Spring 4-27-2020

Reliability-Calibrated ANN-Based Load and Resistance Factor Load Rating for Steel Girder Bridges

Francisco Garcia
University of Nebraska - Lincoln, francisco.garcia@huskers.unl.edu

RELIABILITY-CALIBRATED ANN-BASED LOAD AND RESISTANCE FACTOR LOAD RATING FOR STEEL GIRDER BRIDGES

by

Francisco Garcia

A THESIS

Presented to the Faculty of

The Graduate College at the University of Nebraska

In Partial Fulfillment of Requirements

For the Degree of Master of Science

Major: Civil Engineering

Under the Supervision of Professor Joshua S. Steelman

Lincoln, Nebraska

April 27th, 2020

RELIABILITY-CALIBRATED ANN-BASED LOAD AND RESISTANCE FACTOR LOAD RATING FOR STEEL GIRDER BRIDGES

Francisco Garcia, M.S.

University of Nebraska, 2020

Advisor: Joshua S. Steelman

This research aimed to develop a supplemental ANN-based tool to support the Nebraska Department of Transportation (NDOT) in optimizing bridge management investments when choosing between refined modeling, field testing, retrofitting, or bridge replacement. ANNs require an initial investment to collect data and train a network, but offer future benefits of speed and accessibility to engineers utilizing the trained ANN in the future. As the population of rural bridges in the Midwest approaching the end of their design service lives increases, Departments of Transportation are under mounting pressure to balance safety of the traveling public with fiscal constraints. While it is well-documented that standard code-based evaluation methods tend to conservatively overestimate live load distributions, alternate methods of capturing more accurate live load distributions, such as finite element modeling and diagnostic field testing, are not fiscally justified for broad implementation across bridge inventories. Meanwhile, ANNs trained using comprehensive, representative data are broadly applicable across the bridge population represented by the training data. The ANN tool developed in this research will allow NDOT engineers to predict critical girder distribution factors (GDFs), removing unnecessary conservativism from approximate AASHTO GDFs, potentially justifying load posting removal for existing bridges, and enabling more optimized design for new

construction, using ten readily available parameters, such as bridge span, girder spacing, and deck thickness. A key drawback obstructing implementation of ANNs in bridge rating and design is the potential for unconservative ANN predictions. This research provides a framework to account for increased live load effect uncertainty incurred from neural network prediction errors by performing a reliability calibration philosophically consistent with AASHTO Load and Resistance Factor Rating. The study included detailed FEA for 174 simple span, steel girder bridges with concrete decks. Subsets of 163 and 161 bridges within these available cases comprised the ANN design and training datasets for critical moment and shear live load effects, respectively. The reliability calibration found that the ANN live load effect prediction error with mean absolute independent testing error of 3.65% could be safely accommodated by increasing the live load factor by less than 0.05. The study also demonstrates application of the neural network model validated with a diagnostic field test, including discussion of potential adjustments to account for noncomposite bridge capacity and Load Factor Rating instead of Load and Resistance Factor Rating.

ACKNOWLEDGEMENTS

I'd like to first thank my advisor, Dr. Joshua S. Steelman, for having faith in me throughout my graduate studies. I am thankful and humbled to work under such a knowledgeable, patient, and encouraging advisor. Thank you to Dr. Chung Song and Dr. George Morcous for being on my committee and providing feedback on my research. I'd also like to thank Dr. Fayaz Sofi for all of the help and assistance you provided throughout this project. I appreciate your prompt responses despite the time zone differences.

I'd like to thank NDOT for funding this project and providing me with the opportunity to extend my education. Thanks to the TAC for making this project a possibility and for providing feedback throughout this project. I'd also like to express my gratitude to the University of Nebraska-Lincoln and the Civil and Environmental Engineering department. The faculty, events, and opportunities provided to me by the department made my experience at Nebraska second to none.

I'd like to thank my colleagues for all of their help and encouragement with my studies. I am very fortunate to have studied with intelligent, driven, and fun students. There are too many of you to list out individually, but I'll remember my time at Nebraska with fond memories because of you. Thanks to Khalil Sultani, Xinyu Lin, and Juan Pablo Garfias for your contributions and enthusiasm.

I'd like to thank my family for always encouraging me to follow my dreams. Thank you to my friends including the young men from Piper, my SHPE familia, the friends I made at Kauffman, and everyone from the soccer pitch.

Finally, thank you Anna. I know it was not always easy, but I appreciate you always sticking by me when times were tough.

TABLE OF CONTENTS

LIST OF FIGURES

LIST OF TABLES

1 INTRODUCTION

1.1 Motivation

State governments are required by law to load rate all state-owned structures and to ensure the rating of local government structures (Hearn 2014). Load ratings establish safe loading limits for heavy truck traffic, and load posting is required to restrict bridge use when a bridge is deemed insufficiently safe to support legal loads. Nebraska's bridge inventory is subject to concerns particular to rural Mid-America, where a significant portion of transportation infrastructure was built off-system from state and national highway networks, and in many cases the bridges are aged and approaching or exceeding design lives. These same bridges are now desired to carry heavy husbandry vehicles or crop harvests.

The National Bridge Inventory (NBI 2019) reports that 10% of all bridges in the United States, and 24% of bridges in Nebraska, are posted to limit the allowed load on the bridge. The NBI also reports the design loading for 37% of posted bridges in Nebraska is "unknown", reflecting the bridges' age and off-system locations. Load postings can require truck rerouting, which generates negative economic and environmental impacts. It is therefore desirable to reduce the number of load posted bridges in the existing inventory.

Load posting is generally removed by either retrofitting to enhance the capacity of a particular asset, or performing a more rigorous load rating evaluation with physical load testing and/or refined analysis. Bridges can often carry appreciably higher loads than those used for design, because design procedures typically use conservative analytical modeling simplifications. More rigorous analysis can reveal the margin of reserve capacity beyond design loads accommodated by realistic load distribution among structural elements, but requires time

and expertise on the part of the load rating engineer. The costs of designing, installing, inspecting, and maintaining a retrofit must be compared to the costs of conducting a load test or refined analysis to determine the most efficient bridge management approach for each asset. This study aims to provide a supplementary tool that will enable a load rating engineer to quickly and easily estimate the likely benefit available from more rigorous evaluations.

1.2 Load Ratings

Load ratings are used to assess the load-carrying capacity of bridges, and are expressed as rating factors (RFs). The rating is the ratio of the available capacity of the bridge (i.e., total capacity reduced to account for permanent loads) to the required load effect produced by a rating vehicle. The rating factor is exactly 1 when the available capacity equals the required demand, more than 1 when the bridge has a higher capacity than the demand, and less than 1 when the demand is higher than the available capacity. Typical load rating is performed at two rating levels: Inventory and Operating. Inventory capacity describes the lower bound of the safe load capacity, which can be applied indefinitely, and corresponding to a reliability index that is consistent with current design codes. The operating capacity describes the maximum load capacity that a structure can nominally safely withstand, corresponding to a lower reliability index than the one used in typical design today. Bridges with Operating RFs less than 1 are further assessed using Legal loads, which are typically a suite of truck configurations and can vary by state. A bridge with a Legal RF less than 1 must be posted to warn and restrict heavy vehicles from traversing the bridge.

For girder bridges, engineers determine the RF for each girder of the bridge in question, and the girder with the lowest rating factor governs the load rating. Load rating engineers

analyze each component and connection subjected to a "single force effect" (e.g. axial force, flexure, or shear) (AASHTO LRFD 2013). The general load rating equation, shown in Eqn. 1, is written as a function of nominal capacity (C), dead load (D), live load effect (LL), and impact factor (IM).

$$RF = \frac{\Phi C - \gamma_d * D}{\gamma_L * LL(1 + IM)} \qquad \text{Eqn. 1}$$

AASHTO rating factors tend to be conservative because the derivation of the live load utilizes girder distribution factors (GDFs or DFs). GDFs are intentionally conservative because they are primarily intended to facilitate new design and employ semi-empirical equations that must reasonably represent a wide variety of bridge geometries. Furthermore, AASHTO code neglects some bridge parameters and behavior such as additional stiffness provided by parapets and bridge rails, unintended composite behavior, and additional support restraint (i.e. rotational restraint at nominally simple supports). Since GDFs evaluate each girder as an element with approximated load demands, higher capacities can often be found when evaluating the bridge as a 3D system.

An alternative way to attain a more accurate load rating is to perform diagnostic load tests. The AASHTO Manual for Bridge Evaluation (2013) provides a procedure for adjusting analytic load ratings based on diagnostic tests, and will be discussed in Chapter 8. Load tests reveal live load effects induced in bridge elements by known load magnitudes and placements acting on a bridge. One of the primary benefits of a load test is to capture structural system response, thereby reducing biases introduced by AASHTO GDFs.

Most bridge tests are non-destructive tests. Destructive tests are performed in research labs or on decommissioned bridges in the field to understand how bridge structures behave as the load approaches the ultimate capacity. Diagnostic tests can be performed at a reliably safe load, so that damage to the bridge is highly unlikely. Results of diagnostic tests can be used to calibrate a theoretical prediction of structural response to live loads. Diagnostic tests can be static or moving load tests, depending on the engineer's goals.

Alternatively, a proof test can be performed at a higher load level, by testing a bridge until a target load is reached or the bridge shows signs of distress. Since the load incrementally increases closer to the bridge capacity, damage into the structure is much more likely than a diagnostic load test. For this reason, the testing team must be highly qualified and carefully calculate the appropriate proof load before such a test can be performed.

Finite element analysis (FEA) is a powerful tool that can be used to assess more accurate load ratings. However, FEA takes a considerable amount of time and expertise, as well as investment in analysis software to develop accurate models. Artificial neural networks (ANNs) present an appealing supplementary option to complement AASHTO- and FEA-based computational load ratings. With the increasing accessibility of ANNs in commercial computing software, ANNs have recently been implemented to address an extensive range of complex problems in engineering. The primary benefit of using artificial neural networks is that, after initial development and calibration, ANNs can quickly provide reliable predictions for complex phenomena from readily available known parameter inputs. ANNs implemented in structural engineering do not formulate predictions explicitly from mechanics or advanced structural

analysis. Instead, ANNs formulate predictions implicitly by using relationships detected during training, mimicking the human heuristic thought process.

Typical ANNs in engineering employ a multi-layered feedforward architecture. Multi-layer refers to layers of nodes in between the input and output. All of the nodes from one layer are connected to all of the nodes in the next layer by weighted connections. The weights and biases of the nodes are established and refined during the training of the ANN. The ANN is trained by comparing the desired prediction and the actual ANN prediction. The difference between the ANN prediction and desired prediction is the error. As the ANN trains, the error backpropagates through the node connections and adjusts weights and biases to iteratively mitigate and minimize prediction errors.

In this project, ANNs were trained to predict FEA-based 3D structural system live load effects. The significance of this project is that bridges that are load posted can be load rated by using the ANN predictions to determine whether the investment of more rigorous structural analysis and/or field testing would be warranted to remove load posting.

2 LITERATURE REVIEW

2.1 Scope of Review

Studies on how AASHTO evaluates load ratings and bridge behavior were reviewed. Diagnostic load rating tests were reviewed to seek guidance on how to appropriately perform load testing. AASHTO specifications, manuals, and publications related to load ratings and bridge testing cited by AASHTO were reviewed as well. Finally, artificial neural networks' applications in engineering were reviewed as were common reliability methods to account for the ANN error.

2.2 Studies of Bridge Analysis and Load Ratings

Armendariz, R.R. and Bowman, M.D., 2018, Bridge Load Rating

The Indiana Department of Transportation (INDOT) was posed with the problem of determining bridge load ratings for bridges that had incomplete or no plans at all. The researchers formulated a general load rating plan that can be used for any bridge, regardless of how much information is known. The general procedure, shown in Figure 1, can be summarized by performing the following steps: 1) conduct a bridge characterization, 2) create a bridge database from the previous step, 3) conduct a field survey and inspection, and 4) perform the bridge load rating. INDOT provided the researchers with a list of bridges without plans. The list was made up of 53 bridges, 29 of which were bridges with soil covers. The proposed methodology for load rating the bridges was implemented for several bridges.

The first bridge is a soil covered bridge made up of three corrugated metal pipes. Based on the field inspections and conservative estimates for the three corrugated steel deck pipes,

AASHTO LRFR and LFR load ratings were calculated at inventory and operating rating levels, which were all above 1.

The second bridge, referred to as the Doan's Creek Bridge, was an earthen-filled concrete bridge. The bridge has two symmetrical arches with a pier in the middle that divides oncoming traffic. A SAP2000 model was created to capture axial and bending effects of the bridge. The model was created by dividing the arches in portions. The portions of the arches were approximated by straight frame element members. An interaction diagram was produced that described the failure bounds of the bridge. Finally, the bridge was also load tested with two trucks with strain gauge instrumentation on one of the concrete arches. The model and load test rating factors aligned closely, and showed that the bridge did not need a load posting.

A third bridge, referred to as the Roaring Creek Bridge, was investigated as well. This bridge did have plans, however the open-spandrel reinforced concrete bridge was load posted based on simple analyses performed by INDOT. This bridge was studied more closely with the goal of removing the load posting. This bridge was load tested with two trucks and instrumentation located at the face of the floor beams. A variety of static load tests were performed to use recorded strains to determine elastic neutral axis locations and moments. A 3D FE model was made that used strain measurements from the test in ABAQUS. It was found that the simplified load rating methods used by INDOT were conservative. The measurements from the load test were used to find an experimental load rating that was high enough to remove the load posting.

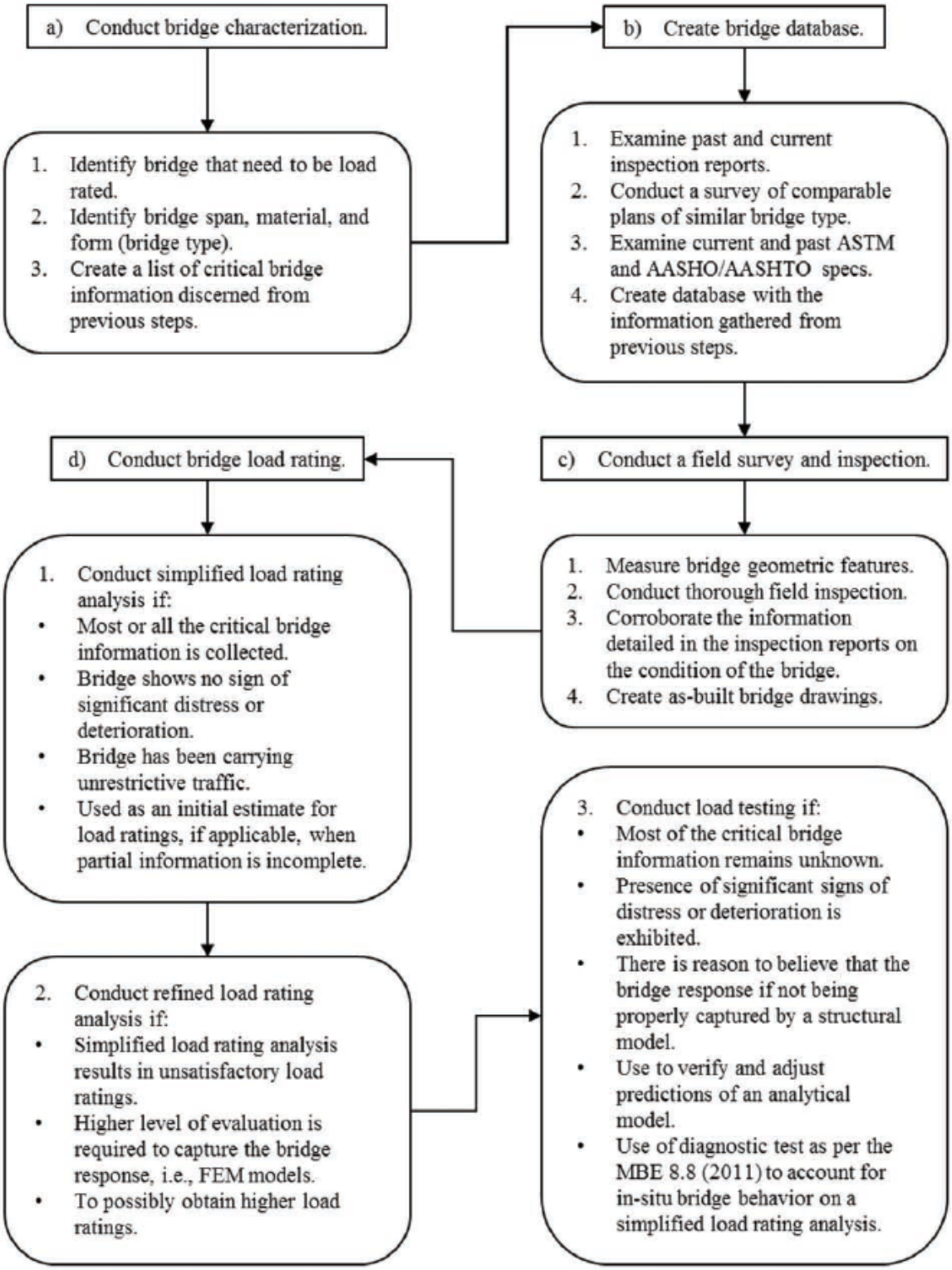

Figure 1. Flowchart of General Rating Procedure

Hearn, G., NCHRP Synthesis 453, 2014, State Bridge Load Posting Processes and Practices

This report gives a summary of the status of bridge load postings, load vehicle types, non-technical load rating processes, load posting signs, and fines associated with overweight vehicle violations. According to the report, ten percent of bridges and culverts in the U.S. are load posted, 77% of load posted bridges and culverts have unknown design live loads or were designed for live loads less than or equal to H15, and 95% of load posted structures are bridges, not culverts. The 10 most numerous structure types and the number of bridges posted is shown in Table 1. Many agencies have vehicles that are exempt from load postings, including vehicles that are related to agriculture, construction, firefighting, forest products, materials, and towing.

Table 1. Ten Most Numerous Structure Types and Load Posting

Item 43 Structure Type, Main		Structures	Posted	% of Group	% of Load Posted
Steel	Stringer/multi-beam or girder	101,454	22,481	22.2	36.8
Concrete	Culvert, includes frame culvert	89,624	2,038	2.3	3.3
Prestressed Concrete	Stringer/multi-beam or girder	54,317	383	0.71	0.63
Steel Continuous	Stringer/multi-beam or girder	47,005	2,710	5.8	4.4
Prestressed Concrete	Box beam or girders—Multiple	40,686	710	1.7	1.2
Concrete	Slab	33,123	3,907	11.8	6.4
Concrete Continuous	Slab	31,940	1,489	4.7	2.4
Concrete Continuous	Culvert, includes frame culvert	27,795	215	0.77	0.35
Concrete	Tee beam	20,295	1,997	9.8	3.3
Wood or Timber	Stringer/multi-beam or girder	18,180	9,373	51.6	15.4

Condition ratings, load rating revaluations, load rating vehicles, load rating signs and installation, and excess weight fines are briefly summarized in the report. The report discusses

ASR, LFR, and LRFR load rating methods and how they differ. The report claims that all of the states surveyed use beam line analysis for load rating, but that 24 of the 43 do refined analysis methods for some load rating computations. Of those 24 agencies, 18 of them perform refined analysis to avoid load postings, 14 of them do it for complex bridges, and six do it for both cases. Of the states surveyed, only 19 states used load tests for rating purposes. Of the states surveyed, 22 states set load postings based on operating rating capacities, 5 set load postings based on inventory rating capacities, and 12 set load postings based on another rating. 4 states used Eqn. 2 from AASHTO, to determine the safe posting load, where W is the gross weight of a rating vehicle and RF is the rating factor for the same vehicle.

$$Safe\ Posting\ Load = \frac{W}{0.7}(RF - 0.3) \qquad \text{Eqn. 2}$$

Legal loads are established by the U.S. Code Title 23; however, states can establish their own legal loads. Code 23 has legal load limits of 20,000 lb. for single axle, 34,000 lb. for tandem axle, and 80,000 lb. for gross vehicle weight. However, legal loads are higher than one or more of the legal loads recommended by Code 23 in 32 states. Nebraska uses the Code 23 single axle and tandem axle limits. However, Nebraska uses 95,000 lb. as the gross vehicle weight maximum legal load instead of 80,000 lb.

According to the report, states can issue overweight permits for vehicles that exceed the legal limit. Typically, overweight permits are issued for non-divisible weights and longer combination vehicles. Overweight permits can be issued for single trips or multiple trips.

The following gaps in knowledge and needs for further research were identified by the author: effectiveness of decisions in load posting, effectiveness of quality control of load rating in load posting, effectiveness of implementation of load postings, effectiveness of load rating in load posting, hazard at un-rated structures, effectiveness of weight limit signs in restricting use of structures, effectiveness of communication of weight restrictions, effectiveness of maintenance of weight limit signs, effectiveness of enforcement, practices of local governments in load posting, and transience of load posting.

2.3 Studies of Neural Networks in Engineering

Sofi, F., 2017, Structural System-Based Evaluation of Steel Girder Highway Bridges and Artificial Neutral Network (ANN) Implementation for Bridge Asset Management

Due to the conservative nature of AASHTO line girder rating methods, Sofi developed a methodology that provides a load rating prediction based on finite element modeling via ANN training. The bridge data in this study is made up of 61 bridges in Nebraska and 193 hypothetically-generated bridges. The scope of the data is limited to single span, multi-girder composite bridges with a concrete deck. The hypothetically generated bridges were randomly made with the most economical rolled W-shapes being used that satisfies AASHTO design requirements.

FEM was performed on ANSYS to obtain girder response to determine a more realistic live load effect that would be used to calculate a refined load rating. An Excel Visual Basic Application (VBA) was used in conjunction with the ANSYS capabilities to perform the analyses. This process modeling technique creates solid elements for the concrete slab. The girders were modeled as shell elements and the cross frames at supports were modeled with

Timoshenko beam elements. The bridges in this study were modeled to act compositely by using multipoint constraint (MPC) rigid beam elements. The modeling process used in this study matched with the results of a full-scale ultimate load test on a simply supported model bridge at the University of Nebraska-Lincoln (Kathol et al.1995) and The Elk River Bridge ultimate load test performed in Tennessee (Burdette and Goodpasture 1971).

The bridge tested at the University of Nebraska-Lincoln, referred to as the Nebraska Bridge, was a steel girder composite bridge with a reinforced concrete deck that was designed in accordance with AASHTO LFD (AASHTO 1992). The test was performed to investigate the load-carrying capacity of the superstructure. Truck loads were applied with post-tensioning rods in 12 locations to simulate two HS-20 design trucks. The longitudinal spacing of the loads was 12 ft. and 15 ft., instead of 14 ft. axle spacing, to match the laboratory's strong floor hole locations. The bridge's geometry and loading configuration is shown in Figure 2.

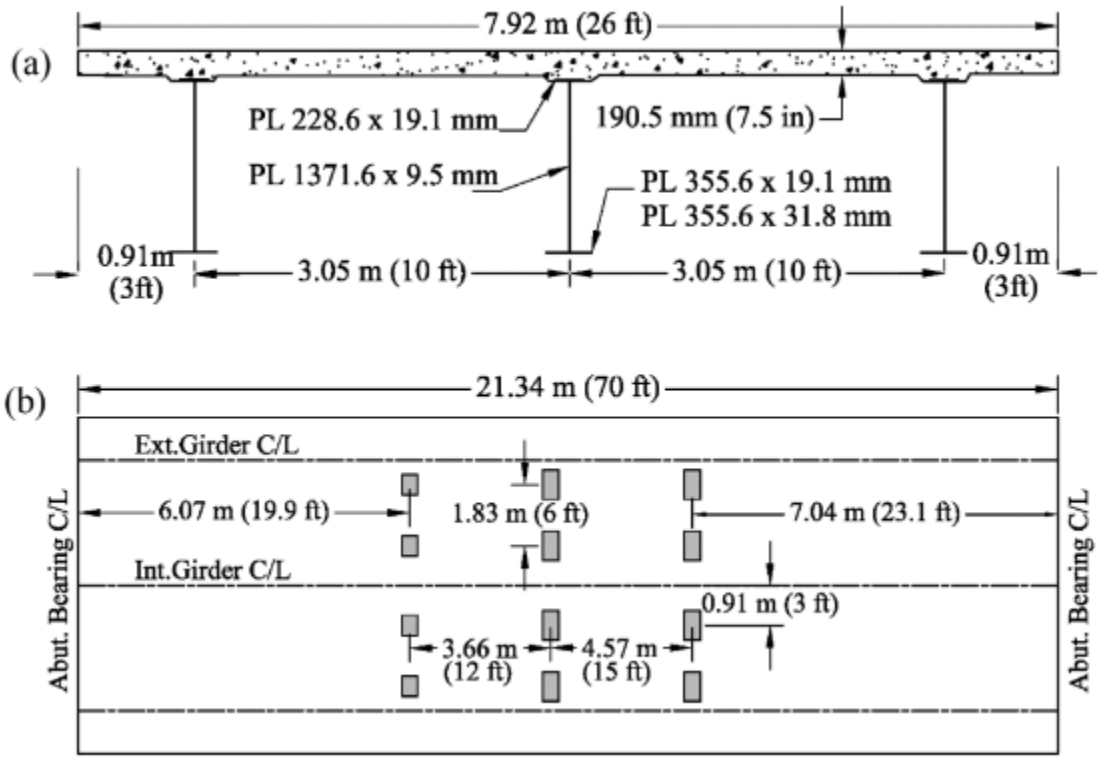

Figure 2. Nebraska Bridge Ultimate Load Test: (a) Cross section; (b) Loading Configuration

Loads were applied in increments of HS-20 trucks (8 kip front axle and 32 kips on middle and back axle). The bridge experienced its first yield after an equivalent weight of 9 HS-20 trucks (648 kips). The exterior girders yielded after an equivalent weight of 12 HS-20 trucks (864 kips). The test came to an end due to local punching shear failure in the concrete after the equivalent weight of 16 HS-20 (1,152 kips) was applied. Girder deflection comparisons between the lab test documentation and the developed models are shown in Figure 3. The maximum interior girder deflection error was 8%, but the mean absolute percent difference was 4%. Sofi claims, “The discrepancy between the load-deflection curve results for the interior girder was attributed to residual stresses in the steel-plate girders and precomposite dead load-induced

stresses unaccounted for in the analytical model, which would cause an earlier onset of inelasticity in the girders than predicted by the FE model."

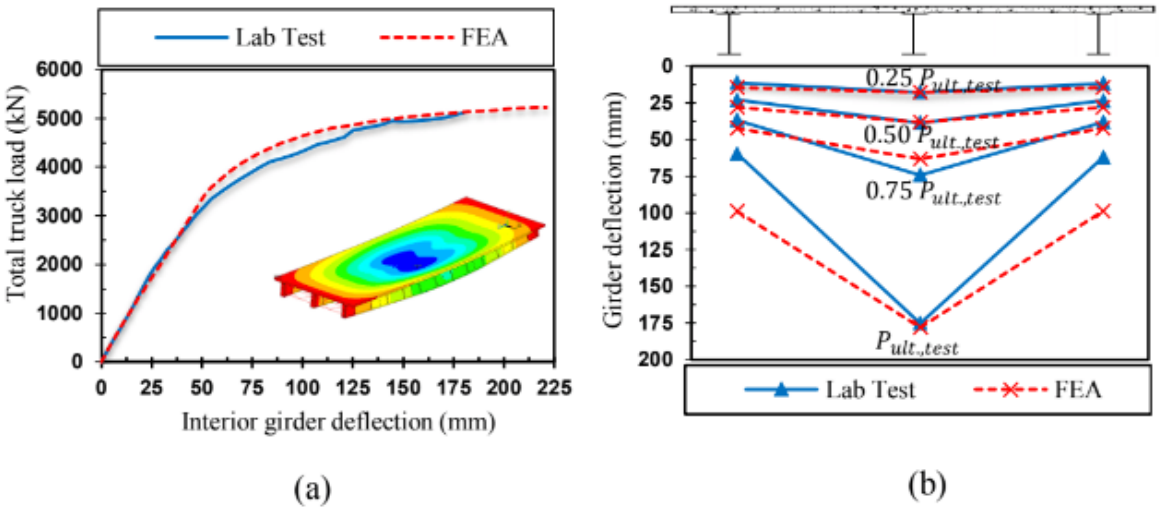

Figure 3. Nebraska Bridge FE Model Comparison with Load Test Results: (a) Interior Girder Deflection; (b) Girder-Deflection Profile at Midspan

Discrepancies between the exterior girder deflections were attributed to a higher stiffness in the experimental exterior girders due to the parapets not being modeled in ANSYS. The difference in deflections became more pronounced at higher loads because more of the loads were distributed to the exterior girders as the interior girders reached their plastic limit.

Once the FEM methodology was validated, the live load distribution of the 243 bridges was used to update load rating predictions and train the ANNs. 10 governing bridge parameters were determined for ANN training. The governing parameters and their effective ranges are shown in Table 2. The ANNs in this study were trained to map the 10 governing inputs to the inventory rating factor of an HS-20 truck. Single ANNs were optimized by creating ANNs with

single or two hidden layers, 2-10 nodes per hidden layer, and either Bayesian-Regularization or Levenberg Marquardt training algorithms. The ANNs were made with 250 retraining iterations to ensure a low mean square error. 15% of the design set was randomly selected for testing. In addition to the 15%, a reduced design set size was used to ensure additional bridges could test the efficacy of the ANN prediction. The ANNs with the best performance were found to have an average absolute error between 6 and 7%.

A shortcoming of a single network is that the error associated for one bridge may be high even though the average error is low. To mitigate this error, Sofi produced committee networks that are made up of subcommittee networks. Subcommittee networks are multiple ANNs of the same architecture. Combined with other subcommittees, the committee network should produce a more robust prediction than a single network. The committee networks produced slightly better predictions on average than the single-best-network. The committee networks and single-best-network had a coefficient-of-correlation with the FEM data of 0.967 and 0.955, respectively.

Table 2. Governing Parameters and their Effective Ranges

Parameter number	Bridge parameter	Effective range
1	Span length (L)	20-89 ft (6.10-27.13 m)
2	Girder spacing (s)	32-99 in (813-2,515 mm)
3	Longitudinal stiffness (Kg)	6,200-325,800 in^4 (2.58×10^9-135.61×10^9 mm^4)
4	Cross frames	Present or absent
5	Number of girders (n_b)	4-11
6	Skew angle (α)	0-45°
7	Barrier distance (d_e)	(-) 8-34 in (-203-864 mm)
8	Deck thickness (t_s)	5-9 in (127-228.6 mm)
9	Conc. compressive strength (f_c')	2.5-4 ksi (17.24-27.58 MPa)
10	Steel yield stress (f_y)	30–50 ksi (206.85–344.75 MPa)

The FEM load ratings produced rating factors that were on average 27% higher than AASHTO. Due to the close agreement between the ANN predictions and the FEM load ratings, Sofi proposes a user application procedure that could be implemented at state agencies.

The first step of the proposed procedure is to create a reliable ANN. Next, the weights and biases should be copied into a spreadsheet where the ANN prediction calculations and nonlinear transfer functions can be programmed. These calculations should be intended to be in hidden sheets so that the user does not have to interact with them. The spreadsheet should prompt the user for the ten governing parameters, normalize the inputs, perform calculations and transfer functions, reverse the normalization, and produce a load rating prediction. Finally, the user should check the applicability of the prediction by ensuring that the governing parameter are

within the design set scatterplot boundaries, otherwise, the ANN would be extrapolating beyond its initial training scope.

2.4 Studies of Structural Reliability

Nowak, A.J., 1999, NCHRP Report 368, Calibration of LRFD Bridge Design Code

The motivation for this research was to produce a bridge design code that is based on probabilistic design. LRFD was created to provide a consistent a "uniform safety level" for bridges – an attribute of LRFD that is not shared with the Allowable Stress Method or Load Factor Design. The probability of failure is described by the reliability index, β, which is shown in Eqn. 3. The reliability index is the inverse standard normal distribution function of the probability of failure. The formula for the reliability index is a function of the nominal resistance (R_n), the resistance bias factor (λ_R), the resistance coefficient of variation (V_R), the mean load (μ_Q), the standard deviation of load (σ_Q), and the parameter k which depends on the location of the design point. Typically, k is taken as 2.

$$\beta = \frac{R_n\lambda_R(1-kV_R)[1-\ln(1-kV_R)]-\mu_Q}{\sqrt{[R_nV_R\lambda_R(1-kV_R)]^2+{\sigma_Q}^2}} \qquad \text{Eqn. 3}$$

A visual representation of the probability failure is shown in Figure 4. The probability of failure and its corresponding reliability index is shown in Table 3.

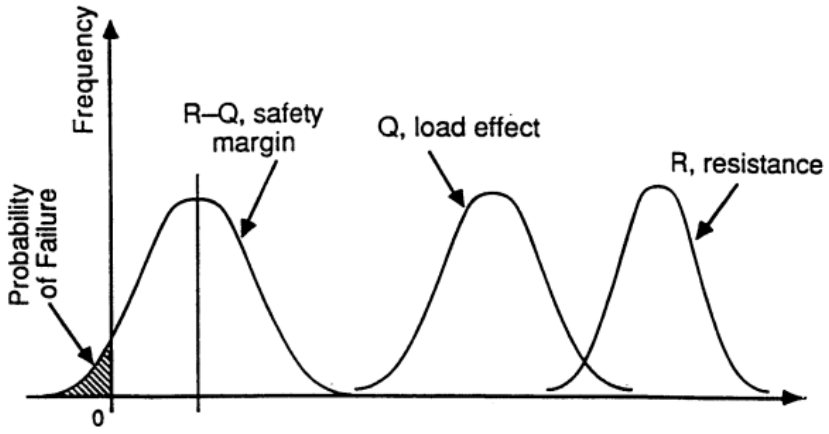

Figure 4. Probability Distribution Functions (PDF) of Load, Resistance, and Safety Reserve

Table 3. Probability of Failure and β.

reliability index β	reliability $S\ (=1-P_f)$	probability of failure P_f
0.0	0.500	$0.500\times10^{+0}$
0.5	0.691	$0.309\times10^{+0}$
1.0	0.841	$0.159\times10^{+0}$
1.5	0.933 2	0.668×10^{-1}
2.0	0.977 2	0.228×10^{-1}
2.5	0.993 79	0.621×10^{-2}
3.0	0.998 65	0.135×10^{-2}
3.5	0.999 767	0.233×10^{-3}
4.0	0.999 968 3	0.317×10^{-4}
4.5	0.999 996 60	0.340×10^{-5}
5.0	0.999 999 713	0.287×10^{-6}
5.5	0.999 999 981 0	0.190×10^{-7}
6.0	0.999 999 999 013	0.987×10^{-9}
6.5	0.999 999 999 959 8	0.402×10^{-10}
7.0	0.999 999 999 998 72	0.128×10^{-11}
7.5	0.999 999 999 999 968 1	0.319×10^{-13}
8.0	0.999 999 999 999 999 389	0.611×10^{-15}

The inconsistent reliability indices are illustrated in Figure 5, Figure 6, Figure 7, and Figure 8. It can be seen that by using the contemporary code, reliability is not consistent for varying span lengths nor girder spacings.

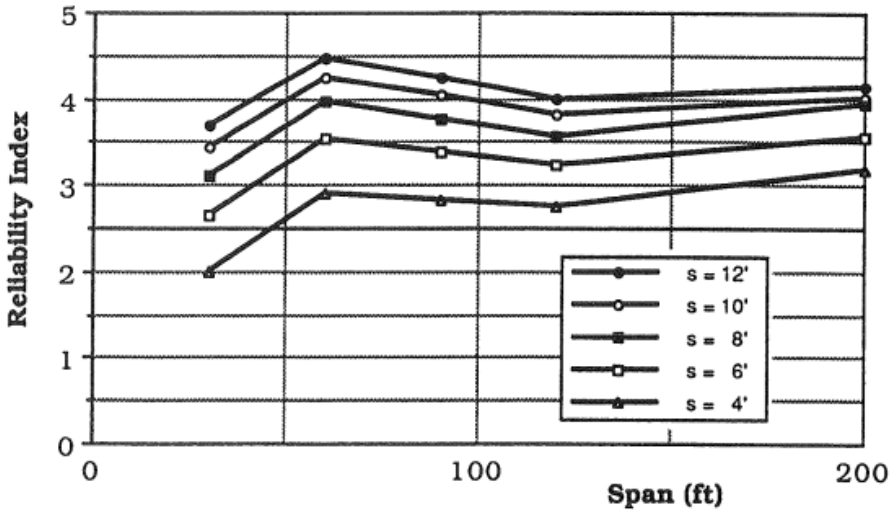

Figure 5. Reliability Indices for Contemporary AASHTO; Simple Span Moment in Noncomposite Steel Girders

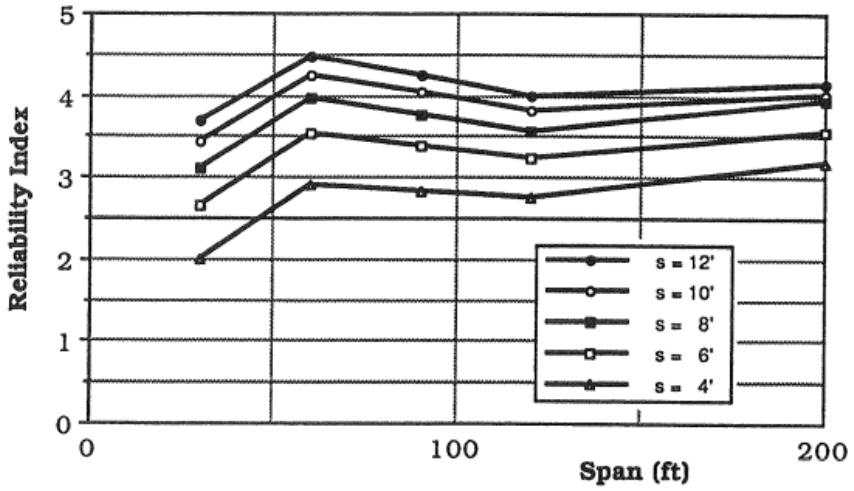

Figure 6. Reliability Indices for Contemporary AASHTO; Simple Span Moment in Composite Steel Girders

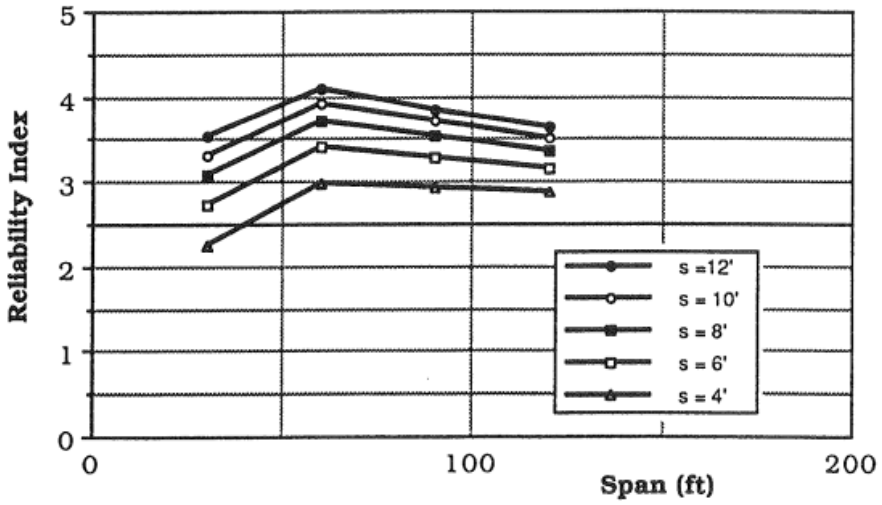

Figure 7. Reliability Indices for Contemporary AASHTO; Simple Span Moment in Reinforced Concrete T-Beams

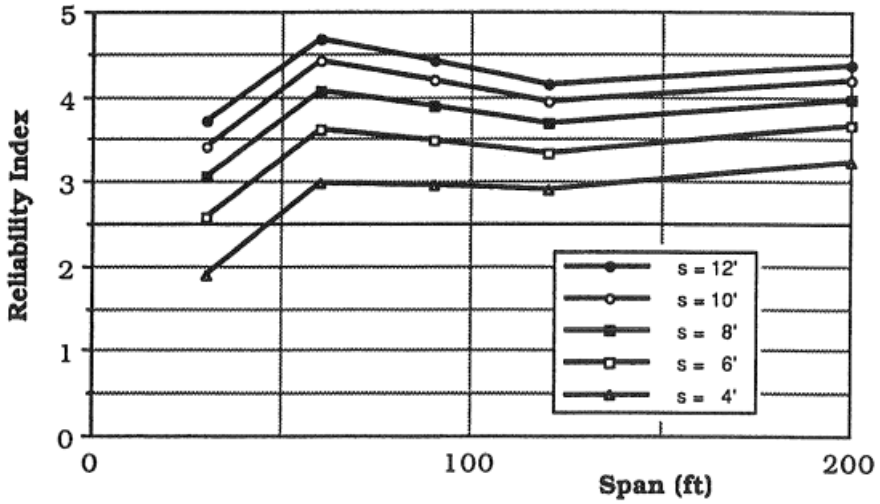

Figure 8. Reliability Indices for Contemporary AASHTO; Simple Span Moment in Prestressed Concrete Girders

The calibration procedure for LRFD is broken down into six steps described below.

1. **Bridge Selection**

   Roughly 200 bridges were selected from various places in the United States. An emphasis was placed on contemporary and future trends instead of focusing on old bridges. Load effects and capacities were evaluated.

2. **Establishing the Statistical Data Base for Load and Resistance Parameters**

   Load data was gathered from surveys, measurements, and weigh-in-motion (WIM) data. Since there is little field data for dynamic loads, a numerical procedure was created to simulate data. As for the resistance parameters, material and component tests were performed.

3. **Development of Load and Resistance Models**

   Cumulative Distribution Functions (CDF) were found for loads by using the available statistical data base. Live load models were created with single and multiple adjacent trucks on the bridge that account for multilane reduction factors for wide bridges.

4. **Development of the Reliability Analysis Procedure**

   Limit states were used to assess the probability of failure and realibility index, β_T, based off of the Rackwitz and Fiessler procedure.

5. **Selection of the Target Reliability Index**

   A target reliability index, which corresponds to a target probability of failure, is selected.

6. **Calculation of Load and Resistance Factors**

   Based off of the target reliability selected in the previous step, load factors, γ, and resistance factors, ϕ, are calculated. Based off of this procedure, a target reliability set at 3.5, and k being equal to 2, load and reliability factors were found. The dead load factor was found to be 1.25 while the asphalt dead load factor was 1.5. The live load factor was found to be approximately 1.6, but a more conservative value of 1.7 was proposed for the LRFD code.

Suggested research topics include creating a large and reliable WIM data base, creating a data base for bridge dynamic loads, further development of serviceability criteria, performing calibration on timber structures, performing calibration on substructures, creating more bridge component test data, creating load models for wind, earthquake, temperature and other load combinations, and investigating how to incorporate bridge component deterioration into the code.

Moses, F., 2001, NCHRP Report 454, Calibration of Load Factors for LRFR Bridge Evaluation

The purpose of this report was to provide the rationale behind the live load factors incorporated to the then proposed AASHTO Manual for Condition Evaluation and Load and Resistance Factor Rating of Highway Bridges. More specifically, the report presents recommendations for legal load rating analysis and permit loadings and postings.

The goal of this project was to select load and resistance factors that correspond to a uniform reliability index. The calibration process was similar to the NCHRP Report 368 (Nowak 1999). First, limit states were checked. The standard limit state function, g, is a function of

random variables. The random variables that the limit state function depends on are resistance, R, dead load effect, D, and live load effect, L. The limit state function is shown below in Eqn. 4.

$$g(R, D, L) = R - D - L = 0 \quad \text{Eqn. 4}$$

Next, the random variables in the limit state function are defined. After that, load and resistance data is gathered for the calibration process. At a minimum, each variable should have a coefficient of variation (COV), which describes the "scatter of the variable", and a bias factor, which is the ratio of mean value to the nominal design value. Finally, a target reliability index is selected and the load and resistance factors can be determined.

The report notes that the NCHRP Report 368 (Nowak 1999) does not specify whether or not site-to-site uncertainties are considered for load intensities. That report used the average beta value from a database using designs that correspond to an extreme loading situation for a very heavy truck volume and weight distribution. However, bridges with lower traffic volumes are expected to have higher reliability indices. Another interpretation is that they did include site-to-site variability. If site-to-site variations are included in the calibration effort and the bias of the extreme loading intensity with respect to average site loading intensity were included, then the target beta of 3.5 would be the average beta of all the bridges. Some bridges would have higher and lower betas than this.

This report claims that they adopted site-to-site variabilities by modeling the live load COV. Furthermore, they used site-specific information such as traffic volume (ADTT) and weight intensities when the data was available.

The data from NCHRP Report 368 was used in this study to find equivalent weight parameters. However, due to the data being recorded for two weeks, heavy trucks avoiding static weight stations, and truck weights changing over time, the researchers decided to consider site-to-site variability and load growth as random variables in this project.

In this research, an operating target beta of 2.5 was used instead of 3.5 for inventory. The reason this is the case is because the 2.5 target beta reflects component failure, not system failure.

Based off of the statistical parameters shown in Table 4, partial safety factors were determined from ranging live-to-dead-load ratios from 0.5 to 2. They found that the required live load factor ranged between 1.65 and 1.77 for a reliability index that corresponds to inventory level rating. For operating level rating, the live load factor ranged between 1.28 and 1.35 for the same live-to-dead-load ratio range. A conservative operating live load factor of 1.35 was recommended by the researchers.

Table 4. Statistics for Safety Index Computations

Case	Bias	COV	Distribution
Dead Load	1.04	8%	Normal
Live Load	1.00	18%	Lognormal
Resistance	1.12	10%	Normal

2.5 Studies of Load Testing

Peiris, A., Harik, I., 2019, Bridge Load Testing Versus Bridge Load Rating

Sensormate's QE-1010 magnetic strain gauge and BDI ST350 strain gauges were evaluated and compared to traditional foil-type strain gauges. The two data acquisition systems were used to instrument members that were also instrumented by foil-type gauges in tensile and flexural laboratory tests. It was found that both systems performed adequately except for the magnetic strain gauge system because they slipped at strains higher than 400 microstrain. The magnetic strain gauge system was used to test a steel girder bridge referred to as the Lewis County Bridge and data was compared to that of foil gauges. The two systems had similar strain profiles, shown in Figure 9, that were interpreted as the bridge performing noncompositely. However, load rating benefits were found since the abutments behave more like fixed supports than simple supports.

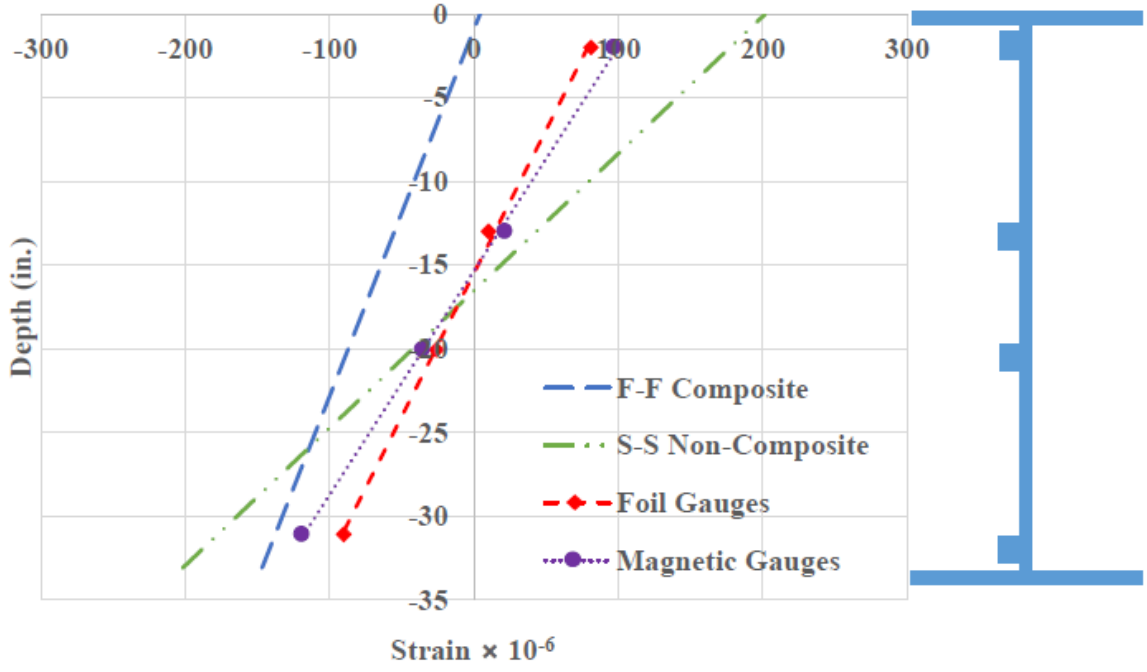

Figure 9. Lewis County Bridge Load Test Strain Data

The Hardin County Bridge was tested using both foil gauges and BDI strain transducers. This test revealed that this bridge benefits largely due to partial composite behavior, illustrated in Figure 10. Although the bridge was performing partially composite, the researchers assumed that the bridge's behavior could be scaled up by 33% since the steel had not yielded yet. It is a well-known that the degree partial composite behavior can decrease as elastic yielding is approached.

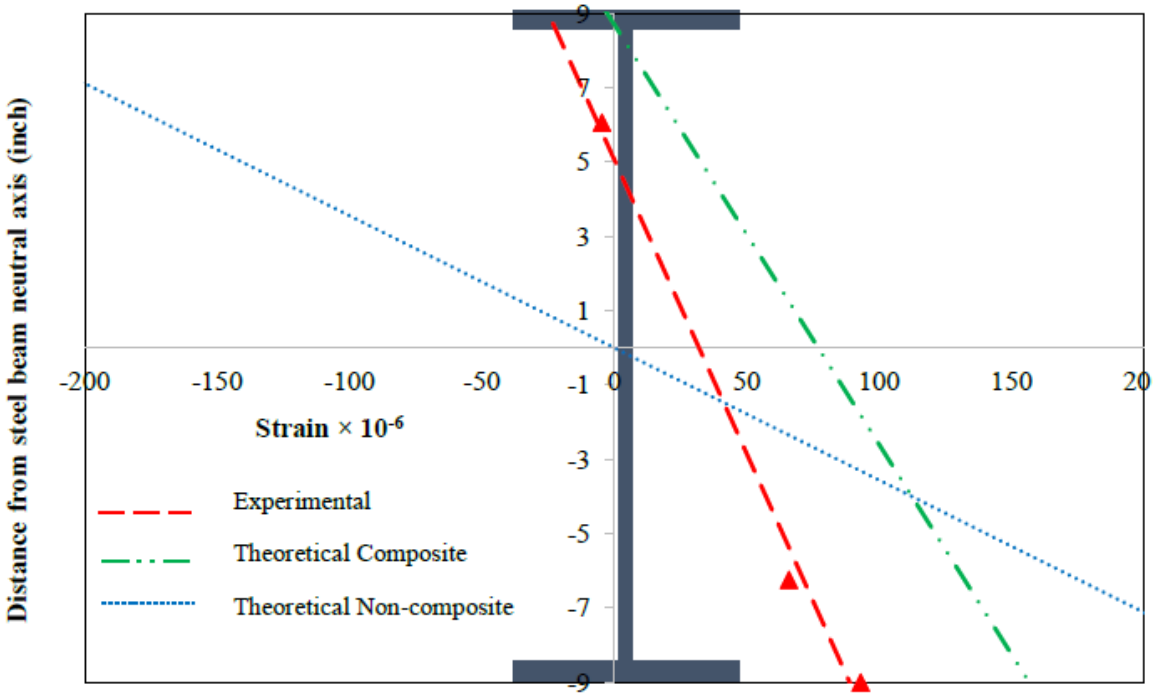

Figure 10. Hardin County Bridge Load Test Strain Data

Both bridges showed significant load carrying capacity benefits in the load test. However, only the Hardin bridge had a load test rating factor that is above 1. The load rating findings are summarized below in Table 5.

Table 5. Load Rating Results

Bridge	Governing Truck Type	AASHTO Analytical Rating Factor	Load Test Rating Factor
KY 1068 – Lewis County	KY Type 3	0.48	0.70
KY 220 – Hardin County	KY Type 3	0.62	1.25

Hosteng, T., and Phares, B., 2013, Demonstration of Load Rating Capabilities Through Physical Load Testing: Sioux County Bridge Case Study

Researchers performed load tests on a two-lane, three-span, continuous steel girder bridge built in 1939. Strain transducers were placed at the top and bottom flanges in locations specified in Figure 11. All of the load tests were performed at crawl speed. The truck locations are shown

Figure 12. Two runs were performed to verify the data. Distribution factors were estimated by taking the ratio of girder strains to the girder strains experienced by all of the girders. The researchers found distribution factors significantly lower than what AASHTO prescribes.

By using the strain data, the researchers developed a two-dimensional FEM to perform LFR load rating analyses on AASHTO rating vehicles. The FEM software that the researchers used is BDI WinGEN and WinSAC was used to do structural analysis and data correlation. WinSAC was used to perform analysis at incremental locations of the truck load. The calibration procedure was done by modifying material properties and stiffnesses until an adequate level of agreement was reached. The calibrated model had a coefficient of correlation of 0.9762. An example of strain comparisons between the analytical model and the field strains is shown in Figure 13.

The operating load ratings for all of the analyses were found to be greater than one despite the bridge being load posted. A summary of the bridge critical rating factors is shown in Table 6.

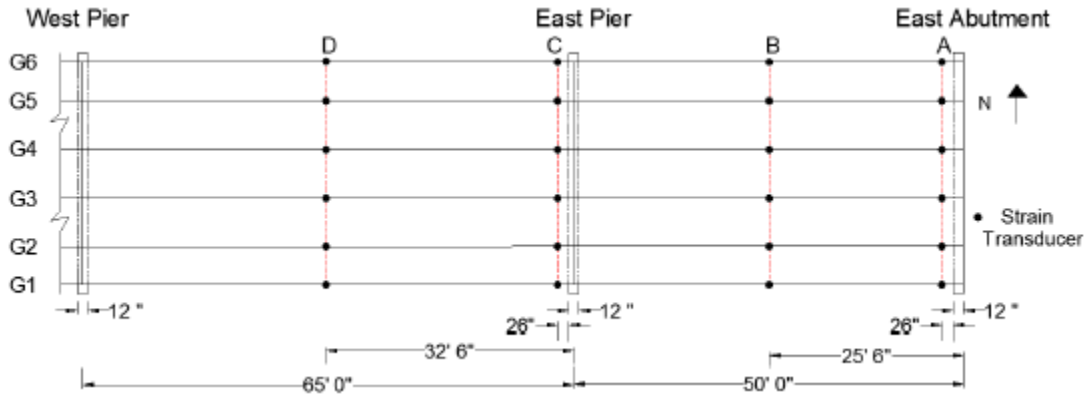

Figure 11. Sioux County Bridge Plan View of Strain Transducer Locations

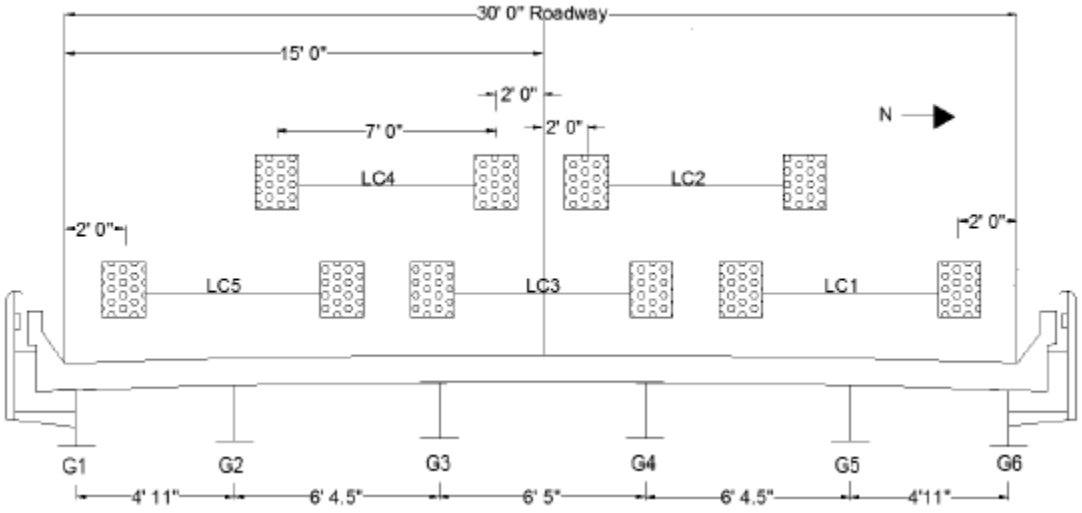

Figure 12. Sioux County Bridge Transverse Load Position

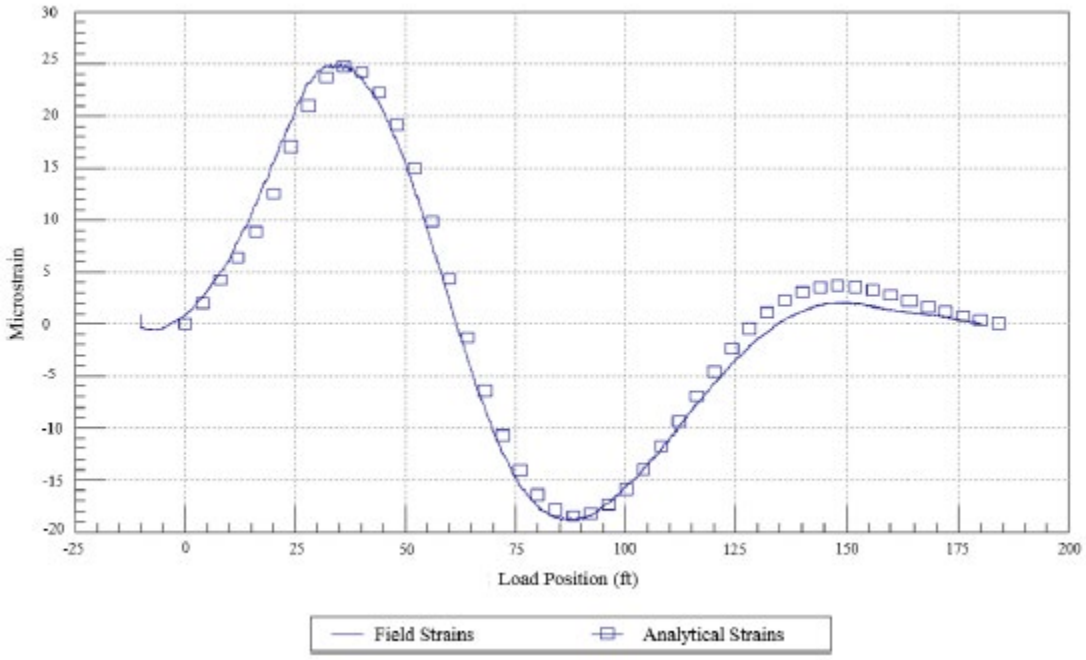

Figure 13. Sioux County Bridge Strain Comparison of G6 on LC3

Table 6. Sioux County Bridge Critical Rating Factors

Rating Vehicle	Location/Limiting Capacity	Inventory Rating Factor		Operating Rating Factor	
		Two Lane	One Lane	Two Lane	One Lane
HS-20(14)	Exterior, Center Span, (+) Flexure	0.61	0.80	1.02	1.33
HS-20(22)	Exterior, Center Span, (+) Flexure	0.72	0.95	1.21	1.59
HS-20(30)	Exterior, Center Span, (+) Flexure	0.86	1.12	1.43	1.88
Type 4	Exterior, Center Span, (+) Flexure	0.73	0.94	1.22	1.57
Type 3S3A	Exterior, Center Span, (+) Flexure	0.75	1.00	1.26	1.66
Type 3-3	Exterior, Center Span, (+) Flexure	0.72	0.96	1.20	1.60
Type 3S3B	Exterior, Center Span, (+) Flexure	0.93	1.16	1.55	1.93
Type 4S3	Exterior, Center Span, (+) Flexure	0.80	1.01	1.34	1.68
Type 3	Exterior, Center Span, (+) Flexure	0.81	1.04	1.35	1.74
Type 3S2B	Exterior, Center Span, (+) Flexure	0.86	1.09	1.43	1.82
Type 3S2A	Exterior, Center Span, (+) Flexure	0.79	1.05	1.32	1.75
Midspan and Endspan Lane Load	Exterior, Center Span, (+) Flexure	0.92	1.19	1.53	1.99
Both Endspans Lane Load	Exterior, Pier, (-) Flexure	1.95	2.61	3.25	4.36
Midspan Lane Load	Exterior, Center Span, (+) Flexure	1.33	1.77	2.23	2.95
Single Endspan Lane Load	Exterior, Pier, (-) Flexure	1.89	2.52	3.15	4.21

3 OBJECTIVE AND SCOPE

3.1 Research Objective

The objective of this research project was to augment and extend existing ANNs that predict the load rating of steel-girder bridges. The ANN modifications include:

- ✓ replacing hypothetical bridge ANN training data with additional existing Nebraska bridge training data,
- ✓ reconfiguring existing ANNs to predict AASHTO truck live load effects rather than load ratings, and
- ✓ accounting for ANN uncertainty in the load rating predictions.

This research was performed with the goal of providing a tool that could be used as a supplement to existing tools available to load rating engineers at the Nebraska Department of Transportation (NDOT).

3.2 Research Scope

Since ANNs were trained using the results of FEMs, the scope of the project is limited by the ranges of attributes represented by the bridges selected for FEM analyses. The bridges selected for training were simple span, steel girder bridges in Nebraska. All bridges were assumed to be composite with concrete decks at the outset of the study, although discussions with state and county bridge engineers during the study revealed that this assumption is not entirely valid. Additional discussion related to composite effectiveness is included with Chapter 8 – Field Testing Case Study.

Ten bridge parameters were used to predict live load distribution factors using ANNs, similarly to Sofi (2017). Sofi selected these parameters because they were believed to be

influential to live load distribution behavior. In order for ANN predictions to be reliable, inputs should be similar to those used in training to avoid extrapolation. ANNs were trained based off of data that excluded outliers in the training. Because of this, ANNs that predict moment and shear rating factors have slightly different ranges of application. Moment ANN and shear ANN ranges of applicability are shown below in Table 7. It should be noted that these are ranges for each individual attribute, but that users should always verify that their inputs are within the scatter of training data shown in Chapter 6.

Table 7. Moment ANN Governing Parameters' Effective Ranges

Bridge Parameters	Effective Range for Moment ANNs	Effective Range for Shear ANNs
Span Length (L)	20-81.6 ft	
Girder Spacing (s)	32-99 in	32-92.5 in
Longitudinal Stiffness (K_g)	11,900-346,225 in^4	7,540.6-415,400.16 in^4
Cross Frames	Present or Absent	
Number of Girders (n_b)	4-11	
Skew Angle (α)	0-45°	
Barrier Distance (d_e)	(-) 4.5-31.25 in	(-) 4.5-32 in
Deck Thickness (t_s)	5-9 in	5-8 in
Concrete Compressive Strength (f_c')	2.5-4 ksi	
Steel Yield Stress (f_y)	30-50 ksi	

Lastly, reliability calibration was performed to augment the AASHTO LRFR paradigm to account for additional live load uncertainty introduced by ANNs. The general methodology

could be implemented with other similar reliability frameworks. AASHTO LFR is not calibrated for a target reliability, and so a direct rigorous extrapolation to LFR is not possible. A short discussion related to LFR is provided at the conclusion of the study.

4 Bridge Population

4.1 Background and Previous Work

Sofi's goal (2017) was to create ANNs that could accurately predict the inventory load rating of a bridge based on 10 governing parameters that are representative of bridge behavior. In order to create ANNs, the 10 governing parameters need target values. For Sofi, every bridge's 10 governing parameters use the inventory rating factor based on FEM load distribution as targets. Before ANN training, bridges needed to be identified and modeled to provide a refined rating factor. The previous work by Sofi, excluding outliers that were not used in ANN training, included 61 real bridges supplemented with 193 hypothetical bridges efficiently designed according to current AASHTO LRFD criteria. Sofi's pilot study created and used hypothetical bridges because retrieving bridge data from DOT records is time-consuming, and Sofi's work focused on FEA and ANN development. Reasonable designs could by generated from hypothetical combinations of governing parameters, allowing Sofi to devote the requisite time for foundational FEA and ANN development and calibration. NDOT bridge documentation often provides only measurement plans. This documentation can be illegible, unclearly organized, or can exclude critical information. Figures 14 through 17 show example measurements available from NDOT for Bridge C007805310P.

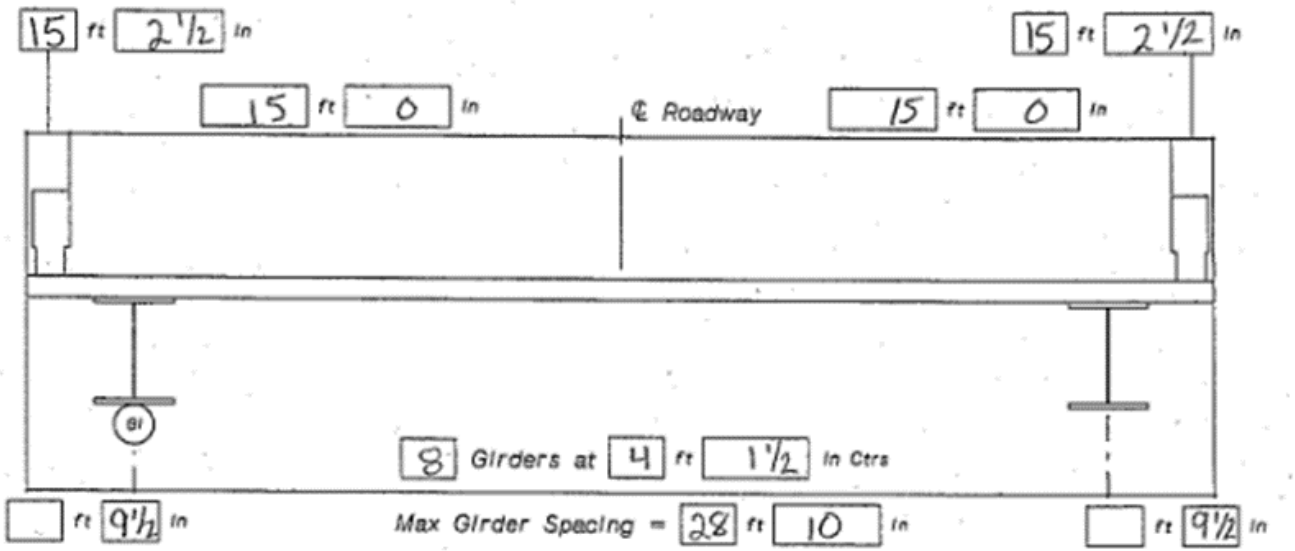

Figure 14. Bridge C007805310P Transverse Measurements

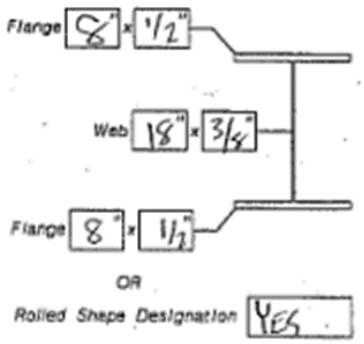

Figure 15. Bridge C007805310P Girder Measurements

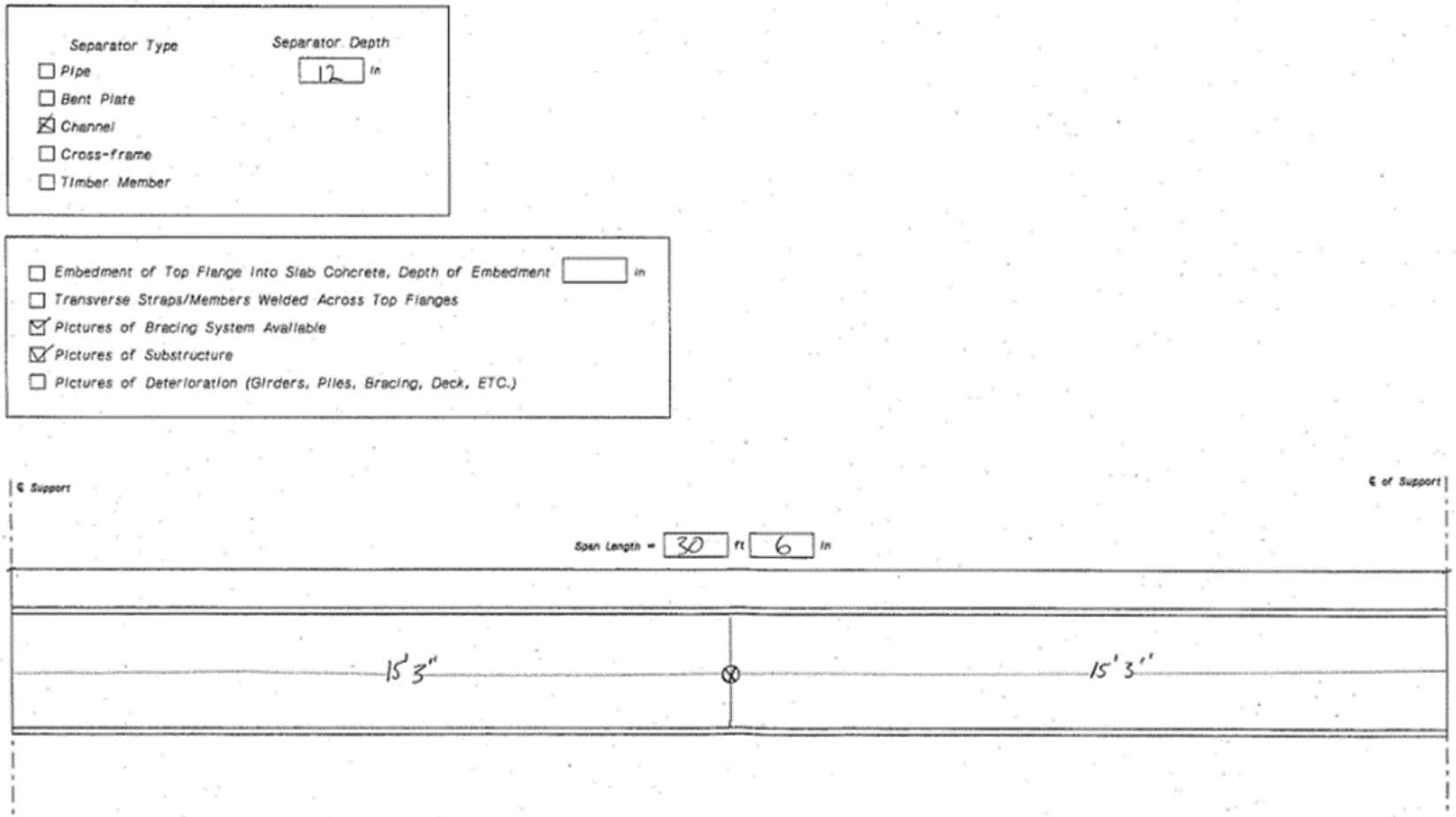

Figure 16. Bridge C007805310P Longitudinal Measurements

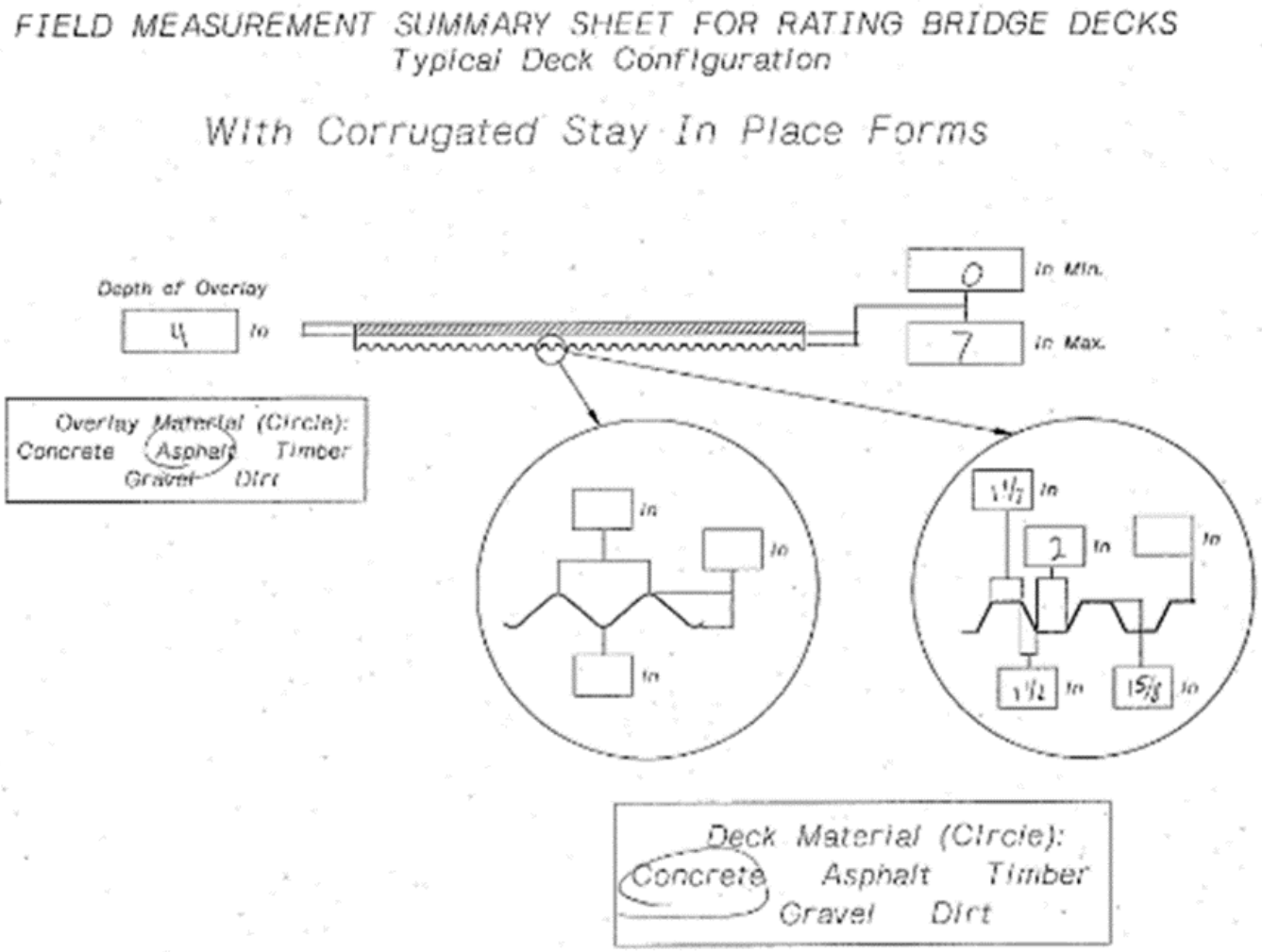

Figure 17. Bridge C007805310P Deck Measurements

4.2 Bridge Population Modifications

The present study included the collection of additional real bridges, allowing hypothetical bridges to be excluded this study to avoid potential bias. 74 Nebraska bridge parameters were made available from Sofi's preliminary pilot study (2017). NDOT aided in retrieving bridge measurement plans and design drawings for 100 additional bridges. The bridges provided from NDOT all have load restrictions, are not fracture critical, and have decks, superstructures, and substructures that have a condition rating of 5 (Fair) or better. Most governing parameter and FEA modeling data were obtained from drawings showing field measurements taken after the bridges' construction. Because of this, details such as presence of composite shear studs or material properties were often undocumented. In such cases, AASHTO 2nd Edition MBE (AASHTO 2013) Tables 6A.5.2.1-1 and 6A.6.2.1-1 were used to select assumed minimum compressive strengths and steel yield strengths, respectively, based on year of construction.

4.3 Bridge Parametric Data

The bridge acquisition task revealed characteristics about single-span bridges in Nebraska. 80% of the bridges were straight and 78% had an assumed concrete compressive strength of 3 ksi. 78% of the bridges had between five and seven girders, with 76% of girder spacings between 3 ft. and 6 ft., and 90% of the bridges span less than 60 ft. Histograms that illustrate the study population's governing parameters are shown in Figures 18 to 27. Appendix 10.1.3.1 includes all of the individual bridge characteristics.

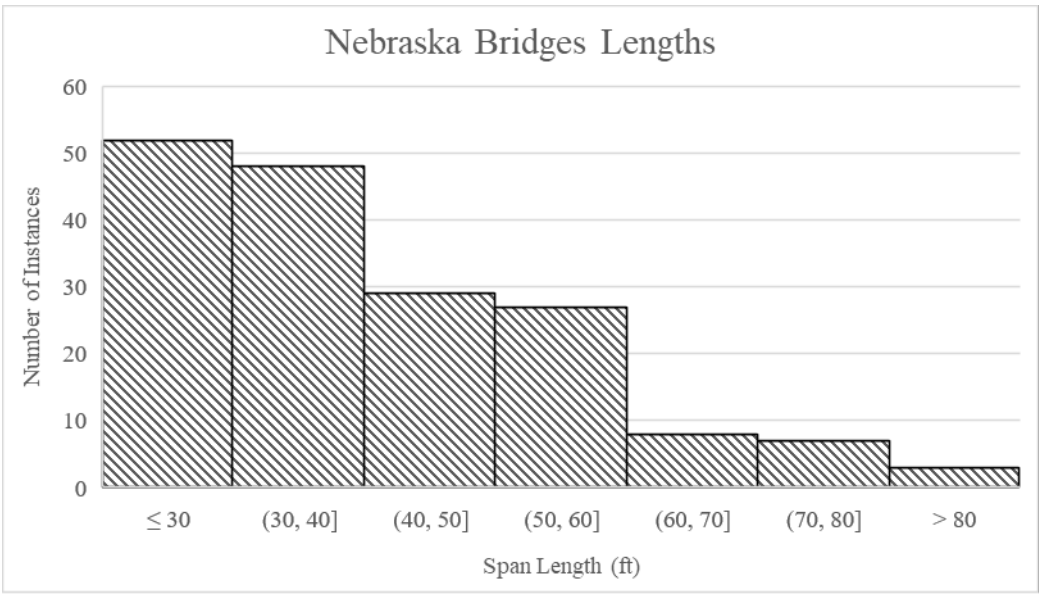

Figure 18. Histogram of Bridge Lengths

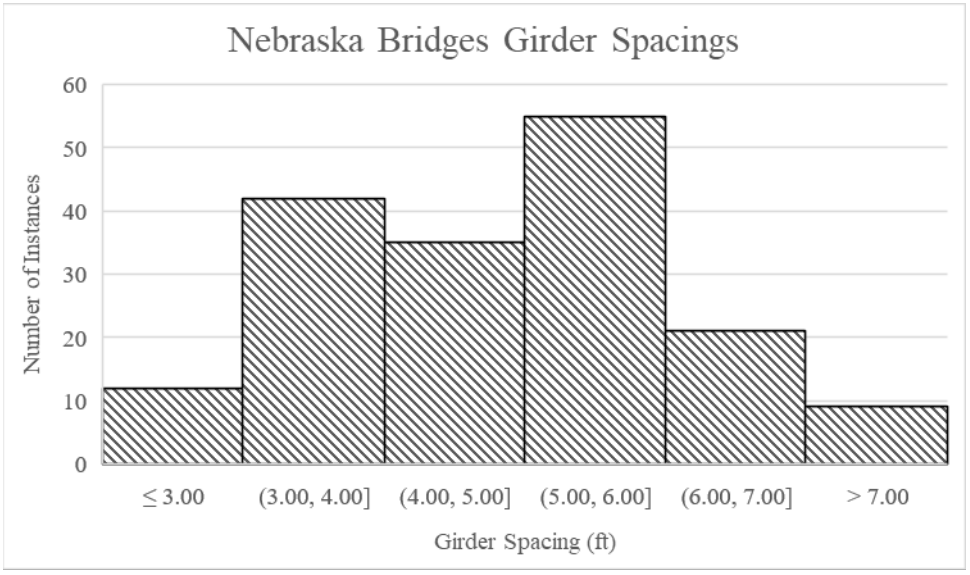

Figure 19. Histogram of Girder Spacings

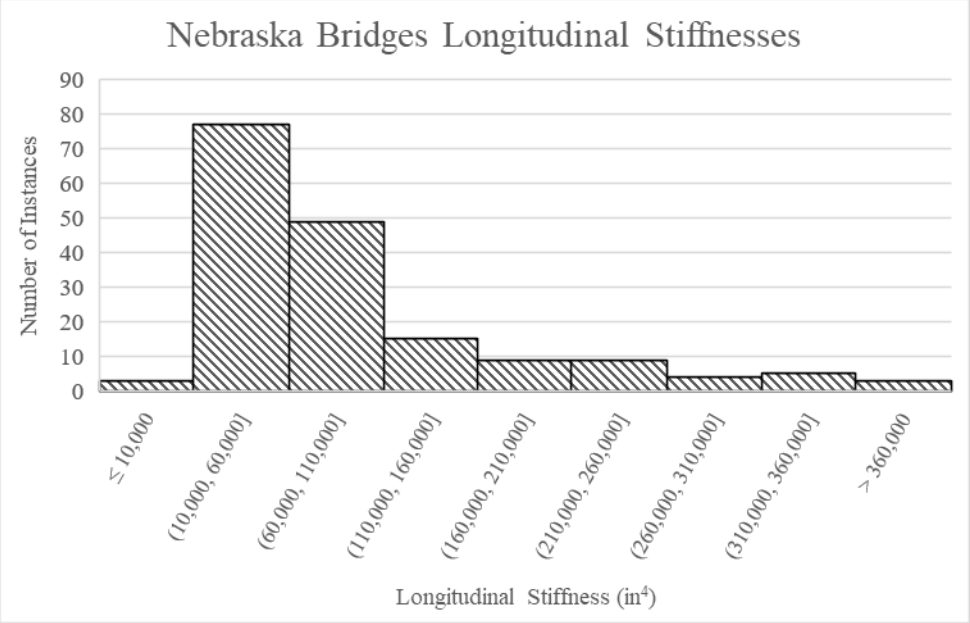

Figure 20. Histogram of Longitudinal Stiffnesses

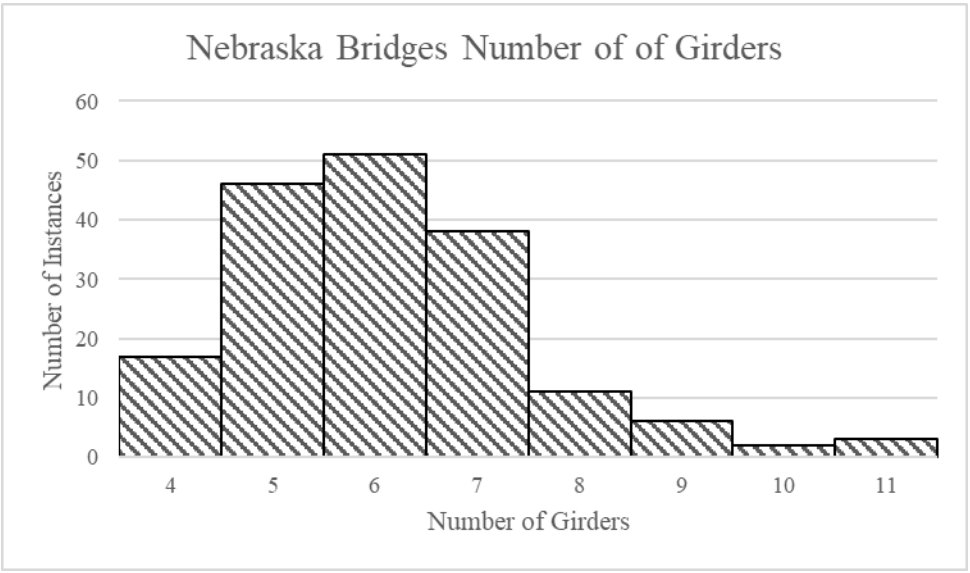

Figure 21. Histogram of Numbers of Girders

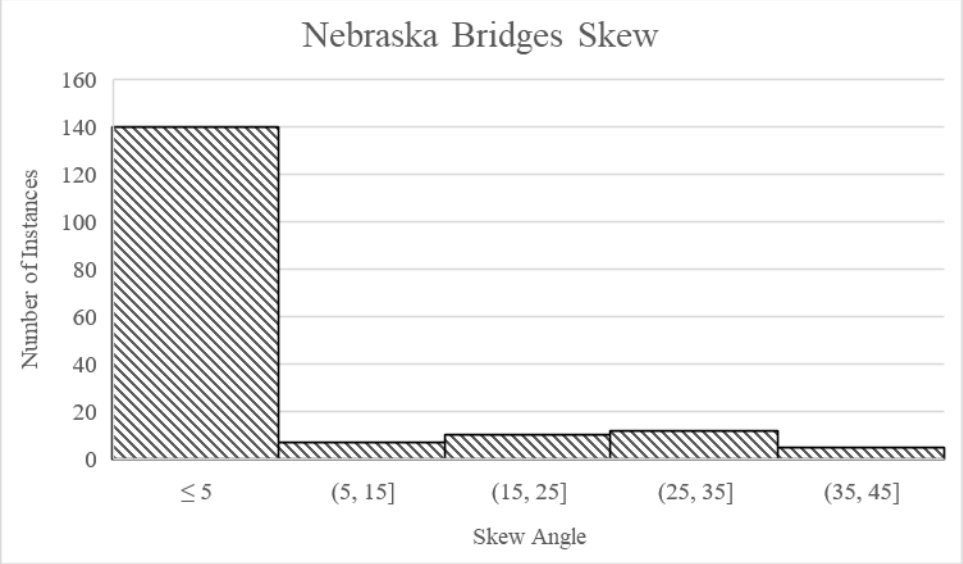

Figure 22. Histogram of Bridge Skews

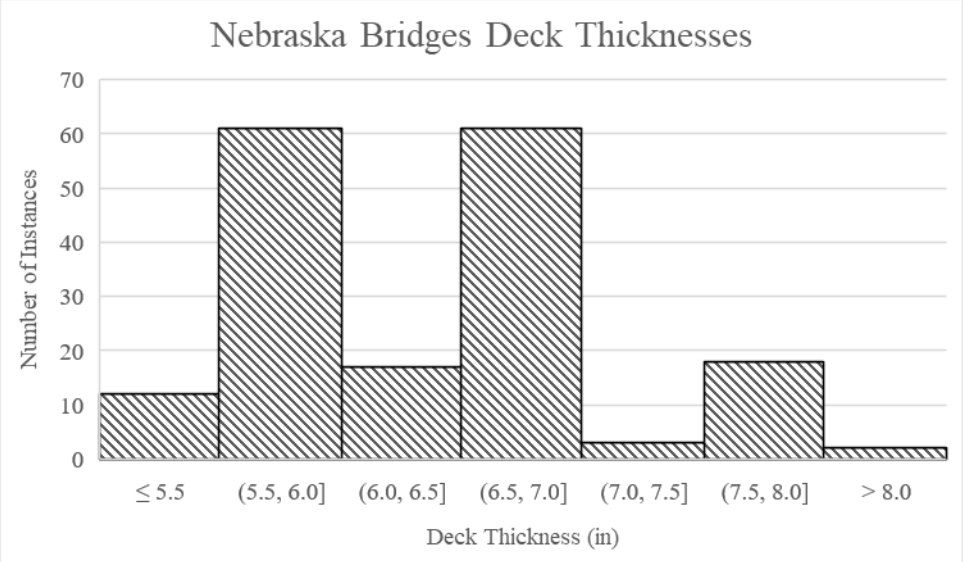

Figure 23. Histogram of Deck Thicknesses

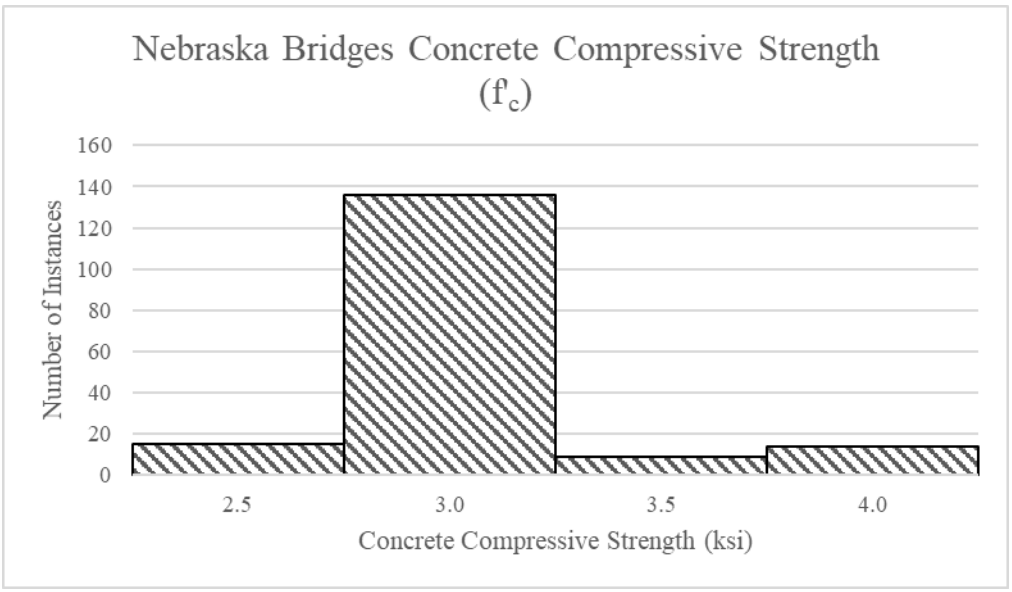

Figure 24. Histogram of Concrete Compressive Strengths

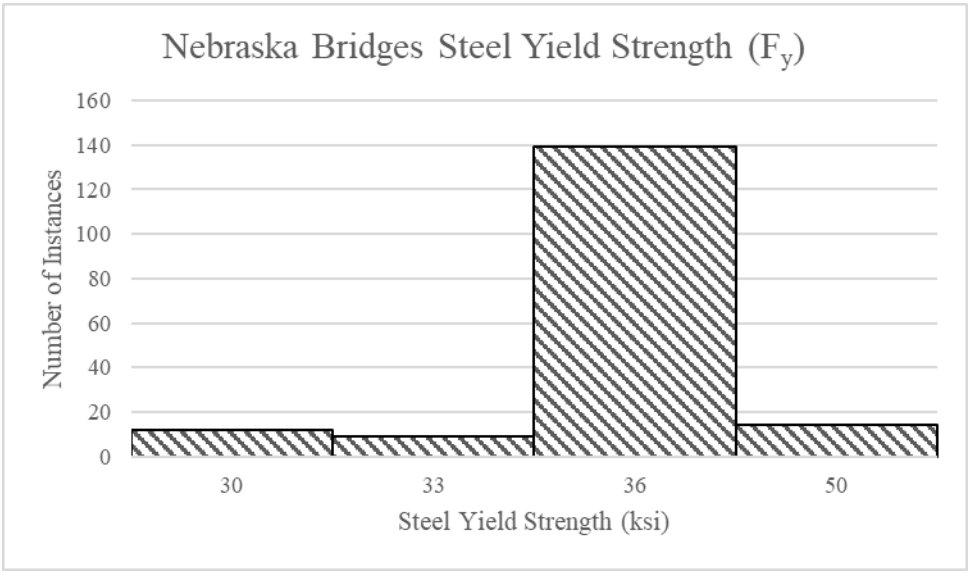

Figure 25. Histogram of Steel Yield Strengths

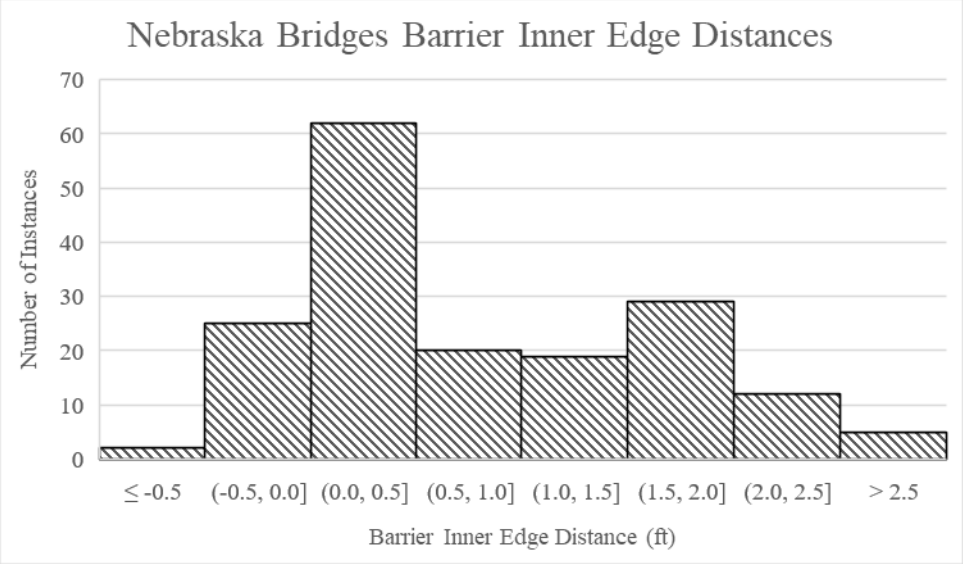

Figure 26. Histogram of Bridge Barrier Inner Edge Distances

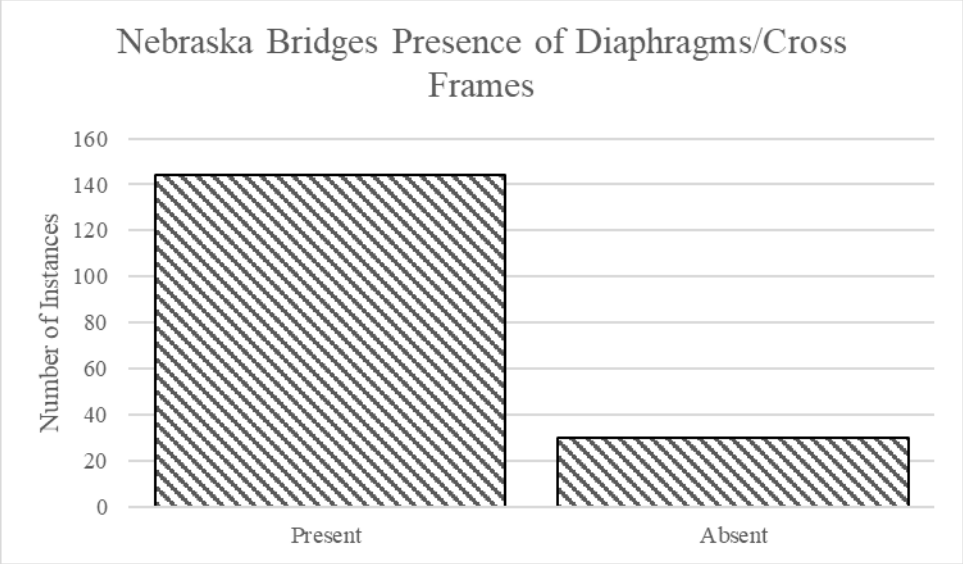

Figure 27. Histogram of Presence of Diaphragms or Cross Frames

5 Finite Element Modeling

5.1 ANSYS Modeling

5.1.1 Background and Previous Modeling Framework

As noted from literature, AASHTO usually estimates live load distribution conservatively, but detailed FEM can capture realistic internal load effects in a structural system closer to those expected from a field load test, which may justify removing load posting from a bridge. It was therefore desirable to generate and implement FEM results as ANN training targets. Sofi (2017) created an FEM procedure to efficiently generate 3D continuum models for single span, composite steel girder bridges. Governing parameters, bridge configuration, loading vehicle details, and FEM meshing details were input into excel sheets for each of the 174 individual bridges from the Nebraska inventory included in this study. Input files for ANSYS were automatically created with an ANSYS parametric design language (APDL) in conjunction with excel VBA macros. The steel girders were modeled as shell elements (Shell 181) and the diaphragms or cross-frames were modeled as beam elements (Beam 188). The bridge deck was modeled using brick elements (Solid65) connected to girders with rigid links (Link180). All bridge models' restraints were modeled as simply supported at the girder ends. Additional details of Sofi's bridge models and validation are available in Sofi and Steelman (2017, 2019). Deck nonlinearity and reinforcement was neglected for these bridge models.

Critical moment loading corresponds to a condition when the loading vehicles' middle axle is located at midspan. However, the maximum moment does not necessarily correspond to the midspan. Sofi specified an analysis location at midspan for bending moments. An example of a bridge FEM is shown in Figure 28 (Sofi and Steelman 2017).

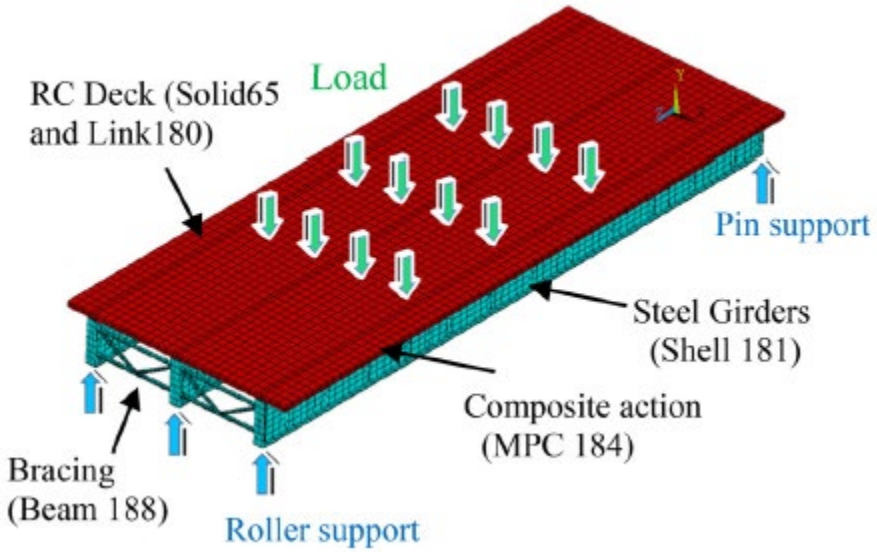

Figure 28. ANSYS Model

5.1.2 Previous ANSYS Modeling and Post-Processing

Sofi's previous work possessed the capability to investigate shear by placing simulated wheel load patches at appropriate alternate locations nearer supports, but primarily focused on flexure. All loads were defined using simulated HS-20 wheel patch loads as described in Sofi and Steelman (2017), and did not account for lane loads in either modeling or post-processing. Four analysis cases were considered: one lane loaded at the critical interior girder position, one lane loaded at the critical exterior girder position, two lanes loaded at the critical interior girder position, and two lanes loaded at the critical exterior girder position. Simulated truck load was placed longitudinally to simulate critical moment demands for all cases.

APDLs were used to post-process element force and stress data to provide the maximum resultant bending moment for each bridge girder following ANSYS analyses. Single lane-loaded analysis results were scaled by a multiple presence factor, *m*, of 1.2. Two-lane loaded analysis

results were not modified to account for multiple presence (i.e., $m = 1$). Maximum moment effects for critical interior and exterior girders were divided by the midspan moment effect of a single lane of HS-20 load. Finally, the analysis results were used to calculate interior and exterior girder moment rating factors, which were then used as output targets in ANN training.

5.1.3 Current Study Modeling and Post-Processing Modifications

As noted previously, Sofi's previous work focused on flexure. The current study expanded to also examine shear. Each bridge was analyzed for eight potential critical scenarios with combinations of: load placement for critical exterior or interior girder loading, load placement for critical shear or moment loading, one- to two-lane loading. A summary of all load cases performed for all bridges in this study is presented in Table 8. Cases 1 to 4 were identical to Sofi's previous work. Transverse load placement correlated to Critical Girder and Lanes Loaded. Longitudinal load placement correlated to the critical Load Effect of interest for the analysis Case.

Table 8. FEM Load Placements

		Critical Girder		Lanes Loaded		Load Effect	
		Interior	Exterior	One	Two	Moment	Shear
Moment ANNs	Case 1	X		X		X	
	Case 2	X			X	X	
	Case 3		X	X		X	
	Case 4		X		X	X	
Shear ANNs	Case 5	X		X			X
	Case 6	X			X		X
	Case 7		X	X			X
	Case 8		X		X		X

The moment GDFs were calculated by dividing maximum moment effects for critical interior and exterior girders by the midspan moment induced by a single lane of HS-20 load. Similarly, the shear GDFs were calculated by dividing maximum shear effects for critical interior and exterior girders by the total shear effect on the critical bridge section under a single lane of HS-20 load.

All modeling in ANSYS assumed composite behavior. However, discussions with NDOT personnel indicated that a significant number of bridges in the anticipated study population were noncomposite. Composite effectiveness will implicitly influence transverse load distribution through the longitudinal stiffness term. Noncomposite bridge models were not included in the study, but the study will extend to load rating noncomposite bridges, provided that the

noncomposite bridge of interest possesses characteristics (particularly longitudinal stiffness) represented in the ANN training data.

5.1.4 ANSYS ANN Training and Testing Data

This study aimed to obtain ANSYS-equivalent GDFs from ANNs. After completing ANSYS analyses for all bridges in the study population, the resulting GDFs were plotted with respect to each governing parameter to identify outliers. Figure 29-Figure 32 and Figure 33-Figure 36 show plots of moment and shear GDFs, respectively. Bridges that were identified as outliers are shown as purple data points and were excluded from ANN training and testing. 11 outliers were identified in the moment GDF scatterplots, which left 163 bridges for moment ANN development. 13 outliers were identified for shear GDF scatterplots, which left 161 bridges for shear ANN development.

It should be noted that some data points may not be outliers in all plots. For example, a bridge may be an outlier because it has a moment GDF and longitudinal stiffness combination that is clearly aberrant compared to the population scatter cloud. However, the same bridge may also have a moment GDF and length that are similar to other bridges. Outliers were assigned a label number so that bridge outlier data points can be noted for multiple plots. Shear ANN outliers do not necessarily correspond to moment ANN outliers.

As anticipated, the GDFs from the modeling procedures were on average lower than AASHTO LRFD GDFs. The AASHTO GDFs were on average 35% and 24% higher than the moment and shear GDFs, respectively. Moment and shear GDF ratios were nearly all between 1 and 1.5, as shown in Figure 37 and Figure 38. The moment and shear GDFs were post-processed and composite operating rating factors were determined. In this study, it was found that 30

bridges were governed by shear. All of these bridges span 35 ft or less. The moment to shear rating factor ratio is 1.87 and is shown in Figure 39.

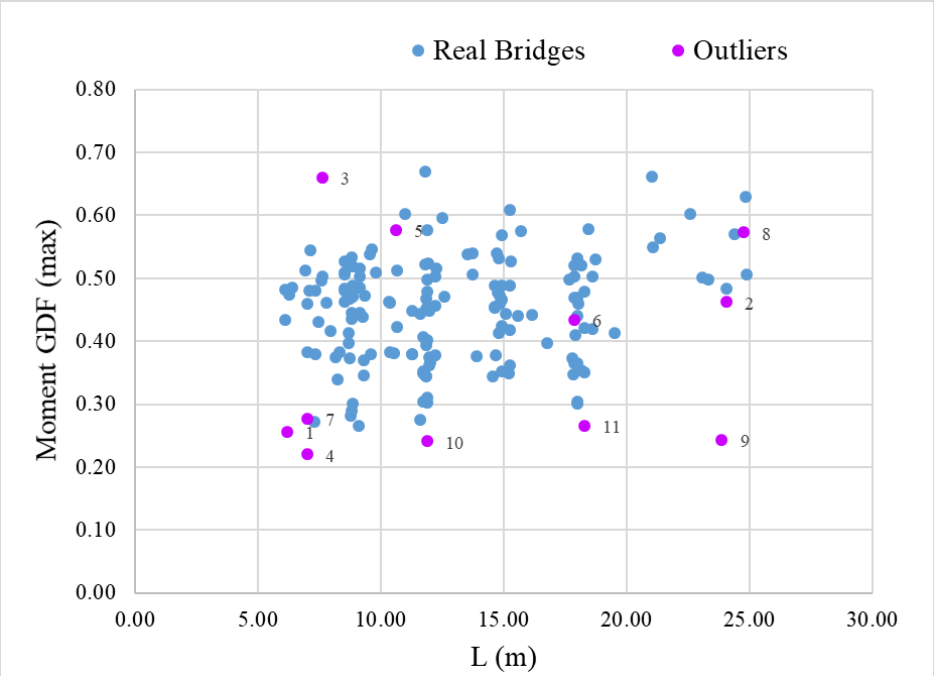

Figure 29. Length vs. FEM-Based Moment GDF

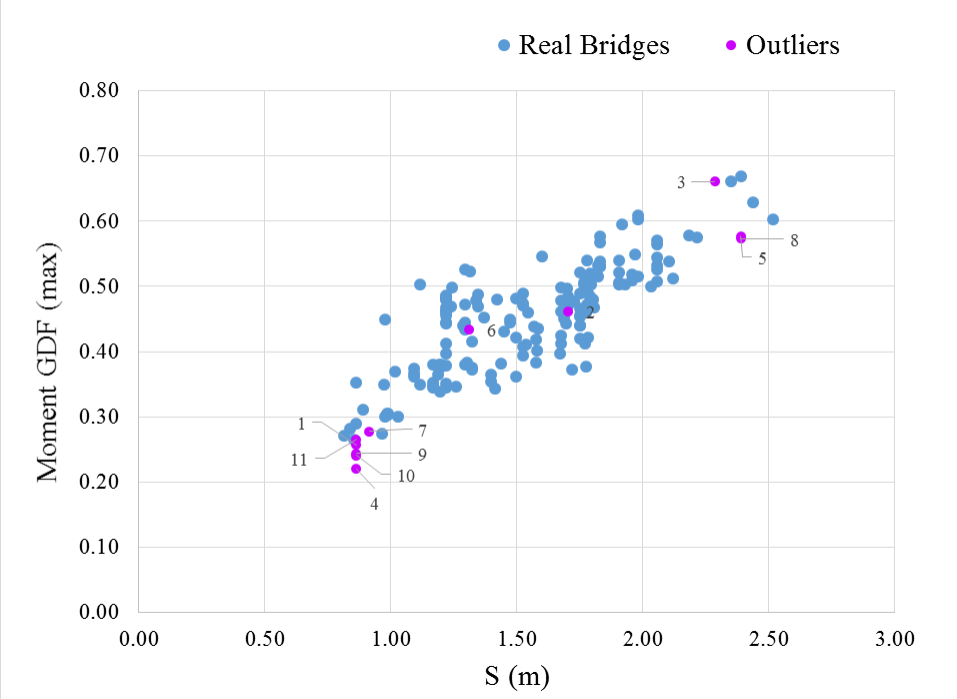

Figure 30. Girder Spacing vs. FEM-Based Moment GDF

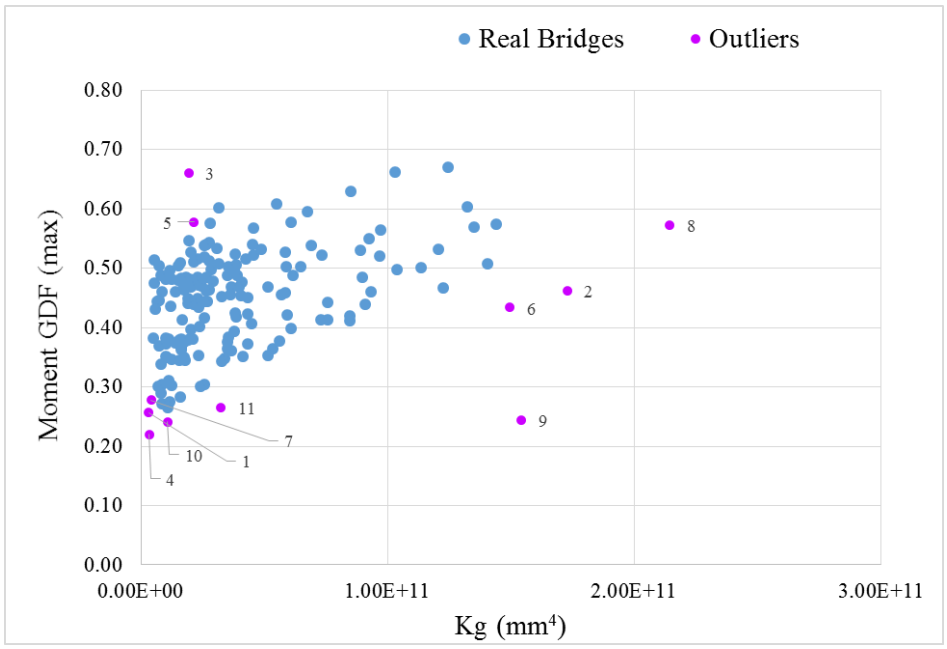

Figure 31. Longitudinal Stiffness vs. FEM-Based Moment GDF

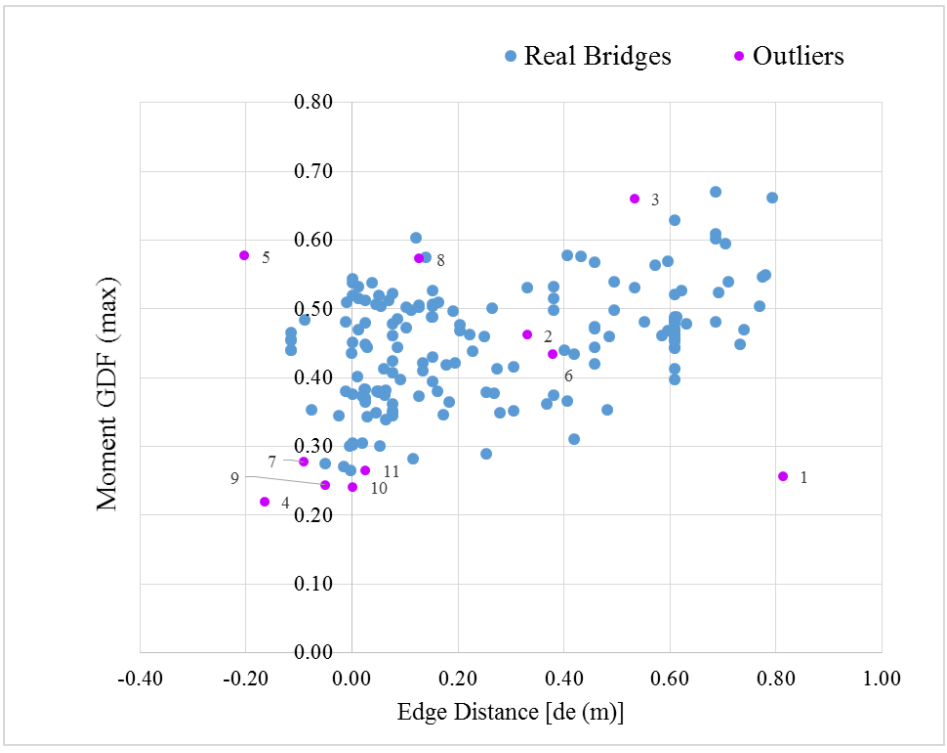

Figure 32. Edge Distance vs FEM-Based Moment GDF

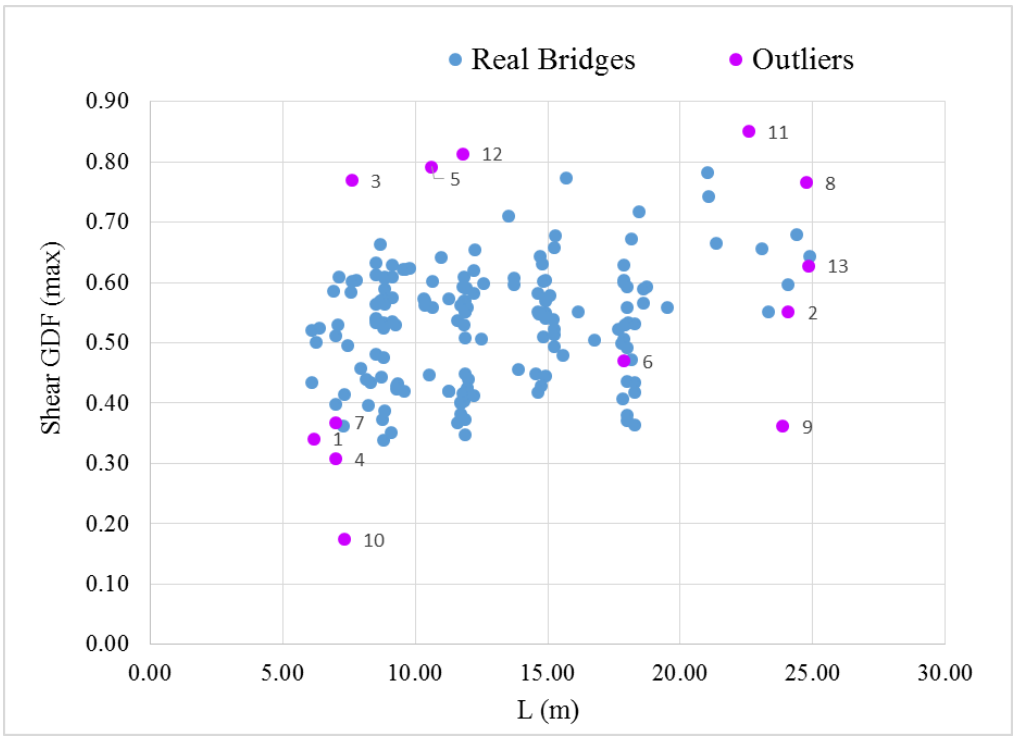

Figure 33. Length vs. FEM-Based Shear GDF

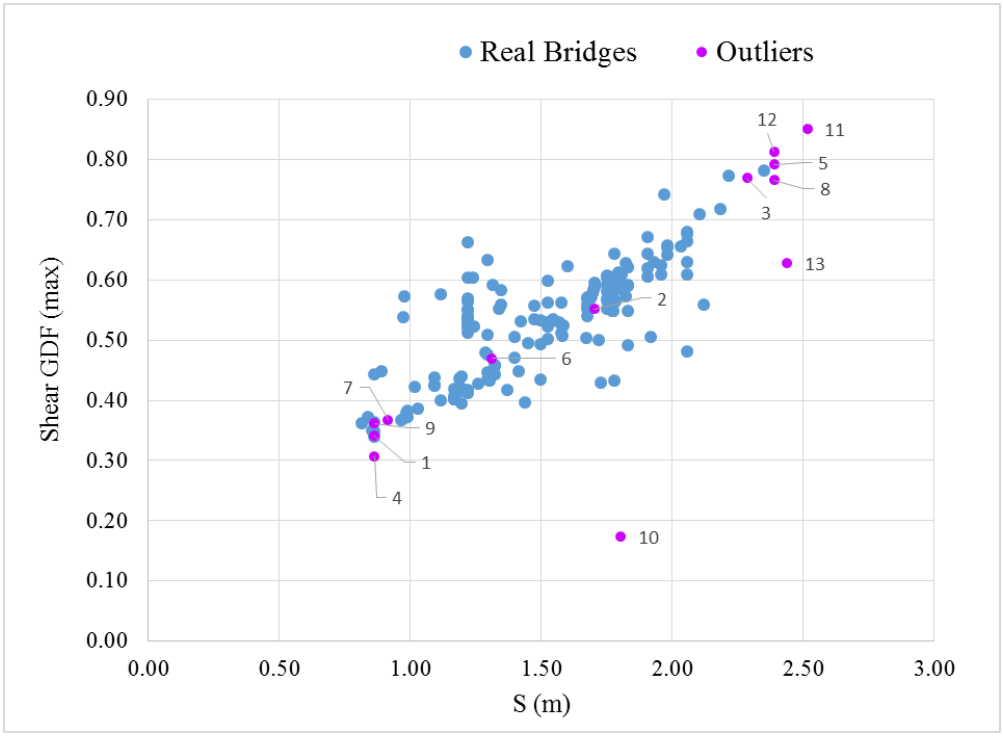

Figure 34. Girder Spacing vs. FEM-Based Shear GDF

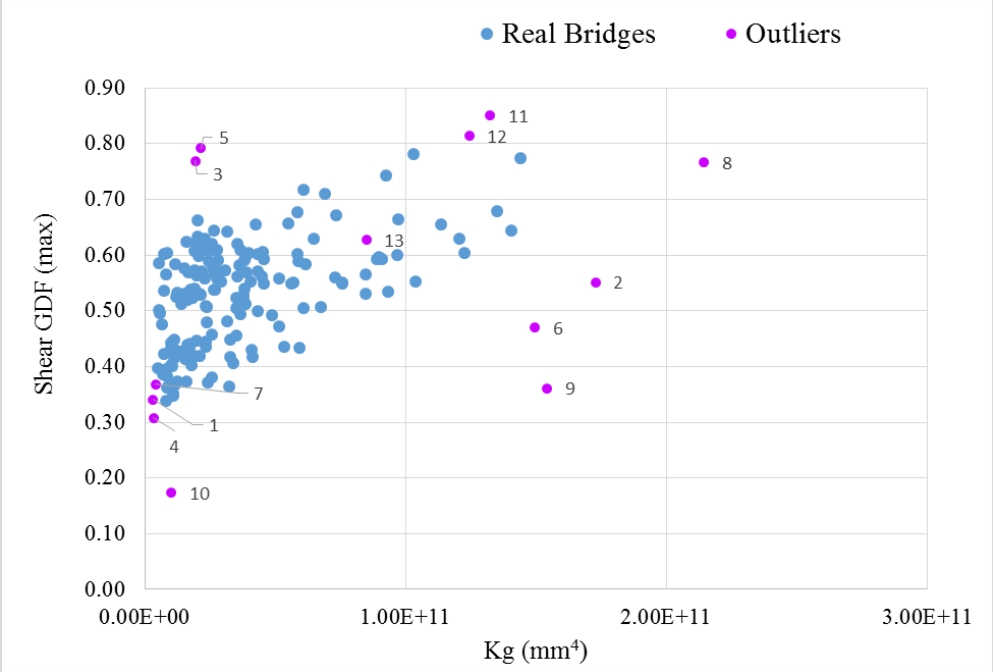

Figure 35. Longitudinal Stiffness vs. FEM-Based Shear GDF

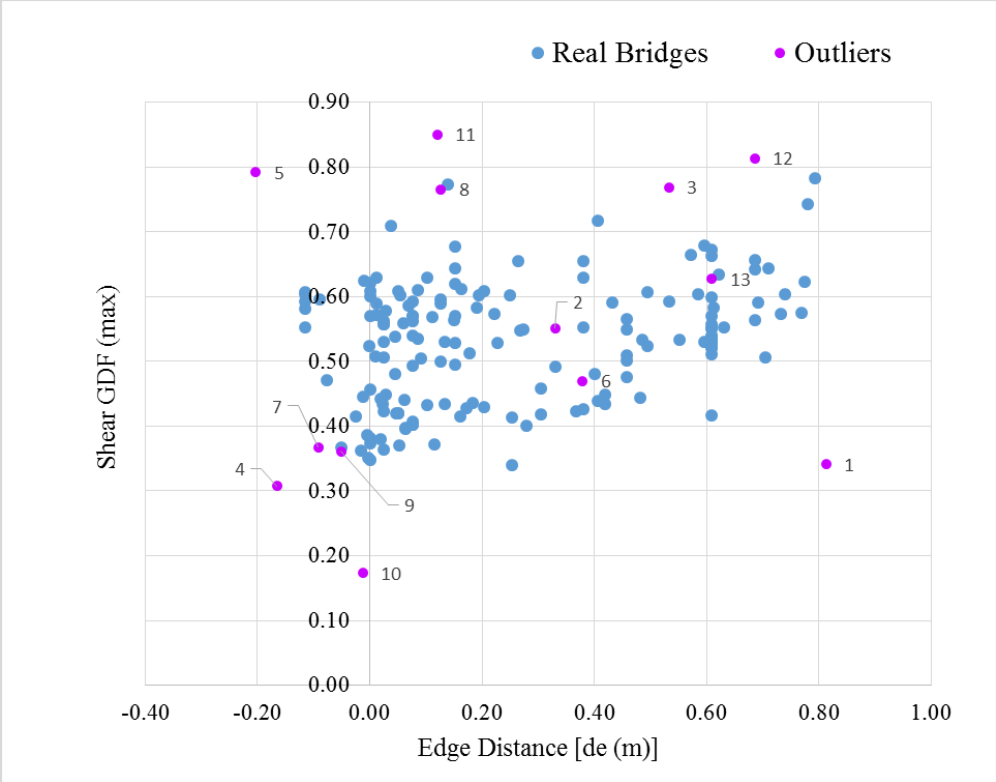

Figure 36. Edge Distance vs FEM-Based Shear GDF

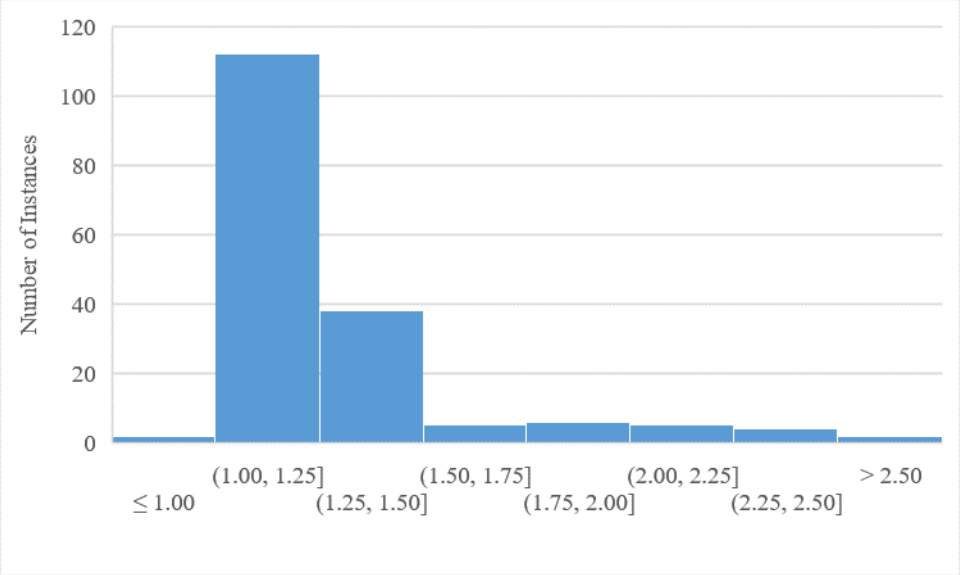

Figure 37. Histogram of Moment GDF Ratio (AASHTO/FEM)

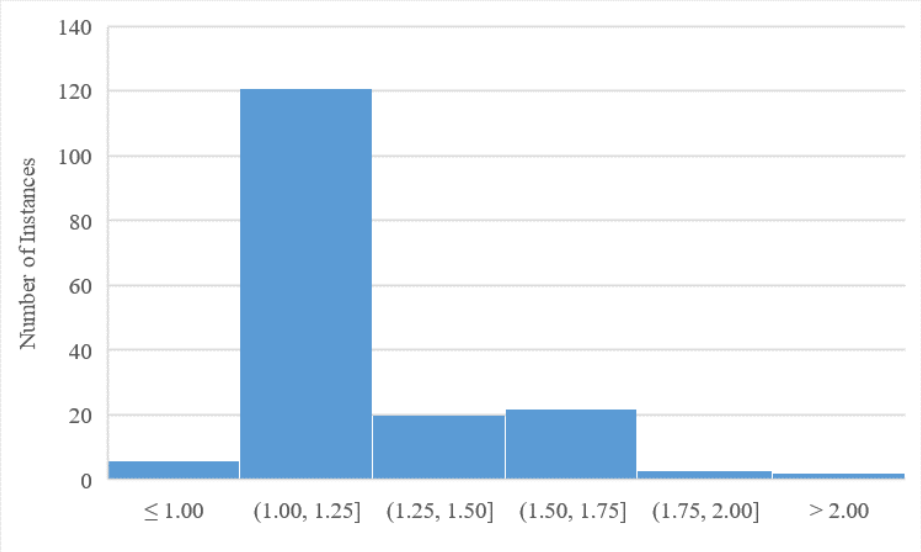

Figure 38. Histogram of Shear GDF Ratio (AASHTO/FEM)

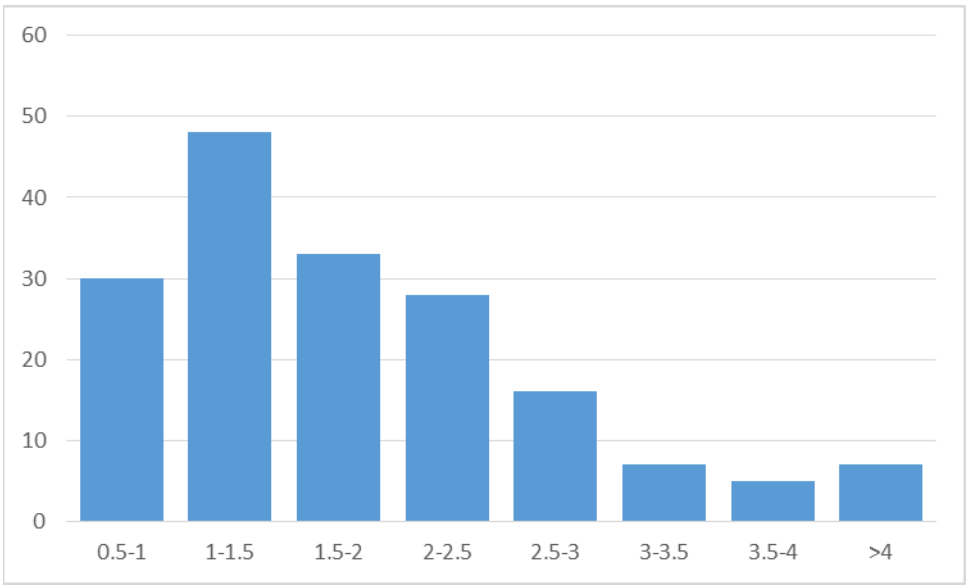

Figure 39. Moment to Shear Operating Rating Factor Ratio

5.2 CSiBridge Modeling

Complementary bridge modeling was performed in CSiBridge for bridges subjected to field load tests. CSiBridge provides a more simplified user experience than ANSYS, and can simulate moving vehicle loads to perform load rating analyses for composite and noncomposite bridges. Both ANSYS and CSiBridge modeled girders with shell elements, but CSiBridge also used shell elements to model the deck, rather than solid elements as in ANSYS.

Four vehicle loading lanes were modeled to represent critical interior and exterior girder load paths in order to be consistent with the loading in the ANSYS models. Material properties, such as yield strength of steel and compressive strength of concrete, were defined identically to those used in ANSYS. Similarly, girder, diaphragm, and deck section properties were identical to ANSYS, except that the deck was specified by its total thickness and axial and flexural shell geometric section properties were internally calculated by CSiBridge.

Once the elements were defined, the bridge was created as an area object model. An HL-93 load pre-defined and available in the software was selected, and an impact factor of 33% was specified consistent with AASHTO LRFR. It should be noted that this load vehicle includes the lane load specified by AASHTO Manual for Bridge Evaluation, which is 0.64 kip/ft for 10 ft wide lanes. Load factors were also specified in accordance with AASHTO LRFR to obtain both inventory and operating load ratings. Load ratings were obtained for both interior and exterior girders, as mentioned previously in the discussion of ANSYS modeling. CSiBridge also allows users specify whether the bridge is composite or noncomposite.

5.3 HS-20 and Tandem GDF Comparison

AASHTO LRFD/LRFR specifies that the maximum moment and shear effects for either HS-20 trucks or tandem loads should be used. For shorter bridge spans, tandem loads have a higher chance of governing moment and shear design. Since this study is predominantly focused on HS-20 loads, a study was performed to compare tandem-based moment and shear GDFs to HS-20 GDFs. The load distributions between HS-20 and tandem loads were compared for bridges C008101013P, C009202210, C003303710, and C006710205 which have span lengths of 20, 40, 60, and 80 ft., respectively. Tandem load GDFs were calculated with the methods mentioned earlier in this chapter. Finally, the percent differences between the GDFs for the two methods were calculated as shown in Eqn. 5. Moment and shear GDF comparisons are summarized below in Table 9-Table 12. Additionally, the governing load effect is provided in Table 13 for the bridges in ascending span length.

$$Percent\ Difference = 100 * (\frac{GDF_{HS-20}}{GDF_{Tandem}} - 1) \quad \text{Eqn. 5}$$

Table 9. Tandem and HS-20 Moment and Shear GDF Difference for Bridge C008101013P (20')

	Moment GDF Difference	**Shear GDF Difference**
1 Truck Interior	0.7%	0.2%
2 Trucks Interior	1.2%	0.7%
1 Truck Exterior	0.6%	2.0%
2 Trucks Exterior	0.9%	-1.8%

Table 10. Tandem and HS-20 Moment and Shear GDF Difference for Bridge C009202210 (40')

	Moment GDF Difference	**Shear GDF Difference**
1 Truck Interior	0.7%	-8.5%
2 Trucks Interior	-0.9%	-2.5%
1 Truck Exterior	0.1%	-4.3%
2 Trucks Exterior	-0.5%	-2.6%

Table 11. Tandem and HS-20 Moment and Shear GDF Difference for Bridge C003303710 (60')

	Moment GDF Difference	**Shear GDF Difference**
1 Truck Interior	-4.4%	-11.5%
2 Trucks Interior	-3.6%	-3.7%
1 Truck Exterior	-0.9%	3.2%
2 Trucks Exterior	0.1%	-0.5%

Table 12. Tandem and HS-20 Moment and Shear GDF Difference for Bridge C006710205 (80')

	Moment GDF Difference	**Shear GDF Difference**
1 Truck Interior	21.5%	21.5%
2 Trucks Interior	19.9%	31.0%
1 Truck Exterior	20.7%	39.4%
2 Trucks Exterior	22.4%	29.3%

Table 13. Governing Load Effect

	Moment		Shear	
Bridge	Tandem	HS-20	Tandem	HS-20
C008101013P	X		X	
C009202210	X			X
C003303710		X		X
C006710205		X		X

In Table 9, the maximum absolute difference between tandem load and HS-20 moment and shear GDFs is 1.2% and 2%, respectively. Results are similar for the 40' bridge, except that the differences in shear GDFs are more pronounced, differing by up to 8.5%. Although this GDFs discrepancy is appreciably large for shear, the governing load effect is produced by the HS-20, as indicated in Table 13, which has a larger gross vehicle weight.

Ultimately, these results indicate that ANNs trained to produce HS-20 GDFs can also be used with tandem loads. A detailed discussion of reliability calibration is presented later, but it is noteworthy for this present discussion that NCHRP 20-07 / 186 (Kulicki et al., 2007) indicated

that the coefficient of variation associated with GDFs was 12%. This aspect of uncertainty is already present and integral within a total 18% coefficient of variation for dynamic live load effects in AASHTO LRFD/R.

GDF predictions for HS-20 loading are generally conservative relative to tandem loading at small loads, to using HS-20 GDFs from ANNs with tandem loads will generally produce slightly conservative results. As span length increases to 40 ft, the HS-20 GDFs initially become unconservative for use with tandem loads, but the effect is only pronounced for shear effects, which are unlikely to govern over moment effects with increasing span lengths. Use of tandem loads with HS-20 GDFs for span lengths of 60 ft or larger is inadvisable. HS-20 loads tend to govern at these span lengths, and the tandem GDFs were also significantly lower for the 80 ft span. Use of tandem loads with HS-20 GDFs may therefore be excessively conservative with increasing span lengths and may negate the benefit of using GDFs from ANNs.

6 Artificial Neural Networks

6.1 Background and Previous Work

Sofi's preliminary study (2017) sought to produce ANNs capable of predicting moment-based load ratings from 10 governing parameters. Figure 40 shows an example of an ANN network architecture (Sofi 2017). Inputs and nodes are connected to each other by weights and each node also has a bias associated to it. Weights and biases are configured during ANN training. Sofi created ANNs using standard machine-learning methods such as using backpropogation algorithms, using testing data to evaluate the generalization of the ANNs, changing ANN architecture to minimize error, and retraining ANNs of the same configuration to account for random initial conditions for weights and biases. The proposed methodology used post-processed FEM live load effects (element-based moment and shear) as ANN training data, rather than extrapolating directly to load ratings within the ANNs.

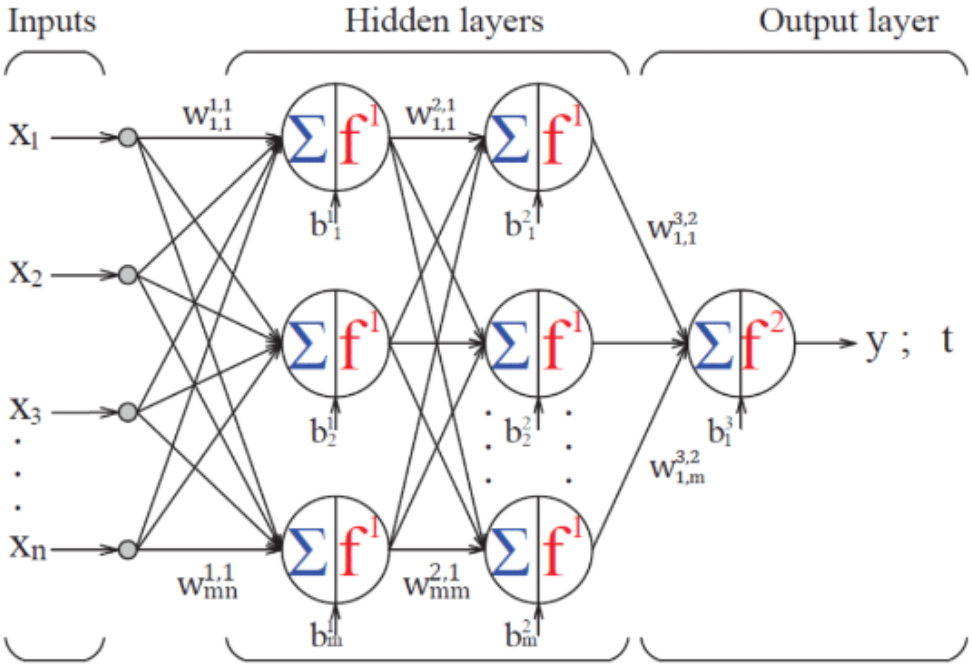

Figure 40. Artificial Neural Network Architecture with Two Hidden Layers and 1 Output

The resulting ANNs in this slightly revised approach can be used to produce rating factors more consistent with realistic bridge behavior when compared to routine AASHTO-based GDFs and load ratings, removing unnecessary conservativism (bias) from anticipated live load effects, similar to Sofi's work. However, the modified approach also facilitates reliability calibration as discussed in detail in Chapter 7 to reflect amplified live load effect uncertainty introduced by ANN prediction errors. The revised methodology also offers increased flexibility and can be easily modified to account for different load vehicles or noncomposite bridges. In addition to the ANN optimization procedure proposed by Sofi, the current study also expanded upon the comparison of ANN performance with varying training set sizes performed by Sofi.

6.2 Artificial Neural Network Training and Testing Data

Neural network modeling for this study was performed using the Neural Network Toolbox available in MATLAB 2017 and implemented a typical feedforward architecture with one input layer comprised of 10 neurons (one for each of the governing parameter inputs), one output layer containing a neuron for the predicted GDF, and either one or two hidden layers. As discussed in the following section, the number of neurons in the hidden layers was varied to optimize network performance.

A total of 163 and 161 bridges remained for moment and shear ANN development, respectively, after excluding outliers as discussed in the previous chapter. Neural network training is commonly performed by partitioning available design data into training, validation, and testing subsets. These design datasets are randomly partitioned during ANN training to ensure that the ANN is sufficiently generalized to avoid overfitting, which would result in very low errors for training data but significantly larger errors for samples outside the training data.

Similar to the Sofi's method, prior to any ANN training, a portion of the study population was partitioned and isolated as an independent testing set, which was distinct from the design testing set typically used in ANN training. Design and independent testing sets were assigned randomly, except that the assignment of bridges to the design set was strategically performed with extreme cases (relatively high and low GDF values with respect to governing parameters) to envelope the design data. The design set envelope was then supplemented with random additional samples to provide internal interpolation points within the population.

The design set ranged from 20 to 130 bridges in increments of 10 to investigate design set size influence on ANN prediction accuracy. Each design set population was randomly subdivided by MATLAB into 70% training, 15% validation, and 15% design testing subsets when the Levenberg-Marquardt algorithm was used. The design set population was randomly subdivided by MATLAB into 85% training and 15% design testing subsets when the Bayesian Regularization algorithm was used. While the design testing set size varied with the overall size of the design set under consideration, the independent testing set comprised 33 and 31 particular bridges for the moment and shear GDFs, respectively, which remained unchanged regardless of the design set size.

When less than the maximum 130 available bridges were used in the design set, the bridges not included in the design set were available for additional testing. Accordingly, these extra bridges excluded from the design set were classified as an "Additional testing set." Figure 41 shows moment GDF vs. governing parameter data points for 130 bridges in the design set and Figure 42 shows moment GDF vs. governing parameter data points for 90 bridges in the design set. The testing set, shown in orange, is the "independent" testing set, and remained the same for

the two design set sizes. The smaller design set left out 40 bridges, shown in magenta, that were used for additional testing (in addition to the independent testing set). The entire moment and shear data sets are in the Appendix 10.1.3.

Figure 41. Moment GDFs vs. Governing Parameters for 130 Bridges in Design Set

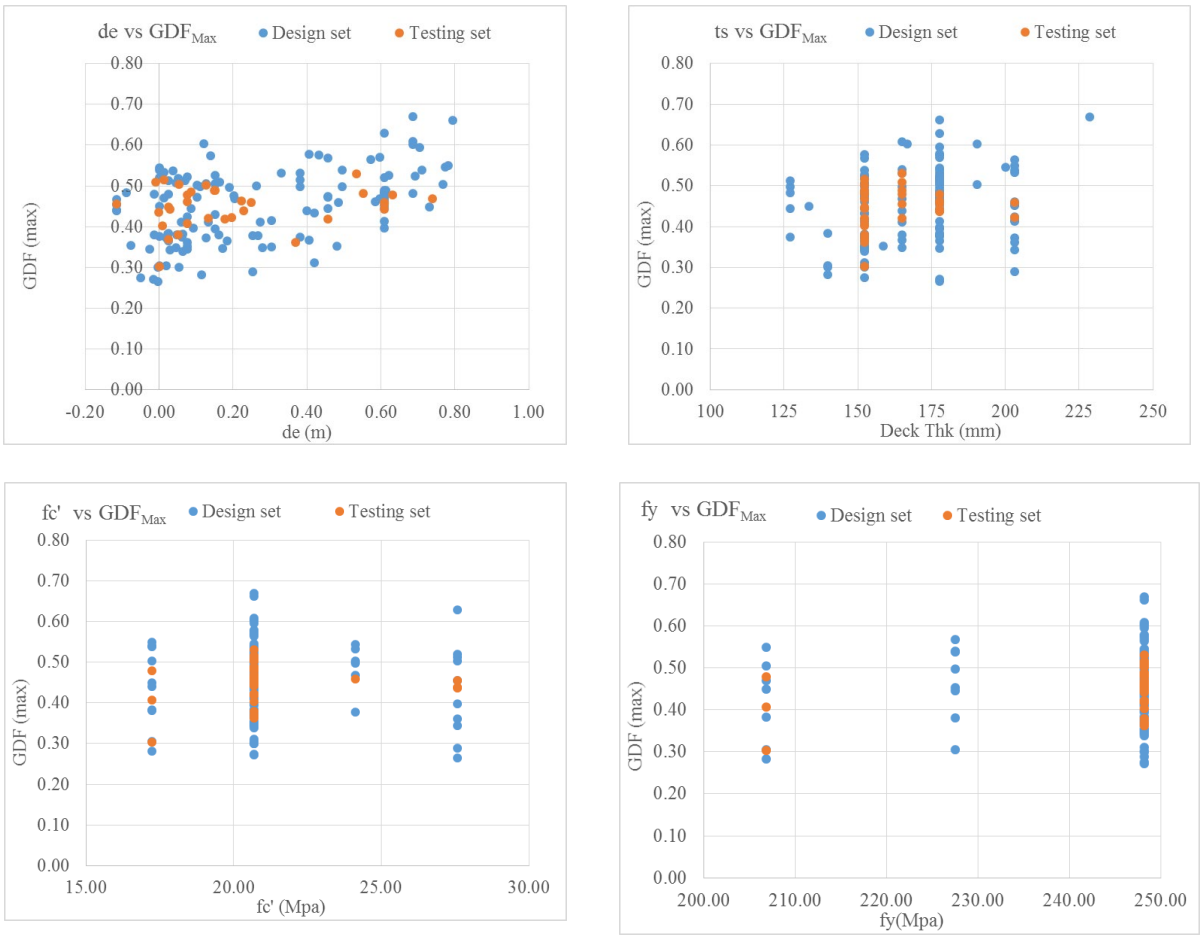

Figure 41. Moment GDFs vs. Governing Parameters for 130 Bridges in Design Set (continued)

Figure 42. Moment GDFs vs. Governing Parameters for 90 Bridges in Design Set

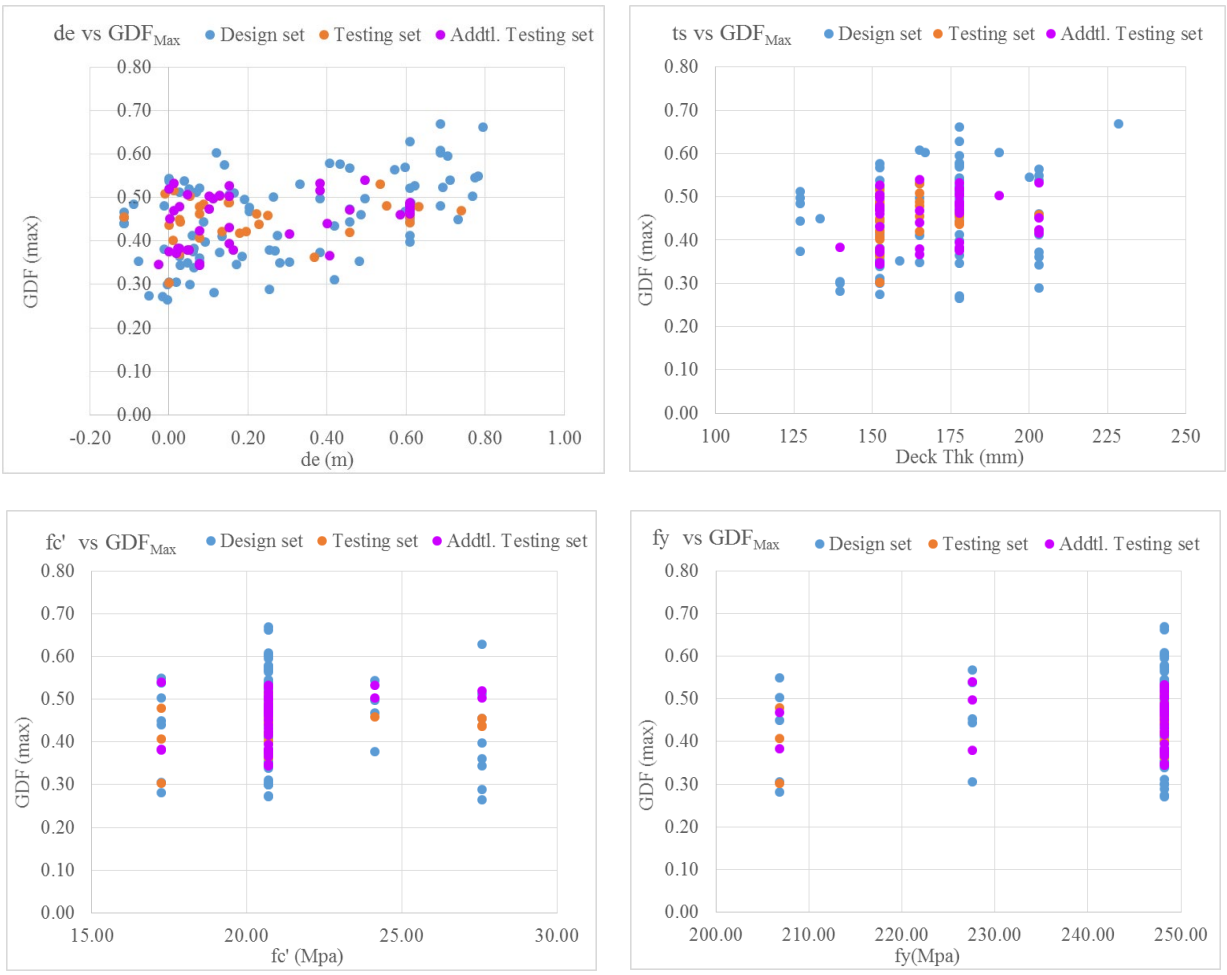

Figure 42. Moment GDFs vs. Governing Parameters for 90 Bridges in Design SetFigure 42. Moment GDFs vs. Governing Parameters for 90 Bridges in Design Set (continued)

6.3 Artificial Neural Network Optimization

The ANNs in this study were optimized with a similar scheme used by Sofi (2017). ANNs of the same design set size were configured and trained with combinations of the following parameters:

1) Training algorithm: ANNs were trained with either Bayesian-Regularization, BR, (MacKay 1992) or Levenberg-Marquardt, LM, (1963) backpropagation algorithms.

2) Number of hidden layers: 1 or 2 hidden layers

3) Number of nodes per hidden layer: 2-9 nodes per hidden layer

The same network architecture naming convention used by Sofi will be used herein. The four combinations are 10-m-1-BR, 10-m-m-1-BR, 10-m-1-LM, and 10-m-m-1-LM where the values read from left to right are the number of inputs (10 governing parameters), number of nodes in hidden layer (m), number of outputs (1 GDF prediction), and training algorithm (BR or LM). The number of nodes per hidden layer was varied between 2 and 10. ANNs with two hidden layers were configured to have the same quantity of nodes in both hidden layers.

ANNs were retrained 250 times with randomly initialized weights and biases. ANN performance was evaluated by mean square error (MSE). The formula for mean squared error is shown below in Eqn. 6, where *n* corresponds to a set of bridge inputs, *T* corresponds to the target value or the expected value of the ANN for a particular bridge (GDF from FEM post-processing), and *Y* is the ANN prediction for a bridge.

$$MSE = \frac{1}{n}\sum_{i}^{n}(T - Y)^2 \qquad \text{Eqn. 6}$$

The optimal ANN for each architecture minimized combined testing set MSE within the 250 ANN trials, where the combined testing set is comprised of the independent testing set and the 15% of the design set used for testing during ANN training. Figure 43 shows an example of how MSE can vary depending on the random initial weights and biases. Figure 44 and Figure 45 are examples of the ANN architecture optimization. The 130 bridge design set single best network that predicts moment GDFs is 10-5-5-1 BR with an average absolute error of 3.65% from independent testing. The single best network of the same for shear GDFs of the same

design set size is 10-3-3-1 BR and has an absolute error of 2.88%. The Appendix 10.1.3 has results for moment and shear neural network optimizations for all design set sizes tested.

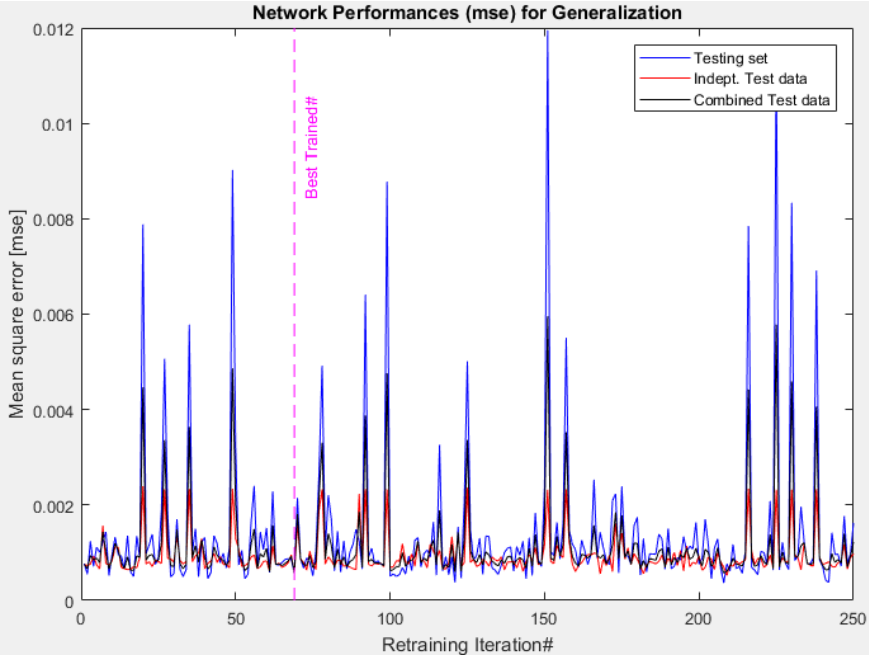

Figure 43. Moment 10-5-5-1 BR Best Network based on MSE of Combined Testing Set

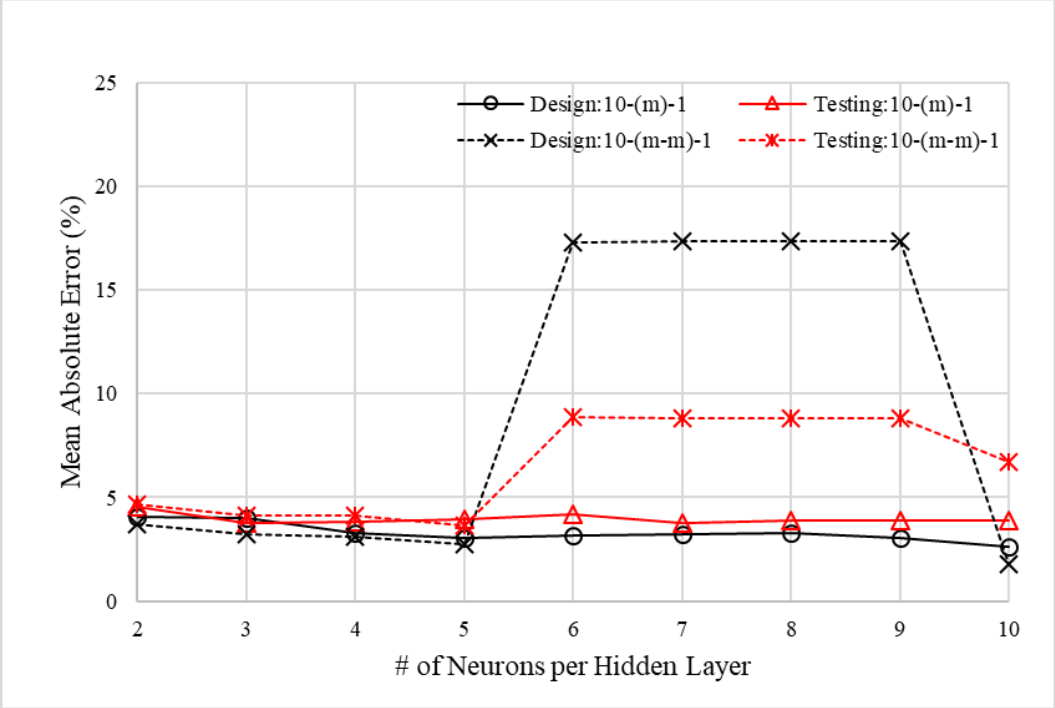

Figure 44. 130 Bridge Design Set Moment ANN Optimization for Bayesian-Regularization

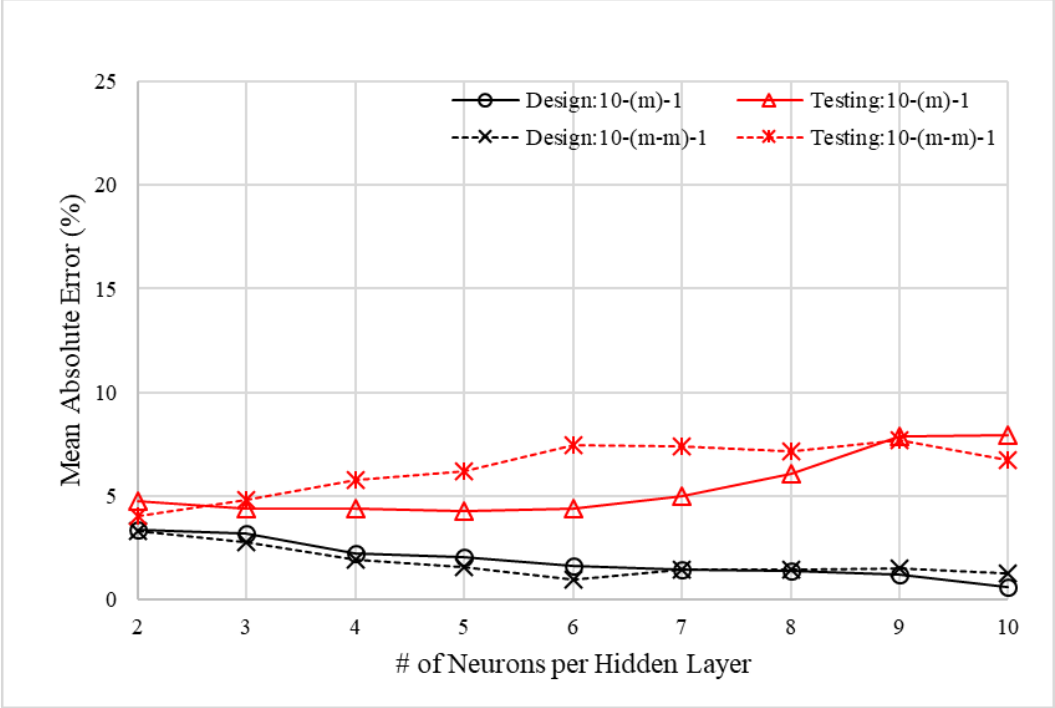

Figure 45. 130 Bridge Design Set Moment ANN Optimization for Levenberg-Marquardt

6.4 Effect of Sample Size

ANN architecture optimization was performed for ANN design sets of varying sizes to investigate ANN error with respect to varying design data sizes. The "best" ANNs for each design set size were defined to be those with the lowest independent testing error. Additional testing and independent testing errors were combined by using a weighted average formula shown in Eqn. 7. Subscripts "1" and "2" correspond to independent and additional testing set errors, respectively. The number of bridges in a testing set is designated by "n". Independent and combined testing errors are plotted for moment ANNs and shear ANNs in Figure 46 and Figure 47.

$$Combined\ Testing\ Error = \frac{Error_1 * n_1 + Error_2 * n_2}{n_1 + n_2} \quad \text{Eqn. 7}$$

As expected, the best-performing moment and shear ANNs were those with the largest number of training bridges. For the moment ANNs, the independent testing error is relatively insensitive to design set size. This is because the data points used for the testing set are within the envelope of the design set. However, the combined testing error increases as the number of training bridges decreases because as more bridges are removed from the training set, additional testing set bridges are increasingly likely to fall at an edge of the population where prediction accuracy begins to degrade. Interestingly, the independent and combined testing error are surprisingly low for an ANN trained using only 20 bridges.

Shear ANNs exhibit similar trends, though with generally higher error, and particularly high sensitivity at very low ANN design set size (sharp jump from 20 to 30 bridges in the design

set). The combined testing error is also higher than the independent testing error by a larger gap for shear than for moment ANNs for most design set sizes.

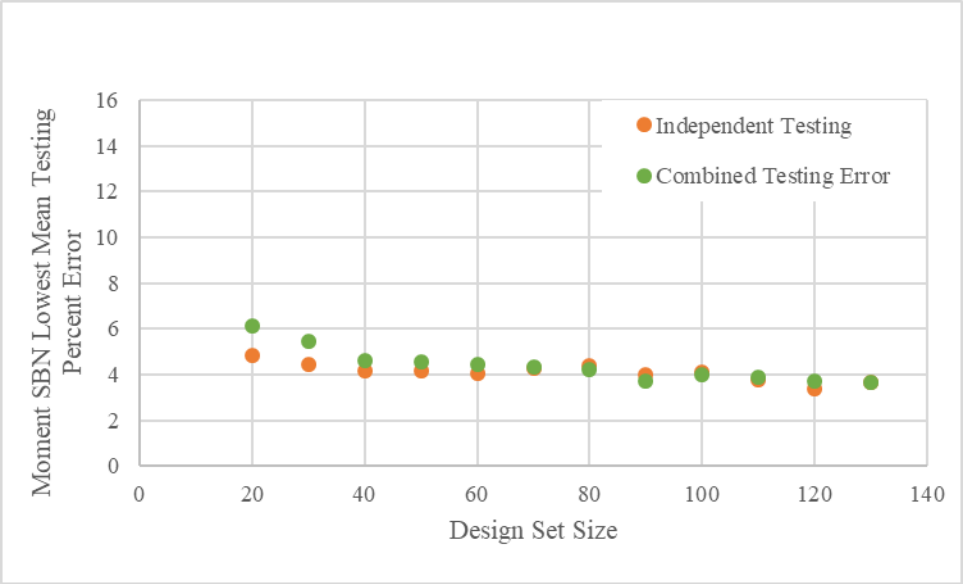

Figure 46. Lowest Mean Absolute Testing Error for Moment ANNs vs. Design Set Size

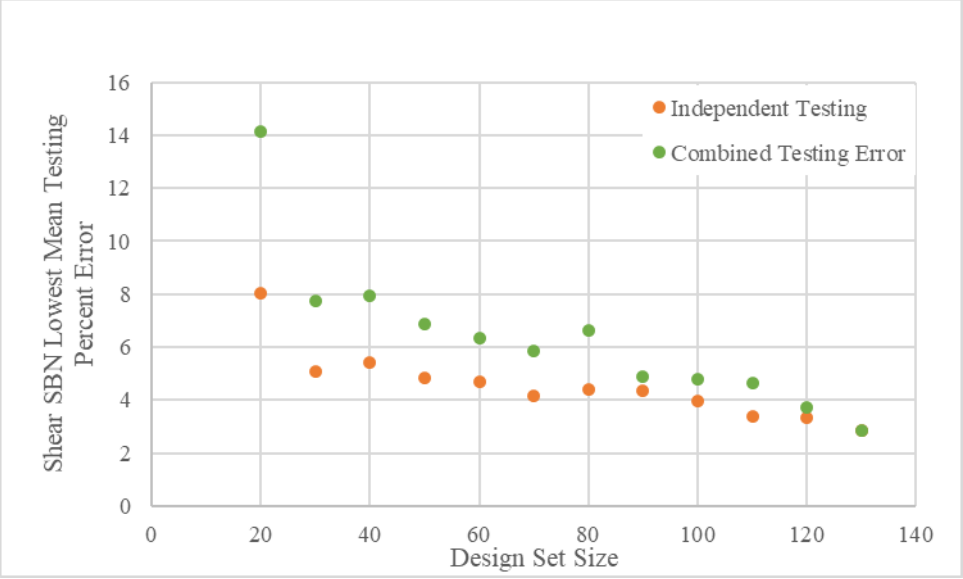

Figure 47. Lowest Mean Absolute Testing Error for Shear ANNs vs. Design Set Size

6.5 Contributions of Governing Parameters

10 governing parameters were used to train ANNs to predict girder distributions factors. Weights connect all of the inputs to all of the nodes in the first hidden layer and are taken as a value between -1 and 1. The weights between the inputs and the first hidden layer for the best moment ANN is shown below in Table 14. The matrix is a 5 by 10 matrix. The 5 corresponds to the best hidden network architecture (10-5-5-1) which has 5 nodes in the first hidden layer. The 10 corresponds to the governing parameters in the following order: length, girder spacing, longitudinal stiffness, cross-frame presence, number of girders, skew, barrier inner edge distance, deck thickness, concrete compressive strength, and steel yield strength.

Table 14. Weights between 10 Inputs and Nodes of 1st Hidden Layer

-0.792	0.309	0.227	-0.312	-0.284	-0.146	-0.106	0.079	-0.180	0.146
0.569	0.069	-0.131	-0.022	-0.353	0.247	-0.030	-0.371	0.246	-0.323
-0.098	-0.145	0.258	-0.029	0.516	0.048	1.014	-0.361	-0.137	0.063
-0.093	-0.368	0.224	-0.229	-0.042	-0.081	0.308	-0.389	-0.124	-0.248
-0.153	-0.351	0.055	-0.118	0.316	0.376	-0.086	-0.082	0.092	0.178

The columns of the weights shown in Table 14 correspond to the weights of the governing parameters. Weights that are close to 0 reflect an inconsequential parameter for the ANN. Each parameter's weight was averaged to examine the relative significance among the parameters with respect to the trained ANN. Table 15 presents the absolute values of arithmetic averages for each column in Table 14. Deck thickness and barrier inner edge distance are observed to have the highest absolute average influence, while concrete compressive stress, steel yield stress, and number of girders had the least absolute average influence. As expected, terms

relating to stiffness (generally depth and span) tend to be more influential than material properties when the objective is to determine girder distribution factors, rather than load ratings (as in Sofi's original study).

Table 15. Absolute Value of the Average Weight for Best Moment ANN

Governing Parameter	Absolute Value of the Average Weight
Deck Thickness	0.22
Barrier Inner Edge Distance	0.22
Presence of Cross Frames/Diaphragms	0.14
Longitudinal Stiffness	0.13
Length	0.11
Girder Spacing	0.10
Skew	0.09
Steel Yield Stress	0.04
Number of Girders	0.03
Concrete Compressive Stress	0.02

7 Reliability Calibration

7.1 Introduction

ANN prediction error introduces additional uncertainty into live loads, which must be integrated into load rating evaluations. Although ANN error is on average small, approximately 50% of rating factors will be unconservative if AASHTO LRFR partial safety factors are used without calibration. To mitigate potentially unconservative load ratings, a reliability calibration was performed to account for additional live load uncertainty from ANN error. The goal of these analyses was to produce an updated live load partial safety factor that corresponds with the same reliability index targeted in AASHTO LRFR. Reliability calibration methods are described in NCHRP Project 20-07, Task 186 (Kulicki et al. 2007), NCHRP Report 368 (Nowak 1999), NCHRP Report 454 (Moses 2001), and Nowak and Collins (2013). Two reliability determination methods described in literature were used in this study: First Order Reliability Method using Rackwitz-Fiessler and Monte Carlo Simulation. Distribution types, coefficient of variations, and dynamic amplification characterization are consistent with NCHRP Project 20-07, Task 186 (Kulicki et al. 2001). All uncertain parameters, including ANN-predicted GDFs, are assumed to be statistically independent.

7.2 Reliability Determination and Calibration Methodology

The objective of this study was to calibrate reliability to reflect ANN prediction uncertainty. However, the suite of bridges in the study reflected a wide range of engineering designers, who could exercise varying levels of diligence and conservativism. Additionally, older bridges were often designed to unknown standards. Such structures may have been designed for lower loads and using either more conservative or liberal practice methodologies. To avoid these

potential sources of bias across the population, baseline reliability indices for each bridge in the study were calculated using FEM live load demands.

The proposed theoretical reliability calibration procedure progresses through two Stages, as summarized in Table 16. The Baseline Stage, which will be indicated in equations with a 0 subscript, represents current AASHTO LRFD/R calibration in the Bridge Design Specifications (2015) and Manual for Bridge Evaluation (2013). The only modification from routine load rating is the use of detailed modeling to determine static live load effects. The load rating factor is therefore generally higher than routine load rating.

When the live load demand is determined from ANN predictions, rather than detailed modeling, the nominal and mean static live loads are nearly identical to those from Baseline detailed modeling. However, the ANN-based live load is more uncertain because of prediction errors. The Updated Stage, which will be indicated in equations with a 1 subscript, produces a load rating factor reflecting an increased live load factor to accommodate additional uncertainty introduced by ANN prediction error.

Table 16. Nomenclature of Live Load, Live Load Partial Safety Factors, and Rating Factors

		L	γ	RF
Stage	Baseline	FEA static live load effect with typical AASHTO live load COV	Unadjusted AASHTO LRFR	Corresponds to FEA live load and unadjusted AASHTO LRFR γ
	Updated	ANN static live load effect with increased COV from ANN uncertainty	Increased for live load, unchanged for other terms	Reduced from Baseline to account for additional LL uncertainty.

7.2.1 AASHTO LRFR Strength I Calibration Format

The general form of the governing AASHTO strength-based limit state function, g, is written below in Eqn. 8:

$$g(R, DC, DW, L) = R - DC - DW - L = 0 \quad \text{Eqn. 8}$$

Where R represents resistance, DC represents dead load from components (e.g., girders, deck), DW represents dead load from a wearing surface, and L represents the effect of traffic live load. Each term represents an uncertain quantity characterized by probabilistic parameters, such as mean and standard deviation, or related terms such as nominal values, biases, and coefficients of variation. Nominal values will be indicated with a subscript *n*. Additionally, AASHTO considers dynamic amplification as an integral component of live load traffic demand on bridge structures. In the following methodology, static and dynamic live loads will be indicated with *st* and *dyn* subscripts, respectively.

A probabilistic limit state function can be characterized with deterministic values for each probabilistic parameter corresponding to the critical design condition (a unique point in hyperdimensional space) along the limit state surface, referred to as the design point:

$$g = x_R{}^* - x_{DC}{}^* - x_{DW}{}^* - x_{L,dyn}{}^* = 0 \quad \text{Eqn. 9}$$

In Eqn. 9, the terms are marked with "*" to indicate that the terms are deterministic values at the design point, rather that uncertain probabilistic terms as in Eqn. 8. A convenient form of the resulting equation at the design point represents parameters mean values, μ, scaled by partial safety factors, γ, as shown in Eqn. 10:

$$g = \gamma_{R,0}\mu_R - \gamma_{DC,0}\mu_{DC} - \gamma_{DW,0}\mu_{DW} - \gamma_{L,0}\mu_{L,dyn,0} = 0 \quad \text{Eqn. 10}$$

Design codes typically implement a format in terms of nominal values, rather than mean values. For example, specified compressive strength of concrete, f'_c, is a nominal value. The actual strength of concrete supplied to job sites will vary from batch to batch, even when supplied by the same manufacturer and using the same raw materials, because of tolerances in measurements and inherent variabilities such as aggregate particle sizes, mixing proportions, heterogeneous distributions of constituent materials, and curing conditions. Actual supplied concrete strength is likely to be higher than the nominal specified value, so the mean-to-nominal concrete strength is expected to be greater than one. The discrepancy between mean and nominal values for each term is incorporated into reliability calibrations through a bias factor, λ, as shown in Eqn. 11 for a general parameter probabilistic parameter X:

$$\mu_X = \lambda_X X_n \quad \text{Eqn. 11}$$

Substituting bias and nominal values for mean values, the governing limit state characterized at the design point becomes:

$$g = \gamma_{R,0}\lambda_R R_n - \gamma_{DC,0}\lambda_{DC} DC_n - \gamma_{DW,0}\lambda_{DW} DW_n - \gamma_{L,0}\lambda_L L_{n,dyn,0} = 0 \quad \text{Eqn. 12}$$

According to NCHRP 20-07 / 186 (Kulicki et al. 2007), AASHTO LRFD has been calibrated based on an assumption that the probabilistic mean live load dynamic amplification

effect relative to static load is 10%. However, the deterministic AASHTO design and evaluation format has been calibrated such that 33% is typically applied to the truck load (lane load is not amplified). Partitioning nominal dynamic live load into nominal static live load and a dynamic amplification factor:

$$x_L{}^* = \gamma_{L,0}\mu_{L,dyn,0} = \gamma_{L,0}\mu_I\mu_{L,st,0} = \ where\ \mu_I = 1.1 \qquad \text{Eqn. 13}$$

The AASHTO LRFD calibration effectively introduces a supplemental bias for dynamic amplification complementary to the general live load bias, $\lambda_{L,dyn}$. The AASHTO code live load amplification is represented below as I_{AASHTO}:

$$x_L{}^* = \gamma_{L,0}\left[\lambda_{L,dyn}L_{n,st,0}\mu_I\right]\frac{(1+I_{AASHTO})}{(1+I_{AASHTO})} \qquad \text{Eqn. 14}$$

Defining the supplemental AASHTO LRFD live load amplification calibration bias as:

$$\lambda_I = \frac{\mu_I}{(1+I_{AASHTO})} \qquad \text{Eqn. 15}$$

Eqn. 14 can be rearranged to a format similar to that found in AASHTO LRFD:

$$x_L{}^* = [\gamma_{L,0}\lambda_{L,st}\lambda_I][L_{n,st,0}(1+I_{AASHTO})] \qquad \text{Eqn. 16}$$

In Eqn. 16, the multiplicative product of terms in the first set of square brackets represent the live load factor adopted in AASHTO LRFD.

The nominal live load term represents an induced load effect in a structural element, and is therefore influenced not only by vehicle weight traveling across a bridge, but also by analysis method. Static traffic gravity load is proportioned to individual girders similar to the approximate analysis method available in AASHTO, using girder distribution factors (GDFs). In the present study, analysis is performed either using detailed FEMs (Baseline, 0), or by substituting ANN-predicted GDFs (Updated, 1). For the Baseline stage:

$$L_{n,st,0} = L_{HL-93} GDF_0 \quad \text{Eqn. 17}$$

For design with LRFD, live load is specified, and a required resistance is calculated that will provide acceptable minimum reliability. For bridge load rating evaluations with LRFR, capacity is known, and the objective is to determine the scaled value of live load that can safely be carried. Multiplying the nominal live load by a scaling factor, RF, theoretically configures the rating evaluation to represent a target reliability.

$$x_L{}^* = [\gamma_{L,0}\lambda_{L,st}\lambda_I][L_{HL-93} GDF_0 RF_0(1 + I_{AASHTO})] \quad \text{Eqn. 18}$$

$$\gamma_L^n = [\gamma_{L,0}\lambda_{L,st}\lambda_I] \quad \text{Eqn. 19}$$

$$Nominal\ Live\ Load\ Term = [L_{HL-93} GDF_0 RF_0(1 + I_{AASHTO})] \quad \text{Eqn. 20}$$

7.2.2 Determining β with the Modified Rackwitz-Fiessler Method

The Rackwitz-Fiessler method was implemented as described in Nowak and Collins (2013). The first step to evaluate bridge reliability for strength is to quantify probabilistic characteristics for live load, dead load, and resistance. The stastistical parameters used in this study are shown in Table 17, which were taken from NCHRP Project 20-07 / 186 (Kulicki et al. 2007). These values correspond to a 75-year bridge design life. Live load uncertainties are associated with the load vehicle (weight, axle spacing, etc.), number of lanes loaded, and dynamic load amplification.

Table 17. Assumed Statistical Parameters

Case	Bias	COV	Distribution
Component Dead Load	1.05	0.1	Normal
Wearing Dead Load	1.00	0.25	Normal
Live Load	1.18	0.18	Normal
Resistance	1.12	0.1	Lognormal

The COV for live load correlates to dynamic live load (static plus dynamic amplification). Dynamic live load amplification was assumed equal to 10% of the static live load, consistent with Kulicki et al (2007). The method to account for probabilistic versus code-based dynamic impact was discussed in the preceding section. The limit state equation is shown below in Eqn. 21. Inclusion of the RF term should result in reasonably uniform reliabilities across the study population. RF values were determined for each bridge using the LRFR method. The anticipated reliability index for the limit state with the inclusion of RF is therefore approximately 2.5.

$$g(R, DC, DW, L) = \mathrm{R} - \mathrm{DC} - \mathrm{DW} - RF_0 * L_{dyn,0} = 0 \quad \text{Eqn. 21}$$

Next, initial design points (x_i^*) are determined. Mean values are used as a starting point for all parameters except live load (Eqns. 22 – 25). The live load initial design point is constrained to coincide with the limit state failure surface (Eqn. 26).

$$g = x_R^* - x_{DC}^* - x_{DW}^* - x_L^* = 0 \quad \text{Eqn. 22}$$

$$x_R^* = \mu_R = \lambda_R * R_n \quad \text{Eqn. 23}$$

$$x_{DC}{}^{*} = \mu_{DC} = \lambda_{DC} * DC_n \quad \text{Eqn. 24}$$

$$x_{DW}{}^{*} = \mu_{DW} = \lambda_{DW} * DW_n \quad \text{Eqn. 25}$$

$$x_{L}{}^{*} = x_{R}{}^{*} - x_{DC}{}^{*} - x_{DW}{}^{*} \quad \text{Eqn. 26}$$

The mean live load, including the rating factor as noted previously, is:

$$\mu_L = \lambda_L RF_0 L_{dyn,0} = \lambda_L RF_0 L_{n,st,0} \mu_I \quad \text{Eqn. 27}$$

Eqns. 28 and 29 convert non-normal random distributions (i.e., lognormal resistance) to equivalent normal distributions at the design point, where Φ and ϕ represent the standard normal cumulative distribution function (CDF) and probability density function (PDF).

$$\sigma_X{}^{e} = \frac{1}{f_X(x_i{}^{*})} \phi[\Phi^{-1}(F_X(x_i{}^{*}))] \quad \text{Eqn. 28}$$

$$\mu_X{}^{e} = x_i{}^{*} - \sigma_X{}^{e}[\Phi^{-1}(F_X(x_i{}^{*}))] \quad \text{Eqn. 29}$$

The limit state function with normalized distributions is next written in terms of reduced variates, $z_i{}^{*}$, as shown in Eqns. 30 and 31. A column vector, $\{G\}$, is then determined by calculating and compiling partial derivatives of the limit state function, as shown in Eqns. 32 and 33.

$$z_i{}^{*} = \frac{x_i{}^{*} - \mu_i}{\sigma_i} \quad \text{Eqn. 30}$$

$$g = \mu_{R,O}{}^{e} + z_R{}^{*}\sigma_R{}^{e} - (\mu_{DC} + z_{DC}{}^{*}\sigma_{DC}) - (\mu_{DW} + z_{DW}{}^{*}\sigma_{DW}) - (\mu_L + z_L{}^{*}\sigma_L) = 0 \quad \text{Eqn. 31}$$

$$\{G\} = \begin{pmatrix} G_1 \\ G_2 \\ \vdots \\ G_n \end{pmatrix}, \text{ where } G_i = -\frac{\partial g}{\partial Z_i} | \{z_i{}^{*}\} \quad \text{Eqn. 32}$$

$$\{G\} = \begin{pmatrix} -\sigma_R{}^{e} \\ \sigma_{DC} \\ RF_0\sigma_{DW} \\ \sigma_L \end{pmatrix} \quad \text{Eqn. 33}$$

Next, α and β can be estimated based on the sensitivy factors, $\{G\}$.

$$\beta = \frac{\{G\}^T * \{z^*\}}{\sqrt{\{G\}^T * \{G\}}} \quad \text{Eqn. 34}$$

$$where\ \{z^*\} = \begin{pmatrix} {z_1}^* \\ {z_2}^* \\ \vdots \\ {z_n}^* \end{pmatrix} \quad \text{Eqn. 35}$$

$$\alpha = \frac{\{G\}}{\sqrt{\{G\}^T\{G\}}} \quad \text{Eqn. 36}$$

Lastly, the design point in reduced variates is updated using α and β and converted back to original coordinates, according to Eqns. 37 – 39. The design point is updated and iterated until β converges to a minimum value.

$${z_i}^* = \alpha_i \beta \quad \text{Eqn. 37}$$

$${x_i}^* = {\mu_{x_i}}^e + {z_i}^* {\sigma_{x_i}}^e \quad \text{Eqn. 38}$$

$${x_L}^* = {x_R}^* - {x_{DC}}^* - {x_{DW}}^* \quad \text{Eqn. 39}$$

7.2.3 Determining β with Monte Carlo Simulation

Monte Carlo Simulation (MCS) was performed to validate the results of the modified Rackwitz-Fiessler Method. MCS is performed by generating an arbitrarily large number of sample points for each random variables according to their respective probabilistic distributions. The limit state equation was evaluated by substituting the randomly generated parameter values, and the probability of failure was determined by counting the number of instances in which the limit state equation was violated (i.e., total dead and live load exceeded capacity) and dividing the number of failure outcomes by total trials. Finally, the reliability index, β, was determined by taking the negative inverse of the standard normal cumulative distribution function evaluated at the sampled failure probability. Eqns. 40 – 43 illustrate the procedure. Sample sizes were

increased until the probability of failure converged. Ultimately, a total of one million samples was used for reported MCS results to reliably capture a probability of failure approximately 0.62% (corresponding to an Operating level reliability index of 2.5).

$$g(R, DC, DW, L) = \mathrm{R} - \mathrm{DC} - \mathrm{DW} - \left(L = RF_0 * L_{0,dyn}\right) = 0 \quad \text{Eqn. 40}$$

$$if\ g_i < 0, Failure\ is\ Recorded \quad \text{Eqn. 41}$$

$$Prob.of\ Failure = \frac{Sum\ of\ Failures\ Recorded}{Number\ of\ Limit\ State\ Scenarios} \quad \text{Eqn. 42}$$

$$\beta = \Phi^{-1}(Prob.of\ Failure) \quad \text{Eqn. 43}$$

7.2.4 Study Population Baseline Reliability

Both the modified Rackwitz-Fiessler and Monte Carlo procedures were performed for all bridges in the inventory. When an Operating rating factor was used in the two procedures with an impact factor of 33%, the resulting reliabilities were found to be very close to the target reliability associated to operating capacities (2.5). The modified Rackwitz-Fiessler method resulted an average β of 2.51, while Monte Carlo produced an average β of 2.53. Histograms of β values from the two methods are shown below in Figures 48 and 49 for moment and shear, respectively, confirming excellent agreement between the two methods. The maximum difference between reliability indexes for a given bridge is less than 1%.

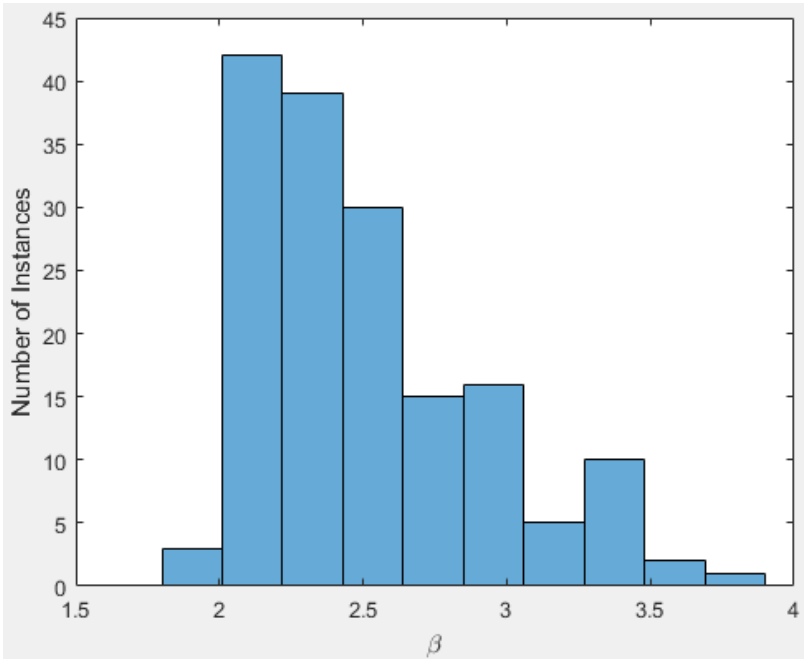

(a)

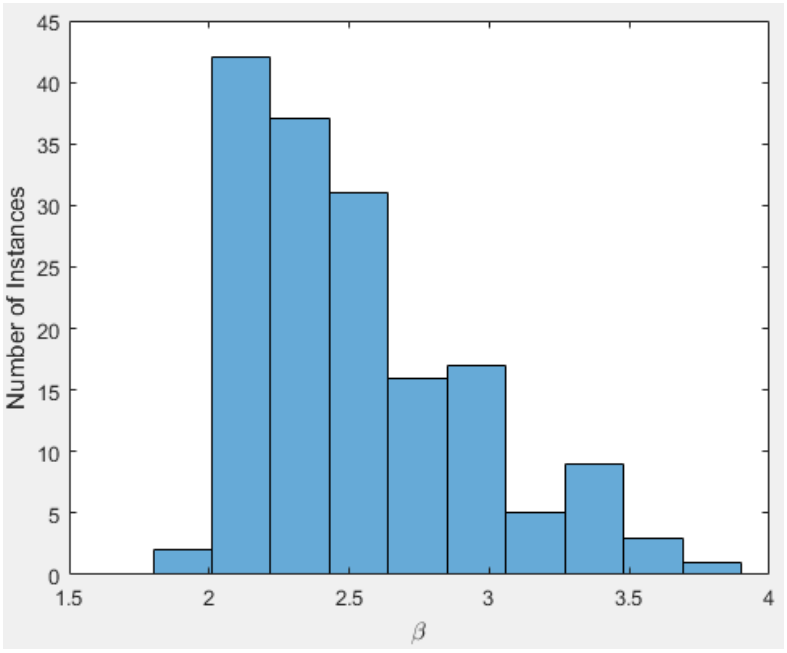

(b)

Figure 48. Histograms of β from FEM Moment reliability analyses using (a) modified Rackwitz-Fiessler Method and (b) Monte Carlo Simulation.

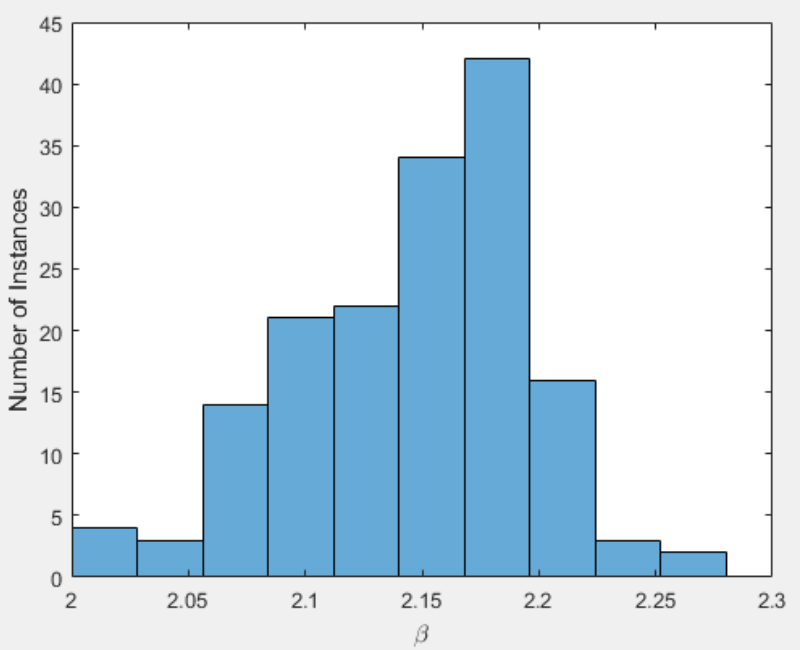

(a)

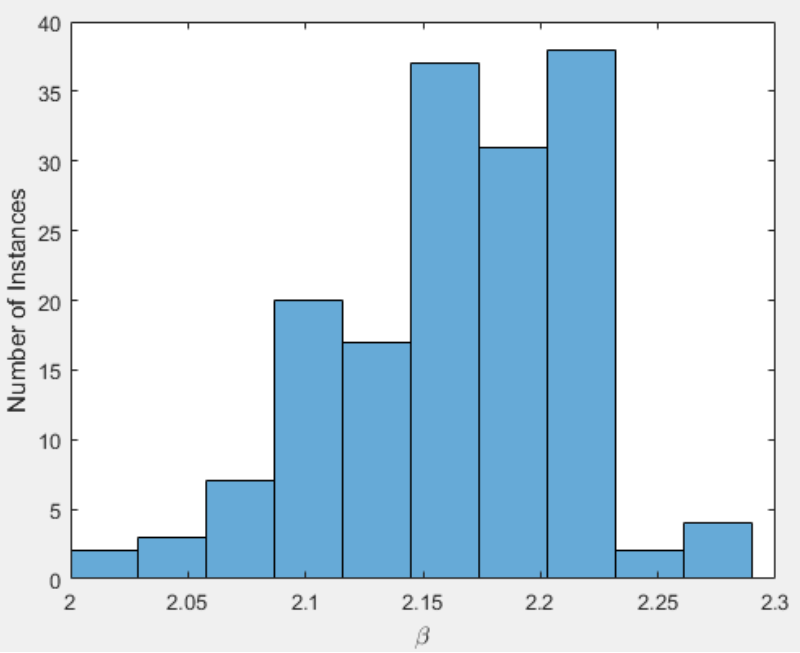

(b)

Figure 49. Histograms of β from FEM Shear reliability analyses using (a) modified Rackwitz-Fiessler Method and (b) Monte Carlo Simulation

7.3 Live Load Statistical Parameters Including Additional ANN Uncertainty

If live load GDFs are determined from ANNs rather than mechanistic models, additional live load uncertainty must be incorporated to account for ANN prediction errors. A numerical method was used to explicitly reflect prediction bias. First, a random normal distribution that corresponds to the live load model was created. For simplicity, a mean of 1 was used. A COV of 18% was used to create an initial distribution, consistent with AASHTO LRFD/R dynamic live load variation. This distribution will be referred to as the original distribution, herein.

In the following step, the ANN uncertainties are used to generate a new random distribution that reflects ANN tendencies. ANN error appears to be roughly normal. The single best moment ANN produced a mean GDF ratio of 1.0 (as expected for a well-trained network) with a standard deviation of 5.70% based on independent testing. Since the live load random variable corresponds to the product of the ANN-produced GDF and the dynamic load effect, the expected mean is the product of the ANN prediction error and the mean of the original distribution. Likewise, the new distribution error will be the product of the ANN standard deviation and the mean of the original distribution. It should be noted that $\mu_{Combined}$ is only used to derive $\sigma_{Combined}$.

$$Error_{ANN,Cal} = \frac{GDF_{FEM}}{GDF_{ANN}} \quad \text{Eqn. 44}$$

$$\mu_{Combined} = \left(Average\ Error_{ANN,Cal}\right) * \mu_{Original} \quad \text{Eqn. 45}$$

$$\sigma_{Combined} = \mu_{Combined} * \sigma_{ANN} \quad \text{Eqn. 46}$$

Finally, the new distribution can be used to find the new COV to use in the rest of the reliability procedure. The new distribution was created by scaling the original distribution by the expected ANN-percent error shown in Eqn. 45. Next, a new point was randomly generated around the updated point with the standard deviation calculated in Eqn. 46. Finally, the new distribution's statistical parameters are calculated. It is anticipated that the COV would be higher, since the live load distribution would be more spread out due to a higher standard deviation caused by ANN error. The new live load COV that accounts for the ANN error is 18.88%, which is higher than the 18% live load COV used to calibrate AASHTO. Figure 50 shows how the updated live load distribution is attenuated and more spread out, however, only slightly. Compared to uncertainties associated to the live load, ANN uncertainty barely adds additional uncertainty.

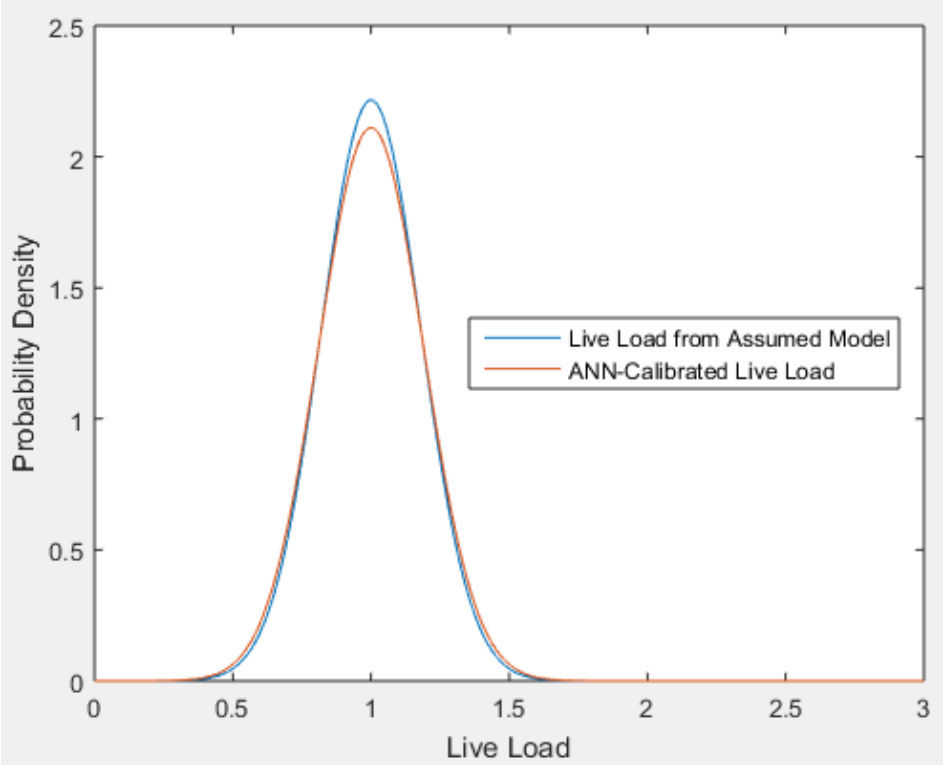

Figure 50. Comparison between Assumed and ANN-Updated Live Load Distributions

A commonly used equation used to combine uncorrelated random distributions is shown below in Eqn. 47 (Nowak and Collins 2013). If the mean values are equivalent, the equation can be rewritten in terms of COV, shown in Eqn 48. Since the updated live load COV was calculated using an assumed distribution used by Kulicki, the additional COV provided by the ANN can be estimated by using Eqn. 50, which is Eqn 49 rewritten.

The COV of the ANN, using Eqn. 50, was found to be 5.70%, which is nearly the standard deviation of the ANN of 5.71 when the mean live load is assumed to be 1. Discrepancies are believed to have been introduced by the fact that the true mean values of the ANN are changed slightly due to the average ANN error bias that is neglected in this calculation.

$$\sigma_{Combined} = \sqrt{{\sigma_1}^2 + {\sigma_2}^2} \quad \text{Eqn. 47}$$

$$COV = \frac{\mu}{\sigma} \quad \text{Eqn. 48}$$

$$COV_{Updated} = \sqrt{{COV_{Live\ Load}}^2 + {COV_{ANN}}^2} \quad \text{Eqn. 49}$$

$$COV_{ANN} = \sqrt{{COV_{Updated}}^2 - {COV_{Live\ Load}}^2} \quad \text{Eqn. 50}$$

Since the best shear ANN performed better than the moment ANN, the COV increase is smaller. The ANN-adjusted COV for the shear ANN was found to be 18.48%.

7.4 Partial Safety Factor Recalibrations

7.4.1 Calibration based on Modified Rackwitz-Fiessler Method

The next step is to update live load and load rating factors by recalibrating to maintain reliability with additional ANN prediction uncertainty. A “1” subscript is now used to indicate

that the reliability calibration reflects additional uncertainty associated with ANN-predicted GDFs.

$$g(R, DC, \mathrm{DW}, L) = 0 = \mathrm{R} - \mathrm{DC} - \mathrm{DW} - RF_1 L_{dyn,1} \quad \text{Eqn. 51}$$

$$g = x_R{}^* - x_{DC}{}^* - x_{DW}{}^* - x_L{}^* = 0 \quad \text{Eqn. 52}$$

The Rackwitz-Fiessler method was implemented similar to the Baseline Stage, except that the reliability index is a target and RF_1 is unknown. As in Stage 0, an initial trial design point was selected using mean values for all parameters except live load, and the live load design point value was calculated to intercept the limit state surface. Accordingly, the initial design point trial was:

$$x_R{}^* = \mu_R = \lambda_R * M_R \quad \text{Eqn. 53}$$

$$x_{DC}{}^* = \mu_{DC} = \lambda_{DC} * M_{DC} \quad \text{Eqn. 54}$$

$$x_{DW}{}^* = \mu_{DW} = \lambda_{DW} * M_{DW} \quad \text{Eqn. 55}$$

$$x_L{}^* = x_R{}^* - x_{DC}{}^* - x_{DW}{}^* \quad \text{Eqn. 56}$$

The mean live load is:

$$\mu_L = \lambda_L RF_1 L_{dyn,1} = \lambda_L RF_1 L_{n,st,1} \mu_I \quad \text{Eqn. 57}$$

$L_{n,st,1}$ differs from $L_{n,st,0}$ only in that the GDF is supplied by an ANN for the Updated (subscript 1) case versus FEMs for the Baseline (subscript 0) case. RF_1 was initially assumed equal to RF_0. Equivalent normal parameters were calculated for the lognormal resistance (recall Eqns. 28 and 29). The remainder of the procedure is the same as described previously to arrive at a converged reliability index and design point for a particular assumed RF_1 value (recall Eqns. 30 – 39).

After the first iteration, the target reliability is not met since the live load COV has increased from Baseline to Updated Stages. The mean live load term is updated for the next iteration by using the following set of equations. Since the uncertainty has increased, the mean live load value has to compensate by decreasing to maintain a consistent probability of failure and reliability index. A scalar, $\zeta_{reduction}$, was introduced to reduce the mean live load. $\zeta_{reduction}$ was incrementally reduced in successive iterations until the target reliability was reached.

$$\mu_L = \lambda_L[RF_1 = \zeta_{reduction} RF_0]L_{1,dyn} \quad \text{Eqn. 58}$$

$$if\ \beta < \beta_{target}, \zeta_{reduction,i+1} = \zeta_{reduction,i} - 0.001 \quad \text{Eqn. 59}$$

Finally, the reduction factor can be related to the updated live load partial safety factor as shown in the following equations. The limit state must be satisfied for Baseline and Updated cases, but the resistance and dead load terms are unchanged. The ratio of GDF_0 to GDF_1 can be neglected (taken as 1) because the ANN-predicted GDF is expected to be very similar to that predicted by FEMs.

$$g = \gamma_{R,0}\lambda_R R_n - \gamma_{DC,0}\lambda_{DC} DC_n - \gamma_{DW,0}\lambda_{DW} DW_n - \gamma_{L,0}\lambda_L L_{n,dyn,0} = 0 \quad \text{Eqn. 60}$$

$$g = \gamma_{R,0}\lambda_R R_n - \gamma_{DC,0}\lambda_{DC} DC_n - \gamma_{DW,0}\lambda_{DW} DW_n - \gamma_{L,1}\lambda_L L_{n,dyn,1} = 0 \quad \text{Eqn. 61}$$

$$\gamma_{L,0}\lambda_L L_{n,dyn,0} = \gamma_{L,1}\lambda_L L_{n,dyn,1} \quad \text{Eqn. 62}$$

$$[\gamma_{L,0}\lambda_{L,st}\lambda_I][L_{HL-93} GDF_0 RF_0(1 + I_{AASHTO})] = [\gamma_{L,1}\lambda_{L,st}\lambda_I][L_{HL-93} GDF_1 RF_1(1 + I_{AASHTO})] \quad \text{Eqn.63}$$

$$\gamma_{L,0} GDF_0 RF_0 = \gamma_{L,1} GDF_1 RF_1 \quad \text{Eqn. 64}$$

$$\gamma_{L,0} GDF_0 RF_0 = \gamma_{L,1} GDF_1 \zeta_{reduction} RF_0 \quad \text{Eqn. 65}$$

$$\gamma_{L,1} = \frac{\gamma_{L,0}}{\zeta_{reduction}}\left(\frac{GDF_0}{GDF_1} \approx 1\right) \quad \text{Eqn.66}$$

7.4.2 Calibration based on Monte Carlo Simulation

MCS was again used to validate the calibration results from the modified Rackwitz-Fiessler method. A similar approach was used to reduce the mean live load until the target reliability is met. The live load reduction factor is called $\xi_{reduction}$ in this section. The live load was successively reduced until the resulting probability of failure and reliability index satisfied the respective target values.

$$g(R, DC, DW, L) = \mathrm{R} - \mathrm{DC} - \mathrm{DW} - \xi_{reduction,n} * RF_0 * L_{,dyn} \quad \text{Eqn. 67}$$

$$if\ g_i < 0, Failure\ is\ Recorded \quad \text{Eqn. 68}$$

$$Prob.of\ Failure = \frac{Sum\ of\ Failures\ Recorded}{Number\ of\ Limit\ State\ Scenarios} \quad \text{Eqn. 69}$$

$$\beta = \Phi^{-1}(Prob.of\ Failure) \quad \text{Eqn. 70}$$

$$If\ \beta < \beta_{Target}, \quad \text{Eqn. 71}$$

$$repeat\ with\ \xi_{reduction,n+1} = \xi_{reduction,n} - 0.001$$

Finally, $\xi_{reduction,n}$was used to update the live load partial safety factor, similar to the procedure shown previously for the modified Rackwitz-Fiessler method.

$$\gamma_{L,1} = \frac{\gamma_{L,0}}{\xi_{reduction,n}} \quad \text{Eqn. 72}$$

7.5 Reliability Calibration Results

Reliability calibration was performed for all of the bridges that had moment and shear GDF predictions. The distribution of live load safety factors that correspond to operating rating capacities for the modified Rackwitz-Fiessler method and Monte Carlo simulation are shown

below in Figure 51 and Figure 53 for moment and shear, respectively. Several bridges have very high moment partial safety factors which was attributed to low original reliability indices, as observed for some cases when determining β with FEM predictions. Additionally, more than half of the bridges were found to have a moment β at or above the target reliability based on FEM live load distribution. Since the ANN live load uncertainty increased only slightly, many bridges did not require an increased live load partial safety factor. Their inherent surplus of reliability accommodated the increase in live load uncertainty without penalizing their load carrying capacity. However, since the shear analyses found lower reliabilities on average than the moment analyses, the shear live load partial safety factor is higher when this approach is used.

Since there is variation in the reliability of the bridges used in this study (recall Figures 48 and 49), an alternative method was chosen characterize the influence of ANN error uncertainty on live load factors for rating. The previously described procedures were repeated with both modified Rackwitz-Fiessler and MCS, targeting original reliability indices of each individual bridge instead of a uniform reliability. Targeting original reliabilities for each individual bridge isolated the influence of amplified live load uncertainty.

The calibrated live load factors obtained by targeting individual original reliabilities instead of a uniform target reliability are shown in Figure 52 and Figure 54 for moment and shear, respectively. In all of the reliability calibration analyses, modified Rackwitz-Fiessler and MCS produced similar results. As expected, the partial safety factors for both moment and shear decrease significantly. Based on this procedure, the maximum partial safety factor for moment and shear are 1.37 and 1.36, respectively. The shear partial safety factor is slightly lower than the

moment partial safety factor because ANN prediction error was smaller for shear than moment GDFs.

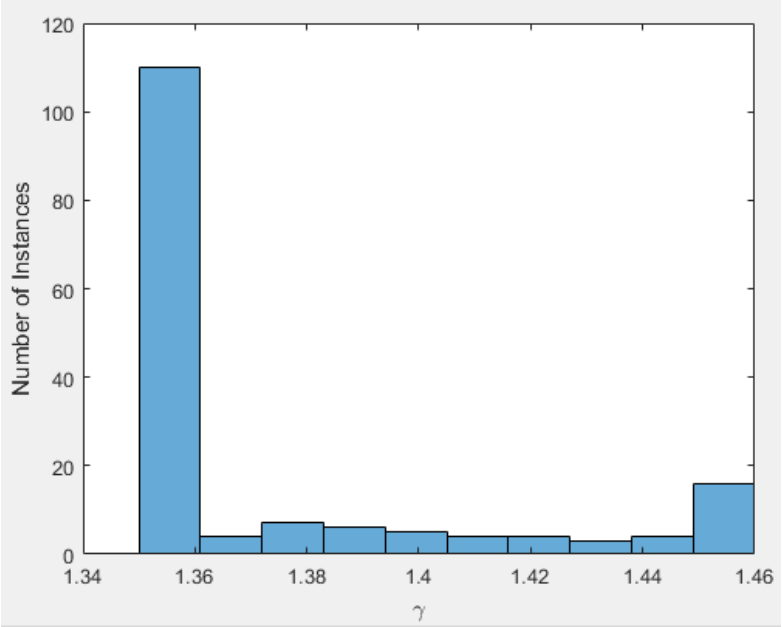

(a)

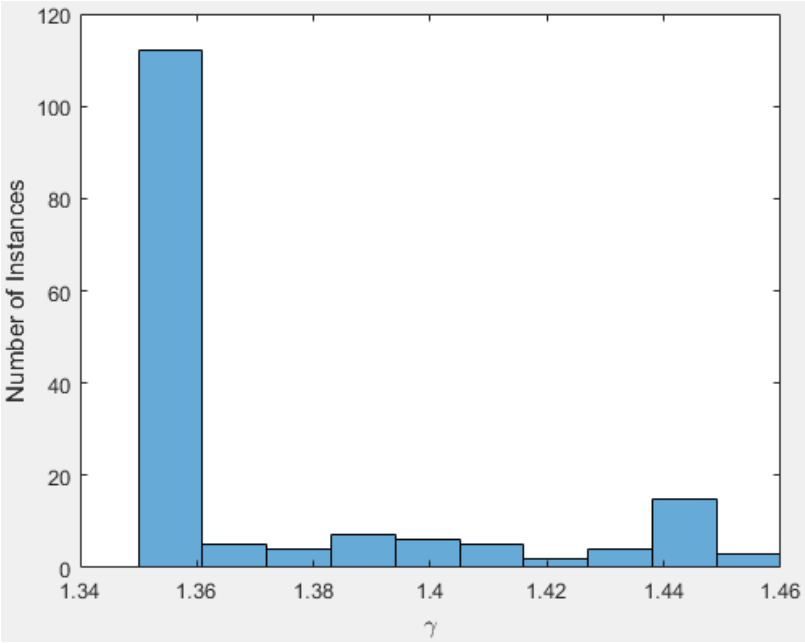

(b)

Figure 51. Calibrated Moment Partial Safety Factor based on a Uniform Target Reliability for (a) Modified Rackwitz-Fiessler Method and (b) Monte Carlo Sampling

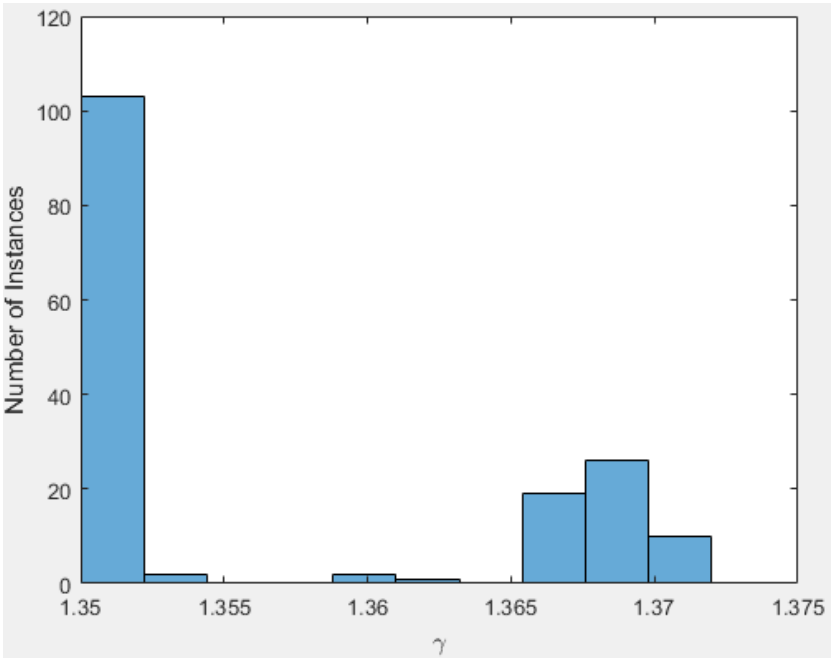

(a)

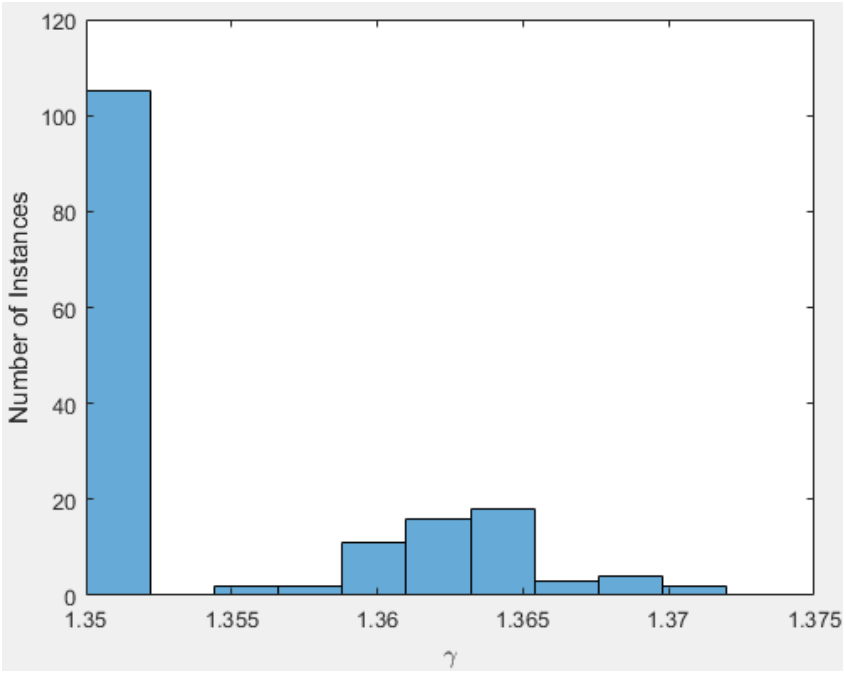

(b)

Figure 52. Calibrated Moment Partial Safety Factor based on FEM Reliability for (a) Modified Rackwitz-Fiessler Method and (b) Monte Carlo Sampling

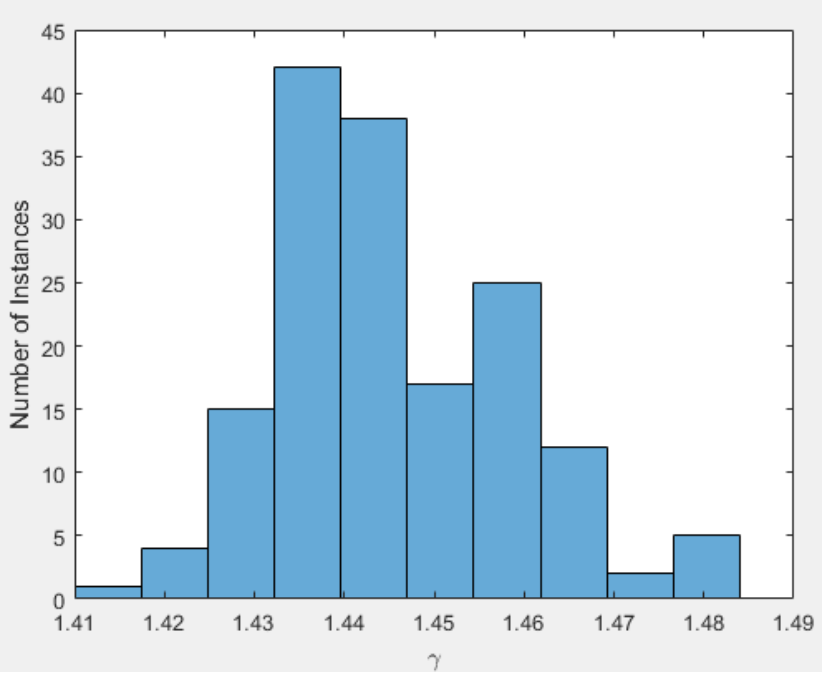

(a)

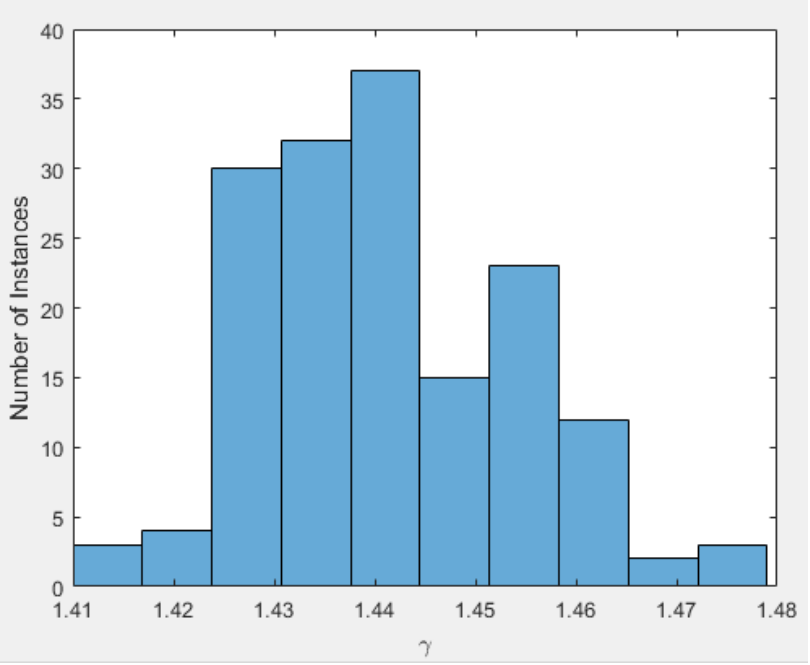

(b)

Figure 53. Calibrated Shear Partial Safety Factor based on a Uniform Target Reliability for (a) Modified Rackwitz-Fiessler Method and (b) Monte Carlo Sampling

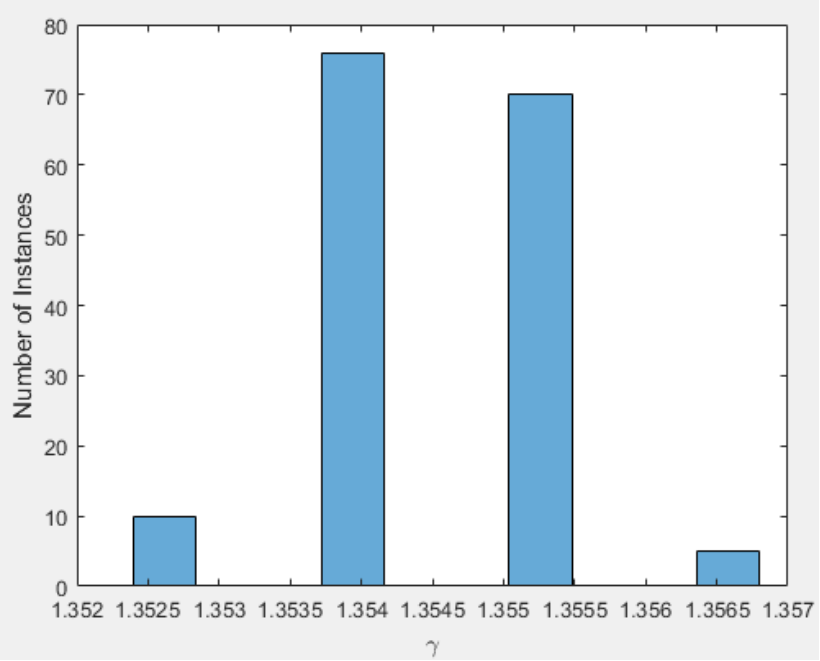

(a)

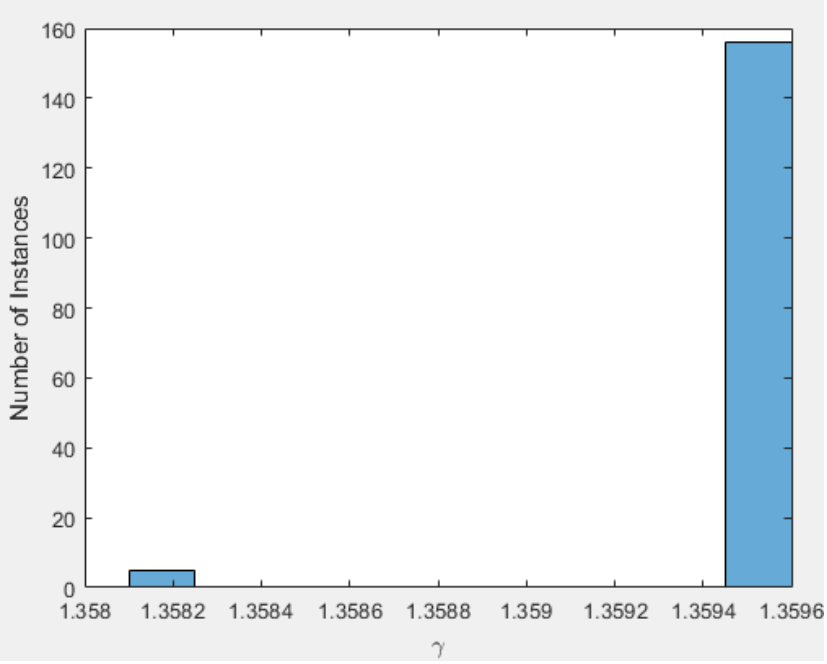

(b)

Figure 54. Calibrated Shear Partial Safety Factor based on FEM Reliability for (a) Modified Rackwitz-Fiessler Method and (b) Monte Carlo Sampling

8 Field Testing Case Study

8.1 Yutan Bridge

8.1.1 Introduction

Bridge C007805310P was identified as a preferred candidate for a diagnostic load test. The bridge has a span length, girder spacing, longitudinal stiffness, number of girders, skew, barrier distance, deck thickness, compressive strength of concrete, and yield strength of steel that are within the appropriate ANN applicability ranges. Additionally, the bridge is located and owned by nearby Saunders County. NDOT documentation indicated that this bridge should be posted, however, a field test was decided to likely be beneficial, suggested by higher ANN and FEM rating factors, and could warrant the removal of the load posting. Line girder analyses showed that this bridge has a noncomposite operating moment rating factor of 0.85.

Besides the potential removal of a load posting, this bridge was load tested to obtain an experimental load rating to compare to a finite element model (FEM) load rating and an ANN load rating. This load test is used to see how well the ANSYS model captures the live load distribution. After analyzing results from the load test, results and limitations from the first load test led NDOT the team to perform a retest on the bridge with instrumentation located on additional bridges.

Figure 55. Yutan Bridge

8.1.2 Instrumentation and Test Procedure for Test 1

Individual sensor dimensions provided by the manufacturer are shown in Figure 56. Sensors were installed near the abutments as well as at the center of the span to investigate both potential restraint and induced negative moments near supports, as well as anticipated critical positive moment.

The strain gauges were instrumented at girders 1-5 and girder 8 for the midspan and the South abutment. The same girders were instrumented for the North abutment with the exception of girder 8 due to safety concerns. For the instrumented girders, two strain gauges were installed at the bottom flange and one strain gauge was mounted on the web near the top flange. Two sensors were used at the bottom flange to investigate the potential presence of lateral bending. Additionally, girders 5 and 8 were instrumented to verify symmetric bridge behavior.

Strain gauges were placed about 6 inches to the South of the midspan because there is a diaphragm at the midspan. Instrumentation was placed near the abutments at about 8 inches from the ends. Instrumentation near the diaphragm at midspan is shown in Figure 57. The gauge near the North abutment for girder 4 and the gauge near the South abutment for girder 1 were placed about 12 inches from the abutments because there were small holes cut in the web at the typical instrumentation location.

Each strain gauge was installed along the longitudinal direction, in accordance to the BDI user manual. Strain gauge installation locations can be seen in Figure 58 and Figure 59. Individual strain gauges can be identified by unique ID numbers. The strain gauge IDs and locations are shown in the appendix.

The BDI software was tared to zero so that only live load strain is detected. The loading vehicle was driven across the bridge at a crawl speed to mitigate potential dynamic amplification effects. The vehicle was driven along three designated loading paths: critical loading for the exterior girder, critical loading for the interior girder, and along the bridge centerline to verify symmetric structural response to applied load. The vehicle was also driven along the three paths at the posted speed limit for the bridge to investigate dynamic amplification effects. A summary of the naming convention for the runs is shown in Table 18. Runs were done going in both directions to ensure that there are two sets of data that correspond to the same anticipated data. The outsides of the tire load paths were painted on the pavement so that the truck driver could easily tell where to drive. The load paths are shown in Figure 60 and the truck axle spacings are shown in Figure 61. Loads paths 1-3 correspond to center load placement, interior girder critical load location, and exterior girder critical load location, respectively.

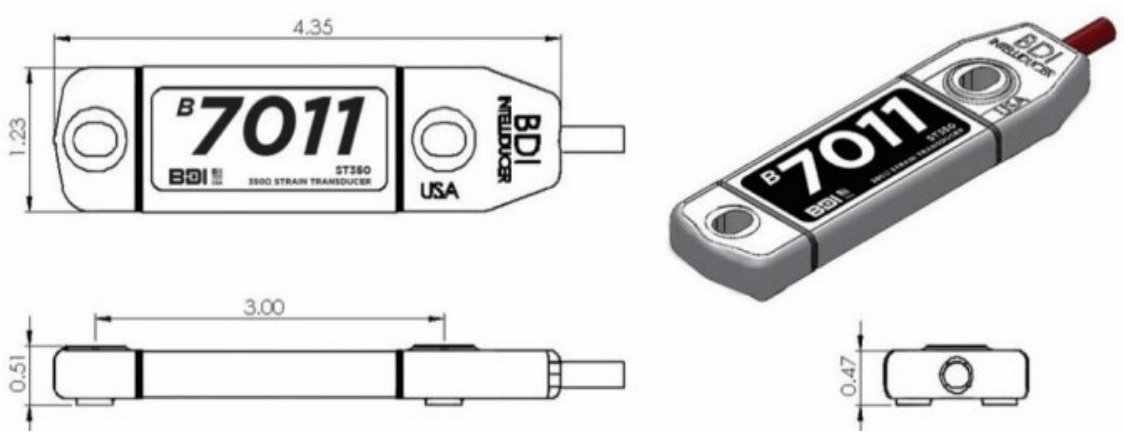

Figure 56. BDI Strain Transducer Dimensions in Inches

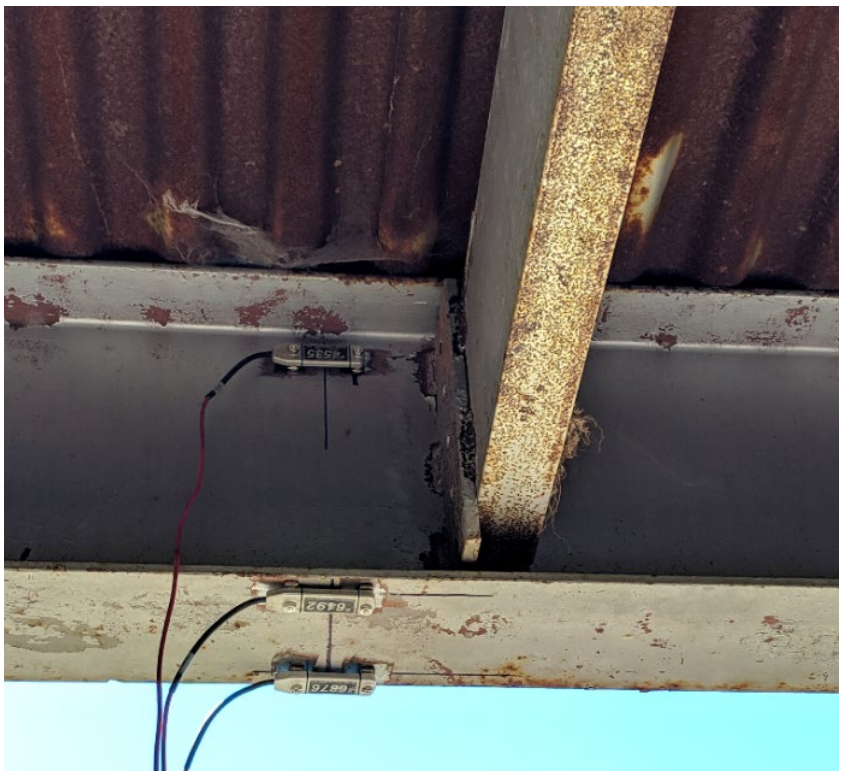

Figure 57. Instrumentation near Midspan for 1st Yutan Bridge Load Test

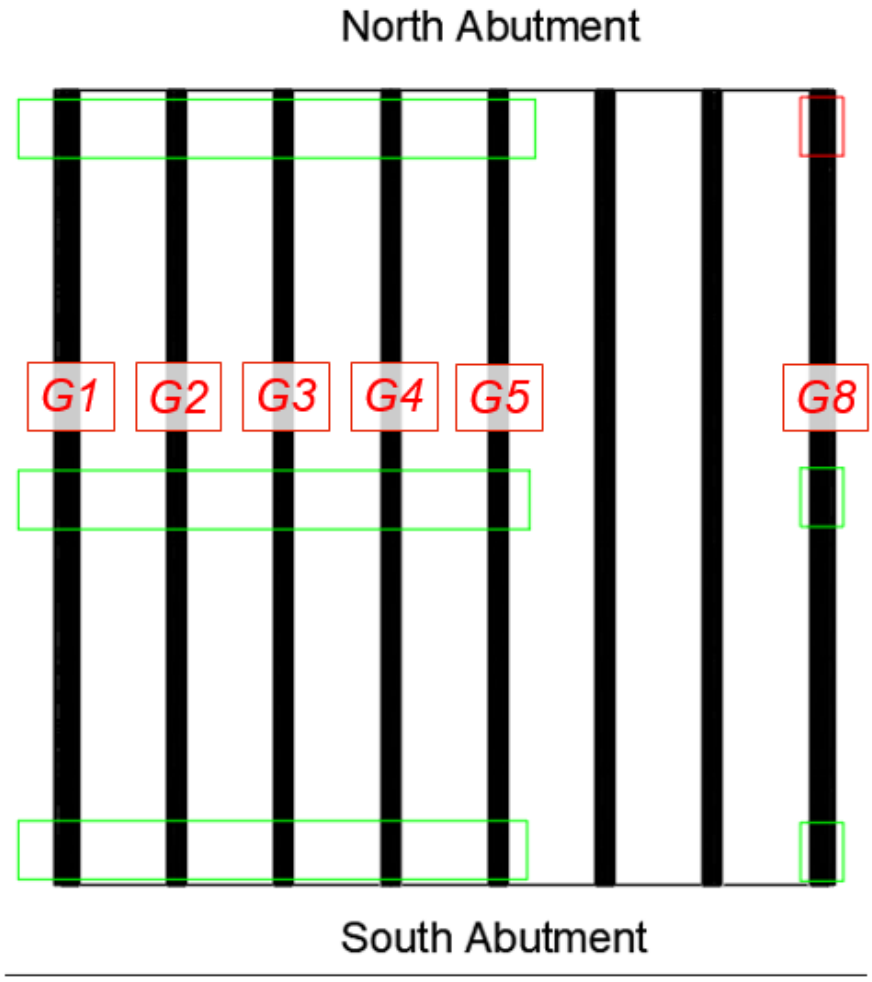

Figure 58. Plan View of Sensor Layout for 1st Yutan Bridge Load Test

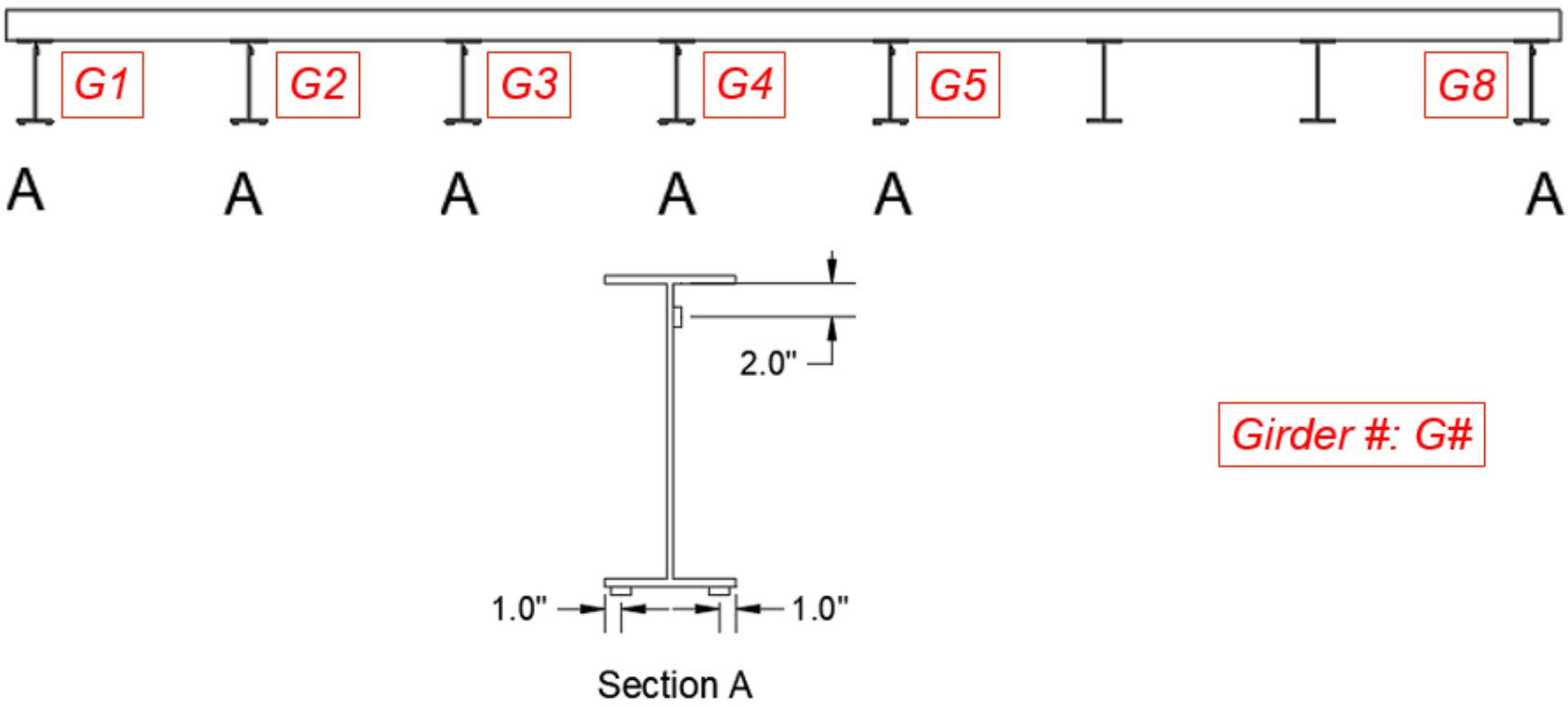

Figure 59. Cross-Section View of Sensor Layout (looking north) for 1st Yutan Bridge Load Test

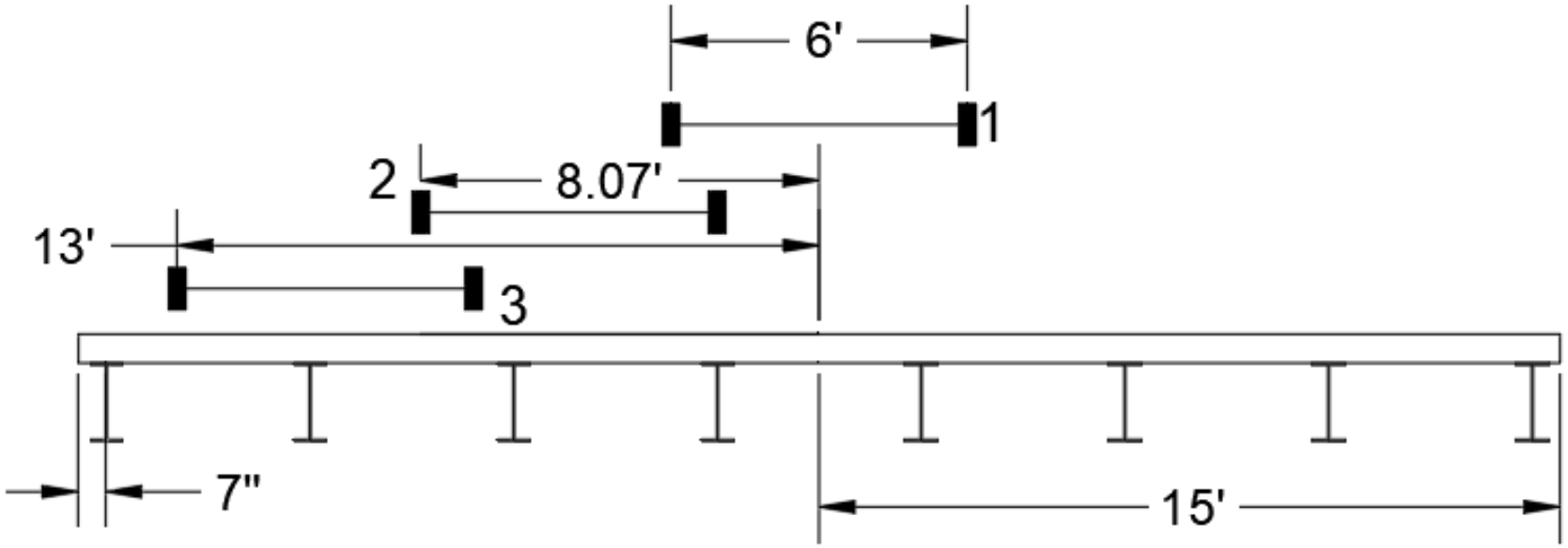

Figure 60. Load Test Plan for 1st Yutan Bridge Load Test

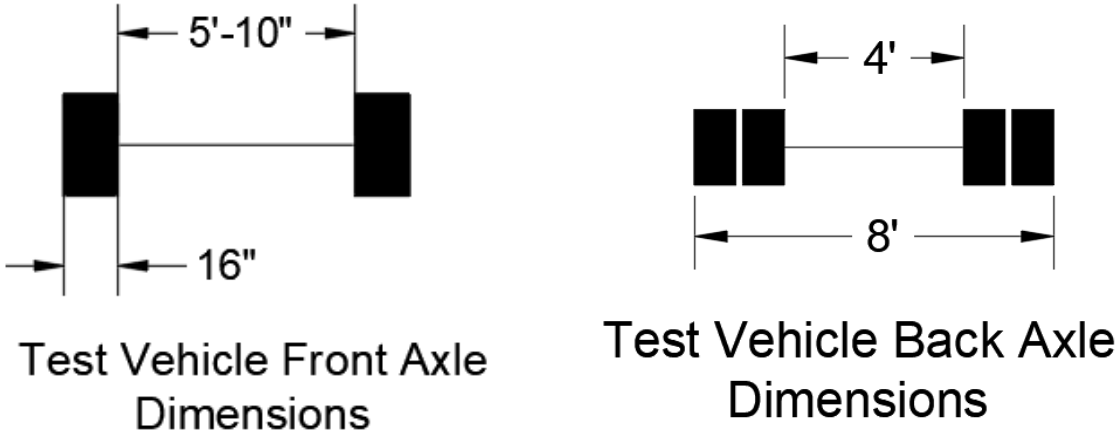

Figure 61. Load Test Vehicle Axle Dimensions for 1st Yutan Bridge Load Test

Table 18. Truck Runs for 1st Yutan Bridge Load Test

Run	Truck Position	Direction	Speed
1	1	N	Slow
2	1	S	Slow
3	1	N	Fast
4	1	S	Fast
5	2	N	Slow
6	2	S	Slow
7	2	N	Fast
8	2	S	Fast
9	3	N	Slow
10	3	S	Slow

8.1.3 Instrumentation and Test Procedure for Test 2

Instrumentation was modified for the second test so that behavior of all of the girders could be analyzed. Instrumentation was left off of girders 7 and 8, as shown in Figure 62, due to hazards introduced by wet conditions. Abutment instrumentation was moved more towards the midspan compared to the first test. Since little differential strain

measurements were picked up from the first load test, it was decided to instrument the bottom flanges with only one strain gauge, as shown in Figure 63. Since additional instrumentation was placed on the East side of the bridge, additional runs were performed over the now instrumented girders. Figure 64 outlines the designated load placements. Locations 1 and 5 correspond to exterior girder critical load placement, locations 2 and 4 correspond to interior girder critical load placement, and location 3 corresponds to geometrical center of load placement. Table 19 summarizes the nomenclature of the runs performed for the 2nd load test.

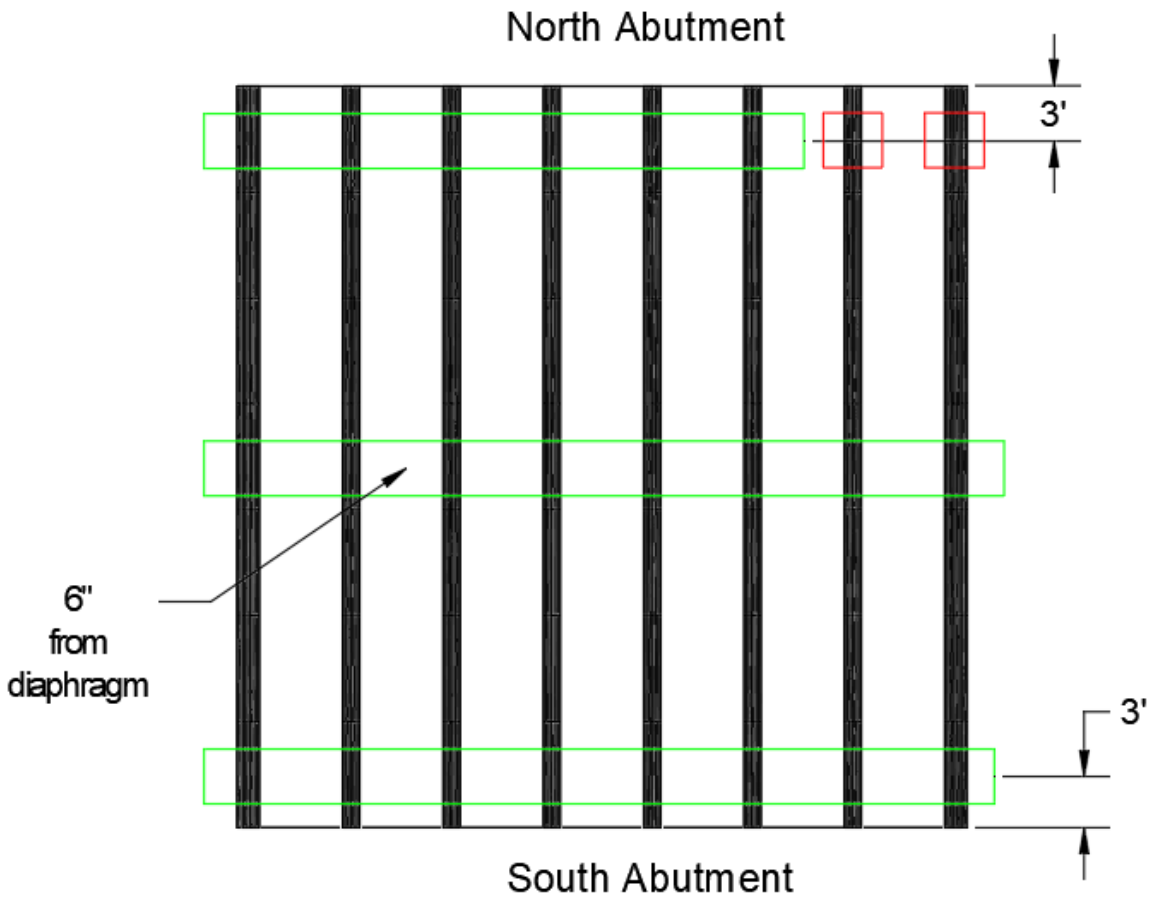

Figure 62. Plan View of Sensor Layout for 2nd Yutan Bridge Load Test

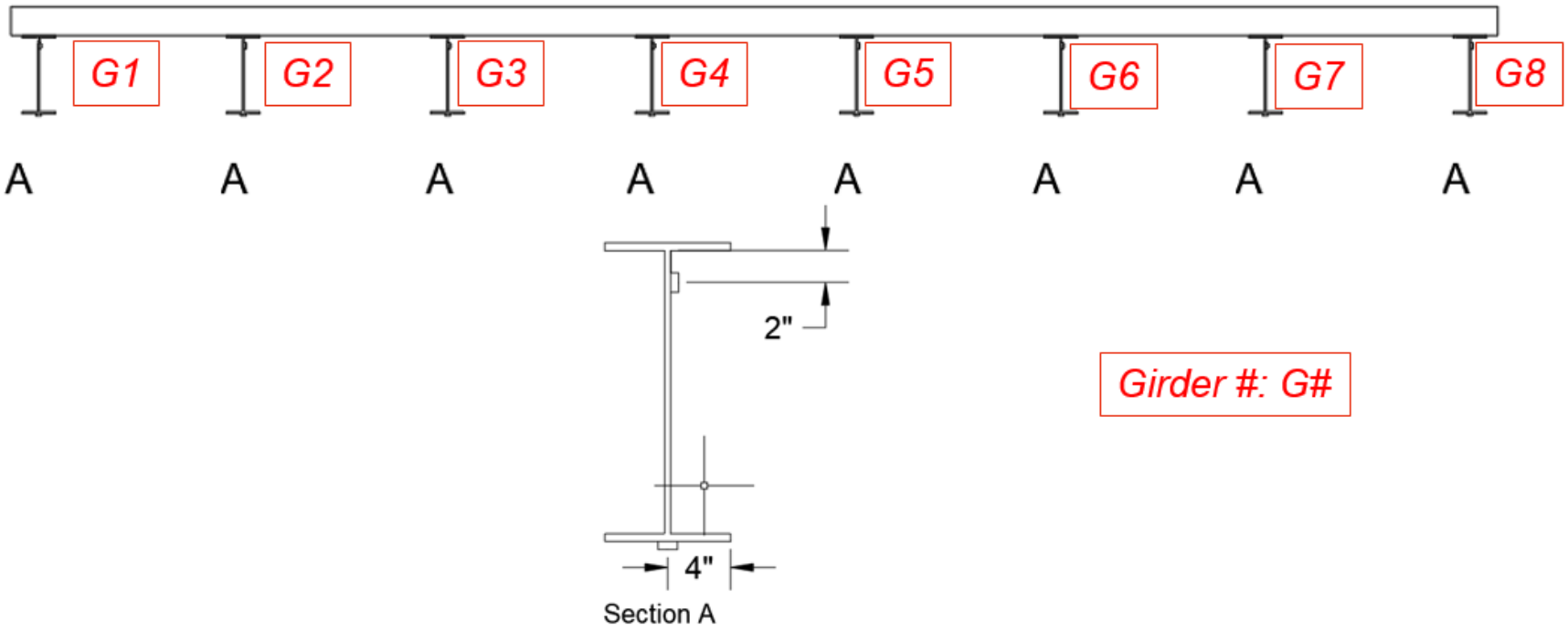

Figure 63. Cross-Section View of Sensor Layout (looking North) for 2nd Yutan Bridge Load Test

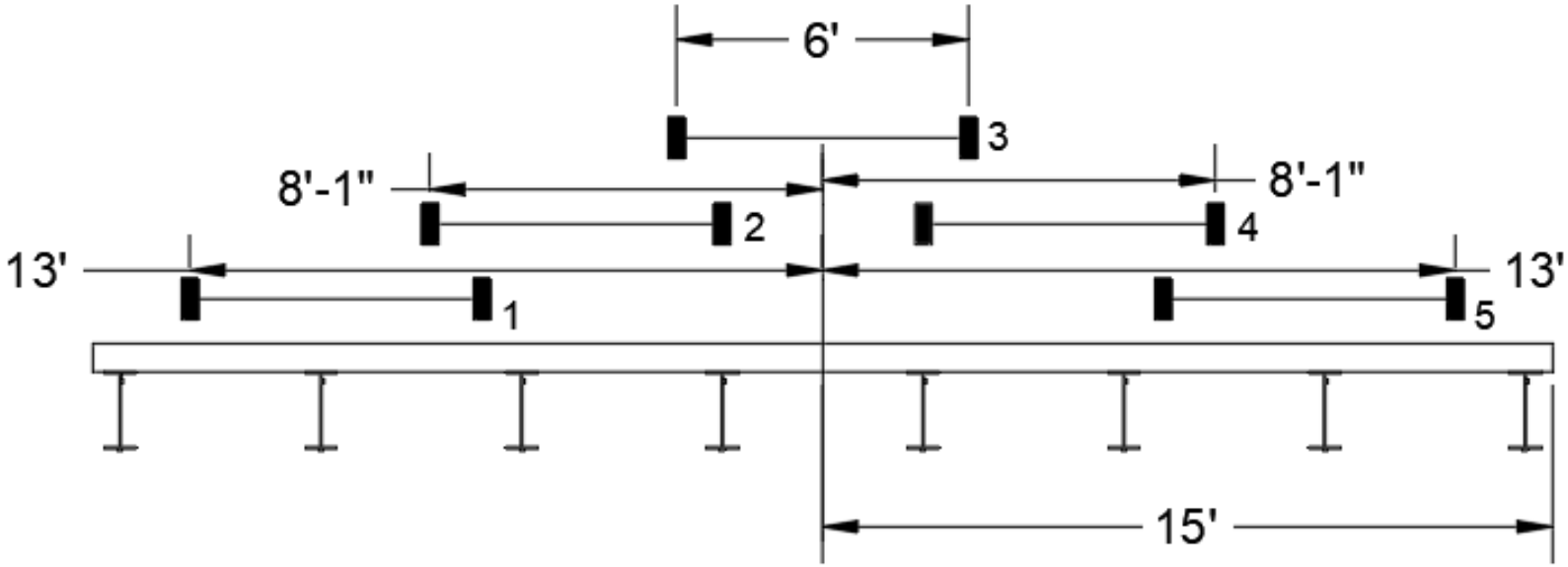

Figure 64. Load Test Plan for 2nd Yutan Bridge Load Test

Table 19. Truck Runs for 2nd Yutan Bridge Load Test

Run	Truck Position	Direction	Speed
1	1	N	Slow
2	1	S	Slow
3	2	N	Slow
4	2	S	Slow
5	2	N	Fast
6	2	S	Fast
7	3	N	Slow
8	3	S	Slow
9	3	N	Fast
10	3	S	Fast
11	4	N	Slow
12	4	S	Slow
13	4	N	Fast
14	4	S	Fast
15	5	N	Slow
16	5	S	Slow

8.1.4 Repeatability of Load Tests

Results of the first and second load test were verified with each other to ensure that consistent data was collected for both load tests. Midspan GDFs were determined by determining the ratio of each girder moment to the sum of all of the girder (1-8) bottom flange strains at midspan. This comparison was done for the load paths that run down the lane that corresponds to the interior critical load placement. As shown in Figure 65, both load tests show very close agreement to each other as expected.

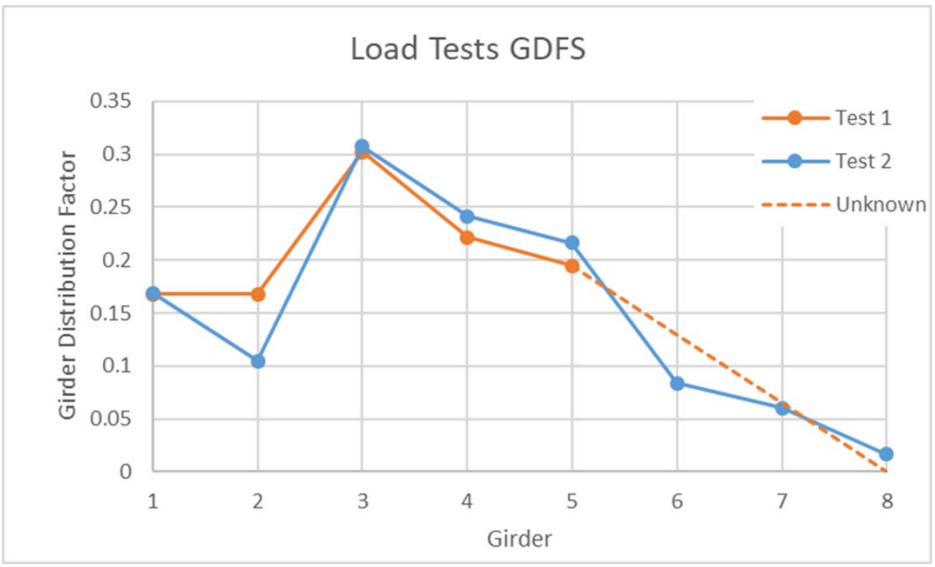

Figure 65. Moment GDF Comparison between Tests 1 and 2 for Load Path at Critical Load at Interior Girder

8.1.5 Unintended Composite Action and Reduced Dynamic Impact

The presence of composite behavior was determined by plotting the strain with respect to time. If a section acts noncompositely, the section would have no benefit from the concrete because there is no shear resistance at the steel and concrete interface. Theoretically, noncomposite sections have an elastic neutral axis, ENA, in the middle of the steel section given that the steel section is symmetric about the center horizontal axis. Since there were strain gauges at the bottom flange and near the top web, the absolute value of the strain measurements should be nearly identical. If the girder was being loaded in positive flexure, the bottom flange would undergo tension and the top flange would experience compression.

Tension and compression strain measurements are expressed as positive and negative microstrains (με), respectively, by the BDI testing system. Of the girders tested in the first load test, girder 2 appears to be noncomposite for all of the runs performed, as shown in Figure 66. A

composite section, shown in Figure 67, differs in the way that the top strain gauge have readings that are closer to zero. This is because the ENA for composite sections are shifted upwards in composite sections since the concrete is acting in compression.

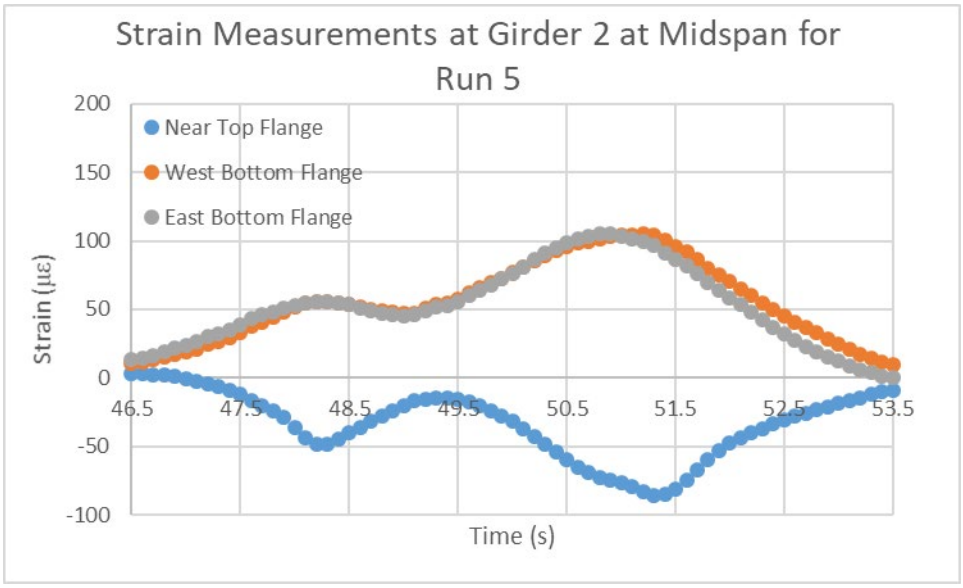

Figure 66. Noncomposite Strain Measurements

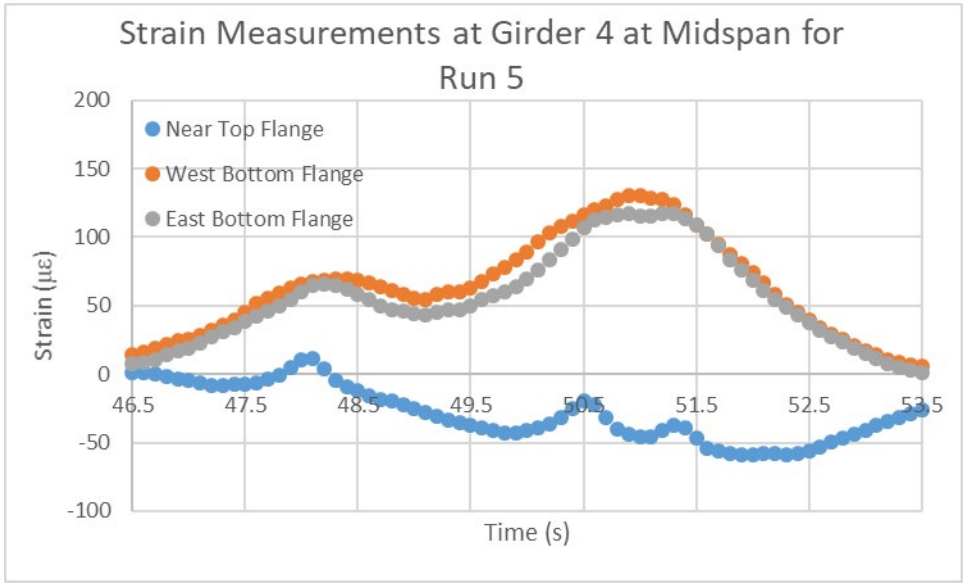

Figure 67. Composite Strain Measurements

The ENA location can be used to determine bridge characteristics such as degree of composite behavior. The expected ENA for a noncomposite and composite section of an interior girder are shown below in Figure 68. The ENA for the composite section is based on AASHTO short-term (n) section properties.

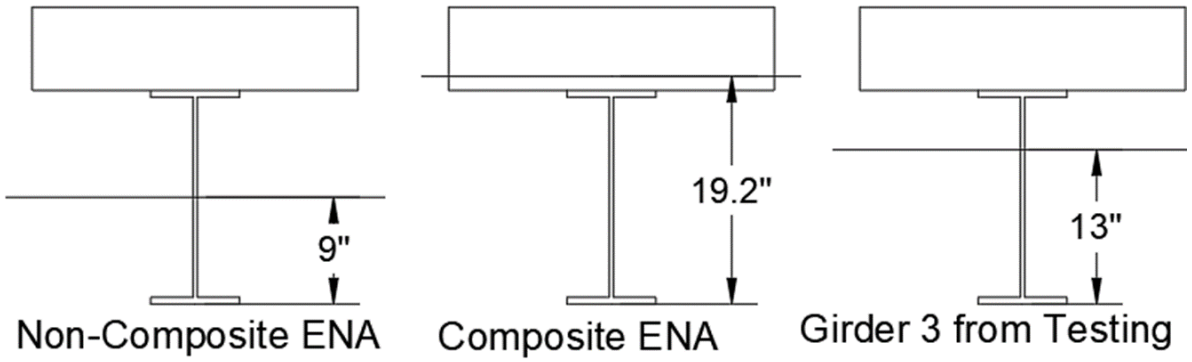

Figure 68. ENA Locations

ENA values for the midspan were determined in a way derived from assuming a linear strain variation across the entire steel section. This method, shown in Eqn. 73 and Eqn. 74, is consistent with the method used in by Jeffrey et al. (2009). The bottom flange strain, ε_{bottom} was taken as an average of the two bottom flange strains. First, the curvature, denoted as m, is determined by the dividing the difference in the strains divided by the distance between them. It should be noted, that Jeffrey et al. (2009) mention that elastic neutral value error can be introduced by the testing setup. For example, wheels that cross over instrumented girders can cause spikes in elastic neutral axis vs. time plots. Additionally, errors in relatively small strain measurements (< 20 με) can result in marginal errors in elastic neutral axis location.

$$m = \frac{\varepsilon_{top} - \varepsilon_{bottom}}{height\ of\ top\ strain\ gauge}\ [in^{-1}] \qquad \text{Eqn. 73}$$

$$y = \frac{-\varepsilon_{bottom}}{m} \ [in] \qquad \text{Eqn. 74}$$

All of the girders from test in the first load test (1-4 and 8) exhibited partial composite behavior, except for girder 2. The second load test revealed that girder 6 was also behaving noncompositely.

Comparisons between crawl speed and dynamic tests of all passes revealed a reduced dynamic amplification factor from those used in standard codes. It was revealed that the maximum amplification of strains was 3%.

8.1.6 Apparent Puddle Welds

It was assumed that this bridge has no shear connectors since it is rated by NDOT as noncomposite. After consulting the Saunders county engineer, it was determined that the county commonly used puddle welds to hold stay-in-place forms onto the steel while pouring concrete during bridge construction. However, construction drawings were unable to be retrieved from NDOT or Saunders County.

The apparent size of puddle welds was estimated in the following manner. First a simple beam model was created to approximate the shear and bending moment of the truck. The loading scenario and shear diagram are shown below in Figure 69 and

Figure 70. The maximum shear scenario corresponds to the back axle being directly over one of the supports. The truck was offset by one section depth and one AASHTO tire width to avoid strut behavior.

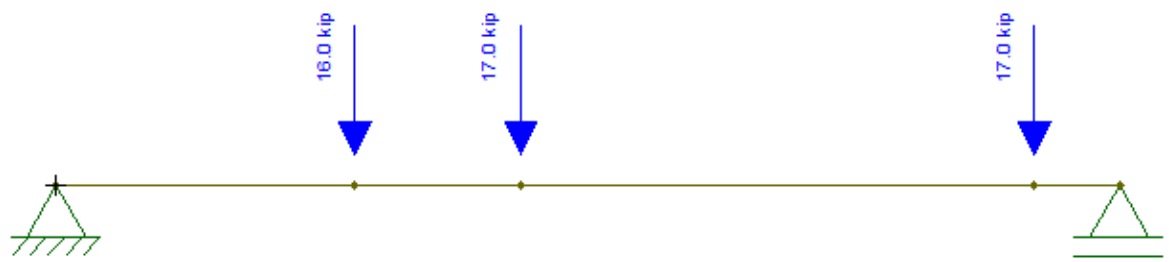

Figure 69. Critical Shear Loading

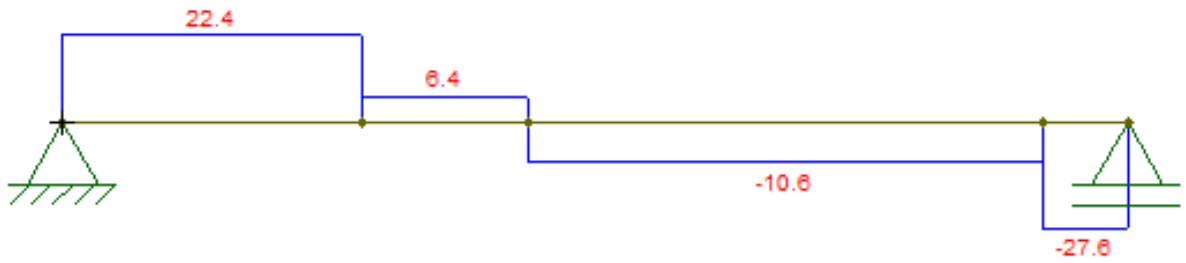

Figure 70. Shear Diagram (kips)

Next, the moment GDFs were used to calculate shear flow acting on the critical girder. The maximum moment GDF was approximated to be 0.29 from the second load test. This was approximated by taking the maximum moment divided by the sum of all of the girder moments. The transverse shear flow is given by Eqn. 75-77.

$$V_{girder} = GDF * V_{theoretical} \quad \text{Eqn. 75}$$

$$q = \frac{VQ}{I} \quad \text{Eqn. 76}$$

$$Q = A' * y_{bar} \quad \text{Eqn. 77}$$

Y_{bar} is the distance of the neutral axis of the composite section to the centroidal axis of the concrete. A' is taken as the product of the transformed width of the concrete and the concrete thickness including the rib concrete. Once q is found, the shear force at the interface, P, is calculated in Eqn. 78.

$$P = q * Puddle\ Weld\ Spacing \quad \text{Eqn. 78}$$

Once the shear force is determined, an AISC design guide (2017) was used to relate the interface shear force to the effective diameter, d_e, of the puddle weld, shown in Eqn. 79. This equation is simply the area of the puddle weld multiplied by the weld strength. However, the π factor was removed since a safety factor of three was used. The effective diameter of the puddle weld is related to the visible diameter, *d*, for a single sheet of steel decking with a thickness of, *t*.

$$P = \frac{{d_e}^2 F_{EXX}}{4} \quad \text{Eqn. 79}$$

$$d_e = \sqrt{\frac{P * F_{EXX}}{4}} \quad \text{Eqn. 80}$$

$$d_e = 0.7d - 1.5t \quad \text{Eqn. 81}$$

$$d = \frac{d_e + 1.5t}{0.7} \quad \text{Eqn. 82}$$

Figure 71 shows a diagram of the effective diameter and visible diameter parameters used in the previous equations.

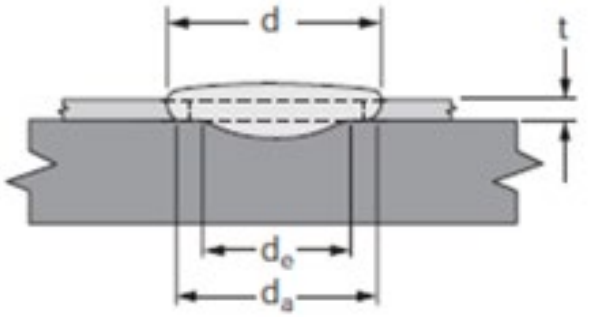

Figure 71. Puddle Weld Dimensions (from AISC Design Guide)

The minimum required puddle weld spacing to satisfy the AISC equations were computed. Since parameters such as the thickness of the corrugated steel decking and the puddle weld spacings are unknown, several possibilities are shown in Table 20 and Table 21. Furthermore, puddle weld spacings without the safety factor of three were computed. The significance of the puddle welds is that their behavior affects K_b which directly affects the experimental load rating. Since K_b is based on whether or not 1.33W can be safely transported, minimum spacings were computed for the legal load scaled up by 33%. Since girders 2 and 6 are interior girders that are closely aligned to the lane paths denoted by traffic lines, it may be that those girders had puddle welds that have deteriorated due to overloading.

Table 20. Puddle Weld Spacing based on Assumed Parameters for a Legal Load

	W											
Thickness of Sheet Metal (in)	0.02	0.02	0.02	0.02	0.04	0.04	0.04	0.04	0.06	0.06	0.06	0.06
F_{EXX} (ksi)	60	60	60	60	60	60	60	60	60	60	60	60
Puddle Weld Diameter	0.375	0.375	0.375	0.375	0.75	0.75	0.75	0.75	1	1	1	1
Required Puddle Weld Spacing with Safety Factor	Not Possible	Not Possible	Not Possible	Not Possible	Every Rib	Every Rib	Every Rib	Every Rib	Every 2nd Rib	Every 2nd Rib	Every 2nd Rib	Every 2nd Rib
Required Puddle Weld Spacing without Safety Factor	Not Possible	Not Possible	Not Possible	Not Possible	Every 3rd Rib	Every 3rd Rib	Every 3rd Rib	Every 3rd Rib	Every 6th Rib	Every 6th Rib	Every 6th Rib	Every 6th Rib

Table 21. Puddle Weld Spacing based on Assumed Parameters for 1.33 * Legal Load

	1.33W											
Thickness of Sheet Metal (in)	0.02	0.02	0.02	0.02	0.04	0.04	0.04	0.04	0.06	0.06	0.06	0.06
F_{EXX} (ksi)	60	60	60	60	60	60	60	60	60	60	60	60
Puddle Weld Diameter	0.375	0.375	0.375	0.375	0.75	0.75	0.75	0.75	1	1	1	1
Required Puddle Weld Spacing with Safety Factor	Not Possible	Not Possible	Not Possible	Not Possible	Not Possible	Not Possible	Not Possible	Not Possible	Every Rib	Every Rib	Every Rib	Every Rib
Required Puddle Weld Spacing without Safety Factor	Not Possible	Not Possible	Not Possible	Not Possible	Every 2nd Rib	Every 2nd Rib	Every 2nd Rib	Every 2nd Rib	Every 4th Rib	Every 4th Rib	Every 4th Rib	Every 4th Rib

8.1.7 FEM Modeling Rating Factors

8.1.7.1 CSiBridge Modeling and Rating Factor

Using the procedure described in Section 5.3, the operating moment rating factor was determined to be 0.96 governed by the exterior girder critical load placement. Differences in rating factors between CSiBridge and ANSYS are attributed to differences in modeling. For example, CSiBridge modeling used shell elements for the girder and deck, whereas ANSYS used shell elements for the girder and brick elements for the deck. Additionally, CSiBridge performs analyses by moving a load across a user-specified lane. A longitudinal stress contour of the Yutan Bridge can be seen below in Figure 72.

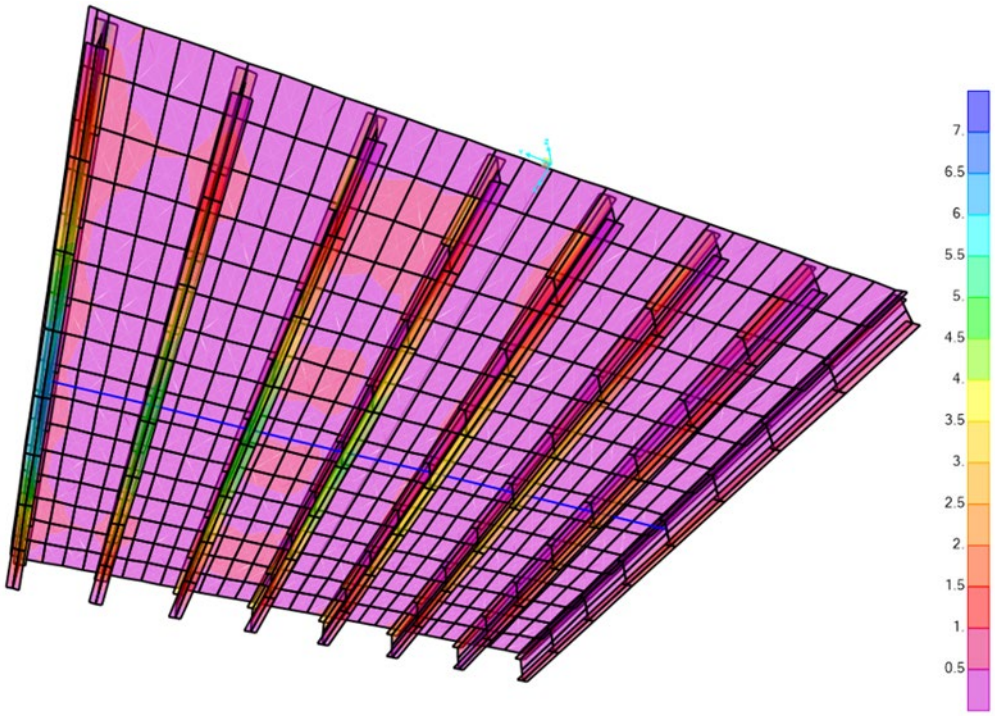

Figure 72. CSiBridge Longitudinal Stress Contour for the Yutan Bridge

8.1.7.2 ANSYS Rating Factor

The ANSYS VBA system described in Chapter 5 was used to find the load rating of the Yutan Bridge. The finite element modeling had to be modified in two ways. Since the bridge was created to perform compositely, the ratio of noncomposite and composite resistance was multiplied so that the rating factor reflects noncomposite section properties. A second modification ratio was multiplied to the rating factor since the ANSYS modeling does not include the lane load prescribed by AASHTO LRFR. The two modifications are shown in detail in the appendix. The operating moment rating factor for this bridge is 1.04 and is governed by the exterior girder critical load placement. A longitudinal stress contour is shown below in Figure 73.

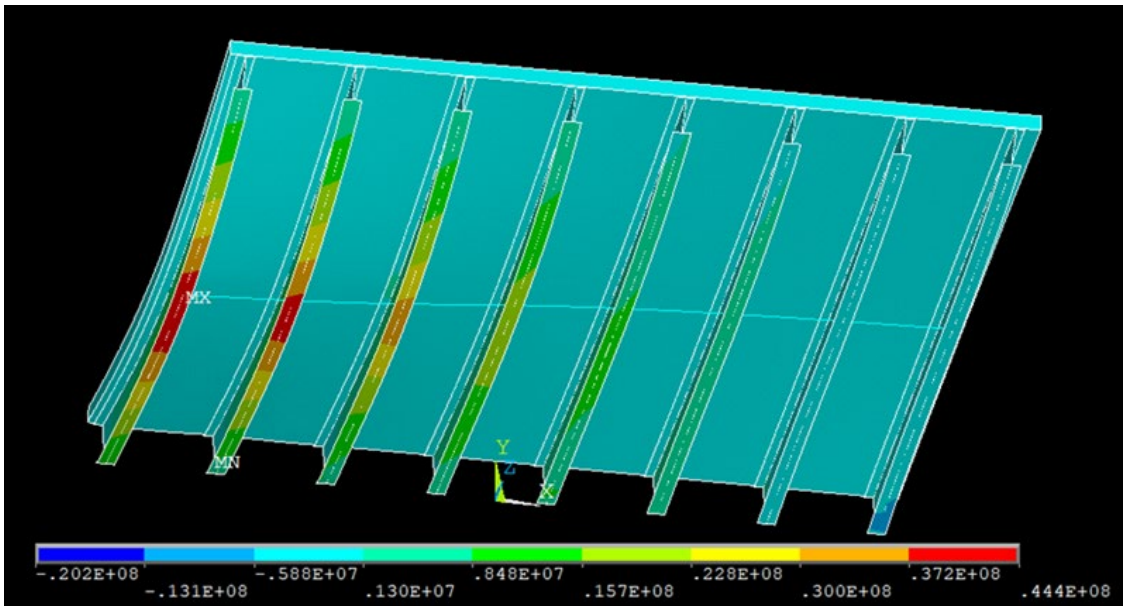

Figure 73. ANSYS Longudinal Stress Contour for the Yutan Bridge

8.1.8 ANN Load Rating Prediction

The best moment ANN, described in chapter 6, was used to calculate a refined rating factor for this bridge. The 10-5-5-1 BR ANN produced an unadjusted rating factor of 1.02. Since the ANSYS rating factor is 1.04, this rating factor appears to be very accurate. If the live load factor of 1.40 is used, the operating rating factor decreases to 0.98. Typically, this would suggest that the bridge should not be load tested. However, since the bridge load rating is very close to 1.0, it was determined that experimental factors could also boost the rating factor.

8.1.9 Experimental Load Rating

The AASHTO Manual for Bridge Evaluation (MBE 2013) outlines a method for updating load ratings based on experimental load ratings. The experimental load rating is shown in Eqn. 83 where subscript "T" denotes data based on testing and subscript "C" corresponds to values based on calculations. K is the adjustment factor for the load rating based on behavior observed from the load test. The overall benefit from the load test, K, is made up of two factors, K_a and K_b, as shown in Eqn. 84. K_a is the direct comparison between theoretical and the load test results, as shown in Eqn. 85. K_b takes the reliability of the bridge performing as noted in the load test at a higher load into account. Table 22 shows the appropriate values for K_b, as shown in AASHTO MBE.

$$RF_T = RF_C * K \quad \text{Eqn. 83}$$

$$K = 1 + K_a K_b \quad \text{Eqn. 84}$$

$$K_a = \frac{\varepsilon_C}{\varepsilon_T} - 1 \quad \text{Eqn. 85}$$

Table 22. Recommended Values for K_b

Can member behavior be extrapolated to 1.33W?		**Magnitude of test load**			**K_b**
Yes	**No**	$\frac{T}{W} < 0.4$	$0.4 \leq \frac{T}{W} \leq 0.7$	$\frac{T}{W} > 0.7$	
✓		✓			0
✓			✓		0.8
✓				✓	1
	✓	✓			0
	✓		✓		0
	✓			✓	0.5

The maximum theoretical strain corresponds to the exterior girder critical load location, as predicted by both CSiBridge and ANSYS models. The maximum experimental strain came from the girder 1 for the exterior girder being loaded. The maximum average bottom flange strains for the exterior critical lane path were 233.9 and 215.9 με, respectively. The average of the two bottom flange strain measurements for the two runs were used for ε_T. ε_C, calculated in Eqn. 86, is based off of theoretical load effect in the member corresponding to ε_T, L_T, the section factor, *SF*, and the modulus of elasticity, *E*. Since the bridge was rated based off of line girder analysis with simply-supported end conditions, L_T was calculated by using the critical moment load placement determined from using influence line analysis and AASHTO exterior girder distribution factors. The section factor is based off of noncomposite section properties. Eqn. 87 shows the resulting K_a.

$$\varepsilon_C = \frac{L_T}{(SF)E} = \frac{DF * M_{Critical}}{(SF)E} = \frac{0.394 * 233.9\ kipft * \frac{12\ in}{1\ ft}}{87.93\ in^3 * 29{,}000\ ksi} = 434\ \mu\varepsilon \qquad \text{Eqn. 86}$$

$$K_a = \frac{434\,\mu\varepsilon}{208\,\mu\varepsilon} - 1 = 1.08 \qquad \text{Eqn. 87}$$

As noted, K_b takes into consideration whether the load test behavior is dependable. The magnitude of the load test is above 0.7 of an HS-20 truck. According to AASHTO MBE, K_b should be taken as either 0.5 or 1.0 for this test magnitude. If K_b is taken as 0.5, then *K* is found to be 1.54. If K_b is taken as 1.0, then *K* is taken as 2.08. The resulting AASHTO experimental operating rating factors would be 1.32 and 1.77 for $K_b = 0.5$ and $K_b = 1.0$, respectively. Since partial composite behavior may not be dependable, a reduced K_b seems appropriate. However, the reduction of K_b to 0.5 seems arbitrary.

In addition, the load distribution from the live load test was used to find a rating factor based on noncomposite behavior, not partial composite behavior. The rating factor based on the distribution from the load test is 1.09, which is significantly lower than the MBE adjusted rating factors. The significant difference between the two rating factors suggests that the reduction of K_b from 1 to 0.5 is non-conservative.

8.1.10 Summary and Recommendations

In conclusion, a methodology was proposed for a modified method for removing load posting based off of load tests and ANNs. The Yutan Bridge was load posted based off of standard AASHTO rating methods. However, ANNs indicated that an improved rating factor is expected for this bridge. A load test found that benefits such as partial composite behavior and a reduced dynamic amplification factor raises the rating factor above 1, which warrants the removal of the load posting. However, the magnitude of benefits from the load may be too high by using MBE adjustment techniques. All of the rating factors calculated are shown in Table 23. These rating factors do not include an improved dynamic load effect found from the 2nd load test.

Table 23. Rating Factor Comparison

Method	**Rating Factor**
AASHTO Line Girder	0.85
Unadjusted ANN	1.02
Calibration-Adjusted ANN	0.98
ANSYS	1.04
CSiBridge	0.96
Load Test GDFs (non-composite)	1.09
AASHTO MBE Adjusted K_b =0.5	1.32
AASHTO MBE Adjusted K_b =1.0	1.77

Removal of the load posting is recommended, however, periodic tests using accelerometers are recommended as well to ensure that the bridge's level of composite behavior does not change. The benefit of using accelerometers is that this could be done in a short amount of time. Changes in the bridge's natural period would indicate that there's been a change in stiffness. A change in the bridge's stiffness would suggest that there may be loss of partial composite behavior in one or more of the girders that were previously behaving partially composite.

9 SUMMARY, CONCLUSIONS, AND RECOMMENDATIONS

This study expanded on a preliminary pilot study conducted by Sofi (2017), which produced an efficient parametric finite element steel girder bridge modeling framework for implementation in ANSYS, together with preliminary ANN development to directly predict bridge load rating factors. The objective of the present study was to enhance the ANN training data and integrate reliability calibration to develop an ANN-based tool, supplementing existing resources available to NDOT load rating engineers and facilitating more cost-effective bridge management decision-making. Although this study focused on using ANNs to support bridge management and load rating, the resulting ANN tool could potentially be used at early design stages to optimally proportion bridge cross-sections for new construction, provided that the parameters of the new construction (e.g. simple span, length, number and spacing of girders) are consistent with the ANN training set.

ANSYS FEMs for a sample of the Nebraska bridge inventory provided refined moment and shear live load demands. Consistent with previous studies in literature, live load demands from FEMs tended to be lower than those typically obtained from AASHTO line girder analysis. ANSYS modeling results were expressed as moment and shear GDFs, which were used to train ANNs.

ANNs were trained to map 10 inputs (e.g., span length, steel yield strength, longitudinal stiffness) to the moment or shear GDFs. ANN architectures were optimized and design dataset sample sizes were compared. Finally, ANN GDF prediction error was incorporated into an updated live load statistical distribution with increased uncertainty, and the live load factor was calibrated using the modified Rackwitz-Fiessler and Monte Carlo Simulation methods to reflect

the updated live load statistical distribution. The two reliability methods produced similar results. In addition to the development of an ANN, two load tests were conducted on a case study bridge in Yutan, NE. Load rating factors for the Yutan bridge were compared among AASHTO, ANSYS, CSiBridge, ANN, and field testing methods.

The following conclusions were drawn from the research presented herein:

1) ANNs trained using a design sample set of 50 bridges were able to predict FEM GDFs with an average testing error of 4.56%. Increasing the design sample size to 130 bridges only reduced testing error to 3.65%.
2) A properly configured and trained ANN should introduce only marginal uncertainty compared to the inherent live load uncertainties routinely accounted for in bridge engineering, such as the vehicle weight, axle spacing, multiple presence in adjacent lanes, and dynamic load amplification. Because the uncertainties routinely attributed to live load effects are statistically independent from ANN-prediction errors, the live load coefficient of variation only increased slightly, from 18% to approximately 19%.
3) Accounting for the additional ANN uncertainty required only a marginally higher live load partial safety factor (corresponding to a marginally lower load rating factor). Moment and shear calibrated live load partial safety factors of 1.4 (vs. 1.35) were found to be adequate.
4) Calibrated ANN-based rating factors provided a net benefit over those obtained from AASHTO line girder analysis, despite a penalty to account for additional ANN prediction error uncertainty. Moment ANN rating factors with calibrated partial safety factors are on

average 16% higher than AASHTO rating factors. Shear ANN rating factors with calibrated partial safety factors are on average 17% higher than AASHTO rating factors.

Outliers were strategically identified and excluded from ANN design data to optimize ANN performance (prediction error minimization). The outliers could have been included and would have increased the range of bridge population applicability. However, broader applicability would be accompanied by higher errors on average, which would then require a higher live load partial safety factor penalty to the entire population.

The study found that ANN prediction errors had only a modest influence on live load factors to account for additional uncertainty. However, this outcome was achievable because the ANN training data was carefully selected to represent extreme cases of parameters in the space. While it is appealing to say that only a handful of bridges are sufficient to develop a reliable ANN, that statement must be coupled with careful review of available data to identify maximally representative training candidates.

While the study was originally limited in scope to composite bridges, discussions with the research sponsor indicated that noncomposite behavior was a significant consideration for older, off-system bridges such as those owned by counties. Transverse live load distribution is believed to be influenced by composite action only through the effect on longitudinal stiffness, as long as all elements are uniformly either composite or noncomposite. Therefore, the ANN-based GDFs provided by this project are also believed to be applicable to noncomposite bridges, provided that longitudinal stiffness for a noncomposite structure is submitted to the ANN and load ratings are calculated using noncomposite rather than composite Capacity.

Diagnostic field tests provide substantial additional load rating benefits, such as revelation of composite behavior and structure-specific (likely reduced) dynamic structural response to vehicle loading. These aspects were observed during two diagnostic load tests on the Yutan Bridge. However, the guidance available to address unintended composite action in AASHTO Manual for Bridge Evaluation appeared potentially unconservative.

Based on the research presented herein, the following topics are recommended for future research:

1) Benefits from ANN-based design and rating tools could be extended to other bridge types, such as prestressed concrete girder bridges and multi-span continuous bridges.
2) Additional research should be performed to clarify appropriate load rating procedures influenced by partial and potentially unreliable composite behavior.

10 APPENDICES

10.1 Extended Literature Review

10.1.1 Studies of Bridge Analysis and Load Rating

Gheitasi, A. and Harris, D.K., 2015, Failure Characteristics and Ultimate Load-Carrying Capacity of Redundant Composite Steel Girder Bridges: Case Study

This investigation included comprehensive nonlinear FEAs of two representative intact composite steel girder bridges (Nebraska Laboratory Bridge Test and the Tennessee Field Bridge Test) that were tested to failure and provided sufficient details for model validation. Both bridges demonstrated additional reserve capacity over the theoretical nominal capacity according to AASHTO LRFD. The researchers categorized the bridges' behavior into four stages; I. flexural cracks in concrete deck II. plasticity initiated in steel girders III. Structural stiffness drops off significantly, and plastic hinges form at the location of the maximum moment IV. local failure after significant plastic deformation and load redistribution within the structural system. The bridges' behavior is shown below in Figure 74.

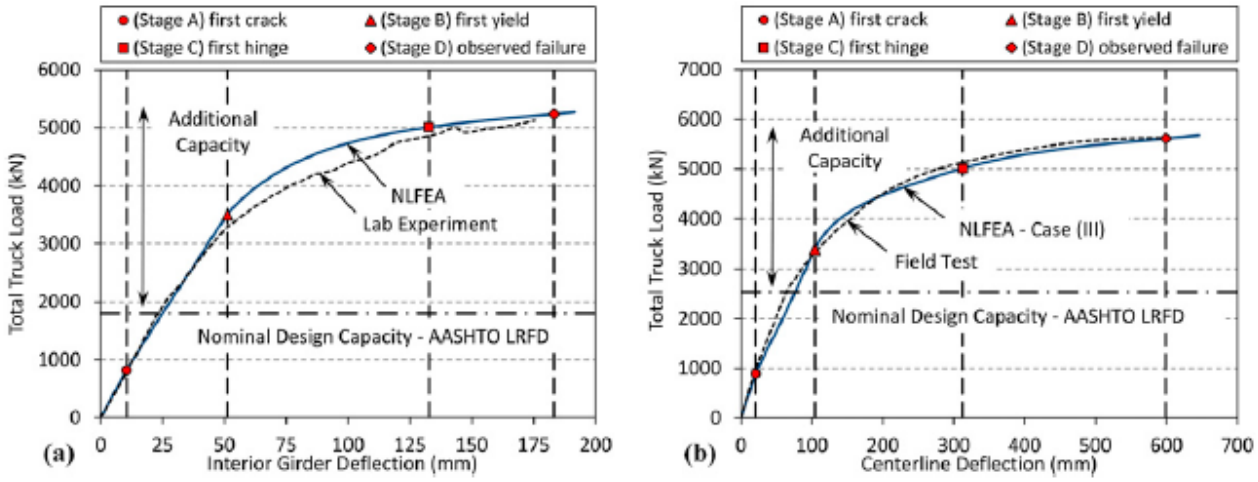

Figure 74. Behavioral Stages: (a) Nebraska Laboratory Test (b) Tennessee Field Test

Gheitasi, A. and Harris, D.K., 2015, Overload Flexural Distribution Behavior of Composite Steel Girder Bridges

A comprehensive study was performed on two in-service bridge superstructures in Michigan to investigate the impact of variations in boundary condition, loading position, and load configuration on the overall structural response and girder distribution behavior of bridges approaching their ultimate capacities. The three parameters were all found to be highly sensitive. Variations in lateral distribution behavior occur once the structure passes the linear-elastic stage of behavior. GDFs published in AASHTO LRFD specifications are usually conservative in

predicting superstructure ultimate capacities. GDFs' level of conservativeness is dependent on loading configuration. Also, AASTHTO GDFs were calibrated based on linear-elastic behavior. Once inelastic behavior is reached, lateral load distribution factors are governed by the geometry of the structure and the loading configuration. Adjustments made to AASHTO LRFD need validation through a parametric study on many geometrically different bridges and different loading configurations.

Bowman, M.D. and Chou, R., 2014, Review of Load Rating and Posting Procedures and Requirements

This report summarizes where load rating specifications can be found for LRFR, LFR, and ASR, as well as the Indiana Department of Transportation (INDOT) Bridge Inspection Manual. The report also summarizes findings from surveys that DOTs completed related to which specifications they use, which design methods (LRFR, LFR, or ASR) they use, and which method they prefer. At the time of the publication, LFR was the preferred method, although many DOTs did not specify a preferred method. The findings are shown below in Figure 75. After reviewing and performing load ratings with the different methods, it was recommended that INDOT follow AASHTO MBE (2011) with AASHTO legal loads for load ratings.

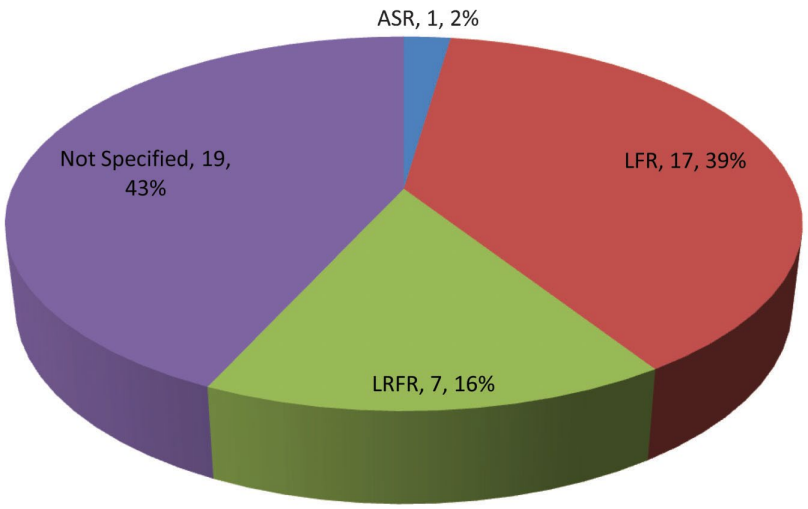

Figure 75. Preferred Method Used for Load Rating and Posting

Harris, D.K. and Gheitasi, A., 2013, Implementation of an Energy –Based Stiffened Plate Formulation for Lateral Distribution Characteristics of Girder-Type Bridges

An analytical approach called the stiffened plate model is presented for determining lateral load distribution characteristics of beam-slab bridges. The methodology was validated using FEM and field investigation of three bridges. The stiffened plate model yielded a more flexible system response compared to upper bound FEM results. The stiffened plate model had lateral load distribution that is similar in the FEM and field measurements. The majority of DFs calculated from the stiffened plate method were within 15% of the measured DFs.

Kim, Y.J., Tanovic, R., and Wight, R.G., 2013, A Parametric Study and Rating of Steel I-Girder Bridges Subjected to Military Load Classification Trucks

The researchers analyzed six simply-supported bridges that were designed with varying span lengths, number of girders, girder spacings, and moments of inertia. The AASHTO LRFD provisions were conservatively rated between 2.46 and 3.87 while the unfactored FEA models yielded an average of 7.01. The geometric parameters influenced the load distribution of the MLC trucks on the superstructure, but none as much as the wheel-line spacing of the MLC trucks. Although the predictive models were conservative, when a bridge is rated higher than MLC50, the margin between FEA and predictive methods decreases considerably.

Razaqpur, A.G., Shedid, M., and Nofal, M., 2012, Inelastic Load Distribution in Multi-Girder Composite Bridges

The researchers used FEMs to analyze fifty bridge cases. Load distribution factors were obtained from the FEMs and compared to AASHTO LRFD. The researchers also analyzed the sensitivities of bridge parameters. For exterior girder load DFs at elastic state, AASHTO LRFD were on average 67% higher than FEA. For interior girders, this value was 73% higher for AASHTO LRFD. At ultimate state, AASHTO was on average 36% higher than FEA.

Bae, H.U. and Oliva, M.G., 2011, Moment and Shear Load Distribution Factors for Multigirder Bridges Subjected to Overloads

The researchers developed new moment and shear load distribution factor equations for oversize, overweight vehicles. 118 multi-girder bridges with 16 load cases of oversize overload vehicles were used to develop FEMs. Distribution factor equations were created and simulated. Furthermore, the researchers performed load tests, and results were found to be within 8% of the predicted deflection. The equations yield results more conservative than FEM, but less conservative than AASHTO equations. Sample moment and shear GDFs are provided in Figure 76.

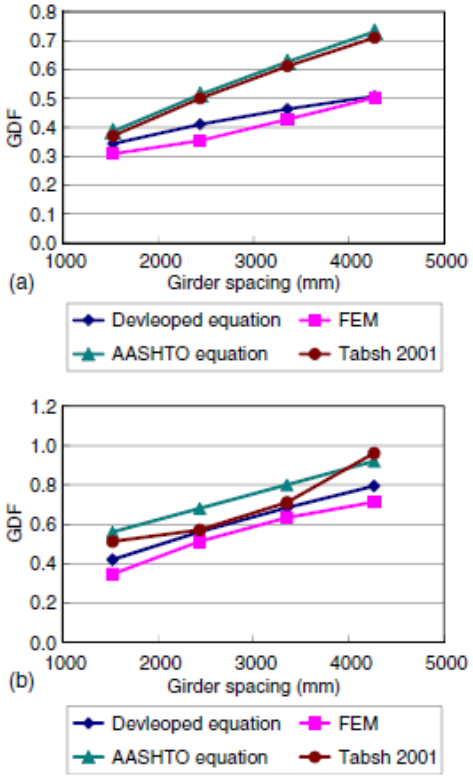

Figure 76. Moment (a) and Shear (b) GDFs based on Girder Spacing from Bae and Oliva (2011)

Harris, D.K., 2010, Assessment of Flexural Lateral Load Distribution Methodologies for Stringer Bridges

The goal of the study was to find the most appropriate analysis method for determining load DFs for slab-girder bridges. Harris validated FEMs for the study using documented field testing, and found that the beam-line method neglects contributions by secondary elements of bridges and concluded that that these contributions should be accounted for in load rating analyses. Furthermore, section response about the composite section neutral axis should be considered for bridges designed for composite action. Harris asserts that boundary conditions had little effect on the distribution factors in the load fraction method, but do affect member response in beam-line analysis.

Murdock, M., 2009, Comparative Load Rating Study Under LRFR and LFR Methodologies for Alabama Highway Bridges

This paper presents major differences between LRFR AND LFR in a comparative study. 95 bridges in Alabama were analyzed using LRFR and LFR rating methods. The researcher concluded that LRFR rating factors correlated well to the estimated probability of failure for interior and exterior girders in moment and shear. LFR rating factors were found to not correlate well to this estimated probability of failure. Main differences between the two rating methodologies can be seen in.

Table 24. Differences between LRFR and LFR from Murdock (2009)

Rating Methodology	LRFR	LFR
Capcity	According to LRFD	According to LFD
Condition and System Factors	ϕ - Resistance ϕ_c - Condtion ϕ_s - System	- - -
Distribution Factors	LRFD Formulas	"S Over" Formulas
Dead Load Factors	λ_{DC} - 1.25 λ_{DW} - 1.5	A_1 - 1.3
Live Load Factors	λ_L Inventory - 1.75 Operating - 1.35 Legal - 1.4 to 1.8 Permit - 1.15 to 1.8	A_2 Inventory - 2.17 Operating - 1.3
Dynamic Load Allowance / Impact Factor	Constant	Span Length Dependent

Kulicki, J.M., Prucz, Z., Clancy, C.M., Mertz, D.R., Nowak, A.S., 2007, Updating the Calibration Report for AASHTO LRFD Code/NCHRP 20-07/186

NCHRP 12-33 Report 368 provided a calibration procedure that did not correspond to a code. The goal of this project was to document calibration of strenght limit state for AASHTO LRFD Bridge Design Specifications. Reliability analyses were performed for representative bridges including beam-slab bridges, composite and noncomposite steel girder bridges, reinforced concrete T-beams, and prestressed concrete bridges. Several adjustments were made to the data used in Report 368, including increasing the ADTT from 1,000 to 5,000, using a lognormal distribution for resistance in reliability analyses, and using a representative bridge database. In this report, Monte Carlo was used and compared to results from the Rackwitz-Fiessler method. Monte Carlo sampling has become more widespread with the advancement in computing power in recent years. As a check, the Rackwitz-Fiessler method was performed and similar results were attained by using both methods. The reliability of the bridges in the dataset used are shown in Figure 77. An interesting observation noted by the researchers is that there is a general decrease in reliability as the length of the bridge increases, as noted by Figure 78. This suggests that there is a correlation between dead to live load ratio and reliability. Lastly, the researchers perturbed load effects to investigate the sensitivity of the reliability index of the bridges. One of their findings is that if they multiply all of the load effects by a scalar, they see a uniform parallel offset in the reliabilities. Furthermore, an increased load effect produced the same results as a resistance that is reduced by the same percentage. Another observation made is that modifying the dead loads by a factor is more sensitive as the length of the bridge increases. This can be explained by the fact that bridges typically have higher dead to live load ratio as the span increases. When only the live load is modified by a scalar, the opposite effect was noted. As the span length increases, the sensitivity of reliability index decreases.

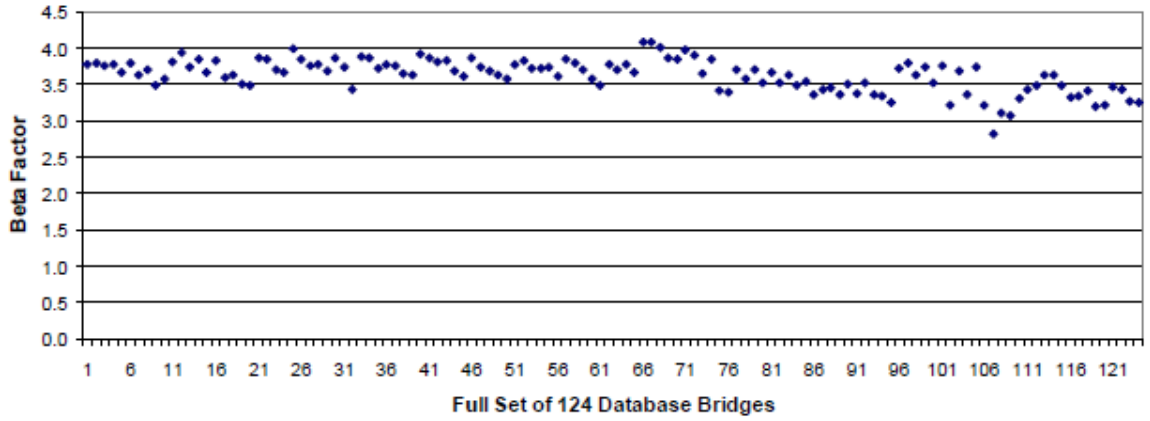

Figure 77. Beta Factors Using Monte Carlo Analysis for Bridge Database

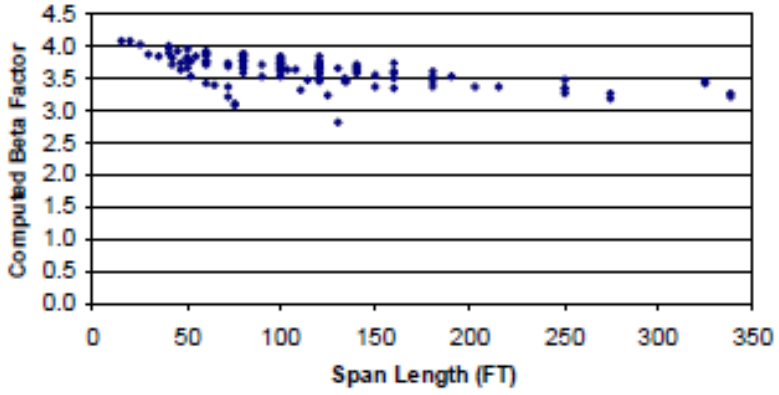

Figure 78. Reliability vs. Span Length

Yousif, Z. and Hindi, R., 2007, AASHTO-LRFD Live Load Distribution for Beam-and-Slab Bridges: Limitations and Applicability

The researchers compared AASHTO LRFD distribution factors to several types of FEM for simple span slab-on-girders concrete bridges. AASHTO LRFD overestimated the live load distribution when compared to FEM for a significant number of cases. AASHTO overestimated the live load distribution a maximum of about 55%. Despite this, AASHTO LRFD did underestimate the distribution factors when compared to FEM in some cases. The range of the limitations specified by AASHTO regarding span length, girder spacing, deck thickness, and longitudinal stiffness all have a significant effect on the live load distribution. Outside of these boundaries, deviations from AASHTO LRFD appear.

Zheng, L., 2007, Comparison of Load Factor Rating (LFR) to Load and Resistance Factor Rating (LRFR) of Prestressed Concrete I-Beam Bridges

This paper presents key differences between LFR and LRFR. Furthermore, the researcher analyzed seven prestressed concrete bridges including one straight, simple span Bulb Tee-girder bridge, three skewed simple span, I-girder, and three skewed continuous multi-span I-girder bridges. They found that the majority of load ratings using LRFR were governed by shear, not flexure. The governing failure mechanism is different from LFR, which has flexural ratings that typically govern.

Moses, J.P., Harries, K.A., Earls, C.J., and Yulismana, W., 2006, Evaluation of Effective Width and Distribution Factors for GFRP Bridge Decks Supported on Steel Girders

Glass fiber-reinforced polymers (GFRP) may be used for replacing concrete decks. Three of these types of bridges underwent situ load tests. Design standards treat GFRP decks similar to noncomposite concrete decks. The researchers found that this may result in nonconservative bridge girder designs. The effective width of the GFRP deck that may be engaged is lower than that of an equivalent concrete deck. This behavior is due to increased horizontal shear lag due to less stiff axial behavior in the GFRP deck and increased vertical shear lag due to the relatively soft in-plane shear stiffness of the GFRP deck. The engaged effective width shows some evidence of degradation with time, which the researchers attributed to the reduction of shear transfer efficiency required for composite behavior.

Chung, W., Liu, J., and Sotelino, E.D., 2006, Influence of Secondary Elements and Deck Cracking on the Lateral Load Distribution of Steel Girder Bridges

The researchers used FEMs to model secondary elements such as diaphragms and parapets. The researchers concluded that the presence of diaphragms and parapets could make girder distribution factors up to 40% lower than the AASHTO values. They also found that longitudinal cracking increased the load distribution factors by up to 17% higher than AASHTO. Transverse cracking was not attributed toimpact the transverse distribution of moment.

Chung, W. and Sotelino, E.D., 2006, Three-Dimensional Finite Element Modeling of Composite Girder Bridges

The researchers created four FEMs with varying modeling parameters. The FEMs' flexural behavior was analyzed and compared to a full–scale lab test and a field test. The first FEM used shell element webs and shell elements flanges. The second FEM used shell element webs and beam element flanges. The third FEM used beam element webs and shell element flanges. The last FEM modeled each girder cross section with a single beam element. All FEMs used shell elements to model the deck. The researchers compared the models' data to physical tests, and differences were attributed to element compatibility as well as geometric discrepancies. The researchers concluded that shell element girder modeling requires a higher level of mesh refinement to converge due to the displacement incompatibility between the drilling DOF of the web element and the rotational DOF of the flange element. The FEM that is the most economical is the fourth model since it is capable of accurately predicting the flexural behavior of the girder bridges including deflection, strain, and lateral load distribution.

Conner, S. and Huo, X.S., 2006, Influence of Parapets and Aspect Ratio on Live-Load Distribution

24 two–span continuous bridges with varying structural parameters were analyzed. FEMs were used to quantify distribution factors and compared to AASHTO distribution factors. The presence of parapets was found to reduce DFs by as much as 36% for exterior girders and 13% for interior girders. Increasing the overhang length decreased the effect of the parapet. AASHTO LRFD was found to be conservative compared to FEMs. Moment DFs were virtually unaffected until the aspect ratio surpassed 1.8. The effect beyond that point, however, was still quite small.

Jaramilla, B. and Huo, S., 2005, Looking to Load and Resistance Factor Rating

This short article describes the differences between LFR and LRFR. LRFR is noted to provide more uniform reliability with HL-93 instead of HS-20 loading. Benefits from nondestructive load testing are noted to be more easily incorporated with LRFR. According to NCHRP Project C12-46, "DOT rating engineers were able to perform the LRFR evaluations without undue difficulty and with relatively few errors." The implementation of LRFD reported at the time of publication is shown in Figure 79.

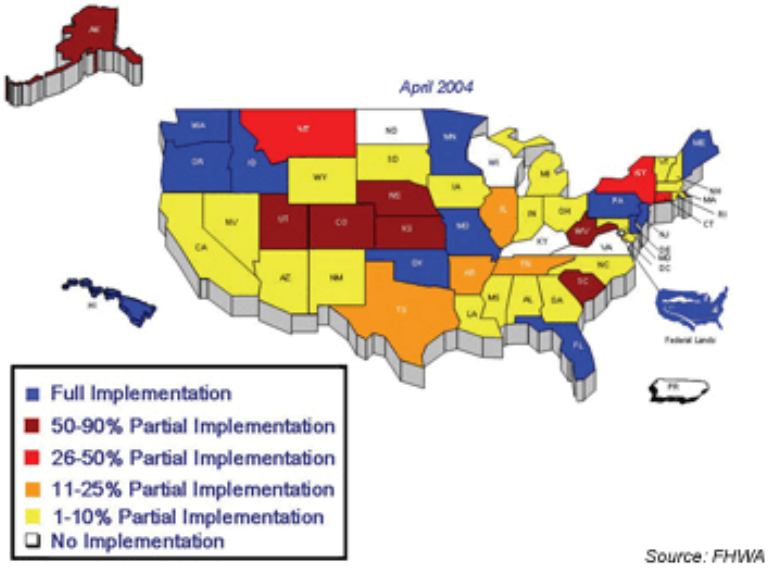

Figure 79. LRFD Implementation as of April of 2004

Sotelino, E.D., Liu, J., Chung, W., and Phuvoravan, K., 2004, Simplified Load Distribution Factor for Use in LRFD Design

AASHTO LDF equation presented in 1994 includes a longitudinal stiffness parameter that is not initially known which makes the procedure iterative. The researchers developed a simplified equation and used it to compare FEMs and AASHTO calculations of 43 steel girder and 17 prestressed concrete girder bridges. The simplified equation always produces conservative LDF values compared to FEA, but larger than the LDFs generated by using AASHTO LRFD. The

researchers did improve the FEM by accounting for secondary elements. They found that the presence of secondary elements produced LDFs that were up to 40% less than AASHTO LRFD values.

F., 2003, Nonlinear Finite-Element Analysis for Highway Bridge Superstructures

Researchers compared the Transformed Area Method and FEM (on FORTRAN) to experimental data of a single concrete deck steel-girder bridge. The FEM process the researchers used for the concrete deck, reinforcement, and steel was discussed extensively. The FEM's deflection was closer to the experimental data than what the design method at the time would have predicted (AASHTO 1996).

Khaloo, A.R. and Mirzabozorg, H., 2003, Load Distribution Factors in Simply Supported Skew Bridges

Simply supported skew bridges were analyzed using FEA in ANSYS. The researchers found that AASHTO DFs are conservative in right bridges and even more conservative for skew bridges. The researchers also concluded that internal transverse diaphragms perpendicular to the longitudinal girders are the best arrangement for load distribution in skew bridges.

Eamon, C.D. and Nowak, A.S., 2002, Effects of Edge-Stiffening Elements and Diaphragms on Bridge Resistance and Load Distribution

These researchers analyzed secondary effects for simple span, two-lane highway girder bridges with composite steel. The researchers also considered prestressed concrete girder bridges in this study. They performed elastic and inelastic analyses for nine bridges modeled in FEM. In the elastic range, secondary elements affected the location and magnitude of moment and were found to experience a 10-40% decrease in GDF, for a typical case. GDFs decrease by an additional 5-20% in inelastic analysis while the ultimate capacity increases 1.1-2.2 times that of the base bridge. Despite the positive influences these elements offer, the researchers seem reluctant to include these benefits in load ratings. "Although ignoring the effects of secondary elements on load distribution and ultimate capacity typically leads to conservative results, their effect varies greatly, depending on bridge geometry and element stiffness. Bridges designed according to the current LRFD code thus have varying levels of safety or reliability, a topic to be investigated in the future."

Eom, J. and Nowak, A.S., 2001, Live Load Distribution for Steel Girder Bridges

The literature at the time of this publication indicated that GDFs appear to be conservative for long spans and large girder spacing, but too permissive for short spans and small girder spacing. The research program field tested 17 steel girder bridges, and the strains were used to calculate GDFs and compare to FEMs with either roller-hinge supports, hinge-hinge supports, or partially fixed supports. Examples of GDFs derived from strain are shown in Figure 80. The absolute value of measured strain was found to be less than that of the FEM. One important reason for this observation is the partial fixity of supports. Measured GDFs were consistently lower than those of the AASHTO code-specified values. FEM and GDFs agree more when the support condition is ideally simply supported. If the reduction of stress due to the partial fixity of supports is considered, then the code-specified girder distribution values are suitable for use in

the rating equations. However, caution must be exercised when relying on partial fixity at supports because the theoretical support restraint may not always be fully available when extremely high loads are present, thereby diminishing the expected beneficial effects.

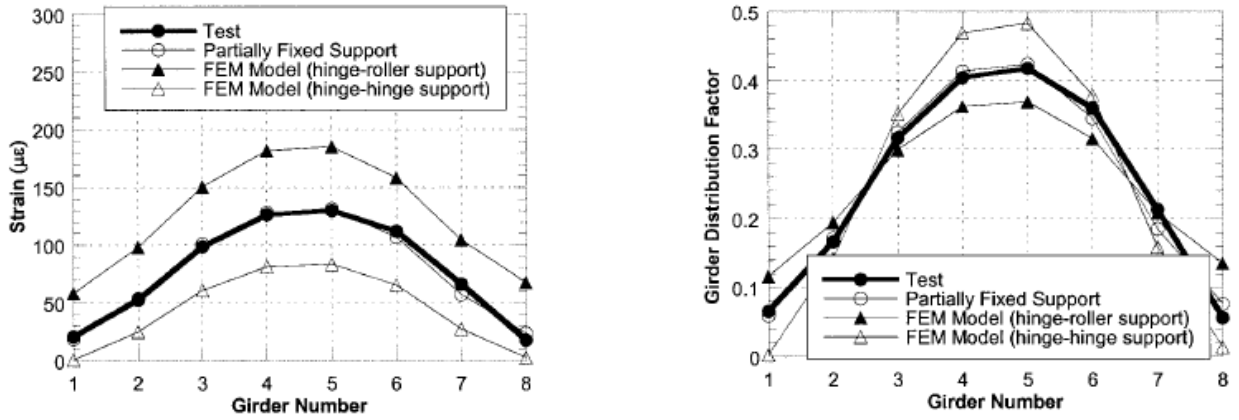

Figure 80. Strain and Resulting GDFs Derived from Strain for Two Lane Loading

Barker, M.G., 2001, Quantifying Field-Test Behavior for Rating Steel Girder Bridges

A systematic approach is presented to separate and quantify the contributions from various effects, such as bearing restraint forces and unintended composite action, in bridge field testing. Bearing restraint was found to increase the capacity by 3.6%. Non-composite sections exhibited composite behavior that increased the capacity an average of 32.3% at those sections. The critical section is composite, so the rating was raised only 4.2%. Load rating engineers should note that bearing restraint contributions may not be reliable over time. The procedure includes inspecting the bridge and determining dimensions and dead loads, determining the experimental impact factor, calculating the experimental distribution factors, determining the bearing restraint forces and moments, calculating the total measured moments, removing the bearing restraint moments, calculating the elastic moments, determining the section moduli, and calculating the elastic longitudinal adjustment moments.

Tabsh, S.W. and Tabatabai, M., 2001, Live Load Distribution in Girder Bridges Subject to Oversized Trucks

FEM was used to develop modification factors for the AASHTO flexure and shear GDFs to account for oversize trucks. Four loading cases were studied; HS20-44, PennDOT P-82 permit truck, Ontario Highway Bridge Design Code's load level 3 truck, and HTL-57 notional truck. The results showed that the modification factors with the specification-based GDFs could help increase the allowable loads on slab-on-girder bridges.

Sebastian, W.M. and McConnel, R.E., 2000, Nonlinear FE Analysis of Steel-Concrete Composite Structures

This paper describes the researchers' FEM process in detail. A verification study was done to assess the FEM's capabilities. The researchers used four structures, tested and published in literature, to validate the FEMs. The FEMs performed well, including those with ribbed reinforced concrete slabs acting compositely with profiled steel sheeting. Internal deformations, crack patterns, and shear connector actions were shown to be modeled accurately.

Zokaie, T., 2000, AASHTO-LRFD Live Load Distribution Specifications

The AASHTO-LRFD Bridge Design Specifications live load distribution equation was only a function of girder spacing. Now, the equations are more complex to account for skew, slab thickness, and length. The researchers tested the accuracy of the new equations and they found that FEM works the best, but the new formulas were within 5% of FEMs' live load distribution. Limitations include that the formulas had uniform spacing, girder inertia, and skew. The researchers also did not include diaphragm effects in the model. Although the formulas are more accurate than S/D factors, they are most accurate when applied to bridges with similar restraints.

Mabsout, M.E., Tarhini, K.M., Frederick, G.R., and Kesserwan, A., 1998, Effect of Continuity on Wheel Load Distribution in Steel Girder Bridges

The researchers made FEMs for 78 two-equal-span, straight, composite, steel girder bridges. Results of the FEMs were used to predict wheel load distribution factors. They were found to generally be less than values obtained using the AASHTO formula (S/5.5). AASHTO overestimated the actual wheel load distribution by as much as 47% depending on the bridge geometry. As the span and girder spacing increases, AASHTO aligns more closely to FEA results.

Chajes, M.J., Mertz, D.R., and Commander, B., 1997, Experimental Load Rating of a Posted Bridge

A posted bridge with non-composite girders was found to have significant bearing restraint. Additionally, the girders were found to act compositely based on data from a diagnostic load test. An FE model was developed and calibrated using the measured response to obtain accurate analytical predictions of bridge structural response to applied live load. Load ratings for Delaware's seven load vehicles increased from the range of 0.72 to 1.39, to 1.38 to 2.55 which justified removing load posting. The authors discussed whether to include unintended composite action in load rating. For this specific case, the researchers recommended including unintended composite action in the load rating since, in the researchers' opinions, the observed structural behavior could be reliably expected for applicable loading patterns and magnitudes. However, they recommend relatively frequent inspection.

Mabsout, M.E., Tarhini, K.M., Frederick, G.R., and Kobrosly, M., 1997, Influence of Sidewalks and Railings on Wheel Load Distribution in Steel Girder Bridges

120 bridges were analyzed using FEMs in a parametric study. AASHTO LRFD wheel load distribution formulas correlated conservatively with the FEM results. Both were less than the AASHTO (S/5.5) formula. NCHRP 12-26 formulas were found to be conservative too, but not as

much as AASHTO except for short spans. Sidewalks and railings were found to increase the load-carrying capacity by upwards of 30% if they are included in the strength evaluation. However, the researchers seemed reluctant to be able to count on the sidewalks and railings when determining the bridge capacity. The researchers' recommendations include, "The results of this research can assist the bridge engineering in determining the actual load-carrying capacity of steel bridges when encountering sidewalks and/or railings in a bridge deck."

Ebeido, T. and Kennedy, J.B., 1996, Shear and Reaction Distributions in Continuous Skew Composite Bridges

AASHTO provisions at the time did not account for skew or continuity; therefore, load ratings could be conservative for continuous skew bridges. FEM was verified with test data and then used to conduct a parametric study on more than 600 prototype cases. The generated data was then used to find expressions for span and support moment DFs for truck loading as well as dead load. Parametric sensitivity was analyzed as well

Ebeido, T. and Kennedy, J.B., 1996, Girder Moments in Continuous Skew Composite Bridges

Six simply supported skew composite steel-concrete bridges were constructed and tested. The researchers included an additional 300+ prototype bridges for a parametric study using FEA. The study produced empirical formulas to evaluate moment DFs for exterior and interior girders. The authors concluded that skew is the most important parameter affecting girder moments in composite bridges. Girder spacing, intermediate transverse diaphragms, and aspect ratio all influence the moment DF as well. Ebeido and Kennedy concluded that, "in the design of continuous skew composite bridges, the exterior girder is the controlling girder in terms of both span and support moments." They found that the higher the skew, the more moment is placed on the exterior girders.

Chen, Y., 1995, Prediction of Lateral Distribution of Vehicular Live Loads on Bridges with Unequally Spaced Girders

Chen proposed an analysis method for predicting the lateral distribution of vehicular live loads on unequally spaced I-shaped bridges. The paper describes the bridge modeling process and verification as well as AASHTO methods of lateral load distribution. Live load distribution factors were obtained using a refined analysis method that uses FEM and compared with data from a parametric study of 13 bridges. The researcher performed nonlinear and linear analysis and found that nonlinear analysis yielded slightly lower DF values. Compared to the refined method presented, AASHTO gave unconvervative distribution factors for exterior girders that are spaced less than six feet.

Helba, A. and Kennedy, J.B., 1994, Parametric Study on Collapse Loads of Skew Composite Bridges

The researchers used FEMs in this parametric study to relate bridge parameters and geometries to failure patterns for the minimum collapse load of simply supported and continuous two-span skewed composite bridges. The analyzed parameters included eccentric and concentric critical loadings, skew, aspect ratio, number of girders, interaction between diaphragms and main

girders, and the number of loaded lanes. For eccentric loading, the "critical crack length" (meaning the transverse distance from the deck edge nearer the applied load to the longitudinal hinging line on the opposite side of the load) was found to be significantly affected by the bridge aspect ratio and slightly by skew. For concentric loading, the inclination of the positive transverse failure line was shown to be related to the number of loaded lanes and skew.

Galambos, T.V., Dishongh, B., Barker, M., Leon, R.T., and French, C.W., 1993, Inelastic Rating Procedures for Steel Beam and Girder Bridges

This project developed a rating methodology for existing bridges that included inelastic capacity available in most multi-girder bridges as well as the redistribution capacity due to composite action. The authors also investigated shakedown – the response of a structure after some initial plastic deformation. Shakedown happens when the structure adapts to prior inelastic excursions and responds in the elastic range to working loads. This study asserts that system-capacity is a more accurate load capacity method than typical element-based approaches. Field tests and experimental studies showed that composite and non-composite compact beams exceeded their theoretical plastic moment capacity and also showed excellent ductility and rotational capacity. The researchers recommended the shakedown method of load testing since bridges are loaded cyclically, which would make the ultimate strength limit state unconservative. One reason they make this assertion is the fact that the friction between slab and girders is overcome at ultimate and composite bridges act noncompositely. Furthermore, "Although the ultimate strength of the composite plate girders can be reached and exceeded by using stiffeners and tension field action, the question of available rotational ductility of the plate girders has not yet been thoroughly researched. It should also be pointed out that plate girders, because of the use of stiffeners and bracing, are very sensitive to fatigue problems." The report goes on to say, "Rather shakedown, or that load causing a set of residual moments throughout the structure such that the bridge responds to subsequent loads of the same magnitude or smaller in an elastic fashion, is the recommended limit state to be used when cyclic loads are present." Shakedown was still in early research phases at the time of this publication, but this article indicated that it will more adequately predict a global failure mechanism instead of local approaches.

Bishara, A.G, Liu, M.C., and El-Ali, N.D., 1993, Wheel Load Distribution on Simply Supported Skew I-Beam Composite Bridges

This paper presents distribution factor expressions for wheel-load distribution for the interior and exterior girders of multi-steel beam composite bridges of medium span length. The researchers used FEMs to determine the wheel load distributions. They also performed sensitivity analysis on parameters such as span lengths, widths, skew angle, and spacing and size of intermediate cross frames. AASHTO wheel-load distribution factors for interior and exterior girders were found to be 5-25% higher than those from FEA. The interior girder distribution factors developed in this study were 30-85% of the contemporary AASHTO distribution factors and exterior girder distribution factors were found to be 30-70% of AASHTO.

Tarhini, K.M. and Frederick, G.R., 1992, Wheel Load Distribution in I-Girder Highway Bridges

FEAs were used to model I-girder highway bridges. Researchers made a wheel load distribution formula by using the FEAs. They used a standard bridge design while they varied one parameter within a specified range while the remaining parameters were the same to measure sensitivity of the parameters. The parameters analyzed were girder size and spacing, cross bracing presence, slab thickness, span length, single or continuous spans, and composite and noncomposite behavior. The formula's DF was compared to AASHTO DFs and other researchers' work and can be seen in Table 25. The sensitivity of the parameters was also analyzed.

Table 25. Comparison of Wheel Load Distribution Factors from Tarhini and Frederick (1992)

Span L (ft) (1)	Beam spacing (ft) (2)	AASHTO $S/5.5$ (3)	S/D_d Bakht and Moses (4)	S/D_d (SALOD) (5)	Proposed DF formula (6)
20	7.5	1.364	1.44	1.85	1.61
50	7.5	1.364	1.33	1.28	1.25
50	6.0	1.09	1.07	1.08	1.04
75	6.0	1.09	1.01	0.96	0.92
75	5.0	0.91	0.84	0.83	0.75
77	8.8	1.60	1.313	—	1.28
100	5.0	0.91	0.82	0.77	0.80
110	8.5	1.545	1.29	—	1.36

Khaleel, M.K. and Itani, R.Y., 1990, Live-Load Moments for Continuous Skew Bridges

Khaleel and Itani modeled a total of 112 pretensioned concrete, 5-girder continuous bridges using FEMs. The researchers found that AASHTO underestimated positive bending moments by as much as 28% for skew bridges. The edge girders controlled the design for a combination of large skew angles, large spans, small girder spacings, and smaller girder-to-slab stiffness ratios. For a skew angle of 60 degrees, the maximum moment in the interior girder is 71% of the corresponding moment for a bridge with no skew. For the exterior girders, the reduction of the moment for the maximum girder is 20%.

Razaqpur, A.G. and Nofal, M., 1990, Analytical Modeling of Nonlinear Behavior of Composite Bridges

Details of modeling bridge deck, steel girders, and reinforcement are discussed. Experimental verification was done using results of the two beam tests and a multi-girder bridge test. FEM accurately determined complete cracking over interior support, bottom flange first yielding, first yielding in the web, and complete cracking with less than 3.5% error and failure load with less than 1% error for the beam test. FEM had similar results to the bridge test with less than 2% difference in failure load.

Bakht, B. and Jaeger, L.G., 1988, Bearing Restraint in Slab-on-Girder Bridges

Researchers found that girder restraint can reduce live load moments in existing single-span slab-on-girder bridges by up to 20%. This paper presents simple expressions for deflection reduction and stress reduction to account for additional girder support restraint. The researchers performed FEA and obtained similar results. The paper provides a procedure to account for additional support restraint. Researchers performed a case study of a short-span simply supported bridge having six rolled-steel girders and a non-composite deck slab that was statically tested. Bearing restraint forces reduced the bending moment at mid-span by at least 12%.

Marx, H.J., Khachaturnian, N., and Gamble, W.L., 1986, Development of Design Criteria for Simply Supported Skew Slab-on-Girder Bridges

Elastic analyses were performed using FEMs on 108 single span skew slab-and-girder bridges. The parametric study was performed to determine the most important bridge variables and to gain insight on how skew bridges respond. AASHTO wheel load (S/5.5) was found to be between 12% unsafe or 32% too large. AASHTO underestimated the actual exterior girder bending moments in most bridges considered – up to 23% too small. It was found that higher skew results in smaller interior girder moments. However, exterior girders are not affected as much as interior girders. Because of this, the exterior girders typically control the design of highly skewed bridges. The presence of end diaphragms can reduce maximum bending moments.

Hall, J.C. and Kostem, CN, 1981, Inelastic Overload Analysis of Continuous Steel Multi-Girder Highway Bridges by the Finite Element Method

This paper describes an analytical technique for predicting the response to overloads of simple-span and continuous multi-girder beam-slab type highway bridge superstructures made of steel beams and concrete slabs by employing a displacement based FEA. This paper was the first study to consider post-plastic stress-strain relationships for the steel girder, strain hardening of steel, buckling of beam compression flanges and plate girder webs, and post-buckling response of the flanges and webs in FEA. Researchers compared the stress and strain of two bridges, two bridge models, two composite beams, and eight plate girder tests to experimental results, and found that the analytical predictions were similar to observed physical responses. The researchers confidently assert that engineers can use the model for structural overload response, regarding stresses, deflections, and damage, for steel beam concrete slab highway bridges, composite beams, and plate girder structures. They also noted that the negative moment regions suffered the most damage.

10.1.2 Studies of Neural Networks in Engineering

Alipour, M., Harris, D.K., Barnes, L.E., Ozbulut, O.E., Carroll, J., 2007, Load-Capacity Rating of Bridge Populations through Machine Learning: Application of Decision Trees and Random Forests

Load rating bridges poses many challenges with limited resources for testing bridges and imcomplete plans. Researchers created neural network models in order to create a data-driven approach to load rating bridges, rather than systematic procedures that are common at state departments of transportation. Data was collected for 47, 385 highway bridges from NBI (2014)

and used to create and test the models. The C4.5 algorithm from Weka machine-learning software. In this project, researchers created decision trees that could predict whether the bridge is posted or not. In addition to decision trees, random forests were created. Random forests are a group of decision trees that are varied in random samples until the optimal number of trees is achieved. Then, the majority prediction between all of the trees is taken. Since the number of posted bridges was about 10% of the entire population, different sampling techniques were used to address class imbalance. Models were created using the original data, majority undersampling so that half of the bridges in the training set are posted, and majority undersampling so that a quarter of the bridges in the training set are posted. Synthetic minority oversampling technique (SMOTE), in conjunction with the two majority undersampling techniques mentioned, were used as alternative models too. The metrics used to evaluate the models are accuracy rate, false positive rate, and false negative rate. Furthemore, a scale factor was used to count false negatives (the model predicting the bridge is posted when it is not according to NBI) more severly. The best model was found to be a random forest made up of 200 trees. This method was found to be suitable for predicting load postings, as shown in Table 26. Comparison of Performance of the Proposed Approach with Contemporary Practices. Furthermore, the team suggests that this tool could be used to identify bridges that may need to be investigated based on false positives or false negatives.

Table 26. Comparison of Performance of the Proposed Approach with Contemporary Practices

Method	FNR (%)	FPR (%)	Accuracy (%)
Proposed method (M3)	9.9	13.5	86.8
Oregon, Washington, Idaho, Kentucky DOT methods	89.5	2.3	90.0
Using condition ratings of Texas DOT flowchart	45.8	14.1	83.1

Bandara, R.P., Chan, T.H.T., and Thambirathnam, D.P., 2014, Frequency Response Function Based Damage Identification Using Principal Component Analysis and Pattern Recognition Technique

Frequency response function (FRF), ANN, and principal component analysis are combined in a procedure for identifying damage to structures. First, FRF data is collected and used to train an ANN. The ANN is then able to predict damage location and severity. The procedure can filter out noise so that the accuracy is not jeopardized. The procedure seems to be adequate at predicting single and multiple damage cases.

Hasancebi, O. and Dumlupinar,T., 2013, Detailed Load Rating Analyses of Bridge Populations Using Nonlinear Finite Element Models and Artificial Neural Networks

T-beam bridges were analyzed using a feed-forward, multi-layer ANN in this study. Governing parameters were span length, skew, bridge width, number of T-beams, beam depth, beam web width, beam spacing, slab thickness, reinforcement detailing, boundary conditions, material properties, and secondary load carrying components such as parapets and diaphragms, as shown

in Figure 81. The study had 90 bridges in the sample set, and it provided enough diversity for training (if 60 are used then the accuracy of the ANN compared to the FEM is reduced by 2-3%). The researchers found that the prediction improves by merely 0.5% if the number of training patterns is increased beyond a total of 200. Single layer architecture was found to be adequate for this study. Results were excellent for both moment and shear load ratings with R-values of 0.997 and 0.996 respectively.

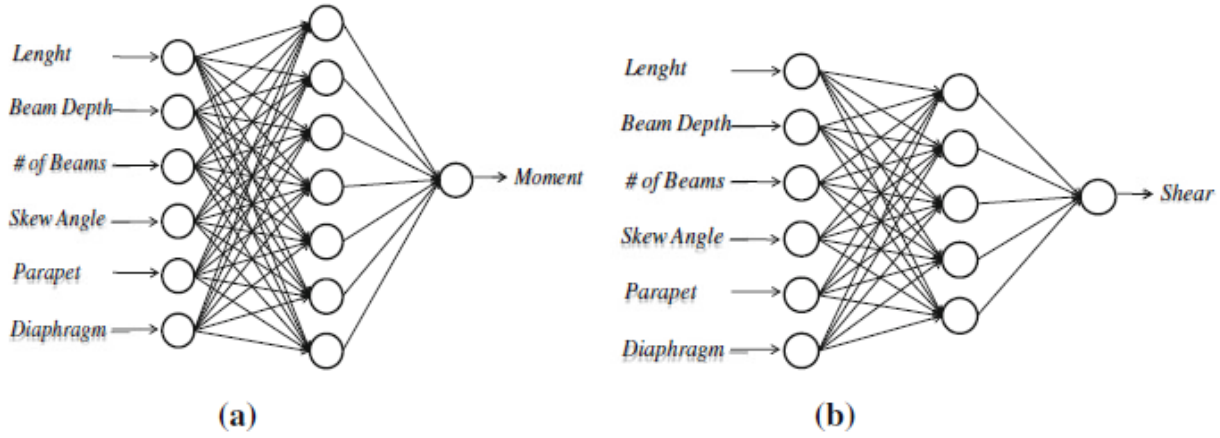

Figure 81. Network Architecture for Moment (a) and Shear (b) from Hasancebi and Dumlupinar (2013)

Shu, J., Zhang, Z., Gonzalez, I., and Karoumi, R., 2013, The Application of a Damage Detection Method Using Artificial Neural Network and Train-Induced Vibrations on a Simplified Railway Bridge Model

A backpropagation ANN was trained to predict damage for a one-span simply supported beam railway bridge. The bridge was modeled using an FEM program. The ANN was found to be able to predict the location and severity of damage. The researchers found that damage in the middle of the bridge is easier to detect than near the supports. Furthermore, the severity estimation depends heavily on an accurate damage location.

Tadesse, Z., Patel, K.A., Chaudhary, S., and Nagpal, A.K., 2012, Neural Networks for Prediction of Deflection in Composite Bridges

Three neural networks were developed to predict the mid-span deflections of simply supported bridges, two-span continuous bridges, and three-span continuous bridges. They made six FEMs for the bridges, and they compared the mid-span deflection to the outputs of the ANNs. The maximum error for any of the spans was 6.4%, and the root mean square error was 3.79%.

Hasancebi, O. and Dumlupinar, T., 2011, A Neural Network Approach for Approximate Force Response Analyses of a Bridge Population

An ANN was used to make an efficient method for approximate force response analyses of a concrete T-beam bridge population. Bridge input parameters were span length, skew, bridge width, number of T-beams, beam depth, beam web width, beam spacing, slab thickness, reinforcement detailing, boundary conditions, and secondary load carrying components such as parapets and end diaphragms, which can be visualized using Figure 83. The researchers also modeled the bridges with FEMs. Results of the ANN were compared to the FEM and found to be very reasonable. The researchers analyzed the parameters' sensitivities. Span length and beam depth were the most sensitive for moment output. Span length, skew angle, and beam depth were the most sensitive for shear output.

Sakr, M.A. and Sakla, S.S.S, 2008, Long-Term Deflection of Cracked Composite Beams with Nonlinear Partial Shear Interaction: Finite Element Modeling

The researchers presented a uniaxial nonlinear FE procedure for modeling the long-term behavior of composite beams at the serviceability limit state in this paper. They performed the procedure on four composite beams from literature. The deflections and stresses of the four beams were within an acceptable degree of accuracy. Neglecting the effect of concrete cracking leads to unrealistic deflection and stress deflections. A parametric study was done to study the effect of the nonlinearity of the load—slip relationship of shear connectors and the cracking the concrete deck on the long-term behavior of simply-supported composite beams. The effect of nonlinearity becomes more significant as the stiffness of the shear connection decreases.

Pendharkar, U., Chaudhary, S., and Nagpal, A.K., 2007, Neural Network for Bending Moment in Continuous Composite Beams Considering Cracking and Time Effects in Concrete

A methodology using an ANN was developed to predict the inelastic moments from the elastic moments while neglecting cracking in continuous composite beams. The eight parameters used as inputs are the age of loading, stiffness ratio of adjacent spans, cracking moment ratio at the support, load ratio of the adjacent spans, composite inertia ratio, cracking moment ratio at left and right adjacent support, and grade of concrete. Four networks with varying architecture details were produced that can all predict inelastic moments with reasonable accuracy.

Sheikh-Ahmad, J.S., Twomey, J., Kalla, D., and Lodhia, P., 2007, Multiple Regression and Committee Neural Network Force Prediction Models in Milling FRP

A tool is used to cut fiber-reinforced polymer chips. The goal of this research was to obtain a continuous specific cutting energy function for given material-cutting tool combination. The parameters were fiber orientation and uncut chip thickness. A committee neural network was used to predict the force of the tool to cut the chips. The neural network did an adequate job of predicting the force when compared to experimental data.

Guzelbey, I.H., Cevik, A., and Gogus, M.T., 2006, Prediction of Rotation Capacity of Wide Flange Beams Using Neural Networks

A backpropagation ANNs was trained to predict the rotation capacity of wide flange beams. The researchers compared its predictions to numerical results from literature at the time of the publication. The ANN inputs are half of the length of flange, the height of the web, the thickness of the flange, the thickness of the web, length of the beam, the yield strength of the flange, and yield strength of the web. The proposed ANN was found to be more accurate than numerical results as well as more practical and fast compared to FEM.

Sirca Jr., G.F. and Adeli, H., 2004, Counterpropagation Neural Network Model for Steel Girder Bridge Structures

The researchers developed a counter-propagation neural network for estimating detailed section properties of steel bridge girders needed in the LFD rating based on just cross-section area, moment of inertia, and section modulus. The motivation of this study was that many old bridges were rated by using working stress design that needed to be updated to LFD. Rating software used by state engineers at the time of the study required unavailable section properties, shown in Figure 82. The ANN used a training set made up of an AISC W-shape database and an additional 100 plate girder designs. The ANN did an adequate job at predicting the needed parameters. State engineers integrated the ANN into an intelligent decision support system that they used at the Ohio Department of Transportation at the time of the study's publication.

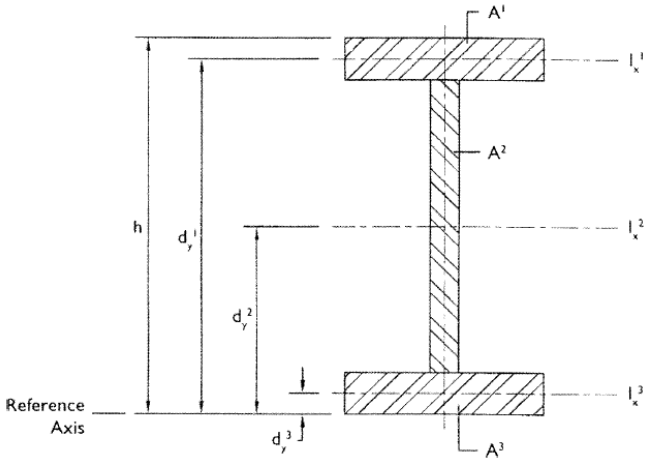

Figure 82. Detailed Description of Geometric Properties Sought After in Ohio

Hadi, M.N.S., 2003, Neural Networks Applications in Concrete Structures

A backpropagation, single-hidden layer ANN was trained to predict optimum beam designs and cost optimization of steel fibrous reinforced concrete beams. The researchers compared several types of backpropagation models and the Levenberg-Marquardt was found to have the least amount of epochs until results converge. The number of samples is a tradeoff: the more samples, the less error the model has, but the longer it takes to get the prediction. ANNs were found to be

a powerful tool that are potentially superior to conventional methods (time spent on calculations, accuracy, ease of use).

Adeli, H., 2001, Neural Networks in Civil Engineering: 1989-2000

This review article sums up neural network implementations in civil engineering. A backpropagation training algorithm has been used in civil engineering because of its simplicity. Estimating a bridge rating is something that has been attempted since 1997 (Cattan and Mohammadi). Neural networks could be used to speed up FEA since linear equations take up a lot of time in large-scale structures. Consolazio (2000) proposed merging neural networks with iterative equation-solving techniques. The author mentions many other applications outside of structural engineering.

Huang, C.C. and Loh, C.H., 2001, Nonlinear Identification of Dynamic Systems Using Neural Networks

This paper discusses the technical details of ANNs. The proposed ANN methodology was put to the test when researchers attempted to find the seismic response of a bridge. The ANN was found to be effective. However, it cannot be applied solely for damage detection. It could be used as a tool for engineers to use before advanced structural analysis is done.

Masri, S.F., Smyth, A.W., Chassiakos, A.G., and Caughey, T.K., 2000, Application of Neural Networks for Detection of Changes in Nonlinear Systems

An ANN was used to try to detect damage in structures. By using vibration measurements from a non-damaged structure, the ANN can detect damage. The ANN was then fed comparable vibration measurements from the same structure but during different episodes. The ANN would then be able to indicate any changes in vibration measurements which would be inferred as damage to the structure. The ANN was successful in detecting changes. However, this was not done on a large, parametric scale.

Chuang, P.H., Anthony, T.C., and Wu, X., 1998, Modeling the Capacity of Pin-Ended Slender Reinforced Concrete Columns Using Neural Networks

A multilayer feedforward neural network was found to be reasonable in predicting concrete column behavior. It could be implemented as a tool to check routine designs since results are instantaneous after training and testing is completed. 54 experimental high strength concrete column tests were adequately predicted using the neural network. The inputs used to train the neural network were b, h, d/h, ρ, $f_{y,}$ f_{cu}, e/h, and L/h.

Mikami, I., Tanaka, S., and Hiwatashi, T., 1998, Neural Network System for reasoning Residual Axial Forces of High-Strength Bolts in Steel Bridges

An automatic looseness detector was developed to measure how loose high-strength bolts are in bridges. The detector, however, cannot determine the residual axial forces of the bolts. The ANN could reasonably predict looseness based on the reaction and acceleration waveforms collected by the new tool.

Hegazy, T., Tully, S., and Marzouk, H., 1998, A Neural Network Approach for Predicting the Structural Behavior of Concrete Slabs

ANNSs were developed to predict the load-deflection behavior of concrete slabs, the final crack-pattern formation, and the reinforcing steel and concrete strain distributions at failure. The researchers used a total of 19 parameters as inputs. They compared the ANN predictions for the four analysis cases to well-documented tests. Considerable amounts of error were found, but the researchers propose that this would decrease with a larger training set. A user-friendly structural engineering tool was formulated using excel to give the engineer the results upon submitting inputs. Input descriptions is shown below in Table 27.

Table 27. Description of Inputs from Hegazy et al. (1998)

Category	Input factor
Slab geometric properties	1. Slab thickness (mm)
	2. Slab depth (mm)
	3. Ratio of rebar depth to slab depth
	4. Slab span (mm)
Aggregate properties	5. Aggregate type (1, sandstone; 2, granite)
	6. Aggregate size (mm)
Concrete properties	7. Concrete compressive strength (MPa)
	8. Concrete tensile strength (MPa)
	9. Concrete modulus of elasticity (MPa)
Reinforcement steel properties	10. Reinforcing steel ratio
	11. Rebar size (1, M10; 2, M15)
	12. Rebar shape (0, smooth; 1, deformed)
	13. Rebar spacing (mm)
	14. Number of rebar layers
	15. Rebar yield strength (×10 000 MPa)
	16. Rebar modulus of elasticity (×10 000 MPa)
	17. Type of shear reinforcement (0, none; 1, hat; 2, U-shape; 3, W-shape)
Loading and boundary conditions	18. Load type (0, axial; 1, bending; 2, axial + bending; 3, cyclic)
	19. Boundary conditions (0, simply supported; 1, fixed; 2, partially fixed)

Anderson, D., Hines, E.L., Arthur, S.J., and Eiap, E.L., 1997, Application of Artificial Neural Networks to the Prediction of Minor Axis Steel Connections

Steel frame designs usually involve minor-axis beam-to-column connections that govern restraint to the columns against buckling. Predicting behavior of those connections has its difficulties. An ANN was trained to predict how these connections will behave. The inputs were column depth of section, column flange thickness, column web thickness, beam flange breadth, beam depth of section, connection number of bolts, and connection plate thickness. The training data was obtained from experiments summarized in the paper. The researchers compared ANN predictions to experimental data, and it suited it well. The researchers attributed the error in the ANN it to the values that were at the edge of the sample space.

Cattan, J. and Mohammadi, J., 1997, Analysis of Bridge Condition Rating Data Using Neural Networks

An ANN was used to predict ratings for Chicago metropolitan railroad bridges. Parameters varied in bridge type, span type, substructure type, deck type, bridge height/clearance, bridge length, number of tracks on the bridge, number of spans composing the bridge, span length, date the span was built, date substructure was built, and date the deck was built. ANNs compared to fuzzy logic and Cooper rating and found to be superior to them. No FEM was performed and compared to the ANN though. The appropriate sample size was determined by using Eqn. 88:

$$\Delta = \frac{K\delta}{\sqrt{n}} \qquad \text{Eqn. 88}$$

where n is sample size, Δ is the confidence interval for the mean as a percentage below and above the mean, and δ is the coefficient of variation. K is obtained based on a confidence level from the table of the normal probability values.

Kushida, M., Miyamoto, A., and Kinoshita, K., 1997, Development of Concrete Bridge Rating Prototype Expert System with Machine Learning

The objective of this study was to evaluate the structural serviceability of concrete bridges by the specifications of the bridges to be evaluated, environmental conditions, traffic volume, and other subjective information gained through visual inspection. The researchers trained the ANN with results of a questionnaire survey conducted with domain experts. The neural network used fuzzy logic. Reasonable agreement between the results attained from the original system and the new system confirmed that knowledge for the new system was successfully acquired from the original system.

Mukherjee, A., Deshpande, J.M., and Anmala, J., 1996, Prediction of Buckling Load of Columns Using Artificial Neural Networks

An ANN was produced to predict the buckling load of columns. The motivation of this study was that semi-empirical formulas typically follow a lower bound to experimental observations which leave a significant portion of the actual column strength unutilized. A total of 20 examples, tested five times each, were used to train the ANN. The researchers found that the ANN could accurately predict the buckling behavior of columns based on the learning based on slenderness ratio, modulus of elasticity, and buckling load. The adequacy of the ANN can be seen in Figure 83.

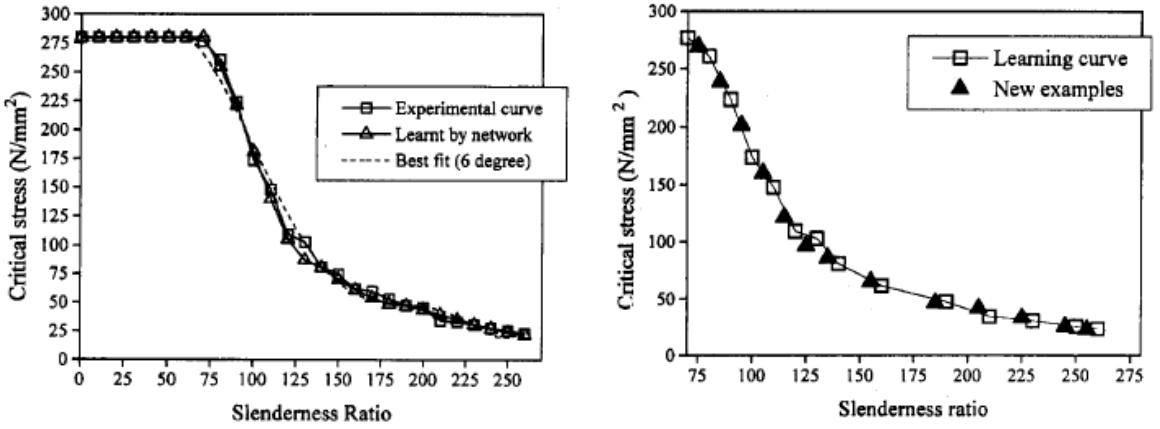

(a) Learning of Critical Stress for Columns (b) Performance Network

Figure 83. Critical column buckling stress by experiments and network predictions from Mukherjee et al. (1996)

Chen, H.M., Tsai, K. H., Qi, G.Z., Yang, J.C.S., and Amini, F., 1995, Neural Network for Structure Control

A backpropagation neural network was used to model the dynamic behavior of an apartment building during an earthquake. The data set used for training was the first 1,000 out of the total 2,000 points from the Morgan Hill earthquake (displacement, velocity, and acceleration). The neural network could then predict and nearly replicate the remaining points of the earthquake record.

Mukherjee, A. and Deshpande, J.M., 1995, Modeling Initial Design Process Using Artificial Neural Networks

It can take years of experience to develop intuition on formulating an initial design. A good initial design can reduce the time and money spent on analysis. The goal of this research project was to make an ANN that could make a preliminary design that includes the amount of tensile reinforcement required, depth of beam, width, cost per meter, and moment capacity. The input parameters are span length, dead load, live load, concrete grade, and steel type. The ANN was suitable at providing a good initial design and could aid structural engineers in the preliminary design stage.

Pandey, P.C. and Barai, S.V., 1995, Multilayer Perceptron in Damage Detection of Bridge Structures

This paper presents an application of multilayer perceptron that learns through backpropagation, in damage detection of steel bridge structures. A total of 40 training patterns and 10 additional testing patterns for verification were used. The engineers used an FE software to design find target outputs. The ANN worked well in determining where the damage is in the bridge. The

engineering significance of the investigation is that the measured data at only a few locations in the structure is needed to train the network for the damage identification.

Masri, S.F., Chassiakos, A.G., and Caughey, T.K., 1993, Identification of Nonlinear Dynamic Systems Using Neural Networks

An ANN was used to predict the internal forces of the same nonlinear oscillator under stochastic excitations of different magnitude. The model was simple, with two inputs and one output, and a total of 15 and 10 nodes in the first and second layers, respectively. This simple three-layer model was adequate to characterize internal forces of the damped Duffing oscillator.

Marquardt, D.W., 1963, An Algorithm for Least-Squares Estimation of Nonlinear Parameters

This paper describes an algorithm that determines the least-square. Like the Taylor series method, it converges rapidly once the vicinity of the converged values is reached. It is like the gradient methods in the way that it may converge from an initial guess which may be outside the region of convergence.

10.1.3 Studies of Static and Dynamic Load Testing

Yarnold, M., Golecki, T., Weidner, J., 2018, Identification of Composite Action Through Truck Load Testing

This paper describes methods that can be used to determine whether or not a slab on girder bridge is behaving compositely. Three cases studies are shown to illustrate the methods.

The first case study is a three span highway bridge in Tennessee. The two lane rural bridge has eight girders, two of which were instrumented for testing. Ambient traffic data was recorded over 10 days. The elastic neutral axis was determined by projecting the elastic strain profile over the entire girder depth. As shown in Figure 84, the elastic neutral axis projection near the top of this girder indicates that it was behaving compositely. Neutral axis projections for all load events were performed and nearly all were found to be around the elastic neutral axis of a truly composite section.

The second case study was carried out on a typical highway bridge with eight spans in Eastern United States. This bridge was selected for monitoring because it exhibited performance problems. Four girder of a single span was tested at quarterspans and midspans. It was found that the exterior girder had an elastic neutral axis very close to a composite neutral axis anywhere along the longitudinal length of the girder. However, girder 3 showed an elastic neutral axis closer to the noncomposite neutral axis.

Finally, a third load test was done to see if the load test would provide an improved load distribution and load rating for a nine girder steel bridge. The bridge was instrumented on all girders at one quarter-span and near the midspan. Although the bridge was rated as noncomposite, it was found that the bridge exhibited substantial partial composite behavior.

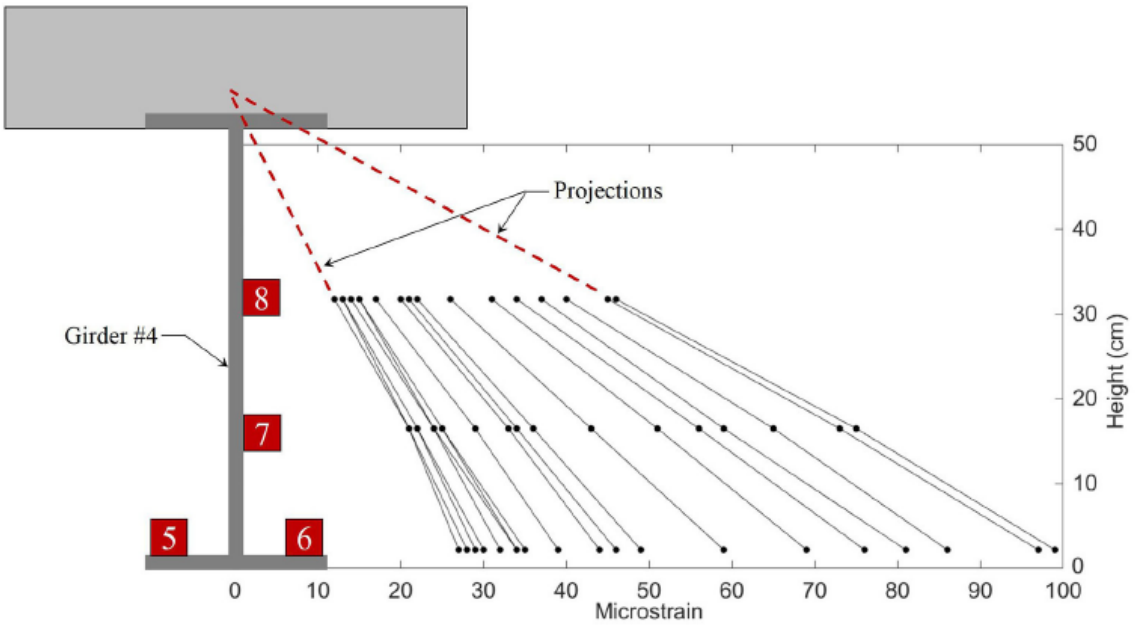

Figure 84. Strain Measurements at Girder #4 for Maximum Truck Events

The researchers recommended two instrumentation profiles for others investigating level of composite behavior in bridges. The two instrumentation profiles can be seen in Figure 85.

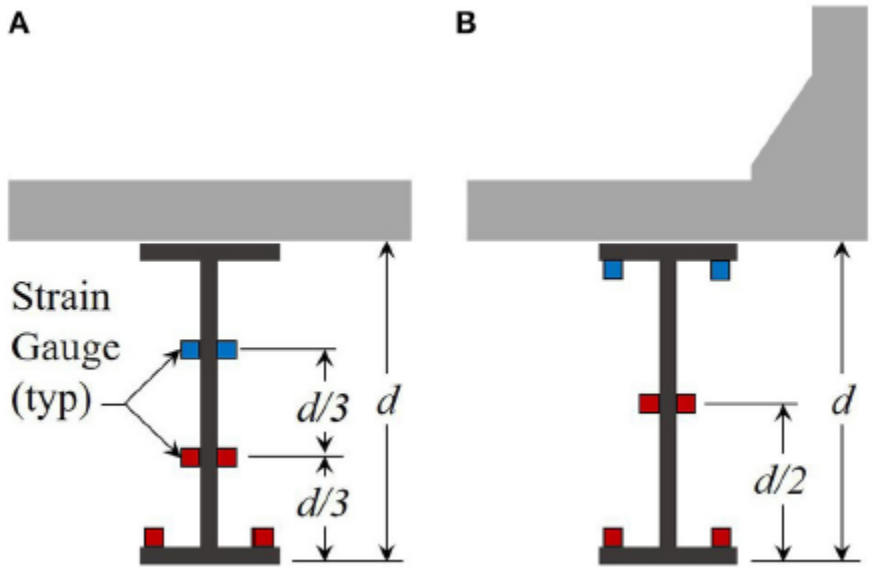

Figure 85. Recommended Strain Gauge Locations for (A) Interior Girder and (B) Exterior Girder with Symmetric Cross-Sections

Harris D.K., Civitillo, J.M., and G heitasi, A., 2016, Performance and Behavior of Hybrid Composite Beam Bridge in Virginia: Live Load Testing

A hybrid composite beam (HCB) was recently implemented in Colonial Beach, VA. The HCB system is made up of a glass fiber-reinforced polymer (FRP) box shell that encases a passively tied concrete arch. The tie reinforcement is an unstressed prestressing strand integrated into the FRP shell during production, and the arch is made up of self-consolidating concrete. This study was focused on evaluating and understanding the in-service performance of the bridge. A conclusion is that the FRP shell does not act compositely with the internal HCB components. The dynamic load allowance was found to be very different than AASHTO recommendations.

McConnell, J., Chajes, M., and Michaud, K., 2015. Field Testing of a Decommissioned Skewed Steel I-Girder Bridge: Analysis of System Effects

Researchers performed a decommissioned field test to calibrate and validate an FEM. The FEM was then used to apply much greater loads than the physical constraints allowed for in the field test. Higher strains in the FEA were attributed to partial fixity at the supports of the decommissioned bridge. The researchers determined that the AASHTO prediction is conservative because it determines load rating by using element-level capacity instead of system-level capacity. The researchers suggest that AASHTO should use a system-level rating system. The researchers also offer a simple upper-bound equation. AASHTO specifications had a capacity of 15 HS-20 trucks, the field test showed a strain that's equivalent to that induced by 17 trucks, and FEA showed that first flexural yielding of a single element was at 19 trucks.

Bell, E.D., Lefebvre, P.J., Sanayei, M., Brenner, B.R., Sipple, J.D., and Peddle, J., 2013, Objective Load Rating of a Steel-Girder Bridge Using Structural Modeling and Health Monitoring

The researchers analyzed and evaluated one bridge in this case study. SAP2000 enhanced designer's model (EDM) was calibrated using bridge data taken during a nondestructive load test and compared to AASHTO LRFR load ratings. EDM RFs were found to be higher than AASHTO in interior girders and nearly identical for exterior girders. They also determined load ratings for hypothetical damage. In a real world setting, load rating engineers would notice the damage during bridge inspection. The researchers analyzed a scenario on SAP2000 for when the section loss is in both an interior and exterior girder, and they found two damage rating factors. One was found assuming the section loss was over the entire length, and the other one assuming the section loss over the noted area only. Although the capacity decreases, system level capacity is still higher than what the LRFR rating would be. The figures shown in Figure 86 compare rating factors of LRFR, EDM, and EDM with the damage considered.

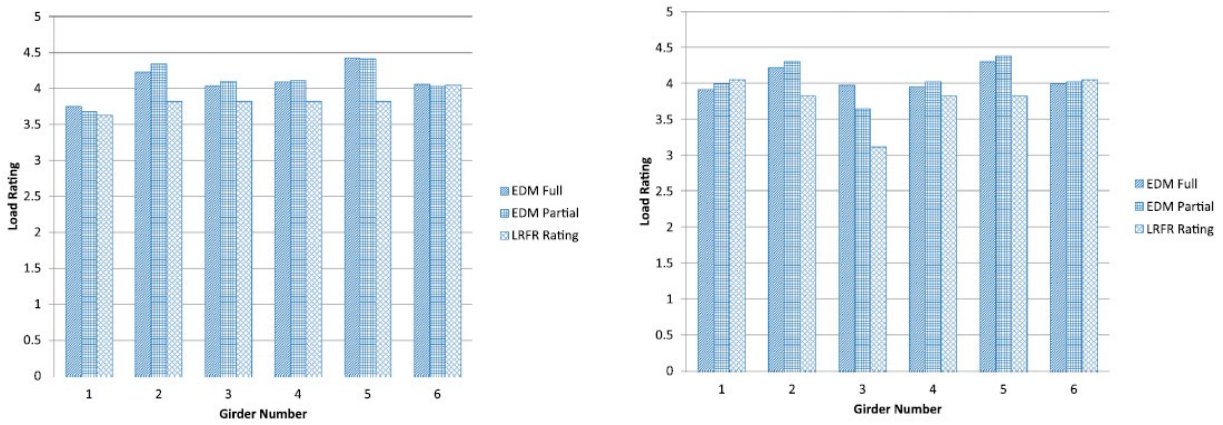

Figure 86. Comparison of RFs for Damage in Girders from Bell et al. (2013)

Hosteng, T., and Phares, B., 2013, Demonstration of Load Rating Capabilities Through Physical Load Testing: Ida County Bridge Case Study

Researchers performed load tests on a two-lane, three-span, continuous steel girder bridge built in 1949. Strain transducers were placed at the top and bottom flanges in locations specified in Figure 87. Trucks passed over the bridge at crawl speed in three locations: two feet away from one barrier, two feet away from the other barrier, and along the center of the roadway. Two runs were performed to verify the data. Distribution factors were estimated by taking the ratio of girder strains to the girder strains experienced by all of the girders. The researchers found distribution factors significantly lower than what AASHTO prescribes. By using the strain data, the researchers developed a two-dimensional finite element model to perform LFR load rating analyses on AASHTO rating vehicles. The operating load ratings for all of the analyses were found to be greater than one despite the bridge being load posted. A summary of the bridge critical rating factors is shown in Table 28.

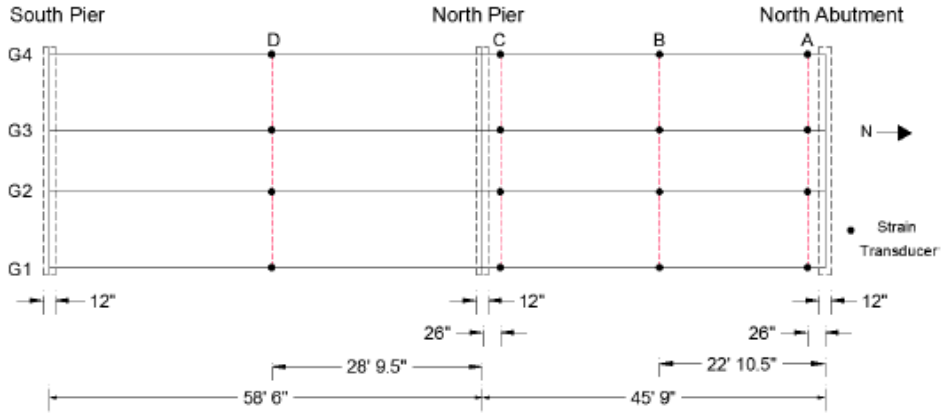

Figure 87. Ida County Bridge Plan View of Strain Transducer Locations

Table 28. Ida County Bridge Critical Rating Factors

Rating Vehicle	Location/Limiting Capacity	Inventory Rating Factor		Operating Rating Factor	
		Two Lane	One Lane	Two Lane	One Lane
HS-20(14)	Two Lane Interior, One Lane Exterior, Center Span, (+) Flexure	0.80	1.10	1.34	1.84
HS-20(22)	Two Lane Interior, One Lane Exterior, Center Span, (+) Flexure	0.96	1.31	1.60	2.19
HS-20(30)	Two Lane Interior, One Lane Exterior, Center Span, (+) Flexure	1.10	1.52	1.84	2.53
Type 4	Two Lane Interior, One Lane Exterior, Center Span, (+) Flexure	0.92	1.27	1.54	2.11
Type 3S3A	Two Lane Interior, One Lane Exterior, Center Span, (+) Flexure	0.98	1.35	1.64	2.26
Type 3-3	Two Lane Interior, One Lane Exterior, Center Span, (+) Flexure	1.00	1.35	1.67	2.26
Type 3S3B	Two Lane Interior, One Lane Exterior, Pier, (-) Flexure	1.01	1.39	1.69	2.32
Type 4S3	Two Lane Interior, One Lane Exterior, Pier, (-) Flexure	0.94	1.27	1.57	2.12
Type 3	Two Lane Interior, One Lane Exterior, Center Span, (+) Flexure	1.01	1.39	1.69	2.32
Type 3S2B	Two Lane Interior, One Lane Exterior, Pier, (-) Flexure	1.06	1.45	1.78	2.42
Type 3S2A	Two Lane Interior, One Lane Exterior, Center Span, (+) Flexure	1.05	1.44	1.75	2.40
Midspan and Endspan Lane Load	Two Lane Interior, One Lane Exterior, Pier, (-) Flexure	1.15	1.39	1.93	2.32
Both Endspans Lane Load	Two Lane Interior, One Lane Exterior, Pier, (-) Flexure	2.11	2.58	3.52	4.31
Midspan Lane Load	Two Lane Interior, One Lane Exterior, Pier, (-) Flexure	1.62	1.94	2.70	3.23
Single Endspan Lane Load	Two Lane Interior, One Lane Exterior, Pier, (-) Flexure	2.03	2.50	3.39	4.18

Sanayei, M., Phelps, J.E., Sipple, J.D., Bell, E.S., and Brenner, B.R., 2012, Instrumentation, Nondestructive Testing, and Finite-Element Model Updating for Bridge Evaluation Using Strain Measurements

An approach is introduced for the instrumentation of a bridge during construction, performing a nondestructive load test before the bridge is opened, creating a detailed FEM, calibrating the model using measured strains, and producing a load rating factor. Three load ratings calculated and compared. One was ASD in accordance to AASHTO load ratings using Virtis. Another was found by NDT strain data. The last one was found by using the calibrated baseline FEM. FEM typically had the highest load rating factors for all of the girders except for exterior girders. The benefits of the NDT are evident in all of the girders, except for the interior girders that govern the rating factor of the bridge. In this case, there is no benefit from testing the bridge. The findings can be seen in Figure 88.

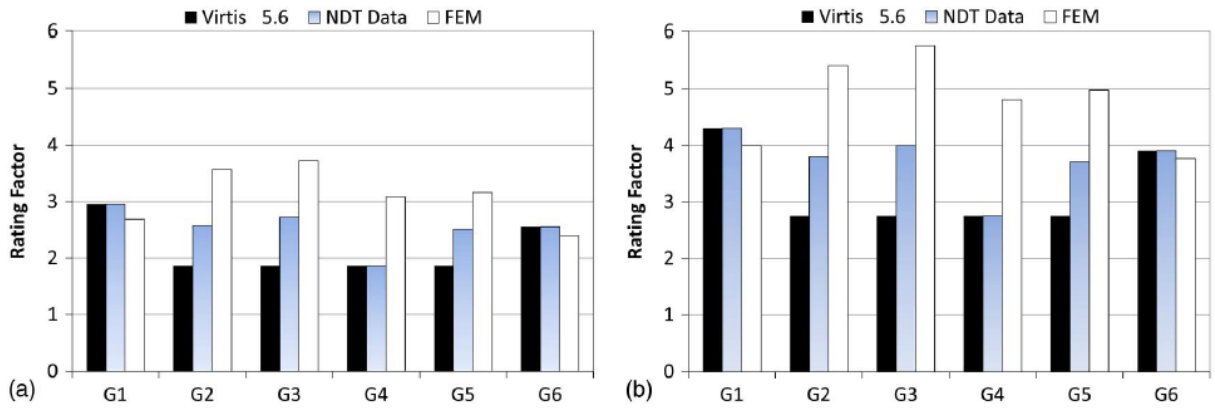

Figure 88. Vernon Avenue Bridge Rating Factors: (a) Inventory and (b) Operating from Sanayei et al. (2012)

Wipf, T.J. and Hosteng, T., 2010, Diagnostic Load Testing May Reduce Embargoes

Load rating engineers performed diagnostic load testing on 17 bridges in Iowa. Six of the 12 bridges were not posted after the test because the diagnostic test found the load rating to be too conservative. A summary of the diagnostic load tests is shown in 9.

Table 9. Effects of Diagnostic Test Results on Bridge Postings

Tested Bridges	Span (#, length)	Bridge Type	Data Analyzed*	Posting before Testing	Posting after Testing
IA-92 west of Massena	1, 40'	Girder	A,B	Yes	Yes
IA-57 in Butler County	1, 50'	Girder	A,B	Yes	Yes
IA-136 in Dubuque County	3, 210'	Girder	A,B	Yes	Yes
US-18 east of Hartley	2, 100'	Girder	A[1],B	Yes	Yes
IA-183 north of Pisgah	3, 96'	Girder	A,B	Yes	Yes
IA-60 near Sibley	1, 43'	Girder	A,B	Yes	Yes
IA-31 west of Quimby	1, 50'	Girder	A,B	Yes	No
US-30 near Wheatland	4, 368'	Girder	A,B,D	Yes	No
US-63 in Davis County	3, 210'	Girder	A,B	Yes	No
IA-78 in Keokuk County	4, 292'	Girder	A,B	Yes	No
IA-93 in Sumner	1, 61' 6"	Girder	A,B	Yes	No
IA-5 in Appanoose County	1, 51' 3"	Girder	A,B	Yes	No
I-80 in Jasper County	3, 100'	Slab	A,C	No	No
I-80 in Jasper County	5, 178'	Slab	A,C	No	No
I-80 in Poweshiek County	3, 114'	Slab	A,C	No	No
US-20 westbnd on-ramp no. Wellsburg	5, 198'	Slab	A,C	No	No

Bechtel, A.J., McConnell, J., and Chajes, M., 2010, Ultimate Capacity Destructive Testing and Finite-Element Analysis of Steel I-Girder Bridges

The problem with bridge evaluation codes is that bridges are rated with component-level capacities, not system-level capacities. A 1/5 scale slab-on-steel girder bridge was tested to ultimate capacity and then analytically modeled to see how different this is compared to bridge evaluation codes. The AASHTO ultimate capacity was found by dividing the plastic capacity of the governing girder by the AASHTO DF. The ultimate capacity of the tested bridge was approximately 9% higher than the AASHTO prediction. The researchers used FEA by using ABAQUS. Strains, deflections, and load distributions were compared between FEA and the physical test and found to be similar. Researchers concluded that FEA is an excellent tool if initial conditions can be properly identified. The testing matched up with the controlling deck failure case for FEA. They found that the deck failed at a load equivalent to 22 scaled AASHTO trucks. Only 30% of the steel in the critical cross section had yielded at the time of deck failure. The concrete deck strengthed also governed for the FEA.

Bechtel, A.J., McConnell, J.R., Chajes, M.J., 2009, Destructive Testing and Finite Element Analysis to Determine Ultimate Capacity of Skewed Steel I-Girder Bridges

The researchers tested a four-girder, simple-span bridge with varying levels of skew and tested it until failure. They compared the bridges' ultimate capacity to AASHTO capacities and FEM produced by Abaqus. The purpose of the study was to investigate how system-level analyses and how it corresponds with skew. The researchers found that the FEA modeled the behavior

adequately. Conclusions from the modeling include that tension softening of the concrete and the internal forces and boundary conditions have to be modeled carefully to get accurate results. The capacities from the destructive tests were higher than AASHTO predictions, as expected. They also found that bridges with higher skews had higher capacities because of the changes in effective length and relative stiffness of the beams running perpendicular to the girders that intersect the support at the obtuse corners of the bridge.

Jeffrey, A., Breña, S.F., Civjan, S.A., 2009, Evaluation of Bridge Performance and Rating through Non-destructive Load Testing

A report was prepared for the Vermont Agency of Transportation which included a literature review and two case study load tests on a 1920's reinforced concrete bridge and an interstate non-composite steel girder bridge that was damaged in three girders from getting hit by trucks passing underneath it. Load ratings were determined for the two bridges based on the load tests. Due to the scope of this project, the steel girder bridge will be described in greater detail.

Two identical and adjacent, three-span continuous steel girder bridges were tested with the goal of removing the load posting. The negative moments over the piers control the rating factor of these bridges. The piers are skewed at just under 42°. The bridges are made up of five A36 rolled shapes that are spaced at 7.5'.

The middle span was instrumented with 30 BDI strain gauges, as shown in Figure 89. One strain gauge was placed at the bottom of the top flange and bottom of the bottom flange for each instrumented location. Three lanes were used for crawl speed tests that correspond to East and West traffic lanes and a lane at the geometric center of the bridge.

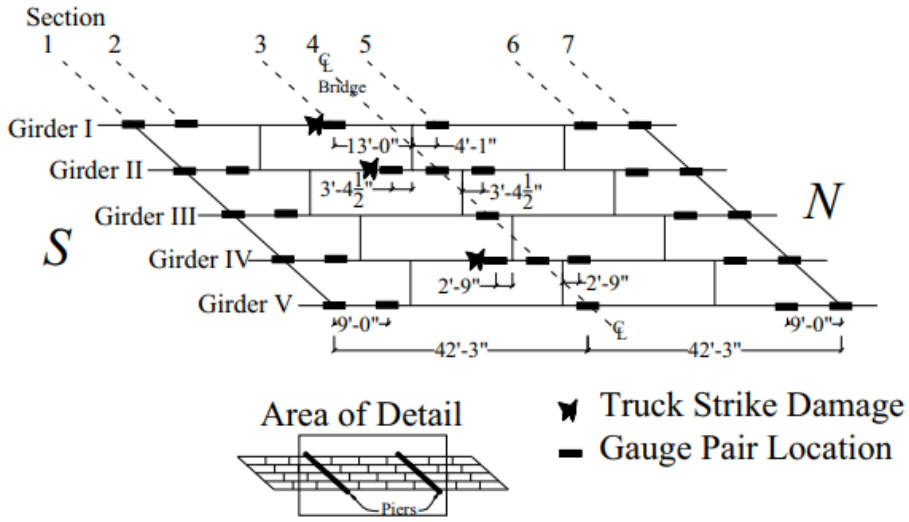

Figure 89. Diagram of Weathersfield Bridge Gauge Locations

Methods were described for deriving positive and negative moment effects and elastic neutral axis locations. To evaluate the performance of the girder with the damaged bottom flange, the

same load trucks were placed on the mirrored side of the bridge and traveling in the opposite direction. Since the bridge is symmetrical, the responses should be the same. Interestingly enough, it appears as though the girder damage is not noticeable in positive bending. However, when the girders' negative bending values were compared, discrepencies were noted.

It was found that neutral axis depths suggest that the bridge was behaving composite and midspan and partially composite at negative moment regions. The researchers noted that neutral axis varied due to multiple reasons. One reason it that error is introduced when the top strain gauge is near the neutral axis. Another reason that error was introduced is because the wheels ran near some of the instrumented girders. This caused for there to be spikes at some locations. Lastly, minimal errors in strain values that are small result in large neutral axis errors. Because of this, the researchers did not use strain measurements less than 20 με for neutral axis calculations.

Rating factors were determined by using AASHTO MBE adjustment factors. Rating factor benefits were observed from the load test. A noncalibrated finite element model was set up to compare to the load test data. The load test data did not match up perfectly with the finite element model, but it was a reasonable uncalibrated model that also yields benefits when compared to line girder analysis. Calibrating it to match up with the load test would yield better results.

Harris, D.K., Cousins, T., Murray, T.M., and Sotelino, E.D., 2008, Field Investigation of a Sandwich Plate System Bridge Deck

The research presented is on the results of a live-load test of the Shenley Bridge – the first bridge to employ the sandwich plate system in North America. The sandwich plate system is made up of a polyurethane core surrounded by two steel plates on the top and bottom. The researchers performed a field test and made an FEM. They compared measured GDFs to AASHTO LRFD, AASHTO standard, and CHBDC. The codes were found to be conservative except for CHBDC for the exterior girder subjected to multiple trucks. The dynamic response from AASHTO LRFD, AASHTO standard, and CHBDC was conservative in two out of three loading configurations (where the truck was positioned to straddle the interior girder).

Barth, K.E. and Wu, H., 2006, Efficient Nonlinear Finite Element Modeling of Slab on Steel Stringer Bridges

ABAQUS was used to capture the behavior of two composite steel girder with high-performance steel and one four-span continuous composite steel bridge that were also tested to failure. FEA matched up well with the testing data. The paper describes two modeling techniques in detail. The smeared crack model captures ultimate behavior well for simple span bridge superstructures. The concrete damage plasticity model is suggested to model continuous span bridges more reasonably than the smeared crack model.

Huang, H., Shenton, H.W., and Chajes, M.J., 2004, Load Distribution for a Highly Skewed Bridge: Testing and Analysis

A highly skewed bridge was tested and modeled using FEM to investigate the influences of model mesh, transverse stiffness, diaphragms, and modeling of the supports. The AASHTO LRFD formulas for transverse load distribution appear to be conservative for positive bending

for the two-span, continuous, slab-on-steel, 60-degree skew bridge. They found that the code is accurate but not conservative for negative bending.

Phares, B.M., Wipf, T.J., Klaiber, F.W., and Abu-Hawash, A., 2003, Bridge Load Rating Using Physical Testing

The researchers tested Boone Country Bridge #11 using Bridge Diagnostic, Inc. (BDI) with three different load vehicles. They found that the BDI found an average of 42% higher flexure capacity and 55% higher shear capacity than that derived from AASHTO LFD. The instrumentation plan can be seen in Figure 90.

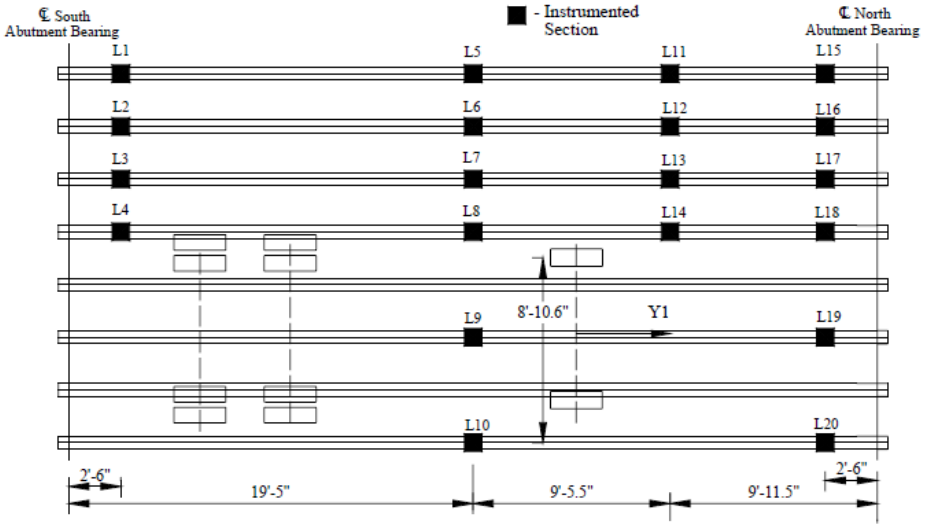

Figure 90. Boone County Bridge #11 Instrumentation Plan

Wipf, T.J., Phares, B.M., Klaiber, F.W., Wood, D.L., Mellingen, E., and Samuelson, A., 2003, Development of Bridge Load Testing Process for Load Evaluation

Bridge Diagnostics, Inc. (BDI) is a software and hardware that engineers developed to perform bridge rating systems based on field data. BDI was used to test three steel-girder bridges with concrete decks, two concrete slab bridges, and two steel-girder bridges with timber decks. The researchers determined that BDI produced accurate models with relative ease. The BDI load ratings were generally greater than AASHTO LFD ratings.

Cai, C.S. and Shahawy, M., 2003, Understanding Capacity Rating of Bridges from Load Tests

Field tests yield different results than analytical methods due to the difference in live load stresses and material conditions. In analytical analyses, some of these parameters are difficult to quantify. A proof load test (lower bound) is done by testing a bridge up to a target load or once the bridge shows any sign of distress. Proof load tests do not require complicated bridge analysis since the target load or a smaller load is reached. However, the risk of damaging the bridge is

higher than in other testing methods. A rating with a diagnosticdiagnostic load test (upper bound) uses a much lower load for testing. This method is preferred if analysis shows that a target load for a proof load test cannot be achieved safely or if the load capacity of the proof load test can't be performed. Reasons for not being able to perform the test include test vehicles not being heavy enough or traffic conditions prohibiting the proof load test. Results of diagnostic tests are used to calibrate a theoretical prediction of live load effects. Load rating using this method is identical to the linear extrapolation method which is the upper bound of the load rating. The total internal moment may be significantly different from applied total external moment due to many field factors that are usually ignored in calculations. Different test interpretations can yield different capacity ratings.

Nowak, A.S., Kim., S., and Stankiewicz, P.R., 2000, Analysis and Diagnostic Testing of a Bridge

The purpose of this study was to find the reasons why transverse crack patterns formed on a seven-span haunched steel-girder bridge built in 1968. As part of the methodology, field tests were performed to investigate what the bridge's actual stresses are under a test truck, and to see what the load distribution and impact factors are. Strain transducers were placed at the top and bottom flanges or near flanges on web. The instrumentation plan is shown below in Figure 91. Strains were collected at crawling-speed and high-speed with single truck and side-by-side trucks. The concrete from the deck was also tested and the water/cement ratio was higher than what AASHTO specifies.

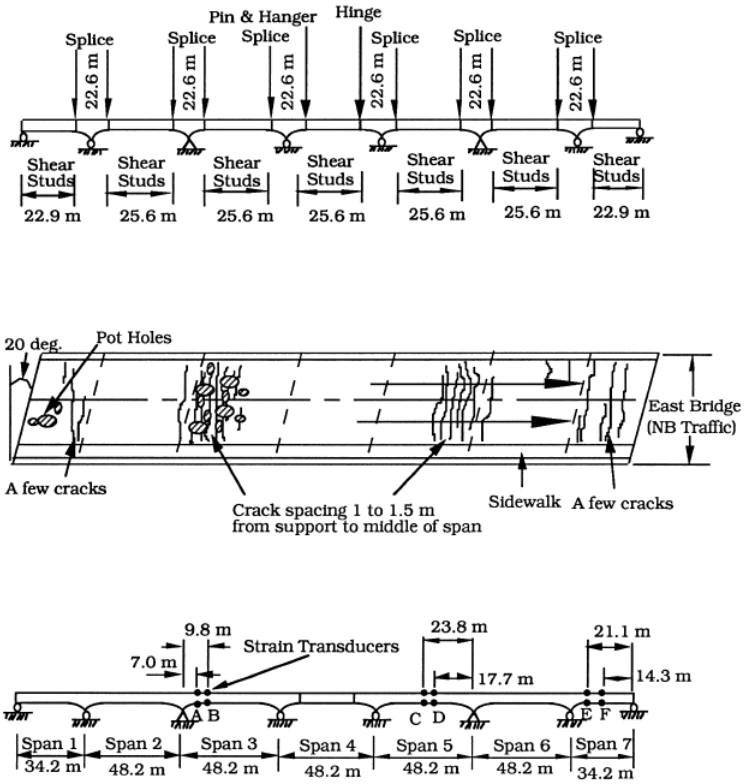

Figure 91. Elevation View of the Bridge, Major Crack Pattern, and Strain Transducer Locations

Distribution factors were determined in two ways: (1) the ratio of girder strains to the sum of all bottom-flange strains and (2) the ratio considering the differences in section modulus between girders because of the sidewalk and parapets. The researchers found that the distribution factors, found by either of the two methods, were much lower than contemporary AASHTO values. Furthermore, the distribution is more uniform when the second method is used.

Impact factors were found to be smaller than the contemporary AASHTO-specified value for all of the girders except for one exterior girder that has "no practical significance since the stress in girder 4 is small compared with stresses in other girders."

Finally, a FEM was made and used to find the causes of the transverse deck cracking. The results of the field test matched well with analyses performed on the FEM. However, the FEA live load stresses do not correspond to the observed crack patterns. Because of this inconsistency, the researchers have attributed the transverse deck cracking to deck pouring sequence and concrete shrinkage due to the high water/cement ratio.

Lichtenstein, A.G., Moses, F., Bakht, B., 1998., Manual for Bridge Rating Through Load Testing

Nondestructive load test applications, considerations and benefits are briefly summarized. The general considerations of bridge load tests, such as dead loads, dynamic and static live loads,

fatigue, impact, and the types of bridges are summarized. The researchers advise the reader to avoid load tests for the following reasons:

- The cost of testing reaches or exceeds the cost of bridge rehabilitation.
- The bridge, according to calculations, cannot sustain even the lowest level of load.
- Calculations of weak components of the bridge indicate that a field test is unlikely to show the prospect of improvement in load-carrying capacity.
- In the case of concrete beam bridges, there is the possibility of sudden shear type of failure.
- The forces due to restrained volume changes from temperature induced stresses may not be accounted for by load tests. Note that significant strains and corresponding stresses induced by temperature changes could invalidate load test results especially when end bearings are frozen.
- There are frozen joints and bearing which could cause sudden release of energy during a load test.
- Load tests may be impractical because of inadequate access to the span.
- Soil and foundation conditions are suspect. The bridge has severely deteriorated piers and pier caps, especially at expansion joints where water and salt have caused severe corrosion of reinforcement.

According to the manual, unintended composite action is a result of noncomposite steel girder bridges acting compositely. However, the composite behavior can be compromised as the load is increased. The researchers propose a limiting bond stress between the concrete slab and steel girders of 70 psi for concrete decks with a compressive strength of 3 ksi. For partially or fully embedded flanges, 100 psi for the limiting bond stress is recommended. Other effects, such as end bearing restraint, additional parapet and sidewalk stiffness, secondary member participation can potentially appear in load test data.

Recommended procedures for planning a load test are outlined in this report. Various data acquisition methods are presented as well. Illustrative diagnostic and proof load test examples are presented for multiple kinds of bridges. This report was cited in the AASHTO MBE in the diagnostic load test section for its walk-through example.

Ghosn, A., Moses, F., 1998, NCHRP Report 406: Redundancy in Highway Bridge Superstructures

In this report, researchers investigate redundancy and they present a methodology on how to consider redundancy in design and load capacity evaluation. The methodology is made up of tables of system factors that can be used to modify AASHTO predictions of ultimate capacities. For bridges outside of the tables' scope, they also present a direct analysis procedure.

Kim, S. and Nowak, A.S., 1997, Load Distribution and Impact Factors for I-Girder Bridges

The researchers monitored two simply supported I-girder bridges for two consecutive days under normal traffic, and captured strain data from the girders. They processed the data, and obtained

the statistical parameters for the girder distribution and impact factors. They found that both the load distribution and impact factors are lower than AASHTO values.

Kathol, S., Azizinamini, A., and Luedke, J., 1995, Strength Capacity of Steel Girder Bridges

Four destructive tests were performed to investigate the global and local behavior of steel girder bridges with and without diaphragms. The study compares the destructive test data to AASHTO LRFD empirical methods of the time. The researchers found that the contributions of diaphragms to capacity was minimal. The deflection of the steel bridge due to shrinkage was found to be less than that predicted by AASHTO. The researchers were also able to make an FEM, that had been validated with test data, which would eliminate specifying distribution factors.

Stallings, J.M. and Yoo, C.H., 1993, Tests and Ratings of Short-Span Steel Bridges

The researchers performed static and dynamic diagnostic tests on three short-span, two-lane, steel-girder bridges. Some of the tests exhibited unintended composite action through friction and bond between the deck and girders. Girder strains calculated using the measured wheel-load distribution factors were consistently larger than the measured strains. They calculated impact factors using various methods. Impact factors based on the combined response of all girders were larger than those values calculated for the most critically loaded girder.

Bakht, B. and Jaeger, L.G. 1990, Bridge Testing – A Surprise Every Time

This paper lists some of the various surprises encountered in bridge testing that may have a significant influence on the load-carrying capacities of bridges. Some surprises include enhanced flexural stiffness of slab-on-girder bridges, composite action in non-composite bridges, the failure mode of cracking deck slab, as well as many others.

Cheung, M.S., Gardner, N.J., NG, S.F., 1987, Load Distribution Characteristics of Slab-on-Girder Bridges at Ultimate

In this study, researchers made a scaled bridge for testing purposes, and strains and deflections were found to be similar to FEA. The values determined from resistant bending moments of the steel girders indicate that there is a significant reduction in load distribution factors between linear elastic and post yielding stages. The shape factor of the girder section can be the reduction factor. The researchers claim that load redistribution and residual stresses are insignificant before the formation of a plastic hinge and can be ignored up until then.

Ghosn, A., Moses, F., and Gobieski, J., 1986, Evaluation of Steel Bridges Using In-Service Testing

This evaluation discusses the benefit of testing bridges to incorporate into rating process. The researchers tested five bridges, and the maximum stresses were below what the conventional procedures would predict. The difference in results are attributed to unintended composite action, secondary elements adding stiffness, girder distributions being more conservative than AASHTO predictions, and impact values being different.

Burdette, E.G., Goodpasture, D.W., 1971, Full-Scale Bridge Testing: An Evaluation of Bridge Design Criteria

The researchers tested girder deck bridges in Tennessee to evaluate bridge design topics such as the lateral distribution of load, dynamic response, ultimate strength, and mode of failure. They found that the load distribution factors are similar to that of other studies. An analytical method based on strain compatibility predicted the ultimate capacity within 9% for three out of the four bridges tested. They also found the AASHTO ultimate loads to be somewhat conservative compared to the load tests.

10.2 Rating Factor Modification Equations

The FEMs' loads were an AASHTO HS-20 load with LRFR load factors. This is inconsistent with LRFR since the load vehicle omits the lane load that the AASHTO HL-93 uses. Because of this inconsistency, two calibration equations were developed to get load ratings consistent with LRFR load ratings and LFR load ratings. Eqn. 89 is the standard load rating equation. In the preexisting model, the equation used a live load induced by an HS-20 (LL), and used LRFR factors. Eqn. 90 is the calibration equation to get a rating factor that is consistent with LFR specifications. Eqn. 91 is the calibration equation to get a rating factor that corresponds to LRFR. The calibration equations were derived by multiplying by the ratio of LRFR to LFR factors and live load effects.

$$RF = \frac{C - \gamma_{DL} * DL}{\gamma_{LL}(LL + IM)} \quad \text{Eqn. 89}$$

$$RF_{LFR} = RF * (\frac{\gamma_{LL,LRFR}}{\gamma_{LL,LFR}}) * (\frac{IM_{LRFR}}{IM_{LFR}}) * (\frac{C - \gamma_{DL,LFR} * DL}{C - \gamma_{DL,LRFR} * DL}) \quad \text{Eqn. 90}$$

$$RF_{LRFR} = RF * (\frac{M_{HS-20}}{M_{HL-93}}) \quad \text{Eqn. 91}$$

The FEM was performed assuming composite action. However, it became apparent that a load rating factor based on noncomposite behavior is desirable to correspond to state load rating summary sheets. Equation 92 shows another calibration to get the noncomposite load rating.

$$RF_{nc} = RF_c * \frac{(C_{nc} - D)}{(C_c - D)} \quad \text{Eqn. 92}$$

10.3 ANN Data

10.3.1 Moment ANN Training and Testing Data

The manila-colored cells designate bridges that were used in the design set. The green-colored cells designate bridges that were used in the design-set size for some ANNs and additional testing bridges in reduced size ANNs. The aqua-colored cells designate bridges that were used in the independent testing set.

Bridge	L (m)	s (m)	Kg (Gmm^4)	CF (1 or 0)	#girders	Skew (deg.)	de (m)	Deck ts(mm)	fc' (MPa)	fy (MPa)	Moment $GDF_{maximum}$
C000621615	11.786	2.388	124.295	1	4	0	0.69	229	20.69	248.22	0.654
C003403910	15.240	1.981	55.171	1	4	0	0.69	165	20.69	248.22	0.601
C007802440	18.440	2.184	60.850	1	4	0	0.41	178	20.69	248.22	0.573
C006500230	9.093	0.854	10.914	1	11	0	0.00	178	27.58	344.75	0.246
C007203715	9.144	1.473	7.518	1	5	0	0.09	152	20.69	248.22	0.414
C006341615	17.983	0.978	24.279	1	7	0	0.05	152	20.69	248.22	0.298
C006301204P	17.983	0.984	25.870	1	7	0	0.02	152	17.24	206.85	0.302
C006313310P	7.010	1.438	4.954	1	6	15	0.06	152	20.69	248.22	0.382
C009202210	12.192	1.219	15.479	1	6	0	0.25	152	20.69	248.22	0.370
C008101013P	6.096	1.295	23.279	1	6	0	0.42	152	20.69	248.22	0.434
C001111430	10.973	1.981	31.674	1	4	0	0.69	191	20.69	248.22	0.585
C007904705	7.141	2.057	27.549	1	5	23	0.00	178	24.13	248.22	0.544
C004702203	6.909	1.791	5.314	0	5	0	0.07	127	20.69	248.22	0.513
C002014017	6.096	1.219	16.448	1	7	0	0.61	178	20.69	248.22	0.482
C005913903	11.735	1.118	10.396	1	8	0	0.28	152	20.69	248.22	0.341
C000602505	9.144	1.118	15.005	1	5	15	0.77	152	17.24	206.85	0.469
C007424540	24.854	2.438	85.164	1	4	15	0.61	178	27.58	344.75	0.626
C009111705	9.626	1.600	19.540	1	5	0	0.77	200	20.69	248.22	0.519

C002001505	8.534	1.295	20.192	0	7	0	0.62	178	20.69	248.22	0.474
C009103005	22.600	2.515	132.446	1	4	0	0.12	167	20.69	248.22	0.600
C007815273	12.497	1.918	67.504	1	4	32	0.70	178	20.69	248.22	0.583
C005463410	7.283	0.813	8.579	1	10	0	-0.02	178	20.69	248.22	0.271
C007603710	11.887	1.829	28.183	1	4	0	0.43	152	20.69	248.22	0.563
C001716105	14.675	1.775	56.245	1	6	45	0.27	178	24.13	344.75	0.373
C006607105P	21.031	2.350	103.109	1	4	0	0.79	178	20.69	248.22	0.657
C007302705P	17.805	1.718	43.257	1	6	30	0.13	203	20.69	344.75	0.370
C000102115	14.561	1.413	32.764	1	7	20	0.03	203	27.58	344.75	0.339
C007010905	11.278	0.975	19.264	1	7	0	0.73	133	17.24	206.85	0.437
C006710205	24.384	2.057	135.193	1	4	0	0.60	178	20.69	248.22	0.568
C007025010	24.866	1.905	140.400	1	5	0	0.15	152	20.69	248.22	0.505
C001403305P	24.079	1.702	89.674	1	5	0	-0.09	127	20.69	248.22	0.482
C007805310P	9.296	1.257	12.586	1	8	0	0.17	178	20.69	248.22	0.325
C007102605	15.240	1.499	36.481	1	7	0	0.08	203	27.58	344.75	0.357
C001401535	10.668	2.121	27.515	1	5	30	0.03	178	27.58	248.22	0.497
C006305115	8.230	1.194	8.161	1	7	20	0.06	152	20.69	248.22	0.313
C000102908	23.063	2.032	113.440	1	5	0	0.26	152	20.69	248.22	0.498
C001712925	11.855	1.808	36.552	1	6	0	0.20	178	24.13	344.75	0.457
C007000515	11.887	0.889	11.428	1	9	0	0.42	152	20.69	248.22	0.304
C007103415	8.807	0.864	8.264	1	11	0	0.25	203	27.58	248.22	0.265
C004803915	8.763	0.838	16.033	0	8	0	0.11	140	17.24	206.85	0.258
C005901825	8.839	1.956	25.751	0	5	45	0.05	152	20.69	248.22	0.476
C001424750	15.697	2.216	144.110	0	5	0	0.14	178	20.69	248.22	0.568
C001210930	14.935	1.753	122.459	1	6	0	-0.11	178	20.69	248.22	0.460
C006311110	17.907	1.537	84.547	0	6	0	0.13	165	20.69	248.22	0.407
C005903110	11.582	0.965	11.722	1	9	0	-0.05	152	20.69	248.22	0.268
C006924230	6.248	1.524	5.333	1	6	0	0.46	178	20.69	248.22	0.474

C005901805	18.161	1.397	51.664	1	7	0	-0.08	152	20.69	248.22	0.351
C001400730	19.507	1.676	72.955	1	6	0	0.06	178	20.69	344.75	0.410
C002003405	8.534	1.219	18.908	0	7	0	0.61	178	20.69	248.22	0.432
C001823610	11.976	1.092	14.176	1	8	0	0.38	127	20.69	248.22	0.365
C009133625	14.935	0.861	23.405	1	7	0	0.48	159	20.69	248.22	0.348
C002602910	17.983	1.188	53.629	1	8	0	0.18	178	20.69	248.22	0.362
C003303710	18.288	1.219	41.497	1	8	0	0.30	152	20.69	248.22	0.348
C001411615P	16.764	1.670	60.705	1	6	20	0.09	178	27.58	248.22	0.394
C007101130	14.780	1.770	75.551	1	6	30	0.27	203	20.69	344.75	0.407
C001224325	17.983	1.753	90.872	1	6	0	-0.11	178	17.24	248.22	0.436
C003413410	21.056	1.969	92.415	1	4	0	0.78	203	17.24	206.85	0.546
C007602705	14.935	1.829	45.661	0	4	0	0.46	152	20.69	227.54	0.561
C005900525	11.735	0.991	8.455	1	7	0	0.00	140	20.69	227.54	0.298
C008803505	8.814	1.295	6.782	1	5	0	0.46	127	20.69	227.54	0.407
C002001220	8.687	1.219	20.175	0	7	40	0.61	178	20.69	248.22	0.361
C001401710	13.503	2.105	69.179	1	5	0	0.04	203	20.69	248.22	0.529
C002001215	8.687	1.219	16.602	0	7	35	0.61	152	20.69	248.22	0.375
C000103420	15.215	0.972	17.697	1	9	0	0.05	165	20.69	248.22	0.345
C005922330	11.735	1.168	9.940	1	6	0	0.08	152	20.69	248.22	0.343
C008722020	11.887	1.753	40.644	1	6	15	-0.11	178	27.58	248.22	0.443
C001202005	11.918	1.314	38.333	0	6	0	0.69	152	20.69	248.22	0.512
C006300825P	8.839	1.029	6.933	1	8	0	0.00	140	20.69	248.22	0.275
C001103815	23.311	1.676	103.774	1	6	0	0.38	165	20.69	248.22	0.496
C000604715	18.034	1.543	93.067	1	6	0	0.49	203	20.69	248.22	0.456
C006602010	21.336	2.057	97.171	1	4	0	0.57	203	20.69	248.22	0.561
C001201410	8.839	1.753	18.992	1	6	30	-0.11	178	20.69	248.22	0.404
C007824260	18.136	1.905	73.369	1	5	0	0.61	178	20.69	248.22	0.517

C002012435	17.678	1.245	38.011	1	7	0	0.50	127	20.69	248.22	0.493
C007932415	14.630	1.372	32.621	1	5	35	0.61	203	20.69	227.54	0.447
C002004730	8.534	1.219	20.044	0	7	0	0.69	178	20.69	248.22	0.433
C002702510	14.732	1.727	40.802	1	5	25	0.20	152	20.69	248.22	0.470
C001205010	14.630	1.346	61.658	0	6	15	0.61	152	20.69	248.22	0.482
C002004725	11.582	1.219	26.896	1	7	0	0.61	178	20.69	248.22	0.433
C001234905	17.983	1.829	48.628	1	4	33	0.33	165	20.69	248.22	0.527
C005900505	11.811	1.753	45.724	0	5	0	0.08	178	20.69	248.22	0.510
C005901410	17.882	1.397	35.029	1	7	0	0.03	152	20.69	248.22	0.362
C002701945	14.707	1.778	26.389	1	5	0	0.71	178	20.69	248.22	0.532
C007910405	8.534	1.794	21.569	1	6	0	0.16	178	20.69	248.22	0.459
C008404020	9.550	1.829	25.698	0	5	0	0.00	152	17.24	227.54	0.510
C003416235	10.541	1.295	20.054	1	7	0	-0.01	178	20.69	248.22	0.368
C004712915	7.588	1.699	11.473	1	6	0	0.19	178	24.13	344.75	0.489
C005901502	7.315	1.803	10.254	1	6	0	-0.01	178	20.69	248.22	0.481
C002004730	8.712	1.219	20.175	0	7	0	0.60	178	20.69	248.22	0.426
C004507603	8.153	1.194	17.564	0	7	0	0.06	152	20.69	248.22	0.349
C003704805P	15.278	2.057	58.662	1	5	0	0.15	152	20.69	248.22	0.520
C002012040	8.534	1.219	26.669	0	7	0	0.61	178	20.69	248.22	0.436
C005914820	11.836	1.524	37.880	1	6	20	0.15	178	20.69	248.22	0.385
C000134022	8.839	1.702	24.582	1	6	0	0.01	152	20.69	248.22	0.431
C004513915	13.884	1.321	35.222	1	7	0	0.00	178	20.69	248.22	0.370
C001705805	7.798	1.219	8.479	1	7	0	0.58	152	20.69	248.22	0.444
C009143435	15.570	1.286	23.607	1	5	0	0.40	165	20.69	248.22	0.434
C007443235	9.347	1.778	17.229	1	5	30	0.10	152	20.69	248.22	0.444
C002001627	6.401	1.219	18.400	0	7	0	0.61	178	20.69	248.22	0.485
C005900915	10.363	1.575	35.508	1	6	30	0.03	178	20.69	248.22	0.370

C005902215	17.831	1.168	34.034	1	7	0	0.08	152	20.69	248.22	0.345
C000602310	11.278	1.168	21.091	0	6	0	0.05	165	17.24	227.54	0.370
C001902340	8.738	1.321	9.940	1	7	0	0.02	152	20.69	248.22	0.340
C009114505	8.306	1.302	9.989	1	6	0	0.02	140	17.24	206.85	0.351
C008511515	7.925	1.321	25.798	0	7	0	0.30	203	20.69	248.22	0.395
C008002310	12.268	1.981	42.313	1	5	0	0.38	178	20.69	248.22	0.504
C005901925	14.834	1.295	23.570	1	5	0	0.46	152	20.69	248.22	0.466
C009314130	11.855	1.686	43.257	1	6	0	0.00	203	20.69	248.22	0.441
C004903005	11.252	1.200	16.496	1	6	0	0.05	152	20.69	248.22	0.370
C002000707P	8.534	1.219	17.487	0	7	0	0.61	178	20.69	248.22	0.417
C005913505	18.288	1.422	20.935	1	6	0	0.03	152	20.69	248.22	0.475
C008602105P	17.888	1.791	96.927	1	5	0	0.00	178	27.58	248.22	0.516
C003302510	13.716	1.765	38.757	1	5	0	0.13	152	20.69	248.22	0.497
C004802905	8.534	2.057	31.555	1	5	45	0.05	178	20.69	248.22	0.456
C007001220	17.983	1.346	51.539	1	6	0	0.61	165	20.69	206.85	0.465
C007213110	11.887	1.773	28.497	1	5	0	0.11	152	20.69	227.54	0.487
C007911205	14.808	2.057	120.415	1	5	20	0.38	203	24.13	248.22	0.525
C005913020	11.836	1.168	18.100	1	7	0	0.08	152	20.69	248.22	0.336
C005901830	14.935	1.676	38.359	1	6	0	0.08	203	20.69	248.22	0.418
C000226205	12.192	1.905	35.412	1	5	0	0.15	191	24.13	248.22	0.492
C001526720	8.785	1.822	30.955	1	5	20	0.01	178	20.69	248.22	0.487
C001800605	11.989	1.092	16.517	1	8	0	0.41	165	20.69	248.22	0.358
C002704210P	15.240	1.524	34.988	1	5	20	0.61	178	20.69	248.22	0.482
C004720810	7.468	1.448	5.617	0	5	0	0.15	152	20.69	248.22	0.430
C009102805	17.856	1.930	64.849	1	5	0	0.10	178	27.58	344.75	0.498
C005900730	11.786	1.219	15.614	1	7	0	-0.03	152	20.69	248.22	0.337
C003406020	12.573	1.524	20.712	1	5	0	0.61	178	20.69	248.22	0.461
C002013720	7.087	1.219	15.218	0	7	0	0.61	178	20.69	248.22	0.480

C000805510P	7.315	1.191	11.320	1	7	0	0.16	178	20.69	248.22	0.380
C001301620	13.716	1.905	45.147	1	4	15	0.50	165	17.24	227.54	0.531
C002000823	7.010	1.219	14.137	0	7	0	0.61	178	20.69	248.22	0.460
C001900130	9.144	1.791	22.898	1	6	0	0.09	152	20.69	248.22	0.451
C004529620	9.601	1.181	19.195	0	7	0	0.05	152	20.69	248.22	0.360
C007202710	11.887	1.581	23.774	1	6	0	0.01	152	20.69	248.22	0.393
C001101705	14.935	1.753	39.173	1	5	0	0.15	165	20.69	248.22	0.482
C004800415	18.745	1.829	88.995	1	5	0	0.53	165	20.69	248.22	0.526
C007602610	11.735	1.524	44.889	0	6	20	0.08	152	17.24	206.85	0.397
C008402410	11.963	1.473	23.128	1	5	0	0.03	152	20.69	248.22	0.439
C005121315P	9.144	1.822	22.898	1	5	0	0.01	152	20.69	248.22	0.480
C001201210	7.620	1.794	7.188	1	6	0	0.05	152	20.69	248.22	0.494
C007012235	11.887	1.339	29.265	1	6	0	0.63	165	17.24	206.85	0.468
C002705115	8.809	1.499	12.300	1	6	0	0.55	152	20.69	248.22	0.441
C006313105	11.887	0.991	12.518	1	7	0	0.00	152	17.24	206.85	0.296
C001814715	11.976	1.092	16.337	1	8	0	0.37	152	20.69	248.22	0.354
C002004010	14.630	1.219	56.953	1	7	0	0.61	178	20.69	248.22	0.449
C009123545	9.805	1.956	15.981	1	5	0	-0.01	165	20.69	248.22	0.488
C007004115	17.882	1.241	39.775	1	6	0	0.74	152	20.69	248.22	0.465
C007203805	8.839	1.784	8.222	1	5	0	0.15	152	20.69	248.22	0.448
C001900815	15.240	1.575	38.726	1	6	0	0.18	152	20.69	248.22	0.413
C005606105	10.331	1.692	27.549	1	6	0	0.22	178	20.69	248.22	0.448
C005901517	8.839	1.676	21.700	1	6	0	0.08	178	20.69	248.22	0.439
C001105220	15.062	1.695	26.289	0	6	0	0.03	152	20.69	248.22	0.438
C005904610	9.296	1.016	7.527	1	8	0	0.03	152	20.69	248.22	0.347
C002003505	16.154	1.219	75.747	1	7	0	0.61	178	20.69	248.22	0.438
C007100625	14.840	1.775	58.437	1	6	0	0.25	203	24.13	344.75	0.453
C005913030	10.363	1.676	26.430	1	6	0	0.08	178	20.69	248.22	0.446

C008902125	12.192	1.753	36.118	1	6	15	-0.11	165	27.58	248.22	0.446
C007112340	10.668	1.781	43.257	1	6	30	0.20	203	20.69	248.22	0.409
C002902505	18.288	1.496	59.278	1	5	30	0.13	152	20.69	248.22	0.418
C000800705	9.246	1.570	21.556	1	6	0	0.23	178	27.58	344.75	0.411
C006514240	8.807	1.583	11.939	1	6	0	0.00	178	27.58	344.75	0.399
C004804115	18.593	1.765	58.865	0	5	0	0.13	152	20.69	248.22	0.499
C003314210	18.593	1.753	84.536	1	5	0	0.46	165	20.69	248.22	0.416

10.3.2 Shear ANN Training and Testing Data

The manila-colored cells designate bridges that were used in the design set. The green-colored cells designate bridges that were used in the design-set size for some ANNs and additional testing bridges in reduced size ANNs. The aqua-colored cells designate bridges that were used in the independent testing set.

Bridges	L (m)	s (m)	Kg (Gmm^4)	CF (1 or 0)	#girders	Skew (deg.)	de (m)	Deck ts(mm)	fc' (MPa)	fy (MPa)	Shear $GDF_{maximum}$
C002001220	8.687	1.219	20.175	0	7	40	0.61	178	20.69	248.22	0.663
C006607105P	21.031	2.350	103.109	1	4	0	0.79	178	20.69	248.22	0.782
C006710205	24.384	2.057	135.193	1	4	0	0.60	178	20.69	248.22	0.679
C007025010	24.866	1.905	140.400	1	5	0	0.15	152	20.69	248.22	0.644
C001403305P	24.079	1.702	89.674	1	5	0	-0.09	127	20.69	248.22	0.596
C004702203	6.909	1.791	5.314	0	5	0	0.07	127	20.69	248.22	0.585
C001903310	11.887	0.864	10.805	1	10	0	0.00	152	20.69	248.22	0.348
C007103415	8.807	0.864	8.264	1	11	0	0.25	203	27.58	248.22	0.339
C005463410	7.283	0.813	8.579	1	10	0	-0.02	178	20.69	248.22	0.363
C006313310P	7.010	1.438	4.954	1	6	15	0.06	152	20.69	248.22	0.397
C002014017	6.096	1.219	16.448	1	7	0	0.61	178	20.69	248.22	0.520
C008101013P	6.096	1.295	23.279	1	6	0	0.42	152	20.69	248.22	0.435
C007932415	14.630	1.372	32.621	1	5	35	0.61	203	20.69	227.54	0.417
C004802905	8.534	2.057	31.555	1	5	45	0.05	178	20.69	248.22	0.480
C007443235	9.347	1.778	17.229	1	5	30	0.10	152	20.69	248.22	0.433
C002702510	14.732	1.727	40.802	1	5	25	0.20	152	20.69	248.22	0.429
C000602505	9.144	1.118	15.005	1	5	15	0.77	152	17.24	206.85	0.576
C007010905	11.278	0.975	19.264	1	7	0	0.73	133	17.24	206.85	0.573
C000103420	15.215	0.972	17.697	1	9	0	0.05	165	20.69	248.22	0.538

C009133625	14.935	0.861	23.405	1	7	0	0.48	159	20.69	248.22	0.444
C006305115	8.230	1.194	8.161	1	7	20	0.06	152	20.69	248.22	0.396
C001424750	15.697	2.216	144.110	0	5	0	0.14	178	20.69	248.22	0.774
C006300825P	8.839	1.029	6.933	1	8	0	0.00	140	20.69	248.22	0.387
C005913903	11.735	1.118	10.396	1	8	0	0.28	152	20.69	248.22	0.400
C001210930	14.935	1.753	122.459	1	6	0	-0.11	178	20.69	248.22	0.604
C006311110	17.907	1.537	84.547	0	6	0	0.13	165	20.69	248.22	0.531
C003303710	18.288	1.219	41.497	1	8	0	0.30	152	20.69	248.22	0.417
C001201210	7.620	1.794	7.188	1	6	0	0.05	152	20.69	248.22	0.603
C009123545	9.805	1.956	15.981	1	5	0	-0.01	165	20.69	248.22	0.624
C004803915	8.763	0.838	16.033	0	8	0	0.11	140	17.24	206.85	0.372
C006341615	17.983	0.978	24.279	1	7	0	0.05	152	20.69	248.22	0.371
C002902505	18.288	1.496	59.278	1	5	30	0.13	152	20.69	248.22	0.434
C002602910	17.983	1.188	53.629	1	8	0	0.18	178	20.69	248.22	0.435
C005903110	11.582	0.965	11.722	1	9	0	-0.05	152	20.69	248.22	0.367
C008002310	12.268	1.981	42.313	1	5	0	0.38	178	20.69	248.22	0.654
C001111430	10.973	1.981	31.674	1	4	0	0.69	191	20.69	248.22	0.642
C009111705	9.626	1.600	19.540	1	5	0	0.77	200	20.69	248.22	0.622
C007802440	18.440	2.184	60.850	1	4	0	0.41	178	20.69	248.22	0.717
C002701945	14.707	1.778	26.389	1	5	0	0.71	178	20.69	248.22	0.644
C001401710	13.503	2.105	69.179	1	5	0	0.04	203	20.69	248.22	0.710
C009002115	18.288	0.864	32.374	0	8	0	0.03	140	17.24	206.85	0.364
C007824260	18.136	1.905	73.369	1	5	0	0.61	178	20.69	248.22	0.672
C007911205	14.808	2.057	120.415	1	5	20	0.38	203	24.13	248.22	0.630
C001103815	23.311	1.676	103.774	1	6	0	0.38	165	20.69	248.22	0.552
C005913505	18.288	1.422	20.935	1	6	0	0.03	152	20.69	248.22	0.531
C003413410	21.056	1.969	92.415	1	4	0	0.78	203	17.24	206.85	0.742
C001401535	10.668	2.121	27.515	1	5	30	0.03	178	27.58	248.22	0.558

C000604715	18.034	1.543	93.067	1	6	0	0.49	203	20.69	248.22	0.534
C007815273	12.497	1.918	67.504	1	4	32	0.70	178	20.69	248.22	0.506
C006924230	6.248	1.524	5.333	1	6	0	0.46	178	20.69	248.22	0.501
C004720810	7.468	1.448	5.617	0	5	0	0.15	152	20.69	248.22	0.496
C005904610	9.296	1.016	7.527	1	8	0	0.03	152	20.69	248.22	0.423
C005901825	8.839	1.956	25.751	0	5	45	0.05	152	20.69	248.22	0.609
C007112340	10.668	1.781	43.257	1	6	30	0.20	203	20.69	248.22	0.603
C008803505	8.814	1.295	6.782	1	5	0	0.46	127	20.69	227.54	0.476
C001201410	8.839	1.753	18.992	1	6	30	-0.11	178	20.69	248.22	0.607
C002001215	8.687	1.219	16.602	0	7	35	0.61	152	20.69	248.22	0.570
C001224325	17.983	1.753	90.872	1	6	0	-0.11	178	17.24	248.22	0.593
C008722020	11.887	1.753	40.644	1	6	15	-0.11	178	27.58	248.22	0.552
C005901805	18.161	1.397	51.664	1	7	0	-0.08	152	20.69	248.22	0.471
C000102908	23.063	2.032	113.440	1	5	0	0.26	152	20.69	248.22	0.656
C007603710	11.887	1.829	28.183	1	4	0	0.43	152	20.69	248.22	0.591
C007904705	7.141	2.057	27.549	1	5	23	0.00	178	24.13	248.22	0.609
C007203715	9.144	1.473	7.518	1	5	0	0.09	152	20.69	248.22	0.535
C002001505	8.534	1.295	20.192	0	7	0	0.62	178	20.69	248.22	0.633
C001205010	14.630	1.346	61.658	0	6	15	0.61	152	20.69	248.22	0.583
C003406020	12.573	1.524	20.712	1	5	0	0.61	178	20.69	248.22	0.599
C009114505	8.306	1.302	9.989	1	6	0	0.02	140	17.24	206.85	0.434
C001705805	7.798	1.219	8.479	1	7	0	0.58	152	20.69	248.22	0.604
C001902340	8.738	1.321	9.940	1	7	0	0.02	152	20.69	248.22	0.443
C009202210	12.192	1.219	15.479	1	6	0	0.25	152	20.69	248.22	0.413
C001823610	11.976	1.092	14.176	1	8	0	0.38	127	20.69	248.22	0.426
C003403910	15.240	1.981	55.171	1	4	0	0.69	165	20.69	248.22	0.657
C001301620	13.716	1.905	45.147	1	4	15	0.50	165	17.24	227.54	0.606

C003704805P	15.278	2.057	58.662	1	5	0	0.15	152	20.69	248.22	0.677
C000226205	12.192	1.905	35.412	1	5	0	0.15	191	24.13	248.22	0.620
C009102805	17.856	1.930	64.849	1	5	0	0.10	178	27.58	344.75	0.630
C008902125	12.192	1.753	36.118	1	6	15	-0.11	165	27.58	248.22	0.582
C008404020	9.550	1.829	25.698	0	5	0	0.00	152	17.24	227.54	0.621
C005900525	11.735	0.991	8.455	1	7	0	0.00	140	20.69	227.54	0.382
C005121315P	9.144	1.822	22.898	1	5	0	0.01	152	20.69	248.22	0.629
C007202710	11.887	1.581	23.774	1	6	0	0.01	152	20.69	248.22	0.507
C006301204P	17.983	0.984	25.870	1	7	0	0.02	152	17.24	206.85	0.380
C001900130	9.144	1.791	22.898	1	6	0	0.09	152	20.69	248.22	0.609
C001716105	14.675	1.775	56.245	1	6	45	0.27	178	24.13	344.75	0.549
C005900505	11.811	1.753	45.724	0	5	0	0.08	178	20.69	248.22	0.592
C005913020	11.836	1.168	18.100	1	7	0	0.08	152	20.69	248.22	0.403
C007910405	8.534	1.794	21.569	1	6	0	0.16	178	20.69	248.22	0.612
C005922330	11.735	1.168	9.940	1	6	0	0.08	152	20.69	248.22	0.402
C002004725	11.582	1.219	26.896	1	7	0	0.61	178	20.69	248.22	0.537
C001712925	11.855	1.808	36.552	1	6	0	0.20	178	24.13	344.75	0.609
C008402410	11.963	1.473	23.128	1	5	0	0.03	152	20.69	248.22	0.558
C004507603	8.153	1.194	17.564	0	7	0	0.06	152	20.69	248.22	0.440
C002012040	8.534	1.219	26.669	0	7	0	0.61	178	20.69	248.22	0.538
C007602705	14.935	1.829	45.661	0	4	0	0.46	152	20.69	227.54	0.549
C004800415	18.745	1.829	88.995	1	5	0	0.53	165	20.69	248.22	0.592
C007102605	15.240	1.499	36.481	1	7	0	0.08	203	27.58	344.75	0.494
C005914820	11.836	1.524	37.880	1	6	20	0.15	178	20.69	248.22	0.529
C000805510P	7.315	1.191	11.320	1	7	0	0.16	178	20.69	248.22	0.415
C004903005	11.252	1.200	16.496	1	6	0	0.05	152	20.69	248.22	0.419
C006313105	11.887	0.991	12.518	1	7	0	0.00	152	17.24	206.85	0.373

C007203805	8.839	1.784	8.222	1	5	0	0.15	152	20.69	248.22	0.565
C007302705P	17.805	1.718	43.257	1	6	30	0.13	203	20.69	344.75	0.499
C001105220	15.062	1.695	26.289	0	6	0	0.03	152	20.69	248.22	0.578
C005902215	17.831	1.168	34.034	1	7	0	0.08	152	20.69	248.22	0.407
C009143435	15.570	1.286	23.607	1	5	0	0.40	165	20.69	248.22	0.480
C000102115	14.561	1.413	32.764	1	7	20	0.03	203	27.58	344.75	0.449
C000602310	11.278	1.168	21.091	0	6	0	0.05	165	17.24	227.54	0.419
C005901517	8.839	1.676	21.700	1	6	0	0.08	178	20.69	248.22	0.570
C002000707P	8.534	1.219	17.487	0	7	0	0.61	178	20.69	248.22	0.532
C006500230	9.093	0.854	10.914	1	11	0	0.00	178	27.58	344.75	0.351
C001400730	19.507	1.676	72.955	1	6	0	0.06	178	20.69	344.75	0.559
C005901830	14.935	1.676	38.359	1	6	0	0.08	203	20.69	248.22	0.540
C002003505	16.154	1.219	75.747	1	7	0	0.61	178	20.69	248.22	0.551
C006514240	8.807	1.583	11.939	1	6	0	0.00	178	27.58	344.75	0.524
C002704210P	15.240	1.524	34.988	1	5	20	0.61	178	20.69	248.22	0.523
C005900730	11.786	1.219	15.614	1	7	0	-0.03	152	20.69	248.22	0.415
C009314130	11.855	1.686	43.257	1	6	0	0.00	203	20.69	248.22	0.570
C002004010	14.630	1.219	56.953	1	7	0	0.61	178	20.69	248.22	0.551
C003314210	18.593	1.753	84.536	1	5	0	0.46	165	20.69	248.22	0.565
C001526720	8.785	1.822	30.955	1	5	20	0.01	178	20.69	248.22	0.572
C002012435	17.678	1.245	38.011	1	7	0	0.50	127	20.69	248.22	0.523
C005901410	17.882	1.397	35.029	1	7	0	0.03	152	20.69	248.22	0.506
C001814715	11.976	1.092	16.337	1	8	0	0.37	152	20.69	248.22	0.424
C001234905	17.983	1.829	48.628	1	4	33	0.33	165	20.69	248.22	0.491
C006602010	21.336	2.057	97.171	1	4	0	0.57	203	20.69	248.22	0.665
C008511515	7.925	1.321	25.798	0	7	0	0.30	203	20.69	248.22	0.458
C004712915	7.588	1.699	11.473	1	6	0	0.19	178	24.13	344.75	0.583
C007805310P	9.296	1.257	12.586	1	8	0	0.17	178	20.69	248.22	0.428

C000134022	8.839	1.702	24.582	1	6	0	0.01	152	20.69	248.22	0.589
C001900815	15.240	1.575	38.726	1	6	0	0.18	152	20.69	248.22	0.513
C002000823	7.010	1.219	14.137	0	7	0	0.61	178	20.69	248.22	0.512
C005900915	10.363	1.575	35.508	1	6	30	0.03	178	20.69	248.22	0.562
C002001627	6.401	1.219	18.400	0	7	0	0.61	178	20.69	248.22	0.524
C005901925	14.834	1.295	23.570	1	5	0	0.46	152	20.69	248.22	0.509
C005913030	10.363	1.676	26.430	1	6	0	0.08	178	20.69	248.22	0.570
C007000515	11.887	0.889	11.428	1	9	0	0.42	152	20.69	248.22	0.448
C001101705	14.935	1.753	39.173	1	5	0	0.15	165	20.69	248.22	0.569
C005606105	10.331	1.692	27.549	1	6	0	0.22	178	20.69	248.22	0.573
C003416235	10.541	1.295	20.054	1	7	0	-0.01	178	20.69	248.22	0.446
C000800705	9.246	1.570	21.556	1	6	0	0.23	178	27.58	344.75	0.529
C001202005	11.918	1.314	38.333	0	6	0	0.69	152	20.69	248.22	0.591
C007101130	14.780	1.770	75.551	1	6	30	0.27	203	20.69	344.75	0.549
C008602105P	17.888	1.791	96.927	1	5	0	0.00	178	27.58	248.22	0.600
C004529620	9.601	1.181	19.195	0	7	0	0.05	152	20.69	248.22	0.419
C002003405	8.534	1.219	18.908	0	7	0	0.61	178	20.69	248.22	0.540
C007602610	11.735	1.524	44.889	0	6	20	0.08	152	17.24	206.85	0.563
C004804115	18.593	1.765	58.865	0	5	0	0.13	152	20.69	248.22	0.589
C007001220	17.983	1.346	51.539	1	6	0	0.61	165	20.69	206.85	0.558
C001800605	11.989	1.092	16.517	1	8	0	0.41	165	20.69	248.22	0.439
C007004115	17.882	1.241	39.775	1	6	0	0.74	152	20.69	248.22	0.605
C002004730	8.712	1.219	20.175	0	7	0	0.60	178	20.69	248.22	0.531
C007213110	11.887	1.773	28.497	1	5	0	0.11	152	20.69	227.54	0.569
C004513915	13.884	1.321	35.222	1	7	0	0.00	178	20.69	248.22	0.456
C001411615P	16.764	1.670	60.705	1	6	20	0.09	178	27.58	248.22	0.504
C003302510	13.716	1.765	38.757	1	5	0	0.13	152	20.69	248.22	0.596
C002004730	8.534	1.219	20.044	0	7	0	0.69	178	20.69	248.22	0.564

C007012235	11.887	1.339	29.265	1	6	0	0.63	165	17.24	206.85	0.552
C007100625	14.840	1.775	58.437	1	6	0	0.25	203	24.13	344.75	0.601
C002705115	8.809	1.499	12.300	1	6	0	0.55	152	20.69	248.22	0.533
C002013720	7.087	1.219	15.218	0	7	0	0.61	178	20.69	248.22	0.530

10.3.3 Moment ANN Optimization Data

FE-based GDF	130 bridges	Training Algorithm: 'trainbr'					
ANN Architecture	10-(2-To-10)-1						
	Mean Error (%)				Max. Error (%)		
m	Design set	Indp. Test.	Addtl. Test.	CombinedTest.	Design set	Indp. Test.	Addtl. Test.
2	4.04	4.55			16.29	24.43	
3	4.00	3.76			15.45	20.46	
4	3.28	3.84			15.83	20.13	
5	3.05	3.96			16.03	23.28	
6	3.17	4.20			16.32	23.77	
7	3.21	3.79			14.66	19.68	
8	3.26	3.87			15.44	21.30	
9	3.03	3.89			15.18	22.17	
10	2.63	3.89			16.34	23.54	

FE-based GDF	130 bridges	Training Algorithm: 'trainbr'					
ANN Architecture	10-(2-To-10)-(2-To-10)-1						
	Mean Error (%)				Max. Error (%)		
m	Design set	Indp. Test.	Addtl. Test.	CombinedTest.	Design set	Indp. Test.	Addtl. Test.
2	3.69	4.68			15.71	22.65	
3	3.22	4.14			16.53	21.72	
4	3.08	4.10			17.22	22.19	
5	2.76	3.65			15.44	18.86	
6	17.31	8.84			69.22	48.00	
7	17.34	8.84			69.93	48.62	
8	17.37	8.83			70.60	49.20	
9	17.36	8.83			70.41	49.04	
10	1.79	6.72			17.46	25.08	

FE-based GDF	130 bridges	Training Algorithm: 'trainlm'					
ANN Architecture	10-(2-To-10)-1						
	Mean Error (%)				Max. Error (%)		
m	Design set	Indp. Test.	Addtl. Test.	CombinedTest.	Design set	Indp. Test.	Addtl. Test.
2	3.38	4.76			15.11	22.15	
3	3.21	4.37			14.56	21.05	
4	2.22	4.36			11.36	23.33	
5	2.05	4.27			13.59	17.29	
6	1.64	4.40			11.71	14.09	
7	1.46	4.99			13.07	19.76	
8	1.35	6.10			22.45	27.73	
9	1.21	7.89			22.89	26.63	
10	0.60	7.96			11.94	29.63	

FE-based GDF	130 bridges	Training Algorithm: 'trainlm'					
ANN Architecture	10-(2-To-10)-(2-To-10)-1						
	Mean Error (%)				Max. Error (%)		
m	Design set	Indp. Test.	Addtl. Test.	CombinedTest.	Design set	Indp. Test.	Addtl. Test.
2	3.31	4.03			13.90	22.78	
3	2.75	4.79			14.87	16.31	
4	1.95	5.79			17.97	19.06	
5	1.58	6.22			20.12	16.34	
6	0.97	7.48			17.20	17.91	
7	1.47	7.39			49.10	21.80	
8	1.46	7.15			31.95	23.50	
9	1.52	7.72			30.90	23.83	
10	1.29	6.73			24.44	24.82	

FE-based GDF	120 bridges	Training Algorithm: 'trainbr'						FE-based GDF	120 bridges	Training Algorithm: 'trainbr'					
ANN Architecture	10-(2-To-10)-1							ANN Architecture	10-(2-To-10)-(2-To-10)-1						
	Mean Error (%)				Max. Error (%)				Mean Error (%)				Max. Error (%)		
m	Design set	Indp. Test.	Addtl. Test.	CombinedTest.	Design set	Indp. Test.	Addtl. Test.	m	Design set	Indp. Test.	Addtl. Test.	CombinedTest.	Design set	Indp. Test.	Addtl. Test.
2	3.98	4.69	4.48	4.64	17.31	25.44	11.90	2	3.60	4.81	4.55	4.75	16.25	23.99	10.96
3	3.23	3.84	4.59	4.01	14.28	21.63	9.65	3	3.29	4.16	4.17	4.16	16.00	22.21	9.72
4	3.13	4.223	4.44	4.27	15.19	21.99	9.49	4	3.03	4.27	5.44	4.55	14.10	22.45	13.38
5	3.15	4.183	4.88	4.35	14.28	20.43	11.77	5	3.14	3.82	4.23	3.92	15.19	21.76	10.47
6	2.91	3.98	4.28	4.05	16.23	22.67	10.99	6	17.60	8.85	13.76	9.99	69.06	47.86	29.86
7	2.89	4.00	4.36	4.09	17.90	22.88	11.97	7	17.61	8.84	13.75	9.98	69.27	48.04	30.02
8	3.39	4.24	4.39	4.28	16.74	21.97	10.37	8	17.65	8.83	13.72	9.97	70.16	48.82	30.70
9	3.22	4.09	4.36	4.15	15.55	22.33	9.99	9	17.65	8.83	13.72	9.97	70.18	48.84	30.72
10	3.29	4.31	4.49	4.35	14.64	22.33	10.04	10	17.71	8.83	13.68	9.96	71.19	49.72	31.49

FE-based GDF	120 bridges	Training Algorithm: 'trainlm'						FE-based GDF	120 bridges	Training Algorithm: 'trainlm'					
ANN Architecture	10-(2-To-10)-1							ANN Architecture	10-(2-To-10)-(2-To-10)-1						
	Mean Error (%)				Max. Error (%)				Mean Error (%)				Max. Error (%)		
m	Design set	Indp. Test.	Addtl. Test.	CombinedTest.	Design set	Indp. Test.	Addtl. Test.	m	Design set	Indp. Test.	Addtl. Test.	CombinedTest.	Design set	Indp. Test.	Addtl. Test.
2	3.71	4.39	3.64	4.21	20.43	24.62	9.17	2	3.73	4.43	4.73	4.50	16.74	25.41	15.25
3	3.23	4.20	5.39	4.48	15.27	17.10	21.33	3	2.89	4.62	4.22	4.52	13.38	21.75	9.15
4	2.43	3.382	4.83	3.72	23.25	17.98	12.80	4	1.62	5.72	7.40	6.11	18.03	23.69	33.10
5	1.91	5.419	2.61	4.77	10.99	27.27	4.67	5	1.12	6.32	9.83	7.14	15.02	20.54	27.91
6	1.94	5.47	5.95	5.58	14.72	22.33	12.02	6	1.27	7.79	8.13	7.87	25.42	24.62	28.00
7	1.21	6.58	5.41	6.31	16.68	24.58	16.13	7	1.34	8.06	6.18	7.62	43.77	31.68	21.66
8	1.02	8.02	5.63	7.47	21.12	31.13	14.71	8	1.23	5.69	5.08	5.54	33.80	16.68	18.61
9	1.25	9.63	11.16	9.99	21.28	32.50	21.04	9	0.90	5.06	5.13	5.08	25.70	18.35	14.22
10	1.30	7.33	5.44	6.89	35.06	35.29	13.61	10	0.97	6.83	6.63	6.79	24.38	25.42	13.47

FE-based GDF	110 bridges	Training Algorithm: 'trainbr'						FE-based GDF	110 bridges	Training Algorithm: 'trainbr'					
ANN Architecture		10-(2-To-10)-1						ANN Architecture		10-(2-To-10)-(2-To-10)-1					
	Mean Error (%)				Max. Error (%)				Mean Error (%)				Max. Error (%)		
m	Design set	Indp. Test.	Addtl. Test.	CombinedTest.	Design set	Indp. Test.	Addtl. Test.	m	Design set	Indp. Test.	Addtl. Test.	CombinedTest.	Design set	Indp. Test.	Addtl. Test.
2	3.92	4.56	4.65	4.59	15.28	23.43	17.50	2	3.58	4.75	4.63	4.71	15.56	23.29	16.23
3	3.31	4.28	4.36	4.31	15.19	20.07	17.19	3	3.09	4.36	4.16	4.28	16.09	20.87	17.46
4	3.00	3.75	4.04	3.86	17.42	21.89	18.60	4	2.89	4.36	4.59	4.45	15.12	22.37	16.99
5	3.09	4.24	4.24	4.24	15.18	22.46	16.40	5	2.46	4.00	4.72	4.27	15.54	20.41	17.14
6	2.59	4.04	4.55	4.23	16.60	22.93	18.17	6	18.06	8.88	13.03	10.44	68.31	47.20	29.66
7	2.34	3.85	4.82	4.21	14.55	22.45	17.98	7	1.81	4.59	5.57	4.96	7.69	19.26	19.23
8	2.27	3.74	4.86	4.16	13.12	21.96	18.46	8	18.08	8.86	12.96	10.41	68.74	47.58	29.99
9	1.95	4.02	4.38	4.16	9.14	19.47	20.55	9	18.20	8.83	12.70	10.29	70.37	49.01	31.25
10	2.03	3.80	4.51	4.07	12.10	20.83	19.68	10	18.12	8.84	12.87	10.36	69.27	48.04	30.39

FE-based GDF	110 bridges	Training Algorithm: 'trainlm'						FE-based GDF	110 bridges	Training Algorithm: 'trainlm'					
ANN Architecture		10-(2-To-10)-1						ANN Architecture		10-(2-To-10)-(2-To-10)-1					
	Mean Error (%)				Max. Error (%)				Mean Error (%)				Max. Error (%)		
m	Design set	Indp. Test.	Addtl. Test.	CombinedTest.	Design set	Indp. Test.	Addtl. Test.	m	Design set	Indp. Test.	Addtl. Test.	CombinedTest.	Design set	Indp. Test.	Addtl. Test.
2	3.46	4.01	5.24	4.47	13.47	20.76	21.35	2	3.21	4.53	4.99	4.70	15.22	16.09	20.05
3	2.72	4.11	5.01	4.45	14.58	25.43	21.03	3	2.28	4.93	4.36	4.71	13.05	17.82	18.90
4	2.07	4.09	4.83	4.37	13.73	19.38	14.96	4	1.81	4.78	5.07	4.89	28.87	16.33	17.43
5	2.40	5.27	7.13	5.97	13.57	16.18	18.69	5	1.48	7.19	7.29	7.23	23.96	21.04	21.10
6	1.38	4.75	6.56	5.44	28.97	23.97	23.44	6	1.00	7.51	8.29	7.81	21.45	28.54	23.64
7	1.35	7.26	10.76	8.58	18.56	24.38	27.31	7	1.16	6.32	6.79	6.50	28.24	23.87	23.38
8	1.07	6.76	8.36	7.37	19.05	23.76	34.61	8	0.69	7.36	7.66	7.47	10.77	22.83	17.68
9	1.36	6.23	10.25	7.75	36.61	24.37	26.17	9	0.61	6.95	6.44	6.76	11.93	25.61	19.57
10	0.85	8.90	7.01	8.19	18.35	29.89	24.02	10	1.02	6.14	5.82	6.02	18.18	26.28	21.02

FE-based GDF	100 bridges	Training Algorithm: 'trainbr'					
ANN Architecture	10-(2-To-10)-1						
	Mean Error (%)				Max. Error (%)		
m	Design set	Indp. Test.	Addtl. Test.	CombinedTest.	Design set	Indp. Test.	Addtl. Test.
2	3.81	4.73	4.36	4.56	17.99	24.17	19.06
3	3.63	4.87	4.48	4.68	15.79	22.99	17.13
4	2.95	4.09	4.01	4.05	16.82	22.23	18.20
5	3.05	4.159	3.96	4.07	15.82	21.39	17.89
6	2.76	4.31	4.41	4.36	17.71	23.47	18.64
7	3.03	4.15	3.98	4.07	15.95	20.99	17.47
8	3.27	4.37	3.94	4.17	16.43	22.19	16.69
9	3.29	4.38	3.92	4.16	16.77	21.27	17.33
10	3.30	4.16	3.77	3.98	15.44	20.82	16.92

FE-based GDF	100 bridges	Training Algorithm: 'trainbr'					
ANN Architecture	10-(2-To-10)-(2-To-10)-1						
	Mean Error (%)				Max. Error (%)		
m	Design set	Indp. Test.	Addtl. Test.	CombinedTest.	Design set	Indp. Test.	Addtl. Test.
2	3.86	4.80	4.58	4.70	16.30	24.07	18.39
3	3.25	4.51	3.65	4.10	15.62	22.73	16.31
4	2.81	4.74	4.80	4.77	16.20	24.71	20.23
5	18.67	8.83	12.94	10.79	70.21	48.86	31.12
6	18.68	8.83	12.93	10.79	70.32	48.96	31.20
7	18.64	8.84	12.96	10.80	69.66	48.38	30.69
8	18.64	8.84	12.96	10.80	69.70	48.42	30.73
9	18.71	8.83	12.93	10.79	70.87	49.44	31.63
10	18.67	8.83	12.94	10.79	70.13	48.79	31.06

FE-based GDF	100 bridges	Training Algorithm: 'trainlm'					
ANN Architecture	10-(2-To-10)-1						
	Mean Error (%)				Max. Error (%)		
m	Design set	Indp. Test.	Addtl. Test.	CombinedTest.	Design set	Indp. Test.	Addtl. Test.
2	3.73	4.27	9.92	6.96	16.83	24.73	103.06
3	2.78	4.76	4.06	4.43	15.78	22.56	16.84
4	2.19	4.20	4.62	4.40	15.09	22.61	22.70
5	2.08	5.060	6.04	5.53	14.36	16.90	17.47
6	1.47	4.98	7.77	6.31	31.73	17.21	24.79
7	1.01	6.47	8.46	7.42	13.78	20.07	22.67
8	1.20	5.55	8.39	6.90	18.47	16.19	21.87
9	1.56	6.50	8.07	7.25	34.24	25.67	21.33
10	1.20	6.50	6.75	6.62	16.95	20.76	29.06

FE-based GDF	100 bridges	Training Algorithm: 'trainlm'					
ANN Architecture	10-(2-To-10)-(2-To-10)-1						
	Mean Error (%)				Max. Error (%)		
m	Design set	Indp. Test.	Addtl. Test.	CombinedTest.	Design set	Indp. Test.	Addtl. Test.
2	3.33	4.62	4.25	4.45	14.35	24.71	18.94
3	2.55	4.65	7.72	6.11	12.44	20.97	90.49
4	1.52	4.81	5.84	5.30	16.57	26.90	25.30
5	1.32	6.60	5.74	6.19	18.64	19.57	21.54
6	0.76	5.90	5.69	5.80	21.68	20.63	19.03
7	0.83	5.69	8.50	7.03	11.87	16.54	27.19
8	0.85	5.91	7.59	6.71	13.82	19.76	31.11
9	1.00	6.07	8.19	7.08	17.33	15.98	57.56
10	0.75	4.41	7.51	5.88	13.97	19.29	44.79

FE-based GDF	90 bridges	Training Algorithm: 'trainbr'					
ANN Architecture	10-(2-To-10)-1						
	Mean Error (%)				Max. Error (%)		
m	Design set	Indp. Test.	Addtl. Test.	CombinedTest.	Design set	Indp. Test.	Addtl. Test.
2	4.01	4.76	3.84	4.26	16.45	24.23	18.66
3	3.72	4.18	3.52	3.82	17.13	22.23	16.51
4	3.35	4.47	4.40	4.43	18.07	25.23	20.90
5	3.19	4.14	3.34	3.70	15.92	20.87	18.72
6	2.84	4.60	4.20	4.38	16.61	23.54	19.00
7	2.39	4.42	5.02	4.75	13.99	22.57	18.54
8	2.71	4.52	4.17	4.33	17.47	23.73	19.44
9	3.60	4.61	3.56	4.04	15.38	21.43	16.66
10	2.91	4.45	4.04	4.23	18.10	24.27	19.00

FE-based GDF	90 bridges	Training Algorithm: 'trainbr'					
ANN Architecture	10-(2-To-10)-(2-To-10)-1						
	Mean Error (%)				Max. Error (%)		
m	Design set	Indp. Test.	Addtl. Test.	CombinedTest.	Design set	Indp. Test.	Addtl. Test.
2	3.89	4.25	4.50	4.39	17.72	23.02	21.13
3	3.34	4.70	4.86	4.79	17.59	22.32	20.04
4	3.32	4.46	4.32	4.39	18.48	25.95	20.48
5	19.78	8.83	12.03	10.59	71.16	49.69	31.85
6	19.64	8.84	12.09	10.62	69.45	48.19	30.53
7	19.75	8.83	12.04	10.59	70.81	49.39	31.58
8	19.61	8.85	12.11	10.64	69.00	47.81	30.19
9	19.67	8.84	12.07	10.61	69.78	48.49	30.79
10	19.81	8.83	12.03	10.58	71.50	50.00	32.12

FE-based GDF	90 bridges	Training Algorithm: 'trainlm'					
ANN Architecture	10-(2-To-10)-1						
	Mean Error (%)				Max. Error (%)		
m	Design set	Indp. Test.	Addtl. Test.	CombinedTest.	Design set	Indp. Test.	Addtl. Test.
2	3.47	4.01	4.76	4.42	17.07	20.51	22.67
3	2.93	4.80	3.59	4.14	15.58	22.59	17.29
4	1.92	4.38	4.39	4.38	11.73	28.28	21.63
5	1.74	5.35	7.84	6.72	14.60	23.10	24.72
6	1.58	6.26	7.13	6.73	23.04	23.26	26.45
7	1.43	8.12	7.86	7.98	20.23	26.35	29.55
8	1.23	6.05	8.00	7.12	24.73	21.30	23.45
9	1.32	5.51	6.59	6.11	23.48	22.41	15.14
10	1.02	6.28	6.34	6.31	19.79	28.84	26.31

FE-based GDF	90 bridges	Training Algorithm: 'trainlm'					
ANN Architecture	10-(2-To-10)-(2-To-10)-1						
	Mean Error (%)				Max. Error (%)		
m	Design set	Indp. Test.	Addtl. Test.	CombinedTest.	Design set	Indp. Test.	Addtl. Test.
2	3.33	4.43	4.14	4.27	15.78	20.03	21.63
3	2.61	5.46	7.14	6.38	14.77	20.05	22.88
4	1.44	7.02	6.57	6.77	18.07	22.94	29.19
5	0.83	7.18	5.14	6.06	12.43	21.02	22.94
6	1.15	6.55	7.92	7.30	21.86	22.77	41.15
7	1.03	6.13	6.29	6.22	16.22	19.85	19.35
8	1.00	6.63	7.15	6.92	18.40	20.94	22.02
9	0.86	5.38	7.72	6.66	13.83	18.36	25.39
10	0.87	5.58	8.91	7.40	10.29	24.43	74.78

FE-based GDF	80 bridges	Training Algorithm: 'trainbr'					
ANN Architecture	10-(2-To-10)-1						
	Mean Error (%)				Max. Error (%)		
m	Design set	Indp. Test.	Addtl. Test.	CombinedTest.	Design set	Indp. Test.	Addtl. Test.
2	3.92	4.84	4.20	4.45	17.41	24.81	18.29
3	3.32	4.75	4.03	4.32	13.25	20.11	18.78
4	3.24	4.540	4.00	4.21	14.82	19.42	19.04
5	2.79	4.474	4.35	4.40	14.11	21.75	17.99
6	2.81	4.69	4.35	4.49	15.56	22.79	17.94
7	2.92	4.50	4.25	4.35	15.99	23.09	18.07
8	3.17	4.77	3.91	4.25	17.03	22.27	16.96
9	2.88	4.48	4.16	4.29	15.60	22.40	17.02
10	2.82	4.55	4.26	4.38	16.18	22.71	17.49

FE-based GDF	80 bridges	Training Algorithm: 'trainbr'					
ANN Architecture	10-(2-To-10)-(2-To-10)-1						
	Mean Error (%)				Max. Error (%)		
m	Design set	Indp. Test.	Addtl. Test.	CombinedTest.	Design set	Indp. Test.	Addtl. Test.
2	3.79	4.97	4.50	4.69	16.73	25.35	20.42
3	3.18	4.71	4.29	4.46	16.40	22.66	17.93
4	20.54	8.83	12.38	10.97	71.24	49.77	31.92
5	20.48	8.83	12.40	10.98	70.79	49.37	31.57
6	20.30	8.85	12.51	11.05	69.01	47.82	30.20
7	20.65	8.85	12.34	10.95	72.10	50.52	32.58
8	20.40	8.84	12.44	11.01	70.00	48.68	30.96
9	20.43	8.83	12.42	11.00	70.31	48.95	31.20
10	20.34	8.84	12.48	11.03	69.37	48.13	30.47

FE-based GDF	80 bridges	Training Algorithm: 'trainlm'					
ANN Architecture	10-(2-To-10)-1						
	Mean Error (%)				Max. Error (%)		
m	Design set	Indp. Test.	Addtl. Test.	CombinedTest.	Design set	Indp. Test.	Addtl. Test.
2	3.69	4.41	4.59	4.52	16.69	22.06	18.08
3	2.32	4.46	5.06	4.82	18.54	23.96	18.94
4	2.58	4.874	4.81	4.83	26.19	16.63	16.35
5	1.74	5.934	6.45	6.24	24.59	22.46	23.54
6	1.29	6.26	6.66	6.50	25.07	23.59	24.34
7	1.30	5.80	6.10	5.98	23.01	20.27	23.29
8	1.13	6.22	9.09	7.95	25.98	16.01	29.95
9	1.25	6.70	8.81	7.97	24.03	23.80	58.06
10	0.95	5.04	6.79	6.09	15.99	25.15	27.36

FE-based GDF	80 bridges	Training Algorithm: 'trainlm'					
ANN Architecture	10-(2-To-10)-(2-To-10)-1						
	Mean Error (%)				Max. Error (%)		
m	Design set	Indp. Test.	Addtl. Test.	CombinedTest.	Design set	Indp. Test.	Addtl. Test.
2	2.81	5.55	5.70	5.64	9.63	18.95	22.13
3	2.34	6.06	6.15	6.11	11.98	23.39	19.32
4	1.34	8.09	9.64	9.02	15.41	40.57	46.92
5	1.25	6.34	6.07	6.18	28.55	25.93	30.42
6	1.19	5.12	6.03	5.67	16.32	23.29	23.38
7	0.86	6.02	6.40	6.25	17.69	21.10	28.52
8	1.24	5.52	5.92	5.76	18.89	19.22	20.85
9	1.01	5.73	4.54	5.01	28.79	23.27	22.80
10	1.26	4.64	5.84	5.36	19.84	18.89	23.32

FE-based GDF	70 bridges	Training Algorithm: 'trainbr'					
ANN Architecture	10-(2-To-10)-1						
	Mean Error (%)				Max. Error (%)		
m	Design set	Indp. Test.	Addtl. Test.	CombinedTest.	Design set	Indp. Test.	Addtl. Test.
2	3.86	4.63	4.18	4.34	16.67	24.53	19.92
3	2.92	4.29	4.42	4.37	14.67	20.54	17.94
4	2.79	4.96	4.77	4.84	16.57	22.46	19.38
5	2.79	4.88	4.77	4.81	15.84	20.79	19.26
6	2.59	4.53	4.37	4.42	15.17	20.73	19.03
7	2.79	5.02	4.68	4.80	16.63	20.94	20.48
8	2.76	4.82	4.78	4.79	16.37	21.80	18.73
9	2.84	4.80	4.43	4.56	16.23	21.32	19.32
10	2.66	4.70	4.97	4.87	14.80	19.39	20.92

FE-based GDF	70 bridges	Training Algorithm: 'trainbr'					
ANN Architecture	10-(2-To-10)-(2-To-10)-1						
	Mean Error (%)				Max. Error (%)		
m	Design set	Indp. Test.	Addtl. Test.	CombinedTest.	Design set	Indp. Test.	Addtl. Test.
2	3.90	4.71	4.59	4.63	16.98	24.72	22.18
3	3.10	4.81	4.30	4.48	13.92	18.11	21.58
4	21.99	8.85	11.84	10.78	69.04	47.84	30.22
5	21.89	8.88	11.92	10.84	68.37	47.26	29.70
6	22.01	8.84	11.83	10.77	69.22	47.99	30.36
7	22.00	8.85	11.84	10.78	69.13	47.92	30.29
8	21.90	8.87	11.91	10.83	68.44	47.31	29.75
9	21.68	8.97	12.11	11.00	66.69	45.78	28.41
10	21.93	8.86	11.88	10.81	68.68	47.53	29.94

FE-based GDF	70 bridges	Training Algorithm: 'trainlm'					
ANN Architecture	10-(2-To-10)-1						
	Mean Error (%)				Max. Error (%)		
m	Design set	Indp. Test.	Addtl. Test.	CombinedTest.	Design set	Indp. Test.	Addtl. Test.
2	3.25	4.94	5.77	5.47	10.71	24.30	24.57
3	2.34	5.11	6.08	5.74	13.70	16.79	25.33
4	1.80	6.24	5.69	5.89	17.83	17.54	25.30
5	1.05	6.07	6.88	6.59	19.58	21.93	27.23
6	1.01	5.28	6.56	6.11	14.84	23.78	21.63
7	1.25	6.06	7.02	6.68	19.20	24.53	42.01
8	1.27	6.64	8.34	7.73	22.91	27.34	33.30
9	1.46	5.47	6.27	5.99	24.08	26.79	28.84
10	1.06	6.47	7.14	6.90	13.74	22.16	32.03

FE-based GDF	70 bridges	Training Algorithm: 'trainlm'					
ANN Architecture	10-(2-To-10)-(2-To-10)-1						
	Mean Error (%)				Max. Error (%)		
m	Design set	Indp. Test.	Addtl. Test.	CombinedTest.	Design set	Indp. Test.	Addtl. Test.
2	2.86	4.51	5.70	5.28	16.49	23.86	27.96
3	1.90	6.74	7.37	7.14	11.44	20.61	26.52
4	0.76	7.31	6.67	6.89	18.66	19.68	22.73
5	1.43	6.57	5.87	6.12	23.16	22.88	19.55
6	1.27	5.88	5.87	5.87	20.29	15.27	25.32
7	0.98	5.77	6.00	5.92	20.81	23.21	27.99
8	1.15	5.81	6.75	6.42	19.27	21.43	33.56
9	0.94	4.93	5.31	5.18	22.01	19.11	20.29
10	0.68	5.18	6.75	6.19	18.18	18.15	24.19

FE-based GDF	60 bridges	Training Algorithm: 'trainbr'						FE-based GDF	60 bridges	Training Algorithm: 'trainbr'					
ANN Architecture	10-(2-To-10)-1							ANN Architecture	10-(2-To-10)-(2-To-10)-1						
	Mean Error (%)				Max. Error (%)				Mean Error (%)				Max. Error (%)		
m	Design set	Indp. Test.	Addtl. Test.	CombinedTest.	Design set	Indp. Test.	Addtl. Test.	m	Design set	Indp. Test.	Addtl. Test.	CombinedTest.	Design set	Indp. Test.	Addtl. Test.
2	2.21	4.75	4.75	4.75	9.45	16.83	20.62	2	2.76	4.91	5.67	5.42	13.46	16.95	22.86
3	2.43	4.75	4.99	4.91	10.58	16.07	20.68	3	2.55	4.85	5.00	4.95	10.80	17.05	20.62
4	2.15	4.23	4.61	4.49	11.91	18.52	20.46	4	22.54	8.94	12.75	11.53	67.16	46.19	47.16
5	1.98	4.45	5.11	4.90	7.16	17.83	21.03	5	22.92	8.84	12.54	11.35	69.76	48.47	49.46
6	2.27	4.04	4.62	4.44	10.27	20.29	19.85	6	22.92	8.84	12.54	11.35	69.79	48.50	49.48
7	1.85	4.35	4.59	4.52	8.09	20.40	20.73	7	22.78	8.86	12.61	11.40	68.92	47.73	48.71
8	1.91	4.26	4.77	4.61	7.32	20.18	20.24	8	22.77	8.86	12.61	11.41	68.86	47.69	48.67
9	2.39	4.71	4.44	4.52	9.00	18.62	21.15	9	23.08	8.83	12.48	11.31	70.70	49.29	50.28
10	2.30	4.53	4.50	4.51	8.65	19.43	19.99	10	22.89	8.84	12.55	11.36	69.61	43.34	49.33

FE-based GDF	60 bridges	Training Algorithm: 'trainlm'						FE-based GDF	60 bridges	Training Algorithm: 'trainlm'					
ANN Architecture	10-(2-To-10)-1							ANN Architecture	10-(2-To-10)-(2-To-10)-1						
	Mean Error (%)				Max. Error (%)				Mean Error (%)				Max. Error (%)		
m	Design set	Indp. Test.	Addtl. Test.	CombinedTest.	Design set	Indp. Test.	Addtl. Test.	m	Design set	Indp. Test.	Addtl. Test.	CombinedTest.	Design set	Indp. Test.	Addtl. Test.
2	2.80	4.67	5.61	5.31	12.30	17.79	20.89	2	2.69	4.69	4.73	4.72	12.40	16.94	21.83
3	2.18	4.78	4.59	4.65	12.43	19.45	21.11	3	1.90	6.29	7.01	6.78	19.93	28.14	38.46
4	0.76	6.161	7.08	6.78	9.61	19.52	60.71	4	0.68	6.16	6.82	6.61	9.63	21.60	25.50
5	0.86	6.116	6.19	6.17	15.55	20.81	21.96	5	0.50	6.90	9.15	8.43	7.26	23.84	62.65
6	0.84	6.14	8.47	7.72	13.02	21.83	55.51	6	0.87	5.20	6.35	5.98	12.02	21.61	26.62
7	1.36	5.14	9.10	7.83	16.65	15.40	52.75	7	0.62	5.92	7.57	7.04	11.32	17.63	30.97
8	1.29	5.13	8.13	7.17	18.75	22.08	58.53	8	0.84	4.87	6.90	6.25	12.11	17.81	24.82
9	0.69	5.43	7.25	6.67	12.01	22.06	30.77	9	0.92	4.94	6.78	6.19	14.27	18.13	21.55
10	0.87	5.45	5.67	5.60	15.60	26.31	22.01	10	0.73	5.03	7.67	6.82	12.65	19.07	42.57

FE-based GDF	50 bridges	Training Algorithm: 'trainbr'					
ANN Architecture	10-(2-To-10)-1						
	Mean Error (%)				Max. Error (%)		
m	Design set	Indp. Test.	Addtl. Test.	CombinedTest.	Design set	Indp. Test.	Addtl. Test.
2	2.63	4.48	5.63	5.30	12.05	17.08	23.15
3	2.39	4.42	4.62	4.56	14.25	17.22	22.25
4	2.33	4.539	5.27	5.06	16.00	21.58	5.27
5	2.15	5.176	5.03	5.07	8.85	17.78	21.87
6	1.88	5.16	5.37	5.31	7.61	17.13	22.44
7	1.48	4.69	4.96	4.88	12.70	17.27	22.92
8	1.85	4.37	4.88	4.73	12.56	17.57	21.73
9	2.13	4.41	5.14	4.93	8.08	16.98	22.56
10	2.08	4.71	5.19	5.05	6.35	15.41	22.83

FE-based GDF	50 bridges	Training Algorithm: 'trainbr'					
ANN Architecture	10-(2-To-10)-(2-To-10)-1						
	Mean Error (%)				Max. Error (%)		
m	Design set	Indp. Test.	Addtl. Test.	CombinedTest.	Design set	Indp. Test.	Addtl. Test.
2	2.47	4.82	5.70	5.44	7.26	17.97	21.93
3	23.95	8.84	13.39	12.06	72.03	50.46	51.46
4	23.74	8.83	13.35	12.03	70.25	48.90	49.89
5	23.75	8.83	13.35	12.03	70.32	48.96	49.95
6	23.84	8.83	13.36	12.04	71.08	49.63	50.62
7	24.01	8.88	13.41	12.08	72.53	50.90	51.90
8	23.82	8.83	13.36	12.04	70.89	49.46	50.45
9	23.84	8.83	13.36	12.04	71.09	49.63	50.62
10	24.02	8.88	13.41	12.09	72.63	50.98	51.98

FE-based GDF	50 bridges	Training Algorithm: 'trainlm'					
ANN Architecture	10-(2-To-10)-1						
	Mean Error (%)				Max. Error (%)		
m	Design set	Indp. Test.	Addtl. Test.	CombinedTest.	Design set	Indp. Test.	Addtl. Test.
2	2.48	4.85	5.79	5.52	11.28	19.94	26.48
3	1.76	4.52	5.09	4.92	22.48	18.21	21.36
4	0.84	6.226	8.13	7.57	12.28	22.68	33.02
5	1.24	4.186	5.57	5.17	29.73	18.78	20.26
6	0.80	5.60	5.77	5.72	11.98	19.74	26.18
7	1.00	5.63	6.78	6.44	12.13	16.87	28.47
8	0.75	5.31	6.33	6.03	9.45	21.09	32.19
9	0.88	5.58	6.68	6.36	16.82	16.74	27.55
10	1.11	4.83	5.48	5.29	18.02	20.58	24.38

FE-based GDF	50 bridges	Training Algorithm: 'trainlm'					
ANN Architecture	10-(2-To-10)-(2-To-10)-1						
	Mean Error (%)				Max. Error (%)		
m	Design set	Indp. Test.	Addtl. Test.	CombinedTest.	Design set	Indp. Test.	Addtl. Test.
2	1.76	5.07	5.64	5.47	9.60	16.63	23.27
3	0.65	5.87	5.58	5.67	9.37	19.91	22.47
4	1.22	5.20	6.39	6.04	15.59	16.21	51.48
5	0.96	5.02	7.78	6.98	13.48	16.82	39.00
6	0.99	5.65	7.58	7.02	11.88	20.66	55.19
7	0.73	5.20	5.75	5.59	7.67	21.46	22.26
8	0.73	5.83	7.37	6.92	8.61	14.56	58.03
9	1.08	5.54	7.55	6.96	18.49	20.40	54.73
10	0.63	5.88	7.81	7.25	10.16	18.51	49.26

FE-based GDF	40 bridges	Training Algorithm: 'trainbr'					
ANN Architecture	10-(2-To-10)-1						
	Mean Error (%)				Max. Error (%)		
m	Design set	Indp. Test.	Addtl. Test.	CombinedTest.	Design set	Indp. Test.	Addtl. Test.
2	3.52	4.80	4.55	4.62	13.64	27.90	20.49
3	25.47	8.89	13.95	12.59	72.68	51.03	66.41
4	2.68	5.282	6.04	5.84	19.12	25.14	23.63
5	1.89	4.437	5.68	5.35	5.94	17.61	25.66
6	1.61	4.67	5.38	5.19	6.74	17.37	23.79
7	1.51	4.55	5.88	5.53	10.40	17.23	23.89
8	1.38	4.80	6.34	5.93	10.22	17.82	25.07
9	1.76	4.51	5.22	5.03	7.22	20.08	21.10
10	1.89	4.16	5.00	4.78	8.54	19.64	20.81

FE-based GDF	40 bridges	Training Algorithm: 'trainbr'					
ANN Architecture	10-(2-To-10)-(2-To-10)-1						
	Mean Error (%)				Max. Error (%)		
m	Design set	Indp. Test.	Addtl. Test.	CombinedTest.	Design set	Indp. Test.	Addtl. Test.
2	1.87	5.17	6.08	5.83	6.10	17.11	25.59
3	25.52	8.92	13.97	12.61	73.12	51.41	66.83
4	25.29	8.83	13.89	12.53	71.17	49.70	64.94
5	25.33	8.83	13.90	12.54	71.55	50.04	65.32
6	25.16	8.84	13.87	12.52	70.07	48.74	63.89
7	25.36	8.83	13.91	12.55	71.75	50.21	65.50
8	25.26	8.83	13.88	12.53	70.93	49.49	64.72
9	25.53	8.93	13.97	12.62	73.23	51.51	66.93
10	25.37	8.84	13.91	12.55	71.82	50.27	65.57

FE-based GDF	40 bridges	Training Algorithm: 'trainlm'					
ANN Architecture	10-(2-To-10)-1						
	Mean Error (%)				Max. Error (%)		
m	Design set	Indp. Test.	Addtl. Test.	CombinedTest.	Design set	Indp. Test.	Addtl. Test.
2	3.24	4.44	5.16	4.97	19.33	27.24	24.80
3	0.82	6.20	6.22	6.22	11.91	26.22	30.95
4	0.65	6.177	7.83	7.39	8.48	17.92	31.62
5	1.00	5.731	7.43	6.97	14.02	23.69	21.39
6	1.24	5.23	5.28	5.27	17.48	20.99	22.62
7	0.95	4.69	6.16	5.77	24.10	16.29	20.01
8	0.88	4.82	6.62	6.14	10.68	17.29	20.47
9	0.59	5.56	6.98	6.59	8.45	19.80	32.72
10	0.99	5.22	5.43	5.37	10.26	19.28	21.72

FE-based GDF	40 bridges	Training Algorithm: 'trainlm'					
ANN Architecture	10-(2-To-10)-(2-To-10)-1						
	Mean Error (%)				Max. Error (%)		
m	Design set	Indp. Test.	Addtl. Test.	CombinedTest.	Design set	Indp. Test.	Addtl. Test.
2	1.64	6.12	7.43	7.08	11.19	18.48	24.80
3	1.56	5.83	7.89	7.33	18.25	24.10	24.16
4	0.46	6.57	8.59	8.05	5.84	21.10	39.97
5	0.88	4.20	6.65	5.99	16.42	15.78	27.05
6	1.17	4.91	7.44	6.76	14.73	21.18	38.28
7	0.80	5.33	8.43	7.60	11.23	25.57	46.07
8	0.88	6.55	8.26	7.80	11.65	23.25	22.66
9	0.85	5.63	7.59	7.07	13.35	22.62	24.97
10	0.38	6.30	7.91	7.48	7.21	15.83	32.61

FE-based GDF	30 bridges	Training Algorithm: 'trainbr'					
ANN Architecture	10-(2-To-10)-1						
	Mean Error (%)				Max. Error (%)		
m	Design set	Indp. Test.	Addtl. Test.	CombinedTest.	Design set	Indp. Test.	Addtl. Test.
2	21.64	8.83	14.30	12.95	67.20	45.77	65.28
3	2.42	5.41	6.59	6.30	15.20	25.14	23.17
4	2.53	5.722	6.51	6.32	15.34	26.35	24.06
5	24.75	10.153	16.24	14.73	79.24	56.76	72.72
6	0.66	5.72	6.07	5.98	9.50	21.44	22.21
7	1.34	4.78	5.47	5.30	19.68	20.72	21.24
8	1.41	5.36	5.57	5.52	5.89	25.49	20.68
9	2.49	5.18	6.28	6.01	14.98	25.84	25.85
10	0.77	4.43	5.81	5.47	8.50	21.56	41.00

FE-based GDF	30 bridges	Training Algorithm: 'trainbr'					
ANN Architecture	10-(2-To-10)-(2-To-10)-1						
	Mean Error (%)				Max. Error (%)		
m	Design set	Indp. Test.	Addtl. Test.	CombinedTest.	Design set	Indp. Test.	Addtl. Test.
2	23.21	9.23	14.79	13.41	71.41	48.76	63.93
3	24.83	10.47	16.51	15.01	80.54	57.90	73.98
4	14.33	8.42	10.20	9.76	43.86	39.34	49.25
5	24.74	10.11	16.20	14.69	79.07	56.61	72.56
6	24.75	10.15	16.24	14.73	79.22	56.74	72.97
7	24.72	10.03	16.13	14.62	78.73	56.31	72.23
8	24.80	10.34	16.40	14.89	80.03	57.45	73.48
9	24.67	9.86	16.01	14.48	78.04	55.71	71.56
10	24.70	9.56	16.08	14.46	78.43	56.05	71.94

FE-based GDF	30 bridges	Training Algorithm: 'trainlm'					
ANN Architecture	10-(2-To-10)-1						
	Mean Error (%)				Max. Error (%)		
m	Design set	Indp. Test.	Addtl. Test.	CombinedTest.	Design set	Indp. Test.	Addtl. Test.
2	1.75	5.90	7.94	7.44	15.69	19.37	49.67
3	1.38	5.49	6.31	6.11	12.11	26.33	36.24
4	0.42	6.119	8.54	7.94	5.57	30.69	75.64
5	0.20	5.260	6.51	6.20	3.57	17.70	32.36
6	0.50	5.12	6.40	6.08	7.10	20.33	26.20
7	0.90	5.40	7.12	6.69	9.87	20.71	23.30
8	0.66	5.17	7.25	6.73	6.34	19.30	67.13
9	0.74	5.42	6.53	6.25	9.19	16.43	28.91
10	1.92	5.01	7.69	7.02	23.64	18.02	26.62

FE-based GDF	30 bridges	Training Algorithm: 'trainlm'					
ANN Architecture	10-(2-To-10)-(2-To-10)-1						
	Mean Error (%)				Max. Error (%)		
m	Design set	Indp. Test.	Addtl. Test.	CombinedTest.	Design set	Indp. Test.	Addtl. Test.
2	0.21	7.24	7.78	7.65	1.94	26.27	31.41
3	1.19	5.56	6.17	6.02	13.12	18.36	35.39
4	0.81	5.83	8.82	8.08	9.00	21.34	44.91
5	0.87	5.89	7.12	6.82	11.49	22.38	30.13
6	0.69	5.85	8.94	8.17	11.52	18.65	40.73
7	0.71	6.29	7.19	6.97	6.05	23.53	39.63
8	1.50	5.76	8.21	7.60	25.59	19.12	30.44
9	1.30	6.95	8.96	8.46	18.65	25.85	41.64
10	0.95	6.03	8.30	7.74	12.96	15.22	28.50

FE-based GDF	20 bridges	Training Algorithm: 'trainbr'					
ANN Architecture	10-(2-To-10)-1						
	Mean Error (%)				Max. Error (%)		
m	Design set	Indp. Test.	Addtl. Test.	CombinedTest.	Design set	Indp. Test.	Addtl. Test.
2	2.07	6.52	8.37	7.94	10.47	27.01	39.45
3	2.11	6.47	7.66	7.39	5.45	26.93	32.89
4	24.05	9.850	16.90	15.27	77.99	55.67	74.05
5	2.14	6.174	7.61	7.28	9.17	26.47	31.07
6	2.38	6.32	7.54	7.26	9.76	27.57	28.52
7	2.26	6.28	7.54	7.25	7.57	27.52	28.71
8	1.86	5.55	7.17	6.79	8.97	27.94	27.29
9	1.75	5.61	7.05	6.72	8.15	27.23	26.27
10	2.34	5.72	6.96	6.67	11.25	24.54	27.42

FE-based GDF	20 bridges	Training Algorithm: 'trainbr'					
ANN Architecture	10-(2-To-10)-(2-To-10)-1						
	Mean Error (%)				Max. Error (%)		
m	Design set	Indp. Test.	Addtl. Test.	CombinedTest.	Design set	Indp. Test.	Addtl. Test.
2	23.63	8.72	16.57	14.76	74.65	52.49	70.39
3	22.05	9.31	15.98	14.44	73.07	50.56	69.01
4	19.08	9.57	13.83	12.85	52.06	36.41	49.19
5	24.06	10.03	17.04	15.42	78.75	56.34	74.80
6	24.07	10.04	17.04	15.42	78.76	56.35	74.81
7	21.20	8.16	15.81	14.04	54.69	38.13	59.58
8	15.83	7.53	13.28	11.95	38.58	21.30	54.24
9	24.08	10.21	17.18	15.57	79.47	56.96	75.50
10	24.10	10.38	17.32	15.72	80.19	57.59	76.20

FE-based GDF	20 bridges	Training Algorithm: 'trainlm'					
ANN Architecture	10-(2-To-10)-1						
	Mean Error (%)				Max. Error (%)		
m	Design set	Indp. Test.	Addtl. Test.	CombinedTest.	Design set	Indp. Test.	Addtl. Test.
2	0.54	6.22	6.07	6.11	5.88	20.82	25.05
3	0.96	5.82	10.02	9.05	13.37	20.06	45.05
4	0.65	5.677	8.28	7.68	9.10	21.84	57.88
5	1.24	6.804	10.61	9.73	14.47	18.59	52.71
6	1.09	5.19	8.29	7.57	9.87	21.05	48.43
7	0.86	4.84	7.73	7.07	9.81	21.66	29.24
8	0.88	6.18	9.11	8.44	6.83	24.99	41.85
9	1.21	5.92	7.65	7.25	10.50	22.96	54.54
10	0.67	5.29	8.50	7.76	10.87	21.98	45.57

FE-based GDF	20 bridges	Training Algorithm: 'trainlm'					
ANN Architecture	10-(2-To-10)-(2-To-10)-1						
	Mean Error (%)				Max. Error (%)		
m	Design set	Indp. Test.	Addtl. Test.	CombinedTest.	Design set	Indp. Test.	Addtl. Test.
2	0.94	6.40	8.60	8.09	9.57	31.52	52.27
3	0.40	6.75	7.01	6.95	5.49	21.28	34.68
4	0.99	6.14	8.35	7.84	13.29	25.97	53.20
5	1.17	6.01	10.55	9.51	16.29	28.38	71.25
6	1.14	5.32	7.51	7.01	16.01	24.32	46.08
7	1.26	6.16	8.70	8.11	12.15	19.70	42.32
8	0.76	6.62	7.96	7.65	7.29	23.13	28.78
9	2.63	5.88	11.61	10.28	34.31	22.20	76.23
10	0.49	7.49	9.65	9.15	6.45	25.04	68.30

10.3.4 Shear ANN Optimzation Data

FE-based GDF	130 bridges	Training Algorithm: 'trainbr'					
ANN Architecture	10-(2-To-10)-1						
	Mean Error (%)				Max. Error (%)		
m	Design set	Indp. Test.	Addtl. Test.	CombinedTest.	Design set	Indp. Test.	Addtl. Test.
2	4.86	4.81			27.26	17.01	
3	4.12	3.94			27.83	13.63	
4	3.69	4.07			27.64	11.38	
5	3.70	4.11			21.27	10.97	
6	3.25	3.75			21.98	9.99	
7	3.42	3.76			22.35	11.79	
8	3.59	4.17			22.54	11.01	
9	3.63	4.02			22.62	11.58	
10	3.46	3.22			22.42	10.43	

FE-based GDF	130 bridges	Training Algorithm: 'trainbr'					
ANN Architecture	10-(2-To-10)-(2-To-10)-1						
	Mean Error (%)				Max. Error (%)		
m	Design set	Indp. Test.	Addtl. Test.	CombinedTest.	Design set	Indp. Test.	Addtl. Test.
2	5.71	4.66			26.61	13.47	
3	4.23	2.88			26.65	15.55	
4	3.78	4.15			23.19	11.33	
5	3.52	3.86			24.06	12.08	
6	16.86	7.92			56.63	26.72	
7	16.84	7.98			56.04	26.25	
8	16.87	7.90			56.90	26.94	
9	16.84	7.96			56.18	26.36	
10	3.59	5.58			51.28	18.61	

FE-based GDF	130 bridges	Training Algorithm: 'trainlm'					
ANN Architecture	10-(2-To-10)-1						
	Mean Error (%)				Max. Error (%)		
m	Design set	Indp. Test.	Addtl. Test.	CombinedTest.	Design set	Indp. Test.	Addtl. Test.
2	6.25	4.15			24.69	15.88	
3	4.07	4.70			28.33	11.52	
4	2.97	4.43			24.28	17.47	
5	2.75	5.21			31.01	12.34	
6	1.95	6.74			14.13	22.57	
7	1.90	7.02			36.53	32.03	
8	2.46	7.22			33.83	43.77	
9	1.67	7.66			39.89	30.96	
10	1.61	6.38			28.85	21.33	

FE-based GDF	130 bridges	Training Algorithm: 'trainlm'					
ANN Architecture	10-(2-To-10)-(2-To-10)-1						
	Mean Error (%)				Max. Error (%)		
m	Design set	Indp. Test.	Addtl. Test.	CombinedTest.	Design set	Indp. Test.	Addtl. Test.
2	5.39	3.67			27.99	11.50	
3	3.35	4.27			29.21	13.74	
4	2.51	6.43			24.61	24.86	
5	1.91	6.02			37.72	19.39	
6	1.79	9.74			32.02	27.18	
7	1.56	5.68			31.27	16.45	
8	1.21	6.96			31.92	19.70	
9	1.41	6.75			39.95	30.40	
10	1.24	6.55			23.76	18.62	

FE-based GDF	120 bridges	Training Algorithm: 'trainbr'						FE-based GDF	120 bridges	Training Algorithm: 'trainbr'					
ANN Architecture	10-(2-To-10)-1							ANN Architecture	10-(2-To-10)-(2-To-10)-1						
	Mean Error (%)				Max. Error (%)				Mean Error (%)				Max. Error (%)		
m	Design set	Indp. Test.	Addtl. Test.	CombinedTest.	Design set	Indp. Test.	Addtl. Test.	m	Design set	Indp. Test.	Addtl. Test.	CombinedTest.	Design set	Indp. Test.	Addtl. Test.
2	5.02	5.11	5.06	5.10	27.45	17.41	12.45	2	6.02	4.14	6.48	4.71	28.67	14.76	16.21
3	4.68	4.10	4.87	4.29	27.60	13.41	12.62	3	4.55	3.54	4.65	3.81	28.05	15.67	7.39
4	4.26	3.971	4.31	4.05	25.12	11.83	10.10	4	3.83	4.29	4.62	4.37	21.58	12.89	9.02
5	3.82	3.849	4.50	4.01	24.52	11.56	8.65	5	3.75	4.35	4.18	4.30	24.06	12.57	8.87
6	3.68	3.87	6.16	4.42	23.35	10.86	14.35	6	17.21	7.95	12.51	9.07	56.25	26.42	24.93
7	3.53	4.03	5.65	4.42	19.85	10.65	15.23	7	17.26	7.88	12.83	9.08	57.76	27.64	26.13
8	3.62	3.34	5.02	3.75	23.40	10.72	12.79	8	3.63	4.73	5.24	4.86	27.06	13.20	15.09
9	3.28	4.00	5.67	4.40	21.28	11.00	14.63	9	3.63	4.73	5.24	4.86	27.06	13.20	15.09
10	3.09	3.45	4.23	3.64	19.79	9.56	15.04	10	17.24	7.88	12.74	9.07	57.34	27.30	25.80

FE-based GDF	120 bridges	Training Algorithm: 'trainlm'						FE-based GDF	120 bridges	Training Algorithm: 'trainlm'					
ANN Architecture	10-(2-To-10)-1							ANN Architecture	10-(2-To-10)-(2-To-10)-1						
	Mean Error (%)				Max. Error (%)				Mean Error (%)				Max. Error (%)		
m	Design set	Indp. Test.	Addtl. Test.	CombinedTest.	Design set	Indp. Test.	Addtl. Test.	m	Design set	Indp. Test.	Addtl. Test.	CombinedTest.	Design set	Indp. Test.	Addtl. Test.
2	5.44	3.91	6.69	4.59	28.55	12.69	15.29	2	5.45	4.38	7.52	5.14	27.78	12.98	23.83
3	4.13	4.93	3.44	4.57	28.80	12.73	6.75	3	2.98	5.10	4.77	5.02	27.26	24.20	11.06
4	3.77	3.760	5.90	4.28	21.21	15.11	13.36	4	2.82	7.11	11.61	8.21	25.55	18.95	40.37
5	3.33	5.281	7.20	5.75	32.38	13.46	22.85	5	1.68	7.97	18.71	10.59	22.06	26.19	66.50
6	1.82	5.41	8.05	6.05	27.15	15.09	22.54	6	1.02	8.98	11.71	9.65	24.16	33.55	58.39
7	2.18	5.88	11.07	7.15	40.63	16.02	34.78	7	1.18	9.06	8.74	8.98	24.95	24.70	25.32
8	1.99	7.42	16.59	9.65	33.26	29.25	54.96	8	1.43	6.01	7.88	6.46	23.01	24.41	22.49
9	1.87	6.71	8.38	7.11	38.88	35.63	20.55	9	0.83	7.55	9.55	8.04	14.95	28.13	19.37
10	1.85	6.43	9.76	7.24	51.19	27.75	29.52	10	1.26	6.94	12.58	8.32	18.09	22.75	30.03

FE-based GDF	110 bridges	Training Algorithm: 'trainbr'						FE-based GDF	110 bridges	Training Algorithm: 'trainbr'					
ANN Architecture	10-(2-To-10)-1							ANN Architecture	10-(2-To-10)-(2-To-10)-1						
	Mean Error (%)				Max. Error (%)				Mean Error (%)				Max. Error (%)		
m	Design set	Indp. Test.	Addtl. Test.	CombinedTest.	Design set	Indp. Test.	Addtl. Test.	m	Design set	Indp. Test.	Addtl. Test.	CombinedTest.	Design set	Indp. Test.	Addtl. Test.
2	5.27	5.85	5.37	5.66	26.32	16.37	14.56	2	5.05	5.47	5.33	5.41	26.92	16.69	12.96
3	4.79	4.69	6.06	5.22	25.64	13.31	13.90	3	4.45	4.56	4.53	4.55	25.95	12.25	17.31
4	3.89	3.96	5.34	4.50	21.48	12.22	34.38	4	3.99	4.21	5.29	4.63	24.31	11.41	14.71
5	3.85	4.40	5.72	4.92	23.77	13.98	10.96	5	3.31	5.44	6.14	5.71	20.16	12.81	25.92
6	3.45	4.13	6.12	4.91	21.35	13.13	15.86	6	3.20	5.92	6.71	6.23	21.27	19.02	15.95
7	3.40	3.46	5.38	4.22	22.28	11.74	10.27	7	3.16	6.71	7.06	6.85	26.61	27.62	21.89
8	3.58	3.68	5.54	4.41	22.45	11.72	11.37	8	17.84	7.88	11.82	9.42	57.62	27.53	52.23
9	3.98	4.47	5.45	4.86	20.74	10.10	19.40	9	17.78	7.97	11.70	9.43	56.14	26.33	50.81
10	2.99	3.40	6.55	4.63	19.04	8.99	27.17	10	17.78	7.92	11.74	9.42	56.60	26.70	51.24

FE-based GDF	110 bridges	Training Algorithm: 'trainlm'						FE-based GDF	110 bridges	Training Algorithm: 'trainlm'					
ANN Architecture	10-(2-To-10)-1							ANN Architecture	10-(2-To-10)-(2-To-10)-1						
	Mean Error (%)				Max. Error (%)				Mean Error (%)				Max. Error (%)		
m	Design set	Indp. Test.	Addtl. Test.	CombinedTest.	Design set	Indp. Test.	Addtl. Test.	m	Design set	Indp. Test.	Addtl. Test.	CombinedTest.	Design set	Indp. Test.	Addtl. Test.
2	5.81	4.71	5.46	5.00	29.50	16.65	12.84	2	5.12	4.07	5.31	4.56	27.47	13.82	16.13
3	3.66	3.74	69.39	29.49	27.08	13.58	1305.61	3	2.97	4.50	7.01	5.49	24.16	13.58	23.21
4	3.39	4.61	8.60	6.17	17.46	15.07	44.97	4	2.58	6.29	12.70	8.80	40.91	26.79	86.86
5	3.09	7.00	7.20	7.08	18.81	21.06	38.36	5	1.51	7.84	7.82	7.83	29.72	34.82	29.18
6	2.39	7.02	15.42	10.31	34.32	20.20	73.45	6	1.20	6.36	7.07	6.64	32.07	17.98	22.01
7	1.87	8.36	10.43	9.17	19.10	49.74	28.11	7	1.51	7.14	16.26	10.72	28.02	29.17	69.71
8	1.58	8.66	12.41	10.13	27.69	40.98	34.86	8	1.33	6.97	9.76	8.06	33.22	23.06	24.44
9	1.55	10.95	15.53	12.74	21.08	39.55	41.47	9	1.18	6.89	12.87	9.23	20.68	30.61	34.08
10	1.78	8.17	19.04	12.43	31.47	23.38	86.53	10	1.56	6.04	10.75	7.89	24.65	21.43	31.95

FE-based GDF	100 bridges	Training Algorithm: 'trainbr'					
ANN Architecture	10-(2-To-10)-1						
	Mean Error (%)				Max. Error (%)		
m	Design set	Indp. Test.	Addtl. Test.	CombinedTest.	Design set	Indp. Test.	Addtl. Test.
2	5.34	5.81	5.80	5.81	25.92	16.07	16.18
3	4.58	4.07	4.52	4.29	27.05	13.00	14.72
4	4.02	4.78	5.82	5.29	21.97	21.02	41.03
5	3.42	4.421	7.80	6.08	18.94	11.99	34.56
6	3.65	4.05	5.55	4.79	20.68	15.69	35.40
7	3.40	4.16	6.53	5.33	18.35	14.55	30.77
8	3.34	4.71	7.12	5.90	19.72	23.65	41.52
9	3.17	4.77	8.68	6.69	18.35	15.54	32.61
10	8.10	4.45	5.82	5.13	25.37	15.17	19.35

FE-based GDF	100 bridges	Training Algorithm: 'trainbr'					
ANN Architecture	10-(2-To-10)-(2-To-10)-1						
	Mean Error (%)				Max. Error (%)		
m	Design set	Indp. Test.	Addtl. Test.	CombinedTest.	Design set	Indp. Test.	Addtl. Test.
2	6.40	4.42	5.02	4.72	26.72	14.52	11.97
3	4.48	5.12	6.69	5.89	25.88	21.15	35.07
4	3.73	4.48	7.14	5.79	21.17	11.68	27.12
5	18.09	7.87	13.37	10.57	58.72	28.42	53.30
6	18.06	7.87	13.30	10.54	58.33	28.10	52.91
7	18.02	7.88	13.13	10.47	57.34	27.30	51.96
8	18.02	7.88	13.11	10.46	57.20	27.19	51.83
9	18.06	7.87	13.28	10.53	58.20	27.99	52.79
10	18.02	7.88	13.15	10.47	57.45	27.39	52.07

FE-based GDF	100 bridges	Training Algorithm: 'trainlm'					
ANN Architecture	10-(2-To-10)-1						
	Mean Error (%)				Max. Error (%)		
m	Design set	Indp. Test.	Addtl. Test.	CombinedTest.	Design set	Indp. Test.	Addtl. Test.
2	6.07	3.97	5.68	4.81	29.04	11.98	15.32
3	4.31	6.22	8.29	7.24	24.60	22.22	38.87
4	2.79	5.37	5.43	5.40	32.15	15.99	47.97
5	3.14	7.347	9.06	8.19	29.86	24.28	33.63
6	2.20	9.26	11.57	10.39	25.35	21.31	38.32
7	2.21	9.91	9.38	9.65	30.66	35.78	38.51
8	1.64	10.08	16.71	13.34	35.12	31.12	70.72
9	0.73	9.80	14.33	12.02	17.68	44.12	65.73
10	1.43	9.90	14.07	11.95	29.75	23.44	75.28

FE-based GDF	100 bridges	Training Algorithm: 'trainlm'					
ANN Architecture	10-(2-To-10)-(2-To-10)-1						
	Mean Error (%)				Max. Error (%)		
m	Design set	Indp. Test.	Addtl. Test.	CombinedTest.	Design set	Indp. Test.	Addtl. Test.
2	5.12	3.88	9.92	6.85	27.31	12.98	125.83
3	3.62	6.18	19.50	12.73	25.44	19.70	343.63
4	2.18	5.53	10.17	7.81	30.86	18.57	35.13
5	1.71	10.35	17.80	14.02	24.03	34.33	56.84
6	1.71	7.16	8.78	7.96	33.41	21.67	28.39
7	1.45	7.53	9.40	8.45	38.33	21.39	51.15
8	1.32	9.21	10.24	9.72	18.86	24.13	32.35
9	0.86	7.82	10.23	9.00	23.77	43.59	28.72
10	1.03	7.96	11.08	9.49	22.19	25.67	55.01

FE-based GDF	90 bridges	Training Algorithm: 'trainbr'						FE-based GDF	90 bridges	Training Algorithm: 'trainbr'					
ANN Architecture	10-(2-To-10)-1							ANN Architecture	10-(2-To-10)-(2-To-10)-1						
	Mean Error (%)				Max. Error (%)				Mean Error (%)				Max. Error (%)		
m	Design set	Indp. Test.	Addtl. Test.	CombinedTest.	Design set	Indp. Test.	Addtl. Test.	m	Design set	Indp. Test.	Addtl. Test.	CombinedTest.	Design set	Indp. Test.	Addtl. Test.
2	5.13	7.65	7.27	7.43	24.64	20.83	19.60	2	6.65	4.35	5.29	4.88	26.92	10.87	22.11
3	4.46	4.98	7.53	6.41	25.17	14.07	28.78	3	4.48	6.29	7.35	6.89	25.35	16.10	23.48
4	3.87	5.22	6.07	5.70	23.49	18.48	29.97	4	4.14	5.81	7.30	6.65	23.21	20.70	37.68
5	4.15	4.24	5.24	4.81	23.81	22.10	31.72	5	18.80	7.87	12.96	10.74	58.74	28.43	53.31
6	3.49	5.82	7.90	6.99	18.30	14.00	31.48	6	18.91	7.89	13.25	10.91	60.19	29.61	54.72
7	3.76	4.51	5.92	5.31	18.84	13.52	20.26	7	4.04	7.57	9.19	8.48	23.59	19.86	34.86
8	4.12	5.70	7.18	6.54	25.57	17.73	25.90	8	18.78	7.87	12.94	10.72	58.57	28.29	53.15
9	4.14	4.44	6.79	5.77	25.03	10.20	22.16	9	18.77	7.87	12.89	10.70	58.24	28.02	52.83
10	4.22	4.82	7.30	6.22	23.85	14.16	31.21	10	18.82	7.86	13.02	10.77	59.05	28.68	53.61

FE-based GDF	90 bridges	Training Algorithm: 'trainlm'						FE-based GDF	90 bridges	Training Algorithm: 'trainlm'					
ANN Architecture	10-(2-To-10)-1							ANN Architecture	10-(2-To-10)-(2-To-10)-1						
	Mean Error (%)				Max. Error (%)				Mean Error (%)				Max. Error (%)		
m	Design set	Indp. Test.	Addtl. Test.	CombinedTest.	Design set	Indp. Test.	Addtl. Test.	m	Design set	Indp. Test.	Addtl. Test.	CombinedTest.	Design set	Indp. Test.	Addtl. Test.
2	5.98	5.12	7.46	6.44	28.02	19.75	24.80	2	5.94	4.58	29.78	18.78	27.99	19.28	946.46
3	3.04	6.59	9.46	8.20	15.94	24.38	54.46	3	3.72	7.62	7.99	7.82	29.80	19.62	22.03
4	2.90	7.80	9.57	8.79	23.40	19.61	58.63	4	2.05	7.50	12.66	10.40	75.29	23.96	72.42
5	2.02	8.80	12.27	10.75	17.92	28.28	40.00	5	1.98	7.58	12.80	10.52	45.14	26.31	47.36
6	2.60	11.54	10.77	11.11	23.99	24.99	35.55	6	1.32	10.26	15.74	13.35	18.52	45.61	51.38
7	1.43	12.28	14.72	13.65	18.47	37.13	58.38	7	1.88	8.91	14.59	12.11	22.66	25.86	90.94
8	1.21	7.79	13.28	10.88	17.35	30.19	72.34	8	1.66	7.17	8.78	8.08	24.40	17.36	28.32
9	1.85	11.20	16.50	14.19	28.81	30.65	72.25	9	1.37	9.09	9.53	9.34	28.01	23.77	30.76
10	0.96	9.09	13.82	11.76	13.77	36.40	67.43	10	1.49	8.13	10.10	9.24	25.28	20.47	39.44

FE-based GDF	80 bridges	Training Algorithm: 'trainbr'						FE-based GDF	80 bridges	Training Algorithm: 'trainbr'					
ANN Architecture	10-(2-To-10)-1							ANN Architecture	10-(2-To-10)-(2-To-10)-1						
	Mean Error (%)				Max. Error (%)				Mean Error (%)				Max. Error (%)		
m	Design set	Indp. Test.	Addtl. Test.	CombinedTest.	Design set	Indp. Test.	Addtl. Test.	m	Design set	Indp. Test.	Addtl. Test.	CombinedTest.	Design set	Indp. Test.	Addtl. Test.
2	5.50	7.23	7.33	7.29	22.92	19.36	22.73	2	6.84	5.17	6.57	6.03	24.64	13.28	25.58
3	4.97	5.23	7.64	6.72	22.54	15.81	26.08	3	4.51	6.16	7.31	6.87	24.38	14.72	26.60
4	4.00	4.473	7.14	6.12	22.73	11.58	26.07	4	19.03	7.88	13.53	11.37	57.68	27.57	52.29
5	4.38	4.946	6.77	6.07	24.23	12.51	24.00	5	19.19	7.88	13.91	11.60	60.13	29.56	54.65
6	4.07	4.87	6.99	6.18	23.53	11.43	27.34	6	19.07	7.87	13.61	11.41	58.38	28.14	52.96
7	4.19	4.54	6.26	5.60	25.34	13.55	23.06	7	19.12	7.86	13.73	11.48	59.14	28.76	53.70
8	8.40	5.10	7.13	6.35	24.93	18.46	24.66	8	19.07	7.87	13.63	11.42	58.48	28.22	53.06
9	4.27	5.48	7.15	6.51	23.49	12.53	26.73	9	19.08	7.87	13.63	11.43	58.54	28.27	53.12
10	3.96	5.31	7.25	6.51	23.01	11.65	29.70	10	19.23	7.90	14.01	11.67	60.68	30.00	55.19

FE-based GDF	80 bridges	Training Algorithm: 'trainlm'						FE-based GDF	80 bridges	Training Algorithm: 'trainlm'					
ANN Architecture	10-(2-To-10)-1							ANN Architecture	10-(2-To-10)-(2-To-10)-1						
	Mean Error (%)				Max. Error (%)				Mean Error (%)				Max. Error (%)		
m	Design set	Indp. Test.	Addtl. Test.	CombinedTest.	Design set	Indp. Test.	Addtl. Test.	m	Design set	Indp. Test.	Addtl. Test.	CombinedTest.	Design set	Indp. Test.	Addtl. Test.
2	5.91	4.57	6.34	5.66	27.28	18.07	21.90	2	5.94	4.40	7.98	6.61	25.82	17.06	49.79
3	3.58	7.52	7.67	7.61	23.19	19.51	21.56	3	3.08	8.59	10.41	9.72	23.10	25.36	69.68
4	3.39	7.268	10.63	9.34	30.71	18.36	57.58	4	1.41	10.57	14.96	13.28	24.94	27.37	67.16
5	2.53	10.143	10.90	10.61	27.70	24.55	41.44	5	1.47	10.49	13.27	12.21	20.91	25.62	50.67
6	2.71	9.67	11.19	10.61	69.91	27.89	38.89	6	1.78	10.61	9.77	10.09	34.59	25.06	49.03
7	2.00	8.74	11.65	10.54	28.67	23.48	97.87	7	1.62	8.04	10.16	9.35	40.01	24.90	89.61
8	2.38	8.97	10.77	10.08	34.95	25.84	29.09	8	1.20	7.97	11.49	10.14	21.06	20.94	60.48
9	1.60	9.64	10.06	9.90	27.98	42.49	51.34	9	1.62	8.64	11.40	10.35	29.81	18.69	67.11
10	1.98	9.35	14.42	12.48	44.07	23.38	64.13	10	1.33	7.53	15.78	12.62	19.37	24.30	90.50

FE-based GDF	70 bridges	Training Algorithm: 'trainbr'						FE-based GDF	70 bridges	Training Algorithm: 'trainbr'					
ANN Architecture	10-(2-To-10)-1							ANN Architecture	10-(2-To-10)-(2-To-10)-1						
	Mean Error (%)				Max. Error (%)				Mean Error (%)				Max. Error (%)		
m	Design set	Indp. Test.	Addtl. Test.	CombinedTest.	Design set	Indp. Test.	Addtl. Test.	m	Design set	Indp. Test.	Addtl. Test.	CombinedTest.	Design set	Indp. Test.	Addtl. Test.
2	7.46	6.60	10.18	8.96	23.73	25.01	59.58	2	5.74	5.56	5.98	5.83	25.25	11.88	20.93
3	5.18	5.34	6.78	6.29	22.46	15.63	23.56	3	5.44	5.73	7.07	6.61	23.53	15.92	31.06
4	4.24	4.97	6.24	5.81	23.61	12.09	33.64	4	19.00	7.87	14.63	12.33	58.53	28.26	53.11
5	9.13	5.30	7.70	6.88	28.93	18.50	26.88	5	18.99	7.87	14.63	12.32	58.47	28.22	53.05
6	8.89	4.85	6.73	6.09	25.47	15.88	23.09	6	19.02	7.87	14.66	12.35	58.83	28.50	53.40
7	8.80	5.88	7.31	6.82	24.73	19.71	27.64	7	18.98	7.87	14.62	12.32	58.38	28.14	52.96
8	4.34	4.14	6.72	5.84	24.51	10.55	27.43	8	18.94	7.88	14.58	12.30	57.83	27.70	52.44
9	8.83	4.87	6.87	6.19	24.94	16.88	22.61	9	19.02	7.87	14.66	12.35	58.83	28.51	53.40
10	8.74	5.36	6.71	6.25	25.56	18.22	25.85	10	19.02	7.87	14.66	12.34	58.81	28.49	53.38

FE-based GDF	70 bridges	Training Algorithm: 'trainlm'						FE-based GDF	70 bridges	Training Algorithm: 'trainlm'					
ANN Architecture	10-(2-To-10)-1							ANN Architecture	10-(2-To-10)-(2-To-10)-1						
	Mean Error (%)				Max. Error (%)				Mean Error (%)				Max. Error (%)		
m	Design set	Indp. Test.	Addtl. Test.	CombinedTest.	Design set	Indp. Test.	Addtl. Test.	m	Design set	Indp. Test.	Addtl. Test.	CombinedTest.	Design set	Indp. Test.	Addtl. Test.
2	6.54	5.77	7.75	7.07	27.90	24.20	28.81	2	6.24	6.37	8.21	7.59	26.15	16.38	31.46
3	4.44	8.30	8.30	8.30	22.29	22.75	76.03	3	3.21	9.38	12.75	11.60	22.30	21.45	74.18
4	3.17	9.47	8.41	8.77	32.05	25.10	30.58	4	2.04	13.90	15.29	14.82	36.82	47.33	69.97
5	2.55	12.11	19.75	17.15	47.05	31.82	293.07	5	1.62	11.36	11.77	11.63	32.79	38.29	73.50
6	1.62	11.59	15.17	13.95	25.70	38.47	72.88	6	1.80	10.73	14.51	13.22	42.58	36.30	68.63
7	2.00	10.57	13.73	12.65	36.97	35.77	86.14	7	2.39	8.69	13.58	11.92	41.97	30.26	53.89
8	1.91	9.23	10.91	10.34	32.43	18.14	58.51	8	1.73	10.09	12.54	11.71	23.90	22.01	71.36
9	1.89	12.22	13.09	12.79	27.59	26.05	69.16	9	1.59	9.56	10.07	9.89	22.90	35.83	38.06
10	1.64	11.56	12.71	12.32	37.74	32.76	49.47	10	2.31	8.93	9.26	9.15	37.29	21.77	55.94

FE-based GDF	60 bridges	Training Algorithm: 'trainbr'						FE-based GDF	60 bridges	Training Algorithm: 'trainbr'					
ANN Architecture	10-(2-To-10)-1							ANN Architecture	10-(2-To-10)-(2-To-10)-1						
	Mean Error (%)				Max. Error (%)				Mean Error (%)				Max. Error (%)		
m	Design set	Indp. Test.	Addtl. Test.	CombinedTest.	Design set	Indp. Test.	Addtl. Test.	m	Design set	Indp. Test.	Addtl. Test.	CombinedTest.	Design set	Indp. Test.	Addtl. Test.
2	6.09	5.39	6.11	5.89	23.59	13.42	19.74	2	6.10	7.81	6.77	7.09	22.87	18.93	24.43
3	4.82	5.37	7.20	6.64	22.10	16.52	27.55	3	4.76	5.15	7.97	7.11	23.81	15.09	36.48
4	9.45	5.07	7.28	6.60	24.54	17.09	23.94	4	19.95	7.87	14.36	12.37	57.98	27.81	52.58
5	9.56	4.80	6.99	6.32	23.72	16.64	22.05	5	19.85	7.89	14.34	12.36	57.15	27.15	51.78
6	9.35	5.16	7.17	6.55	24.41	16.78	25.51	6	19.84	7.89	14.34	12.36	57.05	27.06	51.68
7	8.99	5.06	7.14	6.50	26.14	16.01	24.15	7	19.83	7.90	14.34	12.36	56.98	27.01	51.61
8	9.23	4.69	7.06	6.33	24.77	15.39	22.24	8	19.84	7.89	14.34	12.36	57.06	27.08	51.69
9	9.38	5.05	6.86	6.30	25.39	17.89	23.84	9	19.76	7.99	14.33	12.39	56.01	26.22	50.67
10	9.23	4.96	7.26	6.55	25.05	18.03	24.86	10	19.89	7.88	14.35	12.36	57.55	27.47	52.16

FE-based GDF	60 bridges	Training Algorithm: 'trainlm'						FE-based GDF	60 bridges	Training Algorithm: 'trainlm'					
ANN Architecture	10-(2-To-10)-1							ANN Architecture	10-(2-To-10)-(2-To-10)-1						
	Mean Error (%)				Max. Error (%)				Mean Error (%)				Max. Error (%)		
m	Design set	Indp. Test.	Addtl. Test.	CombinedTest.	Design set	Indp. Test.	Addtl. Test.	m	Design set	Indp. Test.	Addtl. Test.	CombinedTest.	Design set	Indp. Test.	Addtl. Test.
2	6.46	5.65	7.75	7.10	27.62	24.91	33.22	2	6.04	7.16	8.37	8.00	43.96	25.07	38.99
3	3.86	7.35	14.16	12.07	27.85	21.33	74.09	3	1.67	10.49	16.43	14.61	27.37	61.73	226.36
4	2.25	9.198	10.77	10.29	28.00	39.97	49.21	4	2.22	10.35	14.81	13.44	54.62	39.89	58.54
5	2.48	8.467	12.97	11.59	40.28	33.72	52.17	5	2.57	7.62	10.42	9.56	48.51	32.71	50.14
6	1.81	9.70	10.75	10.43	25.54	30.58	39.32	6	1.72	9.63	10.57	10.29	27.50	23.20	45.43
7	1.11	11.83	15.76	14.55	14.67	36.96	87.65	7	2.09	10.06	13.54	12.47	21.86	27.37	67.88
8	2.05	11.14	11.16	11.16	31.40	29.67	46.15	8	1.93	7.78	11.27	10.20	20.58	19.25	98.83
9	1.17	8.22	15.53	13.29	24.17	30.53	141.17	9	1.30	9.14	11.00	10.43	34.74	23.48	36.49
10	1.39	8.37	12.64	11.33	25.03	53.49	100.19	10	1.46	9.86	10.29	10.15	25.68	25.62	39.90

FE-based GDF	50 bridges	Training Algorithm: 'trainbr'						FE-based GDF	50 bridges	Training Algorithm: 'trainbr'					
ANN Architecture	10-(2-To-10)-1							ANN Architecture	10-(2-To-10)-(2-To-10)-1						
	Mean Error (%)				Max. Error (%)				Mean Error (%)				Max. Error (%)		
m	Design set	Indp. Test.	Addtl. Test.	CombinedTest.	Design set	Indp. Test.	Addtl. Test.	m	Design set	Indp. Test.	Addtl. Test.	CombinedTest.	Design set	Indp. Test.	Addtl. Test.
2	5.51	6.87	10.21	9.28	25.61	26.46	51.78	2	5.26	7.56	10.79	9.89	22.84	26.94	60.34
3	4.96	5.69	7.77	7.19	22.69	25.94	29.42	3	21.40	7.99	13.99	12.31	56.01	26.22	50.68
4	8.69	5.159	7.56	6.89	27.67	18.40	23.80	4	21.58	7.88	13.99	12.28	57.57	27.49	52.19
5	8.78	5.150	7.71	6.99	26.96	18.59	23.22	5	21.49	7.90	13.98	12.28	56.89	26.93	51.53
6	8.94	4.97	7.51	6.80	27.83	18.64	23.58	6	21.66	7.87	14.00	12.29	58.06	27.88	52.66
7	8.69	4.87	7.71	6.92	28.98	18.48	22.82	7	21.50	7.90	13.98	12.28	56.96	26.99	51.59
8	8.60	5.30	7.71	7.04	27.72	19.14	23.44	8	21.74	7.87	14.01	12.29	58.53	28.26	53.11
9	9.16	4.82	7.66	6.87	28.71	18.76	23.67	9	21.70	7.87	14.00	12.29	58.33	28.10	52.92
10	8.79	5.03	7.99	7.16	28.91	18.75	23.05	10	21.44	7.92	13.98	12.29	56.53	26.64	51.18

FE-based GDF	50 bridges	Training Algorithm: 'trainlm'						FE-based GDF	50 bridges	Training Algorithm: 'trainlm'					
ANN Architecture	10-(2-To-10)-1							ANN Architecture	10-(2-To-10)-(2-To-10)-1						
	Mean Error (%)				Max. Error (%)				Mean Error (%)				Max. Error (%)		
m	Design set	Indp. Test.	Addtl. Test.	CombinedTest.	Design set	Indp. Test.	Addtl. Test.	m	Design set	Indp. Test.	Addtl. Test.	CombinedTest.	Design set	Indp. Test.	Addtl. Test.
2	4.91	9.62	19.75	16.92	23.05	33.20	456.72	2	4.72	9.09	10.86	10.36	41.24	25.70	40.39
3	2.61	8.29	10.45	9.84	25.14	23.59	47.28	3	3.16	10.66	12.58	12.05	48.56	27.45	37.51
4	2.15	12.139	13.26	12.95	30.99	34.45	55.38	4	1.75	9.08	12.10	11.26	27.45	30.08	64.24
5	1.47	7.521	12.94	11.42	30.85	25.18	84.48	5	2.21	7.89	8.13	8.06	33.77	26.01	30.03
6	1.77	9.70	13.73	12.60	25.66	26.51	143.27	6	2.42	7.90	9.46	9.02	39.47	22.36	32.37
7	1.99	8.41	11.32	10.51	28.82	28.29	38.77	7	1.27	8.27	10.05	9.56	32.90	20.38	65.60
8	1.66	8.40	11.21	10.43	31.26	39.32	71.05	8	1.53	8.87	11.73	10.93	28.17	33.14	43.53
9	1.89	6.73	11.38	10.08	33.33	24.12	83.45	9	0.90	9.17	10.03	9.79	13.10	26.42	50.36
10	1.57	8.40	11.41	10.57	35.48	25.06	57.37	10	1.64	7.05	9.79	9.02	32.78	19.01	51.26

FE-based GDF	40 bridges	Training Algorithm: 'trainbr'						FE-based GDF	40 bridges	Training Algorithm: 'trainbr'					
ANN Architecture	10-(2-To-10)-1							ANN Architecture	10-(2-To-10)-(2-To-10)-1						
	Mean Error (%)				Max. Error (%)				Mean Error (%)				Max. Error (%)		
m	Design set	Indp. Test.	Addtl. Test.	CombinedTest.	Design set	Indp. Test.	Addtl. Test.	m	Design set	Indp. Test.	Addtl. Test.	CombinedTest.	Design set	Indp. Test.	Addtl. Test.
2	8.54	7.24	8.67	8.30	26.00	19.15	28.88	2	23.72	7.88	13.89	12.35	57.64	27.54	52.25
3	8.84	6.43	8.53	7.99	25.69	18.19	26.79	3	23.47	7.96	13.90	12.38	56.18	26.36	50.84
4	8.61	6.825	8.84	8.32	25.17	18.99	28.04	4	23.55	7.91	13.89	12.35	56.73	26.81	51.38
5	8.97	6.512	8.75	8.18	25.59	19.61	28.95	5	23.50	7.94	13.89	12.37	56.38	26.52	51.03
6	8.79	6.41	8.63	8.06	25.41	18.68	26.83	6	23.64	7.89	13.88	12.35	57.19	27.18	51.81
7	8.48	6.26	8.59	8.00	26.03	16.96	26.15	7	23.60	7.90	13.88	12.35	57.00	27.02	51.63
8	8.76	6.28	8.70	8.08	24.82	17.88	27.51	8	23.31	8.14	13.94	12.45	55.14	25.52	49.83
9	8.30	6.57	8.84	8.26	25.82	18.98	27.25	9	23.22	8.25	13.96	12.50	54.56	25.05	49.27
10	8.79	6.12	8.54	7.92	25.79	17.45	26.59	10	23.30	8.16	13.94	12.46	55.05	25.45	49.75

FE-based GDF	40 bridges	Training Algorithm: 'trainlm'						FE-based GDF	40 bridges	Training Algorithm: 'trainlm'					
ANN Architecture	10-(2-To-10)-1							ANN Architecture	10-(2-To-10)-(2-To-10)-1						
	Mean Error (%)				Max. Error (%)				Mean Error (%)				Max. Error (%)		
m	Design set	Indp. Test.	Addtl. Test.	CombinedTest.	Design set	Indp. Test.	Addtl. Test.	m	Design set	Indp. Test.	Addtl. Test.	CombinedTest.	Design set	Indp. Test.	Addtl. Test.
2	23.30	8.16	13.94	12.46	55.05	25.45	49.75	2	1.46	11.97	15.55	14.63	13.57	34.92	68.47
3	2.47	11.24	17.27	15.73	43.82	51.31	87.01	3	2.09	12.47	17.76	16.40	27.25	39.65	112.72
4	1.50	10.267	13.28	12.51	40.92	30.33	78.71	4	1.32	10.74	13.03	12.44	27.48	26.58	90.17
5	1.69	9.351	14.67	13.31	22.56	28.01	69.27	5	1.72	9.45	11.11	10.68	33.83	30.04	56.94
6	1.33	8.69	9.74	9.47	26.58	27.54	50.54	6	2.24	8.92	12.95	11.92	28.23	43.68	71.22
7	2.28	8.73	11.12	10.51	37.61	26.36	74.76	7	1.27	7.71	10.03	9.44	33.58	22.27	64.90
8	1.74	7.52	10.81	9.96	33.77	25.04	59.39	8	0.75	10.69	14.64	13.63	12.67	22.98	117.02
9	1.67	7.04	10.16	9.36	32.02	28.65	54.43	9	1.74	7.38	11.30	10.29	29.51	22.58	85.38
10	1.44	8.68	10.92	10.35	30.67	29.82	37.70	10	2.04	5.40	8.78	7.92	32.72	17.99	57.50

FE-based GDF	30 bridges	Training Algorithm: 'trainbr'						FE-based GDF	30 bridges	Training Algorithm: 'trainbr'					
ANN Architecture	10-(2-To-10)-1							ANN Architecture	10-(2-To-10)-(2-To-10)-1						
	Mean Error (%)				Max. Error (%)				Mean Error (%)				Max. Error (%)		
m	Design set	Indp. Test.	Addtl. Test.	CombinedTest.	Design set	Indp. Test.	Addtl. Test.	m	Design set	Indp. Test.	Addtl. Test.	CombinedTest.	Design set	Indp. Test.	Addtl. Test.
2	11.48	5.94	8.88	8.18	26.55	20.42	30.17	2	22.86	8.00	15.03	13.37	55.95	26.18	50.62
3	11.66	5.85	8.95	8.21	27.99	21.24	31.52	3	22.90	7.97	15.02	13.35	56.14	26.33	50.80
4	10.82	5.839	8.91	8.18	23.38	18.65	28.38	4	22.63	8.22	15.07	13.45	54.71	25.17	49.42
5	11.55	5.076	8.59	7.76	24.55	17.46	28.59	5	22.47	8.40	15.12	13.53	53.86	24.48	48.60
6	10.92	6.01	8.41	7.84	24.51	19.83	28.40	6	22.60	8.24	15.07	13.46	54.56	25.05	49.28
7	11.46	5.73	9.27	8.43	23.62	18.11	30.55	7	22.51	8.35	15.10	13.50	54.06	24.65	48.79
8	11.54	5.44	8.64	7.88	24.14	18.71	29.05	8	22.65	8.20	15.06	13.44	54.83	25.27	49.54
9	10.96	5.59	8.35	7.69	24.44	18.96	28.59	9	22.37	8.52	15.16	13.58	53.30	24.03	48.06
10	10.31	6.27	8.71	8.13	25.01	19.30	29.99	10	22.12	8.88	15.27	13.76	51.65	22.70	46.47

FE-based GDF	30 bridges	Training Algorithm: 'trainlm'						FE-based GDF	30 bridges	Training Algorithm: 'trainlm'					
ANN Architecture	10-(2-To-10)-1							ANN Architecture	10-(2-To-10)-(2-To-10)-1						
	Mean Error (%)				Max. Error (%)				Mean Error (%)				Max. Error (%)		
m	Design set	Indp. Test.	Addtl. Test.	CombinedTest.	Design set	Indp. Test.	Addtl. Test.	m	Design set	Indp. Test.	Addtl. Test.	CombinedTest.	Design set	Indp. Test.	Addtl. Test.
2	3.98	12.05	20.02	18.13	40.55	41.78	76.49	2	22.18	8.79	15.24	13.72	52.04	23.01	46.84
3	1.74	10.77	13.14	12.58	30.57	28.67	83.69	3	1.63	10.33	14.84	13.77	28.93	48.43	49.73
4	2.08	9.412	9.85	9.75	25.71	34.66	31.52	4	1.72	10.63	15.63	14.45	23.39	32.45	52.02
5	2.77	8.649	10.98	10.43	32.95	29.53	45.09	5	0.58	12.01	14.44	13.86	7.70	37.43	47.34
6	3.23	7.36	9.57	9.05	35.84	31.88	30.40	6	2.18	12.12	12.84	12.67	18.40	32.06	48.18
7	2.79	10.60	10.18	10.28	41.60	35.84	53.99	7	1.78	7.92	13.92	12.50	17.46	28.39	81.36
8	2.60	8.24	12.46	11.46	34.88	23.51	72.40	8	2.22	7.30	12.46	11.24	34.34	25.61	72.82
9	1.42	10.30	14.33	13.38	13.73	27.26	68.10	9	0.77	12.44	16.10	15.24	7.16	36.71	102.03
10	2.06	10.32	8.53	8.95	32.33	23.56	45.34	10	2.30	8.42	12.01	11.16	32.83	28.10	55.59

FE-based GDF	20 bridges	Training Algorithm: 'trainbr'						FE-based GDF	20 bridges	Training Algorithm: 'trainbr'					
ANN Architecture	10-(2-To-10)-1							ANN Architecture	10-(2-To-10)-(2-To-10)-1						
	Mean Error (%)				Max. Error (%)				Mean Error (%)				Max. Error (%)		
m	Design set	Indp. Test.	Addtl. Test.	CombinedTest.	Design set	Indp. Test.	Addtl. Test.	m	Design set	Indp. Test.	Addtl. Test.	CombinedTest.	Design set	Indp. Test.	Addtl. Test.
2	22.17	7.97	15.87	14.14	56.15	26.33	50.81	2	22.17	7.97	15.87	14.14	56.15	26.33	50.81
3	22.43	7.88	15.89	14.13	57.41	27.35	52.03	3	22.09	8.03	15.88	14.15	55.78	26.04	50.46
4	22.43	7.881	15.89	14.13	57.41	27.35	52.03	4	22.19	7.95	15.87	14.13	56.26	26.43	50.92
5	22.06	8.053	15.88	14.16	55.63	25.92	50.31	5	22.12	8.00	15.88	14.14	55.94	26.17	50.61
6	22.33	7.90	15.88	14.12	56.95	26.99	51.57	6	21.89	8.20	15.89	14.20	54.80	25.25	49.51
7	22.21	7.94	15.87	14.13	56.38	26.52	51.03	7	21.91	8.18	15.89	14.20	54.91	25.34	49.62
8	22.14	7.98	15.87	14.13	56.05	26.27	50.70	8	22.03	8.08	15.88	14.17	55.49	25.80	50.17
9	22.22	7.93	15.87	14.12	56.44	26.59	51.08	9	21.95	8.15	15.89	14.19	55.10	25.49	49.80
10	22.23	7.93	15.87	14.13	56.48	26.60	51.12	10	21.75	8.34	15.91	14.25	54.12	24.69	48.85

FE-based GDF	20 bridges	Training Algorithm: 'trainlm'						FE-based GDF	20 bridges	Training Algorithm: 'trainlm'					
ANN Architecture	10-(2-To-10)-1							ANN Architecture	10-(2-To-10)-(2-To-10)-1						
	Mean Error (%)				Max. Error (%)				Mean Error (%)				Max. Error (%)		
m	Design set	Indp. Test.	Addtl. Test.	CombinedTest.	Design set	Indp. Test.	Addtl. Test.	m	Design set	Indp. Test.	Addtl. Test.	CombinedTest.	Design set	Indp. Test.	Addtl. Test.
2	2.16	9.65	15.52	14.23	27.94	36.77	65.21	2	4.07	9.73	15.05	13.88	56.09	30.28	66.58
3	2.91	9.27	16.36	14.80	37.48	33.15	82.85	3	1.53	9.28	14.82	13.60	13.25	30.87	66.51
4	3.42	9.932	12.75	12.13	34.45	35.85	46.85	4	0.43	10.88	16.76	15.47	7.52	29.32	75.85
5	4.01	9.285	16.47	14.89	45.91	37.53	85.50	5	2.27	10.34	15.83	14.62	28.29	34.56	81.47
6	1.06	12.13	16.84	15.80	9.71	41.51	72.12	6	2.29	9.54	14.57	13.46	26.66	48.83	68.45
7	2.23	8.68	15.41	13.93	41.68	31.65	67.15	7	5.24	10.20	14.56	13.60	45.04	32.89	51.68
8	3.97	9.62	17.12	15.47	29.43	29.48	62.70	8	0.56	12.38	13.68	13.40	7.37	36.09	61.72
9	1.99	10.01	15.30	14.14	21.73	36.40	74.56	9	3.18	9.12	12.22	11.54	26.33	29.64	53.23
10	4.07	9.73	15.05	13.88	56.09	30.28	66.58	10	0.45	11.42	14.73	14.00	3.69	41.88	68.54

10.4 Rating Factors

Note that ANN rating factors are not shown for bridges that were identified as outliers. Bridges 1-100 are bridges that were gathered for this current study. Bridges 101-174 were made available by Sofi's pilot study (2017).

Table 29. Operating Rating Factors for Bridges in this Study

		Moment LRFR Operating RF			Shear LRFR Operating RF			ANN Benefit	
Bridge #	Bridge ID	AASHTO	FEM	ANN	AASHTO	FEM	ANN	Moment ANN Benefit	Shear ANN Benefit
1	C006313310P	1.48	1.81	1.60	1.27	1.99	1.72	1.08	1.36
2	C006305115	1.78	2.11	2.10	1.85	2.67	2.78	1.18	1.50
3	C001705805	1.61	2.16	2.02	1.89	1.84	1.99	1.25	1.05
4	C001902340	1.82	2.11	1.93	2.22	2.74	2.53	1.06	1.14
5	C005922330	0.92	1.09	1.02	2.03	2.59	2.39	1.12	1.18
6	C001903310	0.74	1.58	#N/A	1.72	2.96	2.65	#N/A	1.54
7	C001823610	1.11	1.41	1.38	2.54	3.00	2.76	1.24	1.09
8	C007443235	1.89	2.24	2.01	2.02	3.50	3.36	1.07	1.66
9	C009133625	0.82	1.40	1.31	2.46	3.32	3.27	1.61	1.33
10	C001111430	1.92	2.20	2.16	2.62	2.88	2.69	1.13	1.03
11	C008402410	1.48	1.59	1.56	2.75	2.88	2.99	1.05	1.08
12	C005901410	1.08	1.24	1.14	3.03	3.38	3.34	1.06	1.10
13	C003403910	1.43	1.63	1.62	3.37	3.63	3.45	1.13	1.02
14	C002902505	1.36	1.61	1.51	3.56	5.41	5.30	1.11	1.49
15	C001403305P	0.99	1.12	0.97	4.27	4.58	4.47	0.98	1.05
16	C007424540	1.18	1.40	1.34	4.25	5.85	#N/A	1.14	#N/A

17	C006710205	1.22	1.45	1.37	4.41	4.71	4.60	1.13	1.04
18	C007025010	1.33	1.55	1.41	4.96	5.31	5.30	1.06	1.07
19	C000102908	1.35	1.59	1.46	5.08	5.58	5.38	1.09	1.06
20	C000134022	2.92	3.18	3.01	3.78	4.11	4.05	1.03	1.07
21	C000602505	1.21	1.65	1.55	1.90	2.30	2.26	1.28	1.19
22	C001101705	1.35	1.60	1.45	2.94	3.37	3.10	1.07	1.05
23	C001800605	1.24	1.65	1.62	2.64	3.03	2.81	1.30	1.07
24	C001814715	1.26	1.62	1.59	2.82	3.35	3.11	1.27	1.10
25	C002000707P	2.37	3.07	2.85	2.98	3.36	3.24	1.20	1.09
26	C002000823	2.59	3.37	3.05	2.60	3.05	2.81	1.18	1.08
27	C002001505	2.58	2.97	3.04	2.85	2.73	3.03	1.17	1.06
28	C002004725	1.60	2.16	2.11	2.89	3.23	3.12	1.32	1.08
29	C002004730	2.44	3.23	2.95	2.69	3.04	2.94	1.21	1.09
30	C002701945	0.94	1.14	1.08	3.08	3.15	2.96	1.15	0.96
31	C002702510	1.48	1.78	1.62	2.80	4.63	4.05	1.10	1.45
32	C002704210P	1.17	1.43	1.37	2.64	3.30	3.19	1.17	1.21
33	C003303710	1.18	1.51	1.35	4.62	5.75	5.09	1.15	1.10
34	C003314210	1.65	2.31	1.82	6.33	7.31	6.80	1.11	1.07
35	C003406020	1.16	1.51	1.38	2.25	2.25	2.27	1.19	1.01
36	C003413410	0.74	1.00	0.94	2.40	2.41	2.36	1.28	0.98
37	C003704805P	1.65	1.81	1.74	3.22	3.45	3.36	1.05	1.05
38	C004800415	1.61	1.79	1.73	4.12	4.67	4.32	1.08	1.05
39	C004802905	3.80	4.72	4.02	2.40	4.44	4.14	1.06	1.73
40	C004803915	1.42	2.72	2.54	2.39	3.84	3.77	1.79	1.58
41	C004804115	1.32	1.38	1.23	2.14	2.38	2.27	0.93	1.06
42	C004813220	1.72	2.19	#N/A	9.01	10.46	#N/A	#N/A	#N/A

43	C005137305	1.83	2.16	#N/A	5.95	6.24	#N/A	#N/A	#N/A
44	C005900525	0.61	0.98	0.92	1.40	2.20	2.24	1.52	1.60
45	C005900730	1.34	1.66	1.46	2.89	3.62	3.30	1.09	1.14
46	C005901502	2.02	2.31	1.99	1.39	5.30	#N/A	0.99	#N/A
47	C005901805	1.30	1.50	1.36	4.68	5.61	5.05	1.05	1.08
48	C005901830	1.41	1.63	1.51	3.08	3.62	3.27	1.07	1.06
49	C005901925	1.00	1.20	1.18	2.89	3.06	3.09	1.18	1.07
50	C005902215	1.12	1.41	1.22	3.20	4.04	3.75	1.09	1.17
51	C005903110	0.87	1.59	1.49	2.52	4.12	3.83	1.71	1.52
52	C005913020	1.56	1.95	1.75	3.36	4.29	4.01	1.13	1.19
53	C005913903	0.99	1.20	1.19	1.47	1.86	1.69	1.20	1.15
54	C005940620	1.11	2.10	#N/A	9.98	16.58	#N/A	#N/A	#N/A
55	C006300507	0.83	1.35	#N/A	0.92	1.50	#N/A	#N/A	#N/A
56	C006300825P	1.10	1.82	1.71	1.90	2.95	2.96	1.56	1.56
57	C006301204P	0.48	0.79	0.71	2.32	3.66	3.41	1.50	1.47
58	C006313105	0.65	1.04	0.99	1.89	3.04	2.95	1.51	1.56
59	C006341615	0.61	1.08	0.95	2.31	3.73	3.50	1.56	1.52
60	C006602010	1.18	1.41	1.40	2.91	3.18	3.04	1.19	1.04
61	C006607105P	1.04	1.30	1.27	2.70	2.86	2.77	1.22	1.02
62	C007001220	0.96	1.23	1.14	3.19	3.43	3.47	1.19	1.09
63	C007004115	0.85	1.20	1.03	2.97	3.25	3.27	1.22	1.10
64	C007010905	0.87	1.26	1.18	1.71	2.01	1.90	1.35	1.11
65	C007012235	1.20	1.53	1.52	2.42	2.67	2.40	1.26	0.99
66	C007202710	1.64	1.90	1.71	2.87	3.45	3.05	1.04	1.07
67	C007203715	1.18	1.29	1.23	1.73	1.88	1.92	1.04	1.11
68	C007203805	1.36	1.61	1.38	1.73	2.02	1.91	1.01	1.11

69	C007213110	1.57	1.82	1.63	2.86	3.31	3.16	1.04	1.10
70	C007602705	1.44	1.48	1.35	2.87	3.50	3.32	0.93	1.16
71	C007603710	1.50	1.75	1.68	2.68	3.05	3.01	1.12	1.12
72	C007802440	1.10	1.29	1.24	2.80	2.95	2.90	1.12	1.04
73	C007805310P	2.00	2.38	2.21	2.45	3.03	2.83	1.11	1.16
74	C007815273	2.54	2.93	2.80	4.59	7.07	6.86	1.10	1.49
75	C007932415	1.12	1.59	1.45	2.53	4.10	3.69	1.29	1.46
76	C008002310	1.99	2.32	2.17	3.04	3.28	3.24	1.09	1.07
77	C008101013P	4.75	5.60	5.28	4.82	5.98	5.22	1.11	1.08
78	C008803505	1.12	1.33	1.27	2.02	2.29	2.19	1.14	1.08
79	C009002115	0.56	0.94	#N/A	2.45	4.04	3.93	#N/A	1.60
80	C009111705	1.88	2.28	2.16	2.55	2.72	2.59	1.15	1.01
81	C009114505	1.47	1.70	1.60	1.92	2.40	2.24	1.09	1.16
82	C009143435	0.87	1.07	1.05	1.93	2.16	2.13	1.20	1.11
83	C009202210	1.24	1.48	1.43	3.34	4.21	3.84	1.15	1.15
84	C000103420	0.68	1.05	1.14	2.62	2.92	3.63	1.69	1.39
85	C001132713	0.93	1.83	#N/A	0.99	1.93	#N/A	#N/A	#N/A
86	C001234905	1.04	1.22	1.16	2.69	4.23	4.18	1.11	1.55
87	C002012435	1.00	1.10	1.14	3.48	3.63	3.68	1.14	1.06
88	C002602910	1.59	1.70	1.75	5.04	5.97	5.39	1.09	1.07
89	C002713535	0.93	2.52	#N/A	0.88	1.92	#N/A	#N/A	#N/A
90	C005904610	0.99	1.33	1.55	1.34	1.91	2.08	1.56	1.55
91	C005913505	0.59	0.55	0.61	2.15	2.31	2.34	1.03	1.09
92	C007000515	0.77	1.46	1.30	1.94	2.60	2.52	1.70	1.30
93	C007824260	1.48	1.84	1.64	4.78	4.91	4.86	1.11	1.02
94	C009123545	1.71	1.90	1.61	2.58	2.89	2.62	0.94	1.02

95	C002705115	1.82	2.18	2.07	2.84	3.15	2.86	1.14	1.01
96	C003302510	1.57	1.81	1.66	3.05	3.35	3.25	1.06	1.07
97	C005121315P	2.45	2.68	2.36	2.99	3.18	3.19	0.97	1.07
98	C001103815	1.30	1.41	1.40	4.51	5.18	4.97	1.08	1.10
99	C001900130	2.41	2.71	2.55	3.03	3.28	3.26	1.06	1.08
100	C001900815	1.41	1.63	1.54	3.14	3.73	3.46	1.09	1.10
101	C000621615	3.89	4.53	4.38	4.74	4.68	#N/A	1.13	#N/A
102	C000800705	3.82	4.39	4.12	4.20	4.83	5.01	1.08	1.19
103	C000805510P	2.69	3.14	2.83	2.69	3.35	3.26	1.05	1.21
104	C001201410	2.61	3.97	2.76	2.35	2.91	2.95	1.06	1.26
105	C001210930	3.39	4.44	3.77	6.25	6.75	6.43	1.11	1.03
106	C001224325	1.79	2.27	2.02	4.08	4.49	3.97	1.13	0.97
107	C000226205	2.13	2.72	2.18	2.62	2.92	2.85	1.02	1.09
108	C001401535	2.39	3.59	2.43	2.23	3.39	3.28	1.02	1.47
109	C001401710	2.43	2.93	2.44	3.65	3.79	3.66	1.00	1.00
110	C001411615P	2.03	2.70	2.12	3.36	4.56	4.36	1.04	1.30
111	C001526720	3.50	4.76	3.48	2.92	3.70	3.47	0.99	1.19
112	C002001220	2.49	3.76	3.56	2.49	2.38	2.42	1.43	0.97
113	C001716105	2.55	3.95	3.55	4.27	6.26	6.16	1.39	1.44
114	C002001627	3.52	4.35	4.06	3.19	3.65	3.43	1.15	1.08
115	C002003405	2.50	3.12	3.00	3.03	3.37	3.29	1.20	1.09
116	C002003505	1.90	2.57	2.46	4.23	4.61	4.56	1.30	1.08
117	C002004010	1.81	2.39	2.36	4.36	4.74	4.70	1.30	1.08
118	C002012040	3.14	3.89	3.71	3.55	3.95	3.83	1.18	1.08
119	C002013720	2.72	3.40	3.19	2.89	3.27	3.12	1.17	1.08
120	C002014017	3.56	4.42	4.27	2.88	3.32	3.16	1.20	1.10

121	C002313205	3.02	3.45	#N/A	6.51	7.53	#N/A	#N/A	#N/A
122	C000604715	1.88	2.25	2.25	4.62	5.19	4.93	1.20	1.07
123	C003416235	2.08	2.45	2.17	2.77	3.35	3.11	1.04	1.12
124	C004507603	3.11	3.97	3.38	3.39	3.97	3.93	1.09	1.16
125	C004513915	1.87	2.24	2.01	3.43	4.11	3.77	1.07	1.10
126	C004712915	3.03	3.49	3.12	2.78	3.05	2.98	1.03	1.07
127	C000201005	3.30	3.69	#N/A	2.10	2.12	#N/A	#N/A	#N/A
128	C005463410	1.67	3.64	2.88	2.24	3.71	3.49	1.73	1.55
129	C005606105	2.22	2.57	2.41	2.84	3.16	3.11	1.08	1.09
130	C005900505	2.62	2.95	2.40	3.47	3.82	3.64	0.91	1.05
131	C005900915	2.91	4.22	3.26	2.97	3.65	3.93	1.12	1.32
132	C005901517	2.81	3.31	2.82	2.68	2.98	2.88	1.00	1.08
133	C005913030	2.24	2.61	2.30	2.42	2.69	2.59	1.03	1.07
134	C005914820	2.29	2.93	2.59	2.97	3.64	3.72	1.13	1.25
135	C007904705	4.01	6.88	4.49	2.70	3.52	3.53	1.12	1.31
136	C006514240	3.06	3.81	3.15	3.14	3.66	3.44	1.03	1.09
137	C007100625	2.55	3.05	2.99	5.18	5.66	5.75	1.17	1.11
138	C007101130	3.02	4.09	3.89	5.16	7.00	6.58	1.29	1.28
139	C007103415	1.54	2.95	2.84	1.70	3.00	2.88	1.84	1.70
140	C001712925	2.69	3.21	3.04	4.25	4.64	4.58	1.13	1.08
141	C007112340	2.78	3.99	3.32	2.97	3.72	3.72	1.19	1.25
142	C007910405	2.78	3.32	2.94	2.97	3.21	3.20	1.06	1.08
143	C007911205	3.10	3.71	3.51	4.47	5.52	5.47	1.13	1.22
144	C008001215	1.83	2.54	#N/A	2.05	2.08	#N/A	#N/A	#N/A
145	C008602105P	2.40	2.84	2.35	4.75	5.24	5.26	0.98	1.11
146	C008722020	2.82	3.74	2.84	3.26	4.09	3.75	1.01	1.15

147	C008902125	2.44	3.21	2.44	3.07	3.65	3.64	1.00	1.19
148	C001201210	1.65	2.02	1.69	1.43	1.57	1.54	1.03	1.08
149	C009102805	2.29	2.71	2.48	5.14	5.67	5.64	1.08	1.10
150	C009314130	2.52	2.99	2.52	3.35	3.74	3.56	1.00	1.06
151	C004702203	1.44	1.79	1.38	1.43	1.62	1.63	0.96	1.14
152	C006924230	1.83	2.08	1.96	1.34	1.60	1.46	1.07	1.09
153	C004720810	1.67	1.77	1.46	1.60	1.86	1.79	0.87	1.12
154	C002004730	2.48	3.15	2.99	2.65	2.97	2.88	1.20	1.08
155	C005901825	3.10	4.74	2.93	2.44	3.41	3.34	0.94	1.37
156	C002001215	2.11	3.07	2.87	2.61	2.79	2.53	1.36	0.97
157	C008511515	4.17	4.63	4.30	3.82	4.56	4.30	1.03	1.13
158	C004529620	2.49	2.95	2.71	2.93	3.60	3.42	1.09	1.17
159	C008404020	2.03	2.49	1.95	2.43	2.62	2.53	0.96	1.04
160	C004903005	1.51	1.84	1.65	2.69	3.32	3.13	1.10	1.16
161	C000602310	1.71	1.84	1.63	3.33	4.08	3.88	0.95	1.17
162	C007602610	1.97	2.70	2.26	3.18	3.62	3.33	1.15	1.05
163	C001202005	1.82	2.22	2.08	3.21	3.46	3.32	1.14	1.03
164	C001301620	1.30	1.56	1.48	2.49	3.00	2.98	1.14	1.20
165	C001105220	1.18	1.26	1.08	2.39	2.64	2.53	0.91	1.06
166	C001205010	1.91	2.35	2.26	4.51	4.65	4.46	1.19	0.99
167	C001424750	3.01	3.66	3.15	5.04	4.97	4.85	1.05	0.96
168	C006311110	2.09	2.35	2.19	5.12	5.79	5.45	1.05	1.06
169	C001400730	2.01	2.43	2.26	5.47	6.20	5.91	1.12	1.08
170	C009103005	1.42	1.74	1.45	3.89	3.80	#N/A	1.02	#N/A
171	C007102605	2.32	2.95	2.76	4.14	4.95	4.75	1.19	1.15
172	C000102115	2.45	3.36	3.04	4.09	5.74	5.47	1.24	1.34

173	C007302705P	1.47	2.08	1.91	3.37	5.07	4.72	1.30	1.40
174	C006500230	2.03	4.35	3.81	3.21	5.48	5.07	1.87	1.58

10.5 Load Test Documentation

Table 30. Strain Gauge ID and Locations for Yutan Load Test 1

Sensor ID	Girder # (1-8)	Cross Section Location (South Abut., Midspan, North Abut.)	Sensor Location (West or East Bottom Flange, Top of Web)	BDI Sensor ID
1	1	South Abutment	Top of Web	5404
2	1	South Abutment	West Bottom Flange	4526
3	1	South Abutment	East Bottom Flange	4523
4	2	South Abutment	Top of Web	4546
5	2	South Abutment	West Bottom Flange	5397
6	2	South Abutment	East Bottom Flange	5328
7	3	South Abutment	Top of Web	5381
8	3	South Abutment	West Bottom Flange	5401
9	3	South Abutment	East Bottom Flange	6182
10	4	South Abutment	Top of Web	5395
11	4	South Abutment	West Bottom Flange	6326
12	4	South Abutment	East Bottom Flange	5410
13	5	South Abutment	Top of Web	7039
14	5	South Abutment	West Bottom Flange	5412
15	5	South Abutment	East Bottom Flange	4520
16	8	South Abutment	Top of Web	6190
17	8	South Abutment	West Bottom Flange	6181
18	8	South Abutment	East Bottom Flange	5406
19	1	Midspan	Top of Web	4535
20	1	Midspan	West Bottom Flange	6876
21	1	Midspan	East Bottom Flange	6192
22	2	Midspan	Top of Web	7033
23	2	Midspan	West Bottom Flange	7030
24	2	Midspan	East Bottom Flange	7032
25	3	Midspan	Top of Web	7051
26	3	Midspan	West Bottom Flange	7041
27	3	Midspan	East Bottom Flange	7040
28	4	Midspan	Top of Web	7035
29	4	Midspan	West Bottom Flange	7052
30	4	Midspan	East Bottom Flange	7054
31	5	Midspan	Top of Web	5408

32	5	Midspan	West Bottom Flange	6178
33	5	Midspan	East Bottom Flange	4524
34	8	Midspan	Top of Web	7031
35	8	Midspan	West Bottom Flange	7044
36	8	Midspan	East Bottom Flange	7042
37	1	North Abutment	Top of Web	7053
38	1	North Abutment	West Bottom Flange	7048
39	1	North Abutment	East Bottom Flange	7050
40	2	North Abutment	Top of Web	7038
41	2	North Abutment	West Bottom Flange	6191
42	2	North Abutment	East Bottom Flange	4531
43	3	North Abutment	Top of Web	7058
44	3	North Abutment	West Bottom Flange	7037
45	3	North Abutment	East Bottom Flange	7060
46	4	North Abutment	Top of Web	5398
47	4	North Abutment	West Bottom Flange	4541
48	4	North Abutment	East Bottom Flange	5411
49	5	North Abutment	Top of Web	7029
50	5	North Abutment	West Bottom Flange	5384
51	5	North Abutment	East Bottom Flange	7055

Table 31. Strain Gauge ID and Locations for Yutan Load Test 2

Sensor ID	**Girder # (1-8)**	**Cross Section Location (South Abut., Midspan, North Abut.)**	**Sensor Location (Bottom Flange, Top of Web)**	**BDI Sensor ID**
1	1	South Abutment	Top of Web	7060
2	1	South Abutment	Bottom Flange	7031
3	2	South Abutment	Top of Web	7057
4	2	South Abutment	Bottom Flange	5395
5	3	South Abutment	Top of Web	7032
6	3	South Abutment	Bottom Flange	7051
7	4	South Abutment	Top of Web	5398
8	4	South Abutment	Bottom Flange	4524
9	5	South Abutment	Top of Web	7029

10	5	South Abutment	Bottom Flange	7045
11	6	South Abutment	Top of Web	6178
12	6	South Abutment	Bottom Flange	7030
13	7	South Abutment	Top of Web	7043
14	7	South Abutment	Bottom Flange	6192
15	8	South Abutment	Top of Web	7040
16	8	South Abutment	Bottom Flange	7047
17	1	Midspan	Top of Web	7049
18	1	Midspan	Bottom Flange	5401
19	2	Midspan	Top of Web	5412
20	2	Midspan	Bottom Flange	4523
21	3	Midspan	Top of Web	7035
22	3	Midspan	Bottom Flange	5384
23	4	Midspan	Top of Web	7053
24	4	Midspan	Bottom Flange	7037
25	5	Midspan	Top of Web	7052
26	5	Midspan	Bottom Flange	6876
27	6	Midspan	Top of Web	7046
28	6	Midspan	Bottom Flange	6181
29	7	Midspan	Top of Web	7042
30	7	Midspan	Bottom Flange	5397
31	8	Midspan	Top of Web	7036
32	8	Midspan	Bottom Flange	5410
33	1	North Abutment	Top of Web	4520
34	1	North Abutment	Bottom Flange	6191
35	2	North Abutment	Top of Web	7041
36	2	North Abutment	Bottom Flange	7056
37	3	North Abutment	Top of Web	7061
38	3	North Abutment	Bottom Flange	4541
39	4	North Abutment	Top of Web	6182
40	4	North Abutment	Bottom Flange	5411
41	5	North Abutment	Top of Web	7055
42	5	North Abutment	Bottom Flange	7054
43	6	North Abutment	Top of Web	4546
44	6	North Abutment	Bottom Flange	4526

11 References

Adeli, H. (2001). Neural Networks in Civil Engineering: 1989-2000. *Computer-Aided Civil and Infrastructure Engineering*, 16(2), pp.126-142.

American Institute of Steel Construction (2017). *Design Guide 21: Welded Connections--A Primer for Engineers*.

Alipour, M., Harris, D., Barnes, L., Ozbulut, O. and Carroll, J. (2017). Load-Capacity Rating of Bridge Populations through Machine Learning: Application of Decision Trees and Random Forests. *Journal of Bridge Engineering*.

American Association of State Highway and Transportation Officials (AASHTO). (2013).*The Manual for Bridge Evaluation*, 2nd Ed., 2011 and 2013 Interim Revisions,Washington, DC.

American Association of State Highway and Transportation Officials (AASHTO). (2015).*AASHTO LRFD Bridge Design Specifications*, 7th Ed., 2015 Interim Revisions,Washington, DC.

Anderson, D., Hines, E., Arthur, S. and Eiap, E. (1997). Application of Artificial Neural Networks to the Prediction of Minor Axis Steel Connections. *Computers & Structures*, 63(4), pp.685-692.

Armendariz, R. and Bowman, M. (2018). Bridge Load Rating. *Joint Transportation Research Program*, (FHWA/IN/JTRP-2018/07).

Bae, H. and Oliva, M. (2012). Moment and Shear Load Distribution Factors for Multigirder Bridges Subjected to Overloads. *Journal of Bridge Engineering*, 17(3), pp.519-527.

Bakht, B. and Jaeger, L. (1990). Bridge Testing—A Surprise Every Time. *Journal of Structural Engineering*, 116(5), pp.1370-1383.

Bakht, B. and Jaeger, L. (1988). Bearing Restraint in Slab-on-Girder Bridges. *Journal of Structural Engineering*, 114(12), pp.2724-2740.

Bandara, R., Chan, T. and Thambiratnam, D. (2014). Frequency Response Function Based damage Identification Using Principal Component Analysis and Pattern Recognition Technique. *Engineering Structures*, 66, pp.116-128.

Barker, M. (2001). Quantifying Field-Test Behavior for Rating Steel Girder Bridges. *Journal of Bridge Engineering*, 6(4), pp.254-261.

Barth, K. and Wu, H. (2006). Efficient Nonlinear Finite Element Modeling of Slab on Steel Stringer Bridges. *Finite Elements in Analysis and Design*, 42(14-15), pp.1304-1313.

Bechtel, A., McConnell, J. and Chajes, M. (2009). Destructive Testing and Finite Element Analysis to Determine Ultimate Capacity of Skewed Steel I-Girder

Bridges. *Transportation Research Record: Journal of the Transportation Research Board*, 2131(1), pp.49-56.

Bechtel, A., McConnell, J. and Chajes, M. (2011). Ultimate Capacity Destructive Testing and Finite-Element Analysis of Steel I-Girder Bridges. *Journal of Bridge Engineering*, 16(2), pp.197-206.

Bell, E., Lefebvre, P., Sanayei, M., Brenner, B., Sipple, J. and Peddle, J. (2013). Objective Load Rating of a Steel-Girder Bridge Using Structural Modeling and Health Monitoring. *Journal of Structural Engineering*, 139(10), pp.1771-1779.

Bishara, A., Liu, M. and El-Ali, N. (1993). Wheel Load Distribution on Simply Supported Skew I-Beam Composite Bridges. *Journal of Structural Engineering*, 119(2), pp.399-419.

Bowman, M. D. and Chou, R. (2014). Review of Load Rating and Posting Procedures and Requirements. *Indiana Department of Transportation*.

Burdette, E. and Goodpasture, D. (1971). Full-Scale Bridge Testing: An Evaluation of Bridge Design Criteria.

Cai, C. and Shahawy, M. (2003). Understanding Capacity Rating of Bridges from Load Tests. *Practice Periodical on Structural Design and Construction*, 8(4), pp.209-216.

Cattan, J. and Mohammadi, J. (1997). Analysis of Bridge Condition Rating Data Using Neural Networks. *Computer-Aided Civil and Infrastructure Engineering*, 12(6), pp.419-429.

Chajes, M., Mertz, D. and Commander, B. (1997). Experimental Load Rating of a Posted Bridge. *Journal of Bridge Engineering*, 2(1), pp.1-10.

Chen, H., Tsai, K., Qi, G., Yang, J. and Amini, F. (1995). Neural Network for Structure Control. *Journal of Computing in Civil Engineering*, 9(2), pp.168-176.

Chen, Y. (1995). Prediction of Lateral Distribution of Vehicular Live Loads on Bridges with Unequally Spaced Girders. *Computers & Structures*, 54(4), pp.609-620.

Cheung, M., Gardner, N. and Ng, S. (1987). Load Distribution Characteristics of Slab-on-Girder Bridges at Ultimate. *Canadian Journal of Civil Engineering*, 14(6), pp.739-752.

Chuang, P., Goh, A. and Wu, X. (1998). Modeling the Capacity of Pin-Ended Slender Reinforced Concrete Columns Using Neural Networks. *Journal of Structural Engineering*, 124(7), pp.830-838.

Chung, W. and Sotelino, E. (2006). Three-dimensional Finite Element Modeling of Composite Girder Bridges. *Engineering Structures*, 28(1), pp.63-71.

Chung, W., Liu, J. and Sotelino, E. (2006). Influence of Secondary Elements and Deck Cracking on the Lateral Load Distribution of Steel Girder Bridges. *Journal of Bridge Engineering*, 11(2), pp.178-187.

Conner, S. and Huo, X. (2006). Influence of Parapets and Aspect Ratio on Live-Load Distribution. *Journal of Bridge Engineering*, 11(2), pp.188-196.

Desayi, P. and Krishnan, S. (1964). Equation for the Stress-Strain Curve of Concrete. *ACI Journal Proceedings*, 61(3).

Eamon, C. and Nowak, A. (2002). Effects of Edge-Stiffening Elements and Diaphragms on Bridge Resistance and Load Distribution. *Journal of Bridge Engineering*, 7(5), pp.258-266.

Ebeido, T. and Kennedy, J. (1996). Girder Moments in Continuous Skew Composite Bridges. *Journal of Bridge Engineering*, 1(1), pp.37-45.

Ebeido, T. and Kennedy, J. (1996). Shear and Reaction Distributions in Continuous Skew Composite Bridges. *Journal of Bridge Engineering*, 1(4), pp.155-165.

Eom, J. and Nowak, A. (2001). Live Load Distribution for Steel Girder Bridges. *Journal of Bridge Engineering*, 6(6), pp.489-497.

Fu, K. and Lu, F. (2003). Nonlinear Finite-Element Analysis for Highway Bridge Superstructures. *Journal of Bridge Engineering*, 8(3), pp.173-179.

Galambos, T., Leon, R., French, C., Barker, M. and Dishongh, B. (1992). Inelastic Rating Procedures for Steel Beam and Girder Bridges. *NCHRP*, Report 352.

Gheitasi, A. and Harris, D. (2015). Failure Characteristics and Ultimate Load-Carrying Capacity of Redundant Composite Steel Girder Bridges: Case Study. *Journal of Bridge Engineering*, 20(3), p.05014012.

Gheitasi, A. and Harris, D. (2015). Overload Flexural Distribution Behavior of Composite Steel Girder Bridges. *Journal of Bridge Engineering*, 20(5).

Ghosn, M. and Moses, F. (1998). Redundancy in Highway Bridge Superstructures. *NCHRP*, Report 406.

Ghosn, M., Moses, F. and Gobieski, J. (1986). Evaluation of Steel Bridges Using In-Service Testing. *Transportation Research Record*.

Guzelbey, I., Cevik, A. and Gögüş, M. (2006). Prediction of Rotation Capacity of Wide Flange Beams Using Neural Networks. *Journal of Constructional Steel Research*, 62(10), pp.950-961.

Hadi, M. (2003). Neural Networks Applications in concrete Structures. *Computers & Structures*, 81(6), pp.373-381.

Hall, J. and Kostem, C. (1981). *Inelastic Overload Analysis of Continuous Steel Multi-Girder Highway Bridges by the Finite Element Method*. Ph.D. Lehigh University.

Harris, D., Civitillo, J. and Gheitasi, A. (2016). Performance and Behavior of Hybrid Composite Beam Bridge in Virginia: Live Load Testing. *Journal of Bridge Engineering*, 21(6), p.04016022.

Harris, D. (2010). Assessment of Flexural Lateral Load Distribution Methodologies for Stringer Bridges. *Engineering Structures*, 32(11), pp.3443-3451.

Harris, D., Cousins, T., Murray, T. and Sotelino, E. (2008). Field Investigation of a Sandwich Plate System Bridge Deck. *Journal of Performance of Constructed Facilities*, 22(5), pp.305-315.

Harris, D. and Gheitasi, A. (2013). Implementation of an Energy-Based Stiffened Plate formulation for Lateral Load Distribution characteristics of Girder-Type Bridges. *Engineering Structures*, 54, pp.168-179.

Hasançebi, O. and Dumlupınar, T. (2013). Detailed Load Rating Analyses of Bridge Populations Using Nonlinear Finite Element Models and Artificial Neural Networks. *Computers & Structures*, 128, pp.48-63.

Hasançebi, O. and Dumlupınar, T. (2011). A Neural Network Approach for Approximate Force Response Analyses of a Bridge Population. *Neural Computing and Applications*, 22(3-4), pp.755-769.

Hearn, G. (2014). *NCHRP Synthesis 453: State Bridge Load Posting Processes and Practices*.

Hegazy, T., Tully, S. and Marzouk, H. (1998). A Neural Network Approach for Predicting the Structural Behavior of Concrete Slabs. *Canadian Journal of Civil Engineering*, 25(4), pp.668-677.

Helba, A. and Kennedy, J. (1994). Parametric Study on Collapse Loads of Skew Composite Bridges. *Journal of Structural Engineering*, 120(5), pp.1415-1433.

Hosteng, T., and Phares, B., (2013) Demonstration of Load Rating Capabilities Through Physical Load Testing: Ida County Bridge Case Study," Iowa. Dept. of Transportation.

Hosteng, T., and Phares, B., (2013) Demonstration of Load Rating Capabilities Through Physical Load Testing: Sioux County Bridge Case Study," Iowa. Dept. of Transportation.

Huang, C. and Loh, C. (2001). Nonlinear Identification of Dynamic Systems Using Neural Networks. *Computer-Aided Civil and Infrastructure Engineering*, 16(1), pp.28-41.

Huang, H., Shenton, H. and Chajes, M. (2004). Load Distribution for a Highly Skewed Bridge: Testing and Analysis. *Journal of Bridge Engineering*, 9(6), pp.558-562.

Jaramilla, B. and Huo, S. (2005). FHWA-HRT-05-006: Looking to Load and Resistance Factor Rating. *Federal Highway Administration*, 69(1).

Jeffrey, A., Breña, S. and Civjan, S. (2009). Evaluation of Bridge Performance and Rating through Non-destructive Load Testing.

Kathol, S., Azizinamini, A. and Luedke, J. (1995). *Strength Capacity of Steel Girder Bridges: Final Report*. Nebraska Department of Roads.

Khaleel, M. and Itani, R. (1990). Live-Load Moments for Continuous Skew Bridges. *Journal of Structural Engineering*, 116(9), pp.2361-2373.

Khaloo, A. and Mirzabozorg, H. (2003). Load Distribution Factors in Simply Supported Skew Bridges. *Journal of Bridge Engineering*, 8(4), pp.241-244.

Kim, S. and Nowak, A. (1997). Load Distribution and Impact Factors for I-Girder Bridges. *Journal of Bridge Engineering*, 2(3), pp.97-104.

Kim, Y., Tanovic, R. and Wight, R. (2013). A Parametric Study and Rating of Steel I-Girder Bridges Subjected to Military Load Classification Trucks. *Engineering Structures*, 56, pp.709-720.

Kulicki, J., Prucz, Z., Clancy, C., Mertz, D. and Nowak, A., 2007. Updating the Calibration Report for AASHTO LRFD Code. *NCHRP*, Project 20-07 Task 186.

Kushida, M., Miyamoto, A. and Kinoshita, K. (1997). Development of Concrete Bridge Rating Prototype Expert System with Machine Learning. *Journal of Computing in Civil Engineering*, 11(4), pp.238-247.

Lichtenstein, A., Moses, F. and Bakht, B. (1998). *Manual for Bridge Rating Through Load Testing*. Research Results Digest Number 234.

Mabsout, M., Tarhini, K., Frederick, G. and Kesserwan, A. (1998). Effect of Continuity on Wheel Load Distribution in Steel Girder Bridges. *Journal of Bridge Engineering*, 3(3), pp.103-110.

Mabsout, M., Tarhini, K., Frederick, G. and Kobrosly, M. (1997). Influence of Sidewalks and Railings on Wheel Load Distribution in Steel Girder Bridges. *Journal of Bridge Engineering*, 2(3), pp.88-96.

MacKay, D.J.C. (1992) “Bayesian Interpolation,” *Neural Comput.*, 4(3), 415-447

Marquardt, D. (1963). An Algorithm for Least-Squares Estimation of Nonlinear Parameters. *Journal of the Society for Industrial and Applied Mathematics*, 11(2), pp.431-441.

Marx, H., Khachaturian, N. and Gamble, W. (1986). *Report FHWA/IL/UI-210: Development of Design Criteria for Simply Supported Skew Slab-And-Girder Bridges*. Illinois Department of Transportation.

Masri, S., Chassiakos, A. and Caughey, T. (1993). Identification of Nonlinear Dynamic Systems Using Neural Networks. *Journal of Applied Mechanics*, 60(1), p.123.

Masri, S., Smyth, A., Chassiakos, A., Caughey, T. and Hunter, N. (2000). Application of Neural Networks for Detection of Changes in Nonlinear Systems. *Journal of Engineering Mechanics*, 126(7), pp.666-676.

McConnell, J., Chajes, M. and Michaud, K. (2015). Field Testing of a Decommissioned Skewed Steel I–Girder Bridge: Analysis of System Effects. *Journal of Structural Engineering*, 141(1), p.D4014010.

Mikami, I., Tanaka, S. and Hiwatashi, T. (1998). Neural Network System for Reasoning Residual Axial Forces of High-Strength Bolts in Steel Bridges. *Computer-Aided Civil and Infrastructure Engineering*, 13(4), pp.237-246.

Moses, F. (2001). NCHRP Report 454, Calibration of Load Factors for LRFR Bridge Evaluation.

Moses, J., Harries, K., Earls, C. and Yulismana, W. (2006). Evaluation of Effective Width and Distribution Factors for GFRP Bridge Decks Supported on Steel Girders. *Journal of Bridge Engineering*, 11(4), pp.401-409.

Mukherjee, A. and Deshpande, J. (1995). Modeling Initial Design Process using Artificial Neural Networks. *Journal of Computing in Civil Engineering*, 9(3), pp.194-200.

Mukherjee, A., Deshpande, J. and Anmala, J. (1996). Prediction of Buckling Load of Columns Using Artificial Neural Networks. *Journal of Structural Engineering*, 122(11), pp.1385-1387.

Murdock, M. (2009). *Comparative Load Rating Study Under LRFR and LFR Methodologies for Alabama Highway Bridges*. Ph.D. Auburn University.

National Cooperative Highway Research Program (1998). *NCHRP Report 406: Redundancy in Highway Bridge Superstructures*. Washington D.C.: National Academy Press.

National Cooperative Highway Research Program (1993). *NCHRP Report 352: Inelastic Rating Procedures for Steel Beam and Girder Bridges*. Washington D.C.: National Academy Press.

NBI (National Bridge Inventory). (2019).

Nowak, A., Kim, S. and Stankiewicz, P. (2000). Analysis and diagnostic testing of a bridge. *Computers & Structures*, 77(1), pp.91-100.

Nowak, A. (1999). NCHRP Report 368, Calibration of LRFD Bridge Design Code.

Pandey, P. and Barai, S. (1995). Multilayer Perceptron in Damage Detection of Bridge Structures. *Computers & Structures*, 54(4), pp.597-608.

Pendharkar, U., Chaudhary, S. and Nagpal, A. (2007). Neural Network for Bending Moment in Continuous Composite Beams Considering Cracking and Time Effects in Concrete. *Engineering Structures*, 29(9), pp.2069-2079.

Phares, B., Wipf, T., Klaiber, F. and Abu-Hawash, A. (2003). Bridge Load Rating Using Physical Testing.

Razaqpur, A.G. and Nofal, M. (1990). Analytical Modeling of Nonlinear Behavior of Composite Bridges. *Journal of Structural Engineering*, 116(6), pp.1715-1733.

Razaqpur, A.G., Shedid, M. and Nofal, M. (2012). Inelastic Load Distribution in Multi-Girder Composite Bridges. *Engineering Structures*, 44, pp.234-247.

Sakr, M. and Sakla, S. (2009). Long-term Deflection of Cracked Composite Beams with Nonlinear Partial Shear Interaction — A Study Using Neural Networks. *Engineering Structures*, 31(12), pp.2988-2997.

Sanayei, M., Phelps, J., Sipple, J., Bell, E. and Brenner, B. (2012). Instrumentation, Nondestructive Testing, and Finite-Element Model Updating for Bridge Evaluation Using Strain Measurements. *Journal of Bridge Engineering*, 17(1), pp.130-138.

Sebastian, W. and McConnel, R. (2000). Nonlinear FE Analysis of Steel-Concrete Composite Structures. *Journal of Structural Engineering*, 126(6), pp.662-674.

Sheikh-Ahmad, J., Twomey, J., Kalla, D. and Lodhia, P. (2007). Multiple Regression and Committee Neural Network Force Prediction Models in Milling FRP. *Machine Science and Technology*, 11(3), pp.391-412.

Shu, J., Zhang, Z., Gonzalez, I. and Karoumi, R. (2013). The Application of a Damage Detection Method using Artificial Neural Network and Train-Induced Vibrations on a Simplified Railway Bridge Model. *Engineering Structures*, 52, pp.408-421.

Sirca, G. and Adeli, H. (2004). Counterpropagation Neural Network Model for Steel Girder Bridge Structures. *Journal of Bridge Engineering*, 9(1), pp.55-65.

Sofi, F. and Steelman, J., (2019). Nonlinear Flexural Distribution Behavior and Ultimate System Capacity of Skewed Steel Girder Bridges. *Engineering Structures*, 197, p.109392.

Sofi, F. and Steelman, J., (2017). Parametric Influence of Bearing Restraint on Nonlinear Flexural Behavior and Ultimate Capacity of Steel Girder Bridges. *Journal of Bridge Engineering*, 22(7), p.04017033.

Sofi, F. (2017). Structural System-Based Evaluation of Steel Girder Highway Bridges and Artificial Neural Network (ANN) Implementation for Bridge Asset Management. Ph.D. University of Nebraska-Lincoln.

Sotelino, E., Liu, J., Chung, W. and Phuvoravan, K. (2004). *FHWA/IN/JTRP-2004/20: Simplified Load Distribution Factor for Use in LRFD Design*.

Stallings, J. and Yoo, C. (1993). Tests and Ratings of Short-Span Steel Bridges. *Journal of Structural Engineering*, 119(7), pp.2150-2168.

Tabsh, S. and Tabatabai, M. (2001). Live Load Distribution in Girder Bridges Subject to Oversized Trucks. *Journal of Bridge Engineering*, 6(1), pp.9-16.

Tadesse, Z., Patel, K., Chaudhary, S. and Nagpal, A. (2012). Neural networks for prediction of deflection in composite bridges. *Journal of Constructional Steel Research*, 68(1), pp.138-149.

Tarhini, K. and Frederick, G. (1992). Wheel Load Distribution in I-Girder Highway Bridges. *Journal of Structural Engineering*, 118(5), pp.1285-1294.

Wipf, T. and Hosteng, T. (2010). *Diagnostic Load Testing May Reduce Embargoes*. Tech Transfer Summary.

Wipf, T., Phares, B., Wood, D., Mellingen, E. and Samuelson, A. (2003). *Iowa DOT Report TR-445: Development of Bridge Load Testing Process for Load Evaluation*. Center for Transportation Research and Education.

Yarnold, M., Golecki, T. and Weidner, J. (2018). Identification of Composite Action Through Truck Load Testing. *Frontiers in Built Environment*, 4.

Yousif, Z. and Hindi, R. (2007). AASHTO-LRFD Live Load Distribution for Beam-and-Slab Bridges: Limitations and Applicability. *Journal of Bridge Engineering*, 12(6), pp.765-773.

Zheng, L., Huo, X. and Hayworth, R. (2007). Comparison of Load Factor Rating (LFR) to Load and Resistance Factor Rating (LRFR) of Prestressed Concrete I-Beam Bridges. *American Society of Civil Engineers Structures Congress*.

Zokaie, T. (2000). AASHTO-LRFD Live Load Distribution Specifications. *Journal of Bridge Engineering*, 5(2), pp.131-138.

END OF DOCUMENT